Parameters and Stability of Surface Waves for Single and Double Layer Liquid Flows: An Experimental and Computational Study

A Thesis Submitted to the College of
Graduate Studies and Research
in Partial Fulfillment of the Requirements
for the Degree of Doctor of Philosophy in
the Department of Chemical Engineering
University of Saskatchewan
Saskatoon

By

Gong Zhang

Summer 1996

University of Saskatchewan

College of Graduate Studies and Research

SUMMARY OF DISSERTATION

Submitted in partial fulfillment
of the requirement for the

DEGREE OF DOCTOR OF PHILOSOPHY

By

Gong Zhang

Department of Chemical Engineering
University of Saskatchewan

Fall 1996

Examining Committee:

Dr. R. Balachandar	~~Dean~~/~~Associate Dean~~/Dean's Designate, Chair College of Graduate Studies and Research
Dr. J. Postlethwaite	Chair of Advisory Committee, Department of Chemical Engineering
Dr. N. N. Bakhshi	Department of Chemical Engineering
Dr. D. Bergstrom	Department of Mechanical Engineering
Dr. M. N. Esmail	Department of Chemical Engineering
Dr. D. -Y. Peng	Department of Chemical Engineering

External Examiner:

Dr. P. Tanguy
Andre-Aisenstadt Building, Room 5515
Ecole Polytechnique
PO Box 6079, Station Centre-Ville
Montreal, PQ
H3C 3A7

Parameters and Stability of Surface Waves for Single and Double Layer Liquid Flows: An Experimental and Computational Study

The flow of thin liquid layers is industrially important, and commonly found in many engineering applications. In modern technology flows of thin liquid films play a major role in fine liquid coating processes, such as the production of photo film and magnetic tape. The principle of such processes is the application of one or more thin layers of coating liquids to a solid substrate. The quality of the products and the efficiency of the coating operation depend to a large extent on the mechanics of the thin film flow. The flow of thin liquid film is known to frequently develop surface waves due to its instability. In liquid coating industry these waves lead to defective products, when the wavy film is dried with a non-uniform thickness.

This work is an experimental and numerical study of the instability and the wave parameters of free-surface waves, running on the surface of falling liquid films over an inclined plane. An experimental procedure employing optic-electric transformation and digital signal processing techniques is designed, and used to obtain the frequency information about waves on the surface of a single layer flow and a double layer flow. Also, the criteria for onset of waves and the transit distance information are experimentally determined for a single layer flow. An unsteady state time-accurate computational model employing finite difference and numerical grid generation techniques is developed and used to simulate the single layer film flow subjected to a minute velocity disturbance. The

method is able to produce stable wavy regimes for a wide range of flow conditions. Wave profile and wave speed reflecting the speed of disturbance propagation over the free-surface were obtained for different liquid properties $0.0467 < \gamma\ [=(\nu 4g)^{-1/3}\sigma/\rho] < 467$, different angles of inclination $0.1° < \theta < 89.9°$, and different Reynolds numbers $Re < 30$. Computations for vertical flow $\theta = 90°$ always diverged. However, any shift in angle from 90° produced stable solutions. Calculations for higher Reynolds numbers consumed increasingly more CPU time.

In presenting this thesis in partial fulfillment of the requirements for a Postgraduate degree from the University of Saskatchewan, I agree that the libraries of this University may make it freely available for inspection. I further agree that permission for copying of this thesis in any manner, in whole or in part, for scholarly purposes may be granted by the professors who supervised my thesis work or, in their absence, by the Head of the Department or the Dean of the College in which my thesis was done. It is understood that any copying or publication or use of this thesis or parts thereof for financial gain shall not be allowed without my written permission. It is also understood that due recognition shall be given to me and the University of Saskatchewan in any scholarly use which may be made of any material in my thesis.

Requests for permission to copy or to make other use of material in this thesis in whole or in part should be addressed to:

The Head of the Department of Chemical Engineering
University of Saskatchewan
Saskatoon, Saskatchewan
Canada, S7N 5C9

ABSTRACT

In modern technology flows of thin liquid films play a major role in fine liquid coating processes, such as the production of photo film and magnetic tape. The principle of such processes is the application of one or more thin layers of coating liquids to a solid substrate. The quality of the products and the efficiency of the coating operation depend to a large extent on the mechanics of the thin film flow. The flow of thin liquid film is known to frequently develop surface waves due to its instability. In liquid coating industry they lead to defective products, when the wavy film is dried with a non-uniform thickness.

This work is an experimental and numerical study of the instability and the wave parameters of the free-surface wave of thin liquid film flow. An experimental procedure employing optic-electric transformation and digital signal processing techniques is designed, and used to obtain the frequency information about waves on the surface of a single layer flow and a double layer flow. Also, the criteria for onset of waves and the transit distance information are experimentally determined for a single layer flow. A computer model employing finite difference and numerical grid generation techniques is developed and used to simulate the single layer film flow subjected to a minute disturbance.

ACKNOWLEDGMENTS

Thanks are due in first place to my supervisor Dr. M. N. Esmail for his sound guidance, assistance, and exceptional support during all stages of my work.

In addition, I would like to thank my committee members: Dr. N. N. Bakhshi, Dr. D. Bergstrom, Dr. D. -Y. Peng, and Dr. J. Postlethwaite for their supervision.

Thanks are also due to Karen Burlock, Debbie Pfeifer, Ted Wallentiny, Al Leyland, and other faculties, staffs, and colleague students in the department.

Financial support came from the Canadian International Development Agency in the form of a graduate scholarship in the first two years of my study, and National Sciences and Engineering Research Council of Canada in the form of research assistantship in the following two and half years.

TABLE OF CONTENTS

LIST OF FIGURES

LIST OF TABLES

INTRODUCTION

THIN LIQUID FILM FLOW

The flow of thin liquid layers is industrially important, and commonly found in many engineering applications. In modern technology flows of thin liquid films play a major role in fine liquid coating processes, such as the production of photo film and magnetic tape. The principle of such processes is the application of one or more thin layers of coating liquids to a solid substrate. The quality of the products and the efficiency of the coating operation depend to a large extent on the mechanics of the thin film flow. The flow of thin liquid film is known to frequently develop surface waves. These waves play different roles in different industrial applications. In liquid coating industry they lead to defective products, when the wavy film is dried with a non-uniform thickness. In cooling towers, wavy film increases the area of heat transfer. Wave motion on the surface of a thin liquid film has been the subject of extensive studies in the past few decades since the pioneering work of Nusselt (1916), and Kapitsa (1948). However, most of the studies were of theoretical nature. Few experimental results exist in this field. A better knowledge and understanding of surface waves, their onset, and decay are important to many industries, particularly those applying liquid coating. In the following section we expand on the concepts of coating technology in order to gain deeper appreciation of the issues surrounding flows of thin liquid films.

LIQUID COATING PROCESSES

Some of the typical products of coating processes are photo-sensitive materials. There are produced in many types such as black and white print film, color print film and slide film, photo paper, medical X-ray film, etc. In order to produce these materials, several silver halide emulsion layers and other auxiliary layers have to be coated on the web of base material. These layers are very thin. For example, the total thickness of the

coating layer of Kodak Ektachrome color slide film is 0.02 mm in dry state (Levey, 1992), and about 0.2 mm before drying.

The coating of modern materials is a complex task and the coating methods in current use are the subject of commercial secrecy. One of the earliest methods of coating flexible supports was 'dip' or 'trough' coating (Figure 1). Dip coating is limited in speed since faster dip-coating results in thicker emulsion layers which are difficult to dry, and which have undesirable photographic properties. This method has been replaced by other coating techniques outlined below.

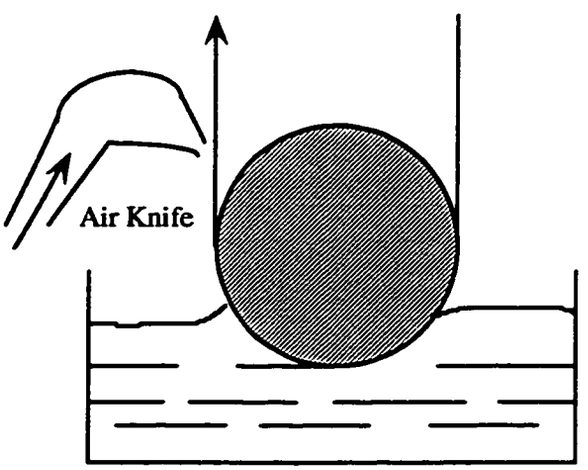

Figure 1 Schematic Diagram of Dip Coating

In order to increase the coating speed dip coating has been modified by the use of an air-knife. It is an accurately machined slot directing a flow of air downwards onto the coated layer. The knife controls the thickness of the coated layer by pushing the excess liquid back into the coating trough. Coating by this method results in faster coating speeds, thinner coating layers, and more concentrated emulsions.

Other coating methods employ accurately machined slots through which emulsion is pumped directly onto the base (slot applicator or extrusions coating) or pumped to flow down a slab before touching the base (slide coating and curtain coating). Figures 2 and

3 show the schematic diagrams of multiple slide coating and multiple curtain coating, respectively. Such coating methods allow coating speeds to be much higher than was possible with the more traditional methods. It is believed (Jacobson, 1988) that in photographic industry coating speeds approaching 60 meters per minute or possibly higher are now being used to coat base material which is approximately 1.4 meters wide.

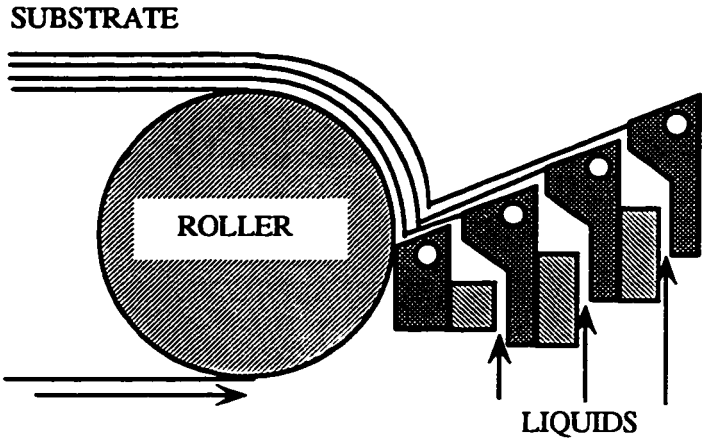

Figure 2 Multi-layer Slide Coating

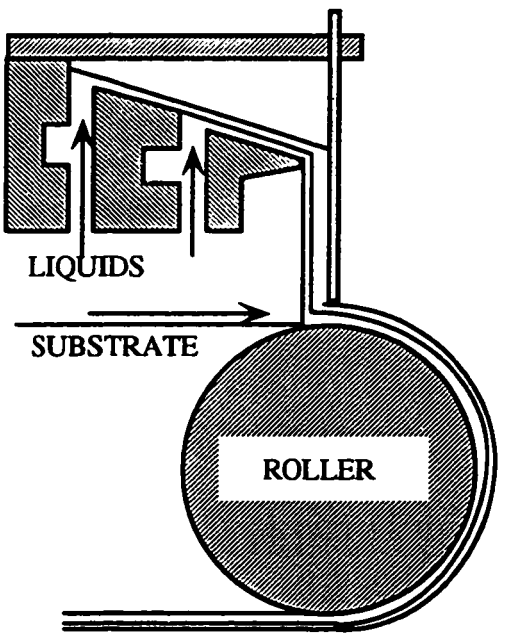

Figure 3 Multi-layer Curtain Coating

Modern monochrome materials are coated with more than one layer. Color materials may have as many as 14 layers. Figure 4 shows a multiple layer structure of a color slide film. In modern coating technology, many layers are coated in a single pass of the base through the coating machine. This is done either by using multiple slots, by using a number of coating stations, or by a combination of both.

It is important that the uniformity and thickness of the applied coating be held to very rigid specifications, because emulsion thickness is very important in controlling the photographic properties of the products. Not only it is essential that the coating be of the proper thickness; but it must be uniform over both the width and the length of the roll, and from one roll of base to another. Thickness and uniformity are controlled by the physical properties of the emulsion, the stability behavior of the flow system involved, and the surrounding conditions.

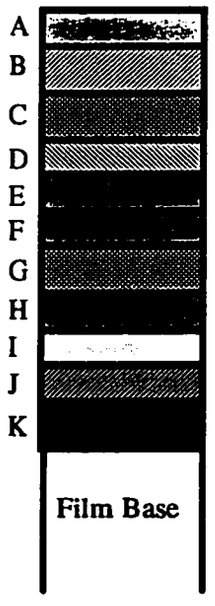

A. Protective layer

B. Blue-sensitive emulsion layer and yellow coupler

C. Yellow filter (colloidal silver)

D. Green-sensitive (fast) emulsion layer and magenta coupler

E. Green-sensitive (medium) emulsion layer and magenta coupler

F. Green-sensitive (slow) emulsion layer and magenta coupler

G. Interlayer

H. Red-sensitive (fast) emulsion layer and cyan coupler

I. Red-sensitive (medium) emulsion layer and cyan coupler

J. Red-sensitive (slow) emulsion layer and cyan coupler

K. Anti-halation coating

Figure 4 Multiple Layer Structure of a Modern Color Slide Film

HYDRODYNAMIC STABILITY OF LIQUID FILM FLOWS

The study of changes which occur in a flowing liquid film when it is subjected to various disturbances has industrial importance. In any processes random disturbances are inevitable. They could be any changes in surrounding conditions such as the changes in fluid properties, or in flow parameters. If the liquid flow is stable as a dynamic system, the disturbance will not alter the system and will disappear in the flow process.

The steady state theoretical solution of the flow of a liquid film describes a flow with uniform thickness, a straight (plane) free surface, and a parabolic distribution of velocity across the film (Nusselt, 1916). In laboratory experiments such a flow is obtained at low speeds and for a limited distance from the starting point of the film. Considering the film flow to be the steady state system subjected to a disturbance, slight shifts in velocities, pressure, and film thickness will occur as a result of the disturbance. The thickness change is particularly visible since it manifests itself by the appearance of a small amplitude surface waves. Similar arguments can be made about multiple layer flows with interfacial waves appearing on the surfaces separating layers as a result of disturbances. If the system is stable the magnitude of this disturbance will gradually decrease, and the free surface and/or the interfaces will gradually become smooth and undisturbed. Stable liquid film flows with uniform thickness are less favorable to the heat/mass transfer across the liquid film. However, the uniformity of the layers is a matter of great importance in coating processes. If the flow system is unstable the disturbance will be amplified in the flow process. Its magnitude will gradually increase, and the free surface and/or the interfaces will be disturbed and become rough. Such wavy surfaces enhance the heat/mass transfer across the liquid film, but are undesirable in coating processes. Wavy coating will eventually appear on the coated product as unevenness. These defects will down-grade the quality.

OBJECTIVES

The purpose of this research work is to study the wave motions on the free surface of single and double layer flow systems. The study includes experimental investigation and numerical simulation.

The objectives are;

1. To design an experimental procedure by employing optic-electric transformation and digital signal processing techniques, and use it to obtain the frequency information about surface wave motions, in a single layer flow.
2. To use the experimental technique to investigate the frequencies of waves on the surface of two liquid layers (double- layer flows).
3. To determine experimentally, the onset condition and the transit distance of the wave motions on the free surface of single layer flow system.
4. To develop a computer model by employing finite difference and numerical grid generation techniques, and use it to simulate the single layer film flow subjected to a minute disturbance.

LITERATURE REVIEW

Wave formations on the free surface and interfaces of thin liquid films have been the subject of extensive studies in the past few decades. However, most of the known studies are of a theoretical nature. Few experimental results exists in this field. Following is a review of the previously known experimental investigations, followed by a review of the more extensive previous theoretical works.

EXPERIMENTS

SINGLE LAYER SYSTEMS

Wave Patterns

Flowing films are stable when their Reynolds number is below a critical value. The film surface is completely smooth and mirror-like, troubled only occasionally by small random "dimples", which rapidly damp out in the direction of film flow. Otherwise, when the Reynolds number is greater than the critical value, the flow will be unstable and waves start to appear on the film surface. In practice, these waves are of a complicated nature. The wave patterns may vary from simple and nearly sinusoidal forms in the wave inception region to complex forms beyond the inception region (Kapitsa & Kapitsa 1949; Tailby & Portalski 1962; Fulford 1964; Krantz & Goren 1971a; Dukler 1972; Chu & Dukler 1974, 1975; Esmail 1980; Sivashinsky & Michelson 1980; Brauner & Maron 1982; Alekseenko et al. 1985; Lin & Wang 1985; Kelly et al. 1989; Goussis & Kelly 1991; Lacy et al. 1991; Liu & Gollub 1993). These complex forms include solitary waves with one or more peaks, the evolution of subsidiary wave fronts, the development of three-dimensional instabilities, the production of irregular fully developed waves, etc. Experimental observations have shown the strong dependence of the evolution of wavy films on the initial wave number.

Critical Reynolds Number

Earlier experimental investigations were concerned only with finding the critical Reynolds number, at which wave motion can be detected (primary instability). The methods used include careful visual observation (Binnie 1957, Fulford 1962), taking photographs of the free surface (Binnie 1959), and employing an electric "feeler" (Brauer 1956). Their results generally lie above the prediction of linear theories (Benjamin 1957), but indicate a similar trend with inclination angle.

According to the stability theory, this critical Reynolds number should be zero for a vertically falling film. But experimental observations show a scatter and the Reynolds number differs from zero. This is mainly due to the fact that although the theory predicts that vertical films will always be unstable, the waves on the free surface may be of too small an amplitude at low flow rate to be observed. The fact that the use of more sensitive methods of wave detection leads to smaller experimental values of the critical Reynolds numbers may be indirect confirmation of this argument (Fulford 1964).

Due to the difficulty in measuring the primary instability at very low flow rates there has been no progress on this subject until a recent work done by Liu et al. (1993). Using fluorescence imaging and computer image processing techniques they were able to dynamically measure the liquid film thickness with a claimed accuracy of several microns. Their result of the critical Reynolds number as a function of inclination angle is in agreement with the linear theory (Benjamin 1957, Yih 1963) for inclination angles of less than 10°. They also measured the growth rates and wave velocities. These experiments demonstrated that overall the linear stability theories are able to give a reasonably accurate prediction of the critical conditions for the onset of surface waves.

Wave Parameters

Tailby & Portalski (1962) reported measurements of the wavelengths near the point of wave inception on vertical films of various liquids. The results were considerably greater than the prediction of Kapitsa theory (1964). Similar results have been obtained

by Fulford (1962) for water films on an inclined wall. These results also show that at a given liquid flow rate, the wavelength increases rapidly as the inclination angle is decreased.

Jones and Whitaker (1966) measured wavelengths and wave velocities of the surface waves on a water film flowing down a vertical plane by optic-electric means. Their results were in agreement with a numerical solution of the Orr-Sommerfeld equation (Whitaker 1964) in the region near the top of the film where the theory of small disturbances is expected to be valid.

After the above work quite a few experiments have been reported (Anshus & Goren 1966, Strobel & Whitaker 1969, Krantz & Goren 1971b, Portalski & Clegg 1972, Portalski 1973, Pierson & Whitaker 1977, Hoffman & Potts 1979, Brauner & Maron 1982, Alekseenko et al 1985, Lin & Wang 1985, Liu et al. 1993). They mainly use local probes and photography. The wave velocity and/or wavelength have been determined for small amplitude waves. The comparison of their experimental results with the fastest growing disturbance in linear theories leads to semi-quantitative agreement with the theoretical predictions of linear theories but with fairly large scatter. Wave motion in the inception region can be described by the linear theories as long as the Reynolds number of film flow is not very high. Measurement of spatial growth rates (Krantz & Goren 1971b, Portalski & Clegg 1972, Alekseenko et al. 1985, Liu et al. 1993) also confirmed this point.

Krantz and Goren (1970) measured the wavelengths, wave velocities, and amplification rates of waves on thin liquid (two kinds of viscous oil) films flowing down an inclined plane (the inclination angle is 74.5°). Their results were in good agreement with the various linear stability analyses and showed that the stability of thin film flow at moderate or low Reynolds numbers is violated by disturbances of long wavelengths compared to the film thickness. But the waves in their experiment are produced by imposing disturbances of controlled amplitude and frequency. They tried to take the

effect of the inclination angle into account by correlating the equilibrium amplitude for the most highly amplified waves with the dimensionless group, $(1.2Re\text{-}\cot\theta)^3We/Re$, where θ is the inclination angle and We the Weber number.

There are very few published experimental reports about the frequency characteristics of free surface waves of thin liquid film flows. For a vertical water film flow Chu & Dukler (1974, 1975) found that there exist at least two classes of random waves, long wavelength waves which carry the bulk of the fluid and small waves which cover a substrate film that exists between large waves. At low Reynolds numbers ($Re < 200$) the frequency of the free surface waves is unimodal and increases with Reynolds number. This is in agreement with Kapitsa's data (1964). With further increase in Reynolds number the frequency becomes bimodal. One mode is associated with small waves and the frequency value continuously increases with Reynolds number. Another mode is associated with large waves, and the frequency value decreases rapidly with increasing Reynolds numbers in the transition periods (up to $Re = 750$), and increases thereafter in almost the same fashion as that of small waves.

For a non-vertical falling film flow Javdani (1976) found that inclination angle is an important parameter in this flow system. The frequency of the most highly amplified wave is expressed in the form:

$$\gamma = aN^n \qquad (a > 0, n < 0)$$

$$\gamma = 2\pi h_0 f/u_0$$

$$N = (1.2Re\text{-}\cot\theta)We/Re$$

$$Re = \rho h_0 u_0/\mu$$

$$We = (\rho h_0 u_0^2)/\sigma$$

where, N is the compact dimensionless number suggested by Yih (1963); h_0 and u_0 are the undisturbed film thickness and mean velocity, respectively; f is the wave frequency, and θ is the inclination angle to horizontal. The power n is a small but fairly constant number, and the coefficient 'a' consistently decreases with the increase in the inclination angle. The wave frequency of developed waves far downstream of the inlet was

reported by Brauner & Maron (1982) for inclined water film flows. Actually, they measured the spectra of the mass transfer rates of a chemical species from the liquid to the solid bottom. However, they experimentally demonstrated that these spectra are close to the wave spectra. Liu et al. (1993) reported two point experimental measurements of most rapidly amplified frequency for glycerin-water solutions at the inclination angle of 4.6°. These results are consistent with Brauner & Maron's (1982) results.

MULTIPLE LAYER SYSTEMS

Much less experimental work has been reported on multiple layer flows of viscous liquids. Earlier work concentrated only on finding the critical Reynolds number for each phase at which the flow becomes turbulent (Charles & Lilleleht 1965, Kao & Park 1972). Both experiments were conducted in a rectangular channel in which oil and water flow concurrently. There was no free surface in these experiments.

Kobayashi et al (1986, 1990) reported experimental work for multiple layer systems. Multiple layer film flow on inclined planes is often encountered in modern coating technology. If the flow on the slide is not stable the effect of instability would appear on the coated web as unevenness. This is the basic idea of their experiments. The pitch of unevenness can be easily obtained by measuring the density fluctuation of the coated web. This pitch is considered as the wavelength of the most rapidly amplified wave. Using this kind of technique they found good agreement between theoretical predictions and experimental results for the wavelengths of most unstable waves in the case of two- and three-layered film flows. Also, their experiment qualitatively supported the theoretical predictions of the effects of various factors, such as viscosity, flow rate, inclination angle, and the length of inclined plane, on the stability of two-layered film flow.

THEORETICAL WORK

SINGLE LAYER SYSTEMS

Linear Theory

The stability problem is formulated by taking the given steady state solution of the equations of motion and superimposing a disturbance of a suitable kind. This results in a set of non-linear disturbance differential equations, which govern the behavior of the disturbance. If the solution of the equations shows that any disturbance ultimately decays to zero, the flow is said to be stable, whereas if the disturbance can be permanently different from zero, the flow is unstable.

Naturally, the solution of the disturbance differential equations is simplified considerably by linearization for small disturbances. In the linear theory (Lin, 1955), the disturbances are assumed to be so small that the effect of the Reynolds stress on the mean motion can be neglected. Squire's theorem (1933) proved that three-dimensional disturbances are less dangerous to stability than their two-dimensional counterpart. This limits the problem of hydrodynamic stability to the two-dimensional case. As a result the stream function formulation of the equations of motion can be used. After that Fourier normal modes in flow direction are used as models for disturbances. These procedures lead to the well-known Orr-Sommerfeld equation.

The stability problem of the flow of thin liquid films was first formulated by Yih (1955). Unfortunately, the results of critical Reynolds number and neutral stability curves were incorrect. Based on Yih's formulation, Benjamin (1957) performed a new but very laborious calculations with the assumption that wave number is small. He found that free surface flows down a vertical plane are unstable for all finite Reynolds numbers.

A new perturbation procedure was introduced by Yih (1963). The advantages of this method were that it was simple and can be applied at low Reynolds numbers to any value of wave number, however large. The results showed: 1) The axis $\alpha = 0$ (α is the

wave number) in the α--Re (Re is the Reynolds number) plane is always a part of the neutral stability curve. 2) The actual rate of damping of very short waves is reduced in magnitude if the viscosity is increased. Also, Yih suggested that there are two kinds of waves, soft waves or surface waves (longer wavelengths), and hard waves or shear waves (shorter wavelengths). At low Reynolds numbers soft waves violated the overall stability of the flow. Graef (1966) and Pierson & Whitaker (1977) extended this work to $Re < 150$ and $Re < 1000$, respectively.

The general features of neutral stability curves were given by Lin (1967a). It was found that surface tension is a stabilizing factor and the inclination angle is a destabilizing factor. For a given inclination angle there exists a critical wave number. If the wavelengths of the free surface disturbances are shorter than this critical value the film flow can become unstable due to shear waves. Otherwise if the wavelengths of the free surface disturbances are longer than this critical value the film flow is always unstable due to surface waves. Later De Bruin (1974) pointed out that an incorrect surface boundary condition was used in Lin's calculation.

For large Reynolds numbers ($1000 < Re < 10000$) Chin et al (1986) numerically investigated the effects of inclination angle, surface tension, and form factor (the ratio of displacement thickness to momentum thickness) for both the surface and shear waves. They concluded that the effects of inclination angle and surface tension are duplex. When inclination angle increases the flow is moderately destabilized for surface waves and slightly stabilized for shear waves. When surface tension increases the flow is stabilized for surface waves and slightly destabilized for shear waves. The form factor has little effect on surface waves and is very important for the shear waves.

Yih (1965) and Lin (1967b) applied the linear theory to the flow of a non-Newtonian inelastic (triply non-linear) liquid films. The flow is always stable with respect to surface waves and the instability of the flow is due to shear waves only. Inclination

angle plays the same role as it does in Newtonian fluid systems and the second viscosity is a stabilizing factor.

Gupta's (1967) study showed that the instability of a visco-elastic (second-order) liquid film flow is governed by shear waves rather than surface waves. This is contrary to the corresponding results for an ordinary viscous fluid. The explanation was given as follows. The shear on an element of the fluid is reversed at such a frequency that the elastic stresses cannot relax when the flow of such a fluid is subjected to a disturbance. This results in a decrease in dissipation of the disturbance energy. So, part of the energy is stored in the element as strain energy and this disturbance makes the flow unstable. It is also shown that the elasticity of fluid is a destabilizing factor. Similar work were done by Gupta & Rai (1967), Lai (1967), Ting (1975), and Dandapat & Gupta (1978). Using Oldroyd-B model to describe a visco-elastic fluid Shaghfeh et al (1989) found out that the elasticity of fluid is actually a stabilizing factor.

Non-Linear Theory

In practice disturbances can be of finite amplitudes, and three-dimensional. For the stability problem with respect to finite amplitude disturbances the interdependence of the mean and disturbance parts of the flow must be taken into account. This creates a set of non-linear equations that fall into the domain of non-linear stability theory. The stream function can not be used for three-dimensional disturbances. Therefore, Orr-Sommerfeld equations are not the governing equations of non-linear stability problem.

Benjamin (1961) considered a three-dimensional small disturbance, introduced a double Fourier integral to represent a bounded disturbance, and found that the disturbance, which is initially concentrated around a point on the free surface, lies mainly within an elliptical region whose area increases linearly with time as it moves downstream and appears as long-crested waves. Photographic records of a growing disturbance on an unstable film indicated that the main features of the wave motions are in agreement with the theory. Gupta and Rai (1968) arrived at an important conclusion, when they

investigated the instability of a visco-elastic liquid system with respect to three-dimensional disturbances. Under certain circumstances these disturbances are more unstable than the two-dimensional ones. This is contrary to Squire's theorem (1933). Similar conclusions were obtained by Krishna (1977) and Lin (1977).

Another important feature (Lin 1969) is that in the neighborhood of the neutral stability curve an exponentially growing infinitesimal disturbance may develop into the supercritical stable wave motion of small but finite amplitude if the surface tension of the liquid is sufficiently large, i.e. the unstable disturbance predicted by linear theory is actually stable under certain conditions. Further investigation about nonlinear surface waves was done by Nakaya (1975), who found that surface waves on the fluid layer resemble gravity waves and capillary waves for small and large wave numbers, respectively.

The profiles of free surface waves were calculated by Esmail (1980) based on a non-linear (with respect to the wave amplitude) dynamic analysis. It was found that once the wavelengths fall into the unstable region, if we gradually move from the region close to the neutral stability curve inside of the unstable region, surface waves will gradually change in shape from nearly sinusoidal waves of small amplitude to the complicated close to solitary waves of high amplitude. The wavelengths will also gradually increase. By examining the profile changes as the inclination angle varies it was also found that any change in the inclination angle from 90° will induce stability in the flow system.

Mechanisms

An early work involving the stability mechanism was reported by Hsieh (1965). He used the kinematic wave theory (Yih, 1955) to predict the wave velocity of the lowest order. A necessary condition for thin film flows was obtained by balancing the inviscid perturbation pressure with the change in the hydrostatic pressure associated with the perturbed surface. The laminar flow of a layer of viscous and electrically conducting fluid down an inclined plane in a transverse magnetic field was analyzed. It was found

that surface tension always tends to stabilize the flow while gravity will tend to stabilize or destabilize the system depending on whether the fluid is flowing down the upper side or the underside of the inclined plane, and the critical Reynolds number obtained agreed with those of Yih's (1963) and Benjamin's (1957).

Following the analysis of Stuart (1960), Lin (1970) discussed the mechanism of non-linear stability from the point of view of energy transfer between the mean flow and disturbance. The results of his analysis were compared with Reynolds & Potter's (1967) results. The comparison showed that for long gravity waves, non-linear stability was found to be due to the large rate of work done by the normal stress to deform the free surface. For relatively short gravity waves, the stability was shown to be mainly due to the generation of higher harmonics that lead to the distortion of the wave form. It was also pointed out that the non-linear stability mechanism for capillary waves was likely to be more complicated due to the possibility of competition between gravity waves and shear waves for instability.

Dagan (1975) found out that the local growth rate of the amplitude of disturbance depends on both the normal pressure gradient and the strain rate on the free surface. It means that there exist two mechanisms associated with the instability of film flow. One is due to the kinematic effect of the strain rate on the free surface and another due to the dynamic effect of the normal pressure gradient. For moderate values of Reynolds number, Goussis & Kelly (1983) examined the equation governing the rate of change of kinetic energy for a spatially periodic disturbance. They found that the dominant energy production term was associated with the rate at which work is done by the perturbation shear stress at the surface. The same conclusion was obtained by Kelly et al (1989), who performed disturbance energy analysis of the film for a disturbance of arbitrary wavelength and identified the various contributions to the disturbance energy. They concluded that: when a film is unstable to long wavelength disturbances, the dominant energy production term is associated with the work done by the perturbation shear stress at the free surface. The mechanism of instability, however, is associated with a

shift of perturbation vorticity relative to the surface displacement resulting from advection.

A two-part-mechanism theory, an initiating mechanism that produces the dominant motion in the film and a growth mechanism that produces the unstable motion of the surface, was proposed by Smith (1990). The initiating mechanism is very similar to the one described by Kelly et al (1989). When the surface is deformed, a perturbation shear stress is induced, but the total surface shear stress at the non-deformed surface position remains constant. The magnitude of this induced shear stress is proportional to the curvature of the basic-state velocity at the surface. The primary effect of this stress is to drive a longitudinal flow perturbation in the film and the work done by this stress is the main energy source for instability. The inertial stresses, which are proportional to the Reynolds number, are produced by the interaction between the leading-order velocity perturbations induced by the initiating mechanism and the basic-state velocity relative to the moving disturbance. When these inertial stresses are positive, they drive the perturbation from crests to troughs and reduce the surface deformation. Such a flow is stable. When these inertial stresses are negative, they do the opposite action to disturbances, and such a flow is unstable. This is the growth mechanism.

Hsieh (1990) interpreted Reynolds number as Froude number. A critical Froude number of O(1) is indeed what we would expect for roll waves in hydraulics. It is also consistent in the context that the perturbed wavelengths are long compared with the depth of the fluid layer. As Reynolds number or Froude number increases, i.e. as inclination angle increases, the gravitational restoration force tends to decrease, while the destabilizing Bernoulli force tends to increase. Thus the system becomes unstable.

MULTIPLE LAYER SYSTEMS

Linear Theory

Kao (1965a, 1965b) first extended Yih's (1963) work to double layer systems, and investigated the stability of a layer of two viscous fluids of different densities but equal viscosity, and found that there exist two modes of long wave instabilities, one is associated with the free surface and another with the fluid-fluid interface. For the case in which the density of the upper layer is somewhat less than that of the lower layer, the interfacial mode is found to govern the stability of the flow. However, when the upper density becomes much smaller, the free surface mode and the interfacial mode compete in dominating this system. It was found that the density stratification can be a stabilizing or destabilizing factor depending on whether the upper density is less than or greater than the lower density, the more stabilizing or destabilizing effect, the more difference in densities; but for the case in which the density ratio is very small, the introduction of an interface is always destabilizing, even though the stratification may be bottom heavy. Later Kao (1968) considered the situation with fluids of different viscosity, and found that viscosity stratification changes the situation dramatically. The interfacial mode is stabilized for the range of viscosity ratio less than unity (bottom viscous system), and the free surface mode is generally the governing mode in that range. The overall effect is stabilizing compared with the equal viscosity system.

Chen's (1993) work showed that the viscosity stratification has two contributions, inertial and non-inertial contributions. They are always competing in the long-wave range, and the outcome depends on Reynolds number. For the lubricated configuration with the less viscous fluid adjacent to the inclined wall the interface mode is always unstable, and it is impossible to stabilize the interface mode and the surface mode simultaneously. For the opposite arrangement with the more viscous fluid occupying the region next to the inclined wall, if a non zero interfacial tension is present to stabilize the short wave instability, linear stability can be achieved by disturbances of all wavelengths at low-Reynolds number.

Kobayashi et al (1986) found out that viscosity stratification is always unstable for double layer systems. Their numerical calculations for the interfacial modes indicated that: 1) The flow rate and viscosity of the upper liquid have stronger effects on flow stability than those of lower liquid. For the bottom viscous system higher viscosity differences increase instability. 2) Surface tension has a very weak effect on flow stability. 3) The density ratio (upper density/lower density) has a strong effect on flow stability and higher density ratios increase instability. 4) Longer inclined planes increase instability. By observing the defects on the coated web they found that theoretical analysis of the effects of these factors on flow stability and the wavelength agrees with their observations.

Akhtaruzzaman et al (1978) formulated the stability problem of n-layer systems, and investigated a triple layer system. For the case of equal kinematic viscosity for all the three liquids and equal thickness for the top and bottom liquids: 1) The wave speed of free surface mode is less than twice the undisturbed free surface velocity for a bottom heavy configuration, and is more than twice the free surface velocity for a top heavy configuration. The speed can be reduced by raising the rate of density increase toward the bottom plane. 2) The wave speed of the interfacial mode is much smaller than that of the free surface mode. The interfacial waves propagate only slightly faster than the fluid particle at the undisturbed interface for a bottom heavy system, and the converse is true for a top heavy system. For the case of equal kinematic viscosity for the top and middle liquids and equal thickness for the top and bottom liquids, if the kinematic viscosity of bottom liquid is small enough, the wave speed of the free surface mode can be greater than that of a single layer system. In addition the wave speed of the interfacial mode is smaller than the speed of a fluid particle at the undisturbed interface in the bottom heavy configuration.

For each mode of wave motion at various values of the thickness of the middle liquid in the case of equal kinematic viscosity for all three liquids and a bottom heavy configuration: 1) The wave motion of the free surface mode is in-phase at all interfaces.

The displacements decrease toward the bottom plane. 2) The wave motion of the second (interfacial) mode is in-phase at the second and the third interfaces, and out-of-phase on the free surface. Moreover, the wave amplitude at the second interface is always greater than that at the other interfaces. When the thickness of the middle layer decreases to zero the amplitude of the free surface wave reduces to a small fraction of the wave amplitude of the other two interfaces. 3) Depending on the values of the dimensionless thickness of the middle layer (the ratio of the thickness of the middle layer to that of the top layer) the wave motion of the third (interfacial) mode is in-phase at the free surface and the second interface, or out-of-phase at the third interface. There exists a critical value of this thickness below which the wave motion at the second and the third interfaces is respectively in phase or out of phase. At this critical value, the second interface is completely flat but the other two interfaces are not.

Wang et al (1978) discussed the stability of the wave motion based on the higher order solution, and described the features of the neutral stability curves for various cases. In the case of a triple layer system of different thickness ratios but of given density, interfacial tension, and viscosity ratios, the third mode instability associated with the step increase in viscosity can be eliminated by an increase in the thickness of the most viscous third layer. However, such a stabilization could not be achieved for the second mode instability associated with the step decrease in viscosity either by reducing or increasing the thickness of the least viscous second layer.

In the case of five liquid layers of equal density, thickness, and interfacial tension but of different viscosity, the neutral curves corresponding to the free surface mode have the same form as that of a single-layered film. The free surface mode instability is obviously caused by the gravitational potential at the free surface, and changes in viscosity stratification merely shift the position of the neutral curves slightly. The slope of the neutral curve for a particular interfacial mode is positive or negative depending on whether there is a downward step decrease or increase in viscosity, at the corresponding interfaces. The instability of the interfacial mode is solely due to the shear waves caused

by viscosity stratification. A downward step decrease in viscosity across an interface makes five-layered systems unstable for all Reynolds numbers if disturbances of all possible wavelengths are present. However, there exists a cutoff wave number below which the film is stable to the relatively long shear waves associated with the step decrease in viscosity across an interface. A downward step increase in viscosity causes quite a different type of instability. The film is unstable to relatively long shear waves with wave numbers smaller than the cutoff wave number, but stable if the Reynolds number is greater than the Reynolds number corresponding to that wave number on the neutral curve.

In the case of the five layers system of equal thickness, viscosity, and interfacial tension, but of different density, it was found that for bottom heavy configuration the film is stable for the interfacial mode but may be unstable for the free surface mode. The film becomes more unstable as the rate of increase in density toward the bottom plate is raised due to the increased gravitational potential. Interfacial instability can only occur in top heavy systems. If the top heavy film is subjected to disturbances of all wavelengths the film is actually unstable at all Reynolds numbers.

They also found that the variation of the inclination angle does not change the character of the instability of various modes, however, the reduction in inclination angle can lead to stabilization of the free surface mode of the wave motion.

Three kinds of stability modes for multiple layer flow systems were proposed by Kobayashi (1990). The surface mode is strongly influenced by surface tension. As surface tension increases it is more effective as a medium of propagating capillary waves (short waves). There are two kinds of surface waves, one that propagates downward and another upward. When the wave number increases the growth rates of these two kinds of waves coincide, i.e. the capillary wave is no longer affected by the base flow. Interfacial tension plays a very important role in the instability of interfacial modes. Each interfacial mode is associated with an interface. When the wave number increases,

the wave velocity of an interfacial mode approaches that of the base flow at the related interface. In other words, the interfacial modes do not influence each other at large wave numbers. This feature is very useful, and makes it easy to estimate the interfacial mode instability of multiple layer flows by using the results of double layer systems. Each shear mode is associated with a layer of most stresses. However, the stability is usually governed by the surface mode or interfacial modes.

Anturkar et al (1990) analyzed the development of the coating film in multiple layer slot coating process by the Reynolds lubrication approximation, which is originally given by Reynolds (1886). They found that: 1) The viscosity ratio does not affect the ultimate stability characteristics of this flow system, although it has some effects on the wave developing process. 2)The larger the surface tension, the longer the downstream distance waves can travel, therefore the more dangerous these waves are. Compared to free surface tension, interfacial tension between two adjacent layers has less effect on wave motion.

Li's (1970) investigation of a double layer system of Oldroyd-B fluid showed that the elasticity of a liquid can stabilize a flow subjected to an interfacial mode of disturbances for certain values of density, viscosity, and elasticity ratios (the upper properties the lower properties). But it can destabilize the flow when viscosity ratio and elasticity ratio are both small enough. The elasticity can also stabilize the flow which is subjected to a free surface mode of disturbances.

Weinstein (1990) considered the effect of shear thinning rheology on the spatial growth of waves for multiple layer systems. The Carreau viscosity constitutive equation was used to model the fluid. Shear thinning behavior affects interfacial and surface modes waves differently. For surface waves, except at very low frequencies, shear thinning results lie between results of the two Newtonian cases corresponding to the maximum and minimum Newtonian viscosity, respectively. This means that surface mode waves propagate as if they were in a Newtonian system, where the viscosity is some average of

the varying viscosity in shear thinning layer. But interfacial modes are largely affected by local viscosity in the vicinity of the interface. Wave propagation can not be governed by some average Newtonian viscosity across the layer. Shear thinning behavior can be stabilizing or destabilizing, depending on the jump in strain across the interface. If it reduces the jump in strain across the interface then it leads to greater stability. If it increases the jump in strain across the interface it is a destabilizing factor.

Non-Linear Theory

There are few papers dealing with nonlinear stability of multiple layer systems. It is predictable that three-dimensional disturbances or those of finite amplitudes will largely change the stability of this flow system. Howard (1963) presented an example of anti-symmetric stratified shear flow and found that in some cases the neutral stability curve is not necessarily the boundary of stability.

CHAPTER I
EXPERIMENTAL METHOD

The experimental setup, the measuring procedures, using optic-electric means for signal detection, and the digital signal processing technique for extracting frequency information, are described in this chapter.

1.1 EXPERIMENTAL SETUP

The test liquid is placed in a reservoir tank A. Pump B (max. 2300ml/min) is used to pump the liquid into the flow loop (Figure 1-1) through a control valve C and a flow meter D. The liquid is delivered to a buffer chamber E, where a layer of sponge material F lines the bottom. The bottom of the buffer chamber is extended into the flat surface G, where a layer of the experimental liquid runs down. The liquid then pours into the liquid reservoir tank. The purpose of the sponge material at the bottom of the buffer chamber is to minimize flow disturbances as the liquid starts its free surface layer motion.

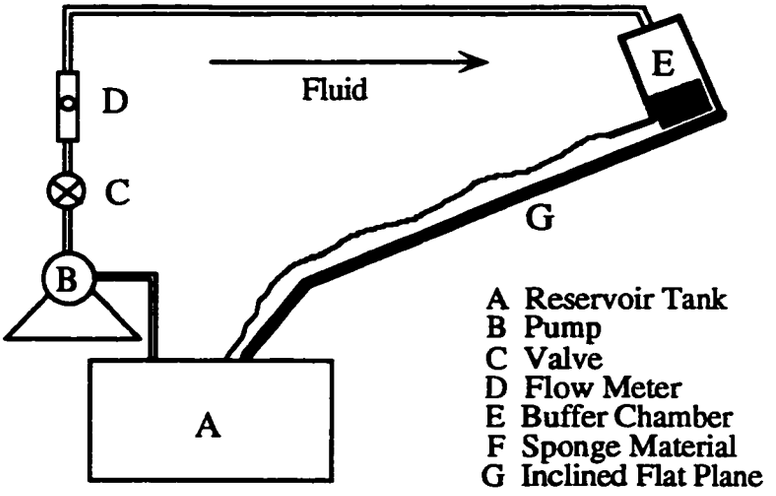

(a) Single Layer System

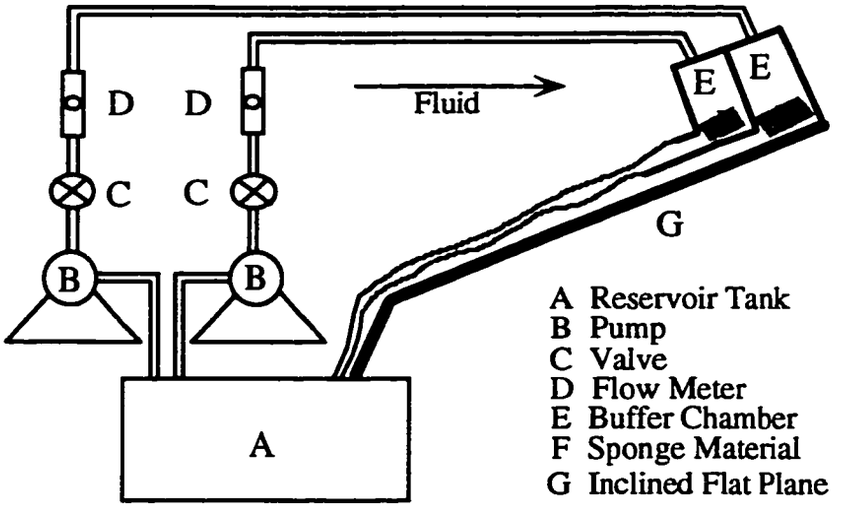

(b) Double Layer System

Figure 1-1 Flow Loop of Experiment Setup

A narrow beam of light from a fiber optic lamp H (Figure 1-2) penetrates the bottom plate of the channel and the fluid film. A portion of the light intensity is absorbed by the fluid. The rest reaches a light sensor "I" mounted above the liquid layer. The output current signal from the sensor contains information about the frequency of waves. A pre-amplifier J is used to amplify this weak current signal and to transform it to a voltage signal for easier recording and detection. This voltage signal is the input to a read-out unit K for detection and regulation. The scaled signal is sampled by a

computer sampling processor consisting of an analog-to-digital (A/D) converter K and a computer M.

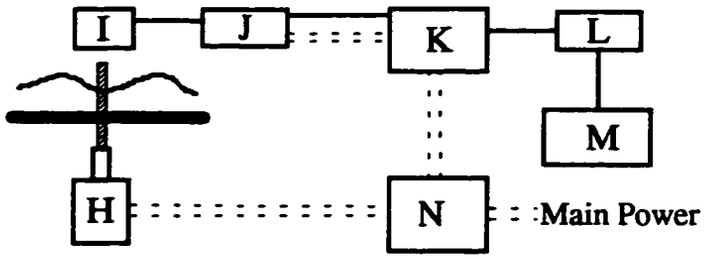

H Light Source I Light Sensor J Pre-amplifier
K Read-out Unit L A/D Converter M Computer
N Constant Voltage Transformer

Figure 1-2 Optical Measurement System

In this work the elimination of the effects of external vibrations is a very important issue. In addition to those mentioned measures, a constant-voltage transformer is used to provide stable power to the lamp and the read-out unit. All experiments are conducted late into the night for minimizing the effect of surrounding vibrations and voltage fluctuations in main power. Table 1-1 is a list of the instruments and chemicals used in this work.

Table 1-1 A List of the Instruments and Chemicals Used

Item	Name	Model	Manufacturer
B	Pump	7144-00	Cole-Parmer Instrument Co. Chicago, IL. U.S.A.
D	Flow Meter	No. 3 No. 4	Gilmont Instruments Inc. Great Neck, NY. U.S.A.
H	Lamp	FO-150	Chiu Technical Corp. Kings Park, NY. U.S.A.
I	Photo Diode	71802	Oriel Corporation Stratford, CONN. U.S.A.
J	Pre-amplifier	70710	*ibid.*
K	Read-out Unit	70701	*ibid.*
L	A/D Board	DAS-8	Keithley Instruments Inc. Taunton, MA. U.S.A.
M	Computer	PC6300	AT & T
N	Transformer	23-22-150	Sola Electric Elkgrove Village, IL. U.S.A.
	Viscometer	A-120	Burrell Corp. Pittsburgh, PA. U.S.A.
	Tension Meter	21	Fisher Scientific U.S.A.
	Surface Active Agent	Extran 300	BDH Inc. Toronto and Branches Canada
	Dye	Basic Blue 9	Matheson Coleman & Bell Manufacturing Chemists Norwood, Ohio U.S.A.

1.2 THE FLUIDS

Test fluids are a mixture of water and glycerol. Surface active agent is added to the solutions to lower the surface tension of the fluids and to increase their wettability with respect to Plexiglas. A blue dye is added into the fluids used for the frequency measurement for enhancing the light absorptivity of the fluids. Tables 1-2 and 1-3 show the physical properties of the fluids used in this work for single layer and double layer experiments, respectively. The physical properties of test liquids are measured at room temperature (23° C ± 1.0° C).

Table 1-2 Physical Properties of Test Fluids
(Single Layer System)

Experiment	Density g/ml	Viscosity cp	Surface Tension dyne/cm	γ Number $(\nu^4 g)^{-1/3}\sigma/\rho$
Critical Reynolds Number	1.08	3.10	32.60	346
	1.09	3.30	34.20	335
	1.16	7.93	45.03	140
Transit Distance	1.02	1.05	34.23	1508
	1.07	2.53	44.20	613
	1.14	4.32	31.00	215
	1.16	8.05	30.11	92
Frequency	1.04	1.10	31.08	1296
	1.11	3.34	35.53	344
	1.16	7.93	45.03	140
	1.19	23.00	32.30	25

Table 1-3 Physical Properties of Test Fluids
(Double Layers System)

Density ρ g/ml	Viscosity μ cp	Surface Tension σ dyne/cm	γ Number $(\nu^4 g)^{-1/3}\sigma/\rho$
1.04	1.10	31.08	1296
1.14	5.14	36.03	198
1.21	67.95	39.87	7

1.3 FREQUENCIES AND AMPLITUDE

1.3.1 An Example

For the flow system considered in this work the highest frequency component is less than 30 cycles per second according to previous work (Jones & Whitaker, 1966; Javdani, 1976). Our experiments also support this point. So, 120 samples/second is a proper sampling frequency in this work. The sampling duration is 20 seconds. It is much longer than the longest period (about 0.5 second) presented.

Figure 1-3 shows a raw signal in our experiments. In the post signal process high frequency noises are filtered by a double exponential digital filter. The corresponding signal after a double exponential filter (filter constant is 0.7) is shown in Figure 1-4. The filtered signal will be normalized before being analyzed according to Fourier method. Figure 1-5 is the corresponding normalized signal. Obviously, it is much less rippled (noised) than its raw form. Fourier analysis will produce the energy spectrum plot (Figure 1-6) in the form of relative energy level vs. frequency.

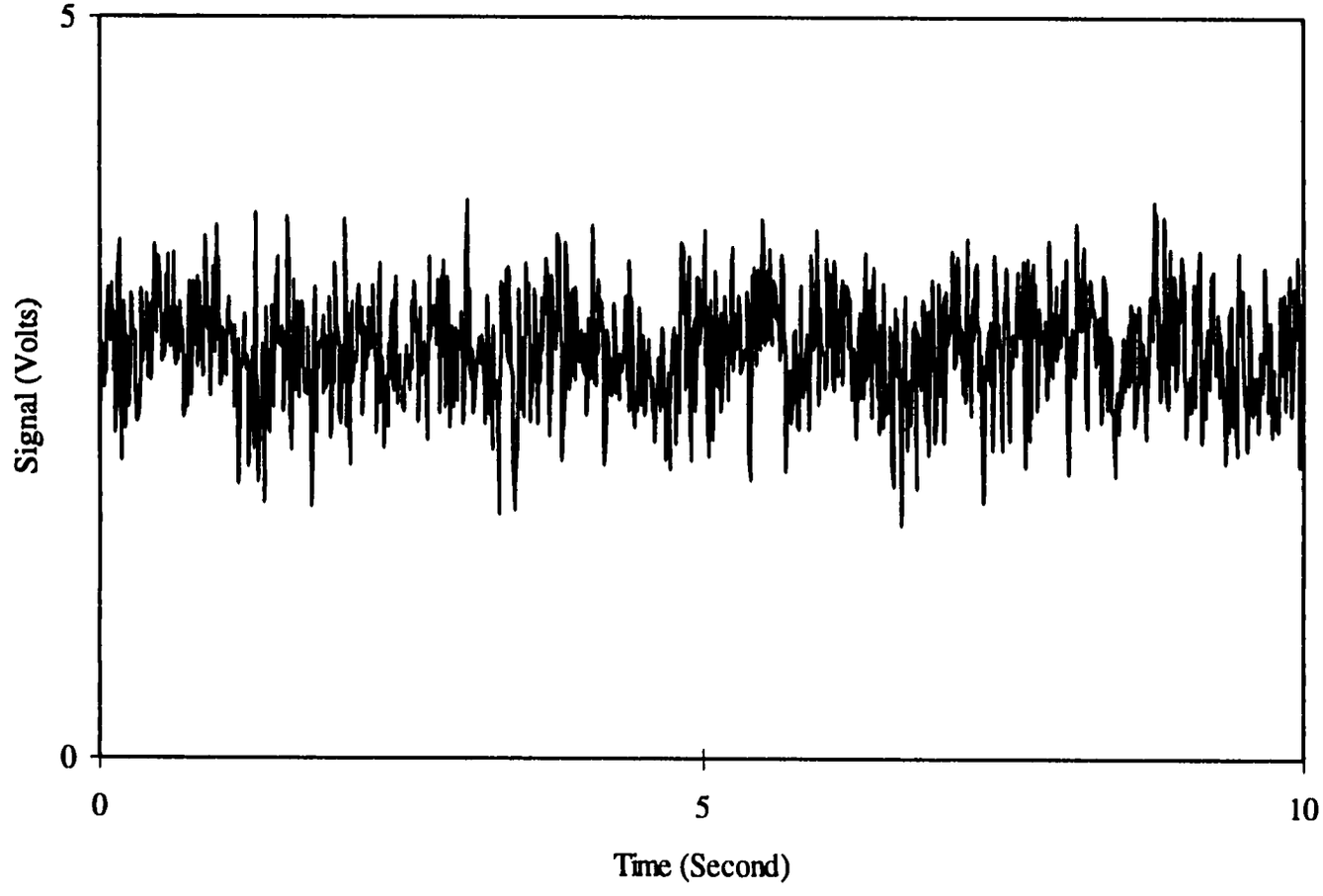

Figure 1-3 A Raw Signal in Real Situation

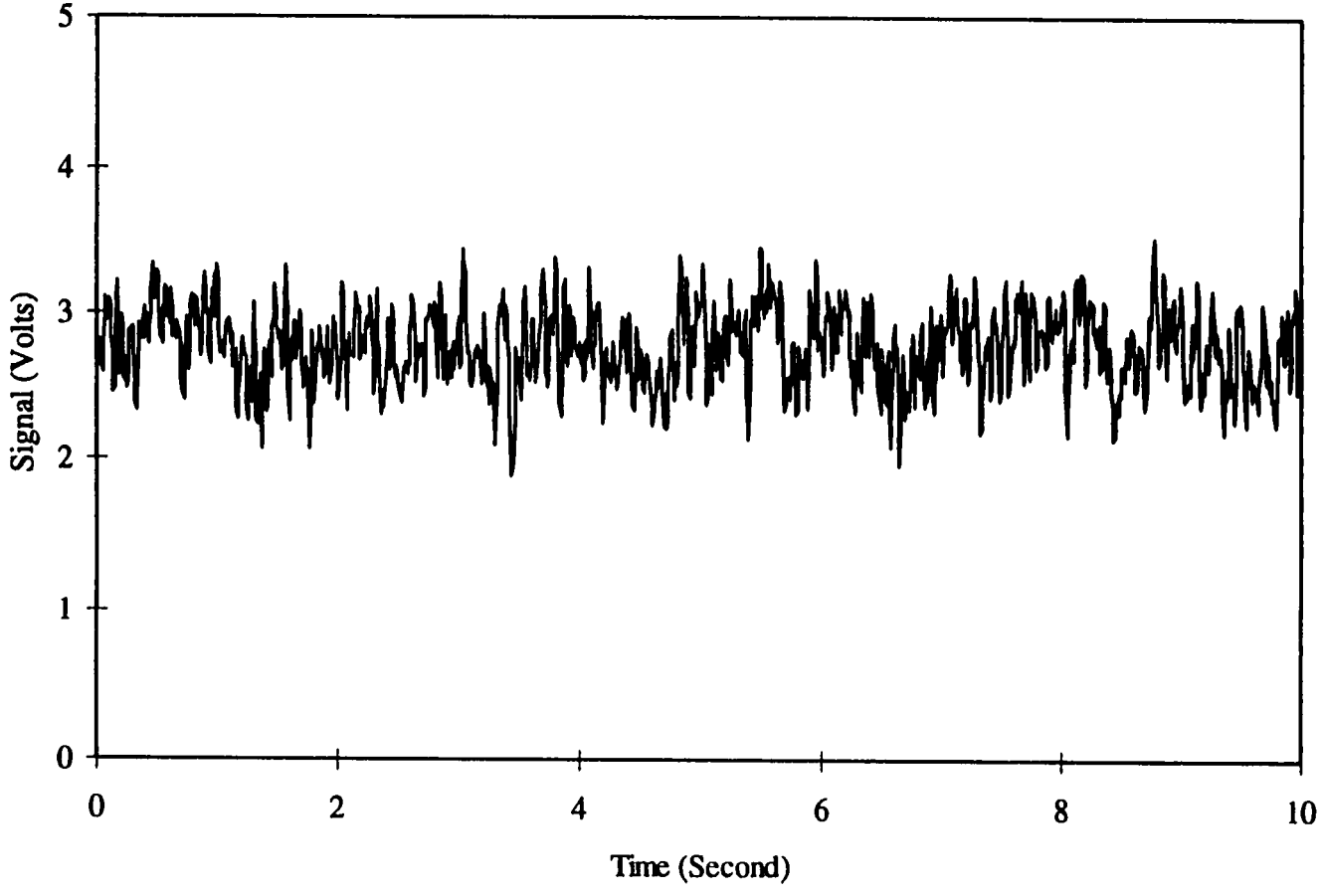

Figure 1-4 The Corresponding Signal After the Filter

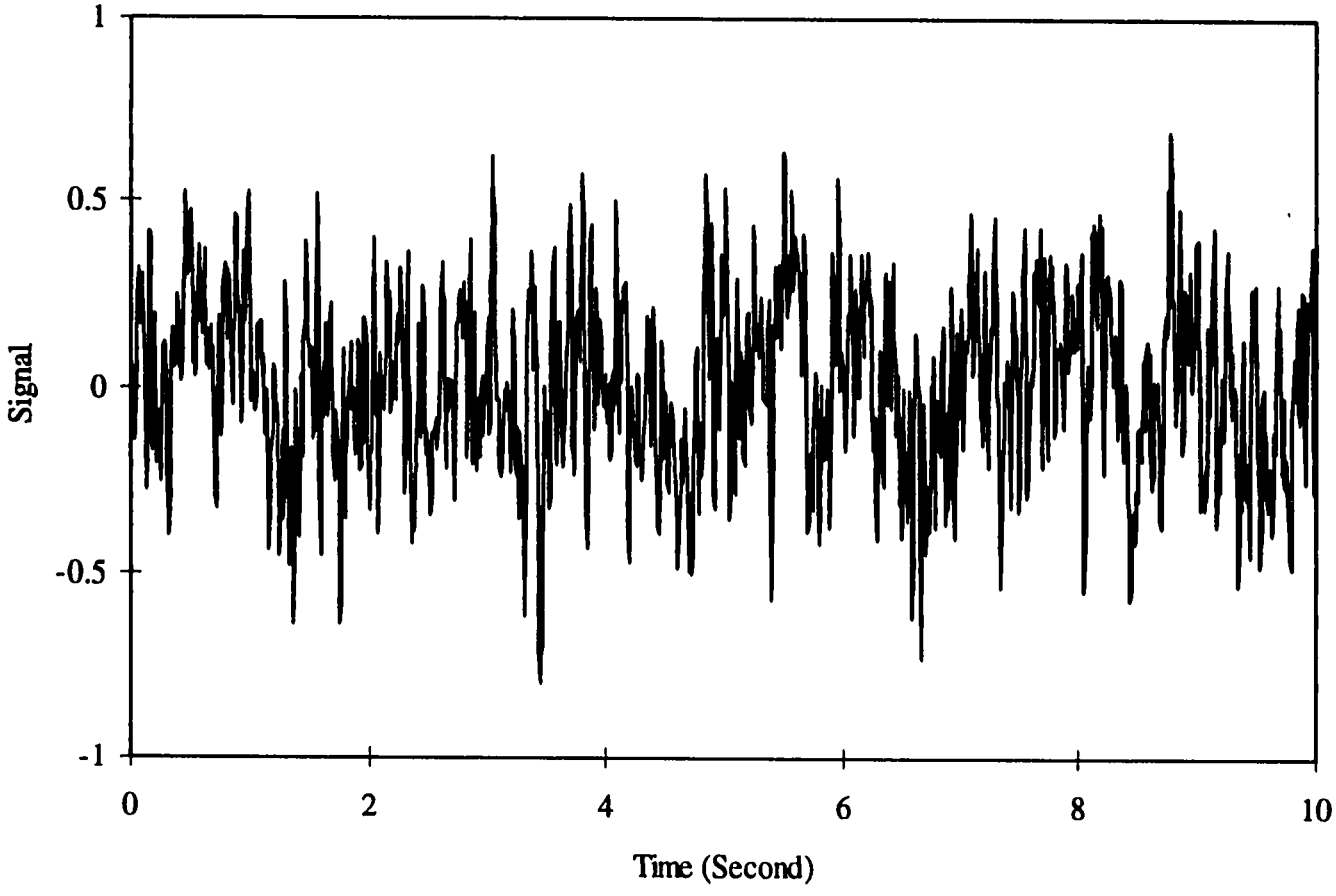

Figure 1-5 The Corresponding Normalized Signal

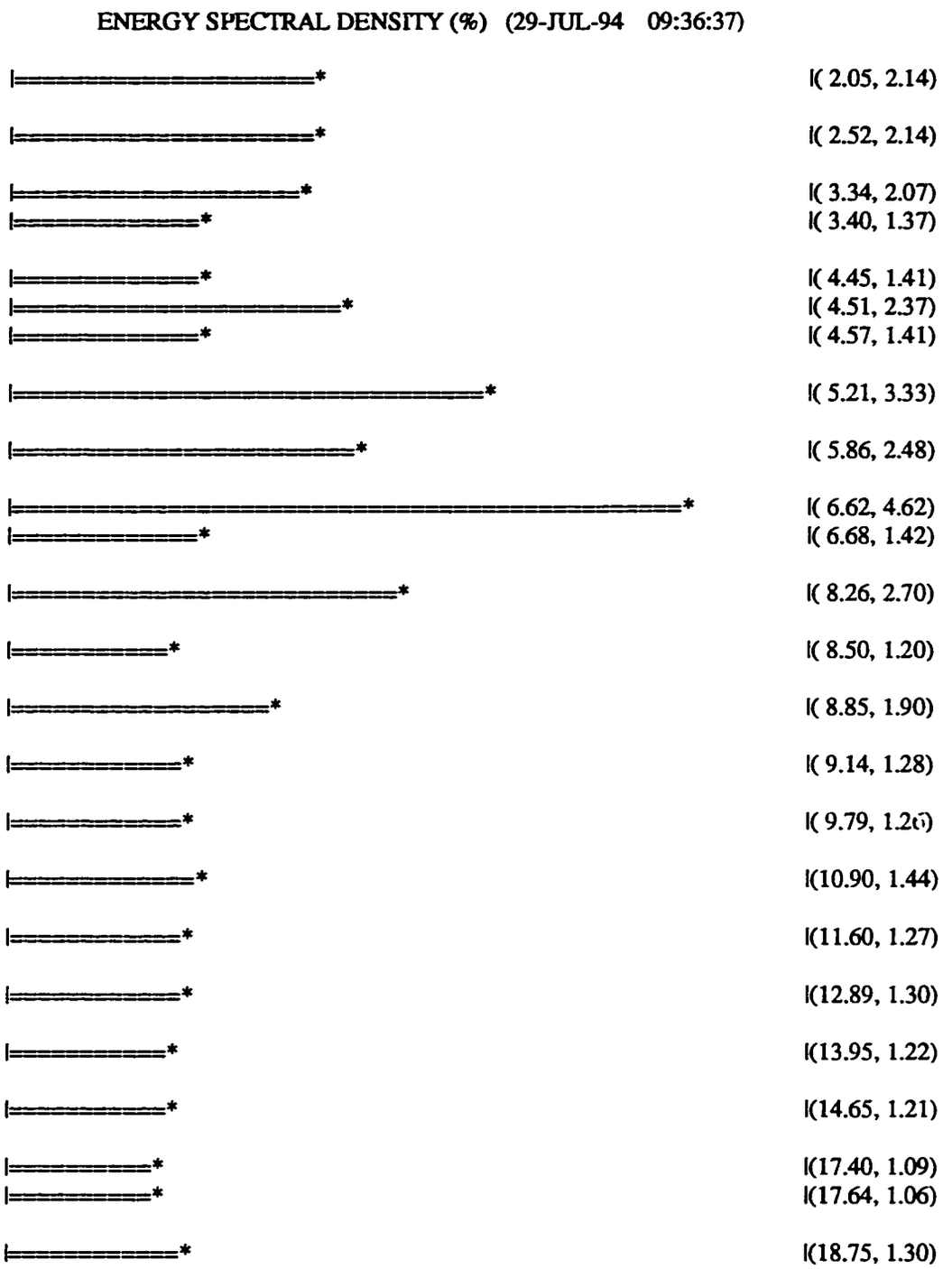

Figure 1-6 The Energy Spectrum Plot

1.3.2 Frequency

Due to the complex nature of free surface waves, energy spectral analysis produced numerous frequency components (Figure 1-6). Some have larger portion of energy, and some have a much smaller portion. In our calculations the frequency components having a relative energy level of less than 0.5% are eliminated. Also, the characteristic frequency components of white noise are picked out from the energy spectral plot. The white noise is obtained right before every experimental run by making the final arrangements for the run without allowing liquid on the surface. Three frequency terms are used to represent the remaining frequency components. Upper Limit Frequency (ULF) and Low Limit Frequency (LLF) are respectively the highest and the lowest frequency components that appear in the energy spectral plot. The Dominant Frequency (DF) has the highest relative energy level in the plot.

1.3.3 Maximum Relative Amplitude

Higher flow rates correspond to the thicker fluid films. So more light will be absorbed by the fluid and the output signal in these cases is smaller. Experiments show that the average signal level does decrease with the increase in flow rate as we expected. A theoretical model on the relation between signal level and film thickness is needed for the extraction of amplitude information. The experimental data strongly support the linear model,

$$\Delta S = kh_0 \qquad (1\text{-}1)$$

where ΔS is the signal level drop, k the model coefficient, and h_0 the total theoretical steady-state film thickness.

The average signal drop from the reference signal (S_0, when no fluid flows) $\Delta S = S\text{-}S_0$, will represent the average thickness of the fluid film, and the maximum signal deviation S_{max}, represents the maximum amplitude of the surface waves. Actually, in this work for better representation, we take S_{max} as the mean value of the several biggest signal deviations in the sampling history. The maximum relative amplitude (MRA) will be

$$MRA = S_{max}/\Delta S \times 100\% \qquad (1\text{-}2)$$

1.4 EXPERIMENTAL ERRORS

1.4.1 Frequency Measurement

Experimental error in frequency measurement is mainly contributed by the resolution of the instrument used to digitize the analog voltage signals and the interference of the surrounding vibrations. DAS-8 is used in our work to transform the analog voltage signal to digital form, and has the resolution of 1.4 mV. The absolute value of the voltage signal occurred in experiments is between 1 to 5 Volts. So, the measurement error caused by the instrument is less than 0.15% (1.4/1000*100%) and is negligible.

The major experimental error in frequency measurement came from the surrounding vibrations. In order to minimize the effect of the surrounding vibrations we put a layer of foam rubber sheet between our experimental setup and experimental table to damp the surrounding vibrations. The experimental table is fixed firmly on the floor and will create no additional vibrations. Besides, experimental runs were made in late evening and early weekend morning when the building was quite.

According to Pierson & Whitaker (1977) the building itself had a characteristic frequency of the order of 4 Hz, and pump and fan motors provided frequencies in the range of 20 to 30 Hz. By processing the white noise (reference signal) we are able to identify these two frequencies. The characteristic frequency of the pump and fan motors is around 23 Hz in this work. Our experimental results of wave frequencies suggested that the frequencies of the wave motions on the free surface of thin liquid film are less than 20 Hz. So, the pump and fan motors do not interfere with our measurement results of wave frequencies. The frequency of the building vibration changes slightly from case to case, and was in the range of 3.75 to 4.16 Hz. This frequency clearly interfered with the experimental measurements. However, as we said before, this frequency is removed by picking it out from the frequency spectrum.

In our work, the light source is operated at low intensity range (< 20% of full scale). The light is the range of orange, and is close to the red-end of the visible light spectrum. Water has good absorptivity with respect to the red-end light. Besides, a blue dye is added into the experimental fluids to further enhance the light absorptivity of the fluid. When a narrow beam of the light (approximately 4 mm in diameter) penetrates a layer of the test fluid, a portion of the light intensity is absorbed by the test fluid, a small portion of the intensity is deflected by the wavy free surface (acting like a convex or concave lens), and the remaining intensity reaches a light sensor that is 3 cm above the light source. In addition to the above mentioned facts, the wave motion detected in this work is a small-scale phenomenon and has a limited deflection ability to the light. So, compared to the amount of absorbed intensity, the amount of deflected intensity is small.

When a wave peak moves to the measurement position the liquid film has larger thickness, and more light intensity is absorbed. The light sensor will catch less light intensity, and produce weaker signal. When a wave valley moves to the measurement position the liquid film has smaller thickness, and less light intensity is absorbed. The light sensor will catch more light intensity, and produce stronger signal. In order to achieve higher experimental accuracy of frequency measurement, we want the signal to vary more significantly with wave motion. Let us consider the deflection effect of the wavy surface. When a wave peak moves to the measurement position the deflection action of the liquid film will turn away a small portion of light intensity from the measurement point like a convex lens does. This will cause the light sensor to catch less light intensity and to produce weaker signal. When a wave valley moves to the measurement position the deflection action of the liquid film will focus a small portion of light intensity toward the measurement point like a concave lens does. This will cause the light sensor to catch more light intensity and to produce stronger signal. From the above argument we can conclude that the deflection effect of the liquid film actually benefits the frequency measurement.

1.4.2 Amplitude

In order to obtain the information about the maximum wave amplitude we need a model to describe the relation between the amount of the voltage signal drop from the reference signal and the thickness of the liquid film. Based on all of that and the experimental results (refer to Table) we could suggest the following linear model (1-1).

Table 1-4 Experimental k Value of The Linear Model (Based on The Mean Thickness)

Test	Number of Data Points	Arithmetic Mean k Value, (Volts/mm)	Maximum Relative Error, (%)
#1	2	1.1426	3.07
#2	5	1.3319	2.00
#3	6	1.3080	4.52
#4	5	1.4792	4.54
#5	5	1.4884	8.45

The above tests were conducted for the same fluid and at different times of the day. Considering that the reference signal (i.e. the setting of the light intensity at the start of experiment) is different each time we can say that this linear model is appropriate for our work.

CHAPTER II
EXPERIMENTAL RESULTS AND DISCUSSION

The experimental results are obtained by employing the optic-electric detection system and digital signal processing techniques described in the previous chapter. We apply the experimental techniques to a single layer liquid system, and a double layer liquid system. The frequency characteristics of the waves running on the free surface of single and double layer system are studied. Also, the inception and development of the free surface waves of single layer system are investigated.

2.1 DIMENSIONAL ANALYSIS

In this work, the parameters are liquid properties ρ (density), μ (viscosity), and σ (surface tension coefficient); the acceleration of gravity g; and two reference quantities u_0 (mean velocity of the liquid film in x-direction) and h_0 (mean thickness of the liquid film). All the physical values we want to know, such as transit distance, wave frequencies, and wave speed, are expected to be the functions of these six parameters.

The Buckingham Pi theorem (Shames 1962) provides the maximum number of dimensionless groups which govern our flow system as independent variables. This is equal to the number of parameters (six) less the number of primary dimensions (three: mass, length, and time). So, only three dimensionless groups could be independent.

The same conclusion may be reached when we consider the various acting forces involved in this flow system. They are: gravity, inertial, surface, and viscous forces. These four forces provide at least six well known dimensionless groups which can be used as governing parameters (Esmail & Ghannam 1990). They are Re (Reynolds

number), Fr (Froude number), We (Weber number), Ca (Capillary number), Bo (Bond number), and Dr (Deryagin number), and defined as following:

$$Re = \rho u_0 h_0/\mu \quad (2\text{-}1)$$

$$Fr = u_0^2/h_0 g \quad (2\text{-}2)$$

$$We = \rho u_0^2 h_0/\sigma \quad (2\text{-}3)$$

$$Ca = \mu u_0/\sigma \quad (2\text{-}4)$$

$$Bo = \rho g h_0^2/\sigma \quad (2\text{-}5)$$

$$Dr = \rho g h_0^2/\mu u_0 \quad (2\text{-}6)$$

In addition, the physical properties number introduced by Esmail (1980) γ is an important parameter in the system. It is defined as

$$\gamma = \sigma(\nu^4 g)^{-1/3}/\rho \quad (2\text{-}7)$$

where, $\nu = \mu/\rho$ is kinematic viscosity. Four independent relationships exist between the described seven parameters (considered as entities in their own right rather than as products of dimensional variables or their reciprocals):

$$We = ReCa \quad (2\text{-}8)$$

$$We = FrBo \quad (2\text{-}9)$$

$$Fr = Re/Dr \quad (2\text{-}10)$$

$$We = Re^2 Bo^{1/2} \gamma^{-3/2} \quad (2\text{-}11)$$

This leaves three independent parameters for our flow system. We chose Re, We, and γ in this work. All the physical values we want to know will be the functions of these three independent dimensionless groups.

2.2 SINGLE LAYER SYSTEM

In these experiments a single layer of a glycerol solution was allowed to flow down the inclined plane at a controlled flow rate. The inclination angle of the plane was also controlled. Several glycerol solutions were tested. Properties number is used to characterize the physical properties of the test liquid. Glycerol solutions are uniquely

characterized by their γ number. Correlating the results to this dimensionless number makes it possible to generalize the conclusions to all liquids sharing the same value of the number.

2.2.1 Critical Reynolds Number

Viscous liquids flow in undisturbed thin layers of uniform thickness in laminar regimes. Such flows occur at very small speeds. As the speed increases the stability of thin liquid layers decreases. At a certain critical speed random disturbances in the flow system induce a transition from the laminar uniform thickness flow to a laminar flow with waves running over the layer surface. At high speeds the laminar wavy regimes of thin liquid layers turn into turbulent regimes.

In this work we are concerned with thin liquid layers in the laminar uniform thickness flows, their transition to wavy laminar regimes, and the description of these wavy regimes. The critical speed of transition to laminar wavy regimes is associated with a critical Reynolds number, $Re_c = h_0 u_0 \rho/\mu$, where h_0 is the mean thickness of the liquid layer, u_0 the mean velocity, ρ the density, and μ the viscosity of the liquid. For purpose of mechanical similarity between flows the Reynolds number is used.

Experimental measurements of the critical Reynolds number are shown in Figure 2-1. The experimental points divide the Re versus angle space into two regions. Flows that fall under the points are stable uniform thickness laminar regimes. Flows that fall above the points are wavy regimes. In Figure 2-2 a comparison between our measurements and those of previous authors shows our experiments in variance with previous work which covered a higher range of inclination angles. It is also notable that our measurements show higher values than those in previous work.

As we described earlier our experimental apparatus and procedures included a number of measures to eliminate disturbances from the flow prior to its entrance to the test

section. This should account for higher critical Reynolds number, since such measures will help push the limit of stability upward.

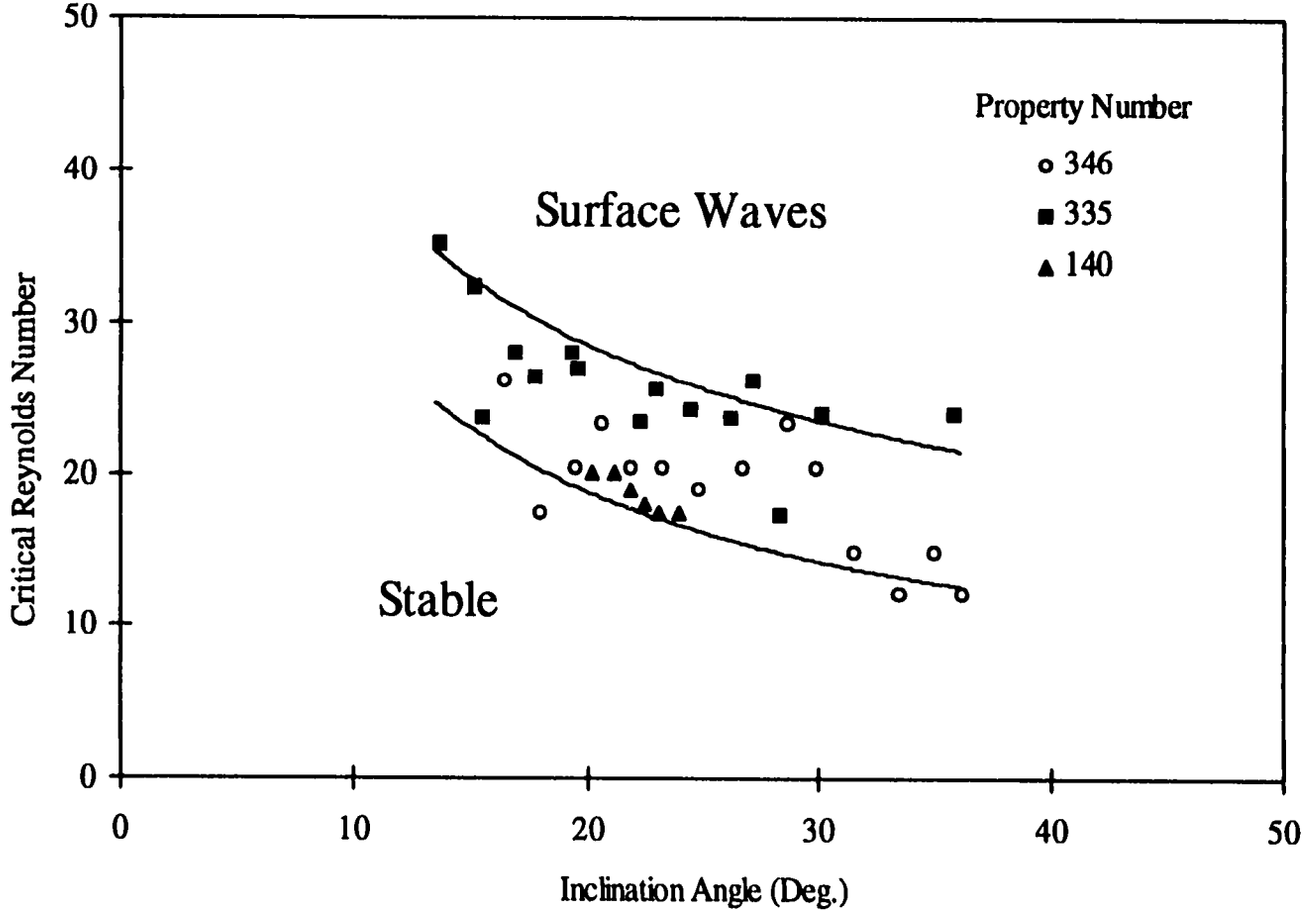

Figure 2-1 Experimental Stability Criteria

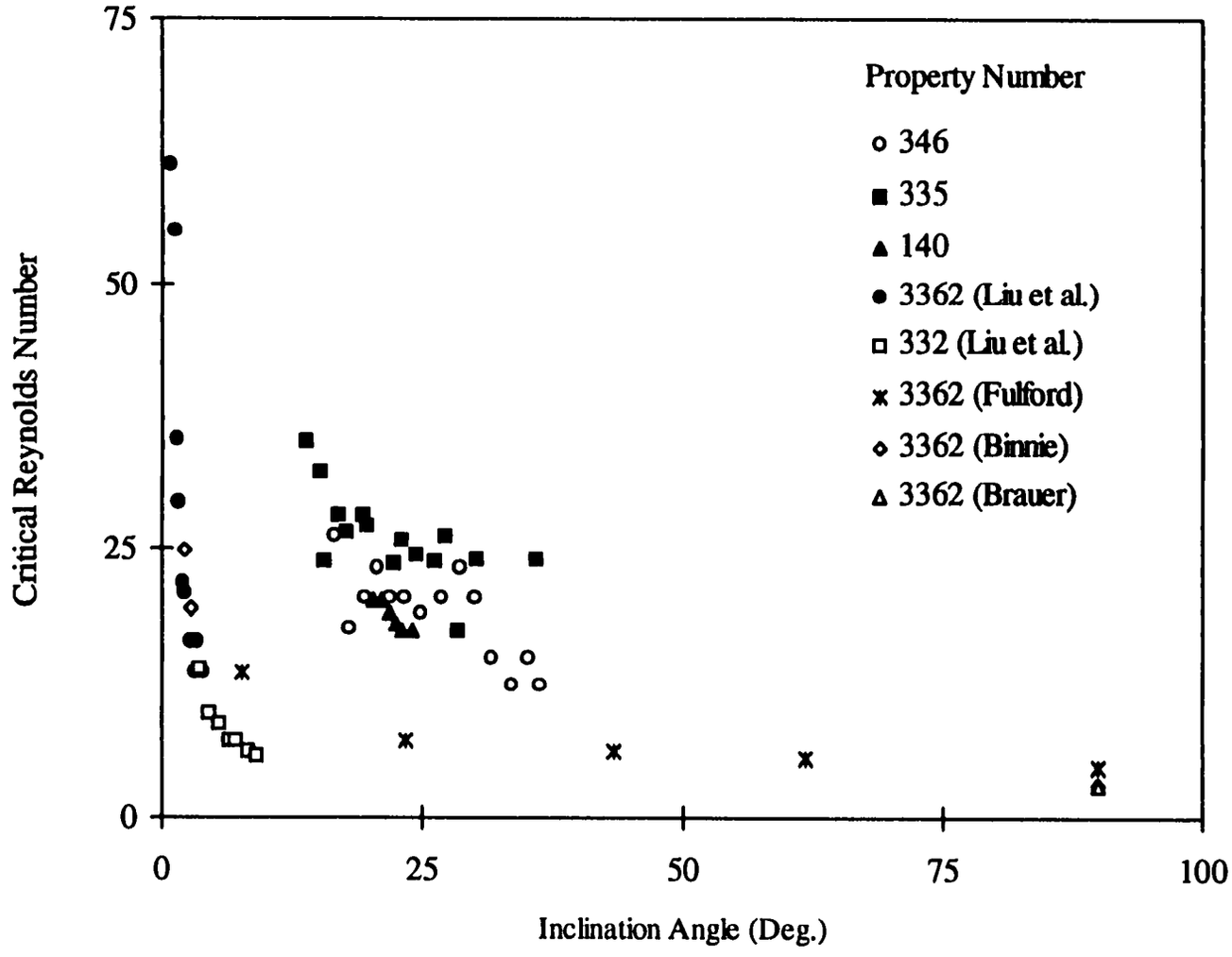

Figure 2-2 Experimental Stability Criteria

It is also interesting to compare experimental results with theoretical predictions. The stability of laminar uniform thickness thin layers has been studied by linear analysis. The basic linear stability theory (Benjamin 1957, Yih 1963) sets the critical Reynolds number of transition from uniform laminar layer to a wavy regime at:

$$Re_c = 5\cot\theta/6 \qquad (2\text{-}12)$$

More recently Smith (1990) obtained two limiting cases for the linear stability analysis. In the first case the flowing film is subjected to a shear stress τ, and consequently a tangential stress boundary condition is used in the perturbation analysis (Yih, 1963). The critical Reynolds number according to this model is:

$$Re_c = 5\cot\theta/[6(1+\tau)] \qquad (2\text{-}13)$$

In the second model Smith (1990) assumes that the flowing film is bounded by a perfect elastic compliant surface that is moving with the velocity U. This surface has no mass, no bending stiffness, and no damping. Consequently a no-slip velocity boundary condition is used in the perturbation analysis (Yih, 1963). The critical Reynolds number according to the second model is:

$$Re_c = 40\cot\theta/[3(1-4U^2)] \qquad (2\text{-}14)$$

The only driving force in the thin layers investigated in our work is gravity. When the additional forces of shear τ, and inertia U are driven to zero in the analysis of the two models, two limiting cases criteria are obtained for the Reynolds number

$$Re_c = \cot\theta \qquad (2\text{-}15)$$

$$Re_c = 48\cot\theta/3 \qquad (2\text{-}16)$$

respectively.

Figure 2-3 shows the critical Reynolds number according to the linear stability theory of Benjamin (1957), and the limiting cases of Smith (1990). Our experimental points are located well above the linear theory but just below the inertia driven limiting case.

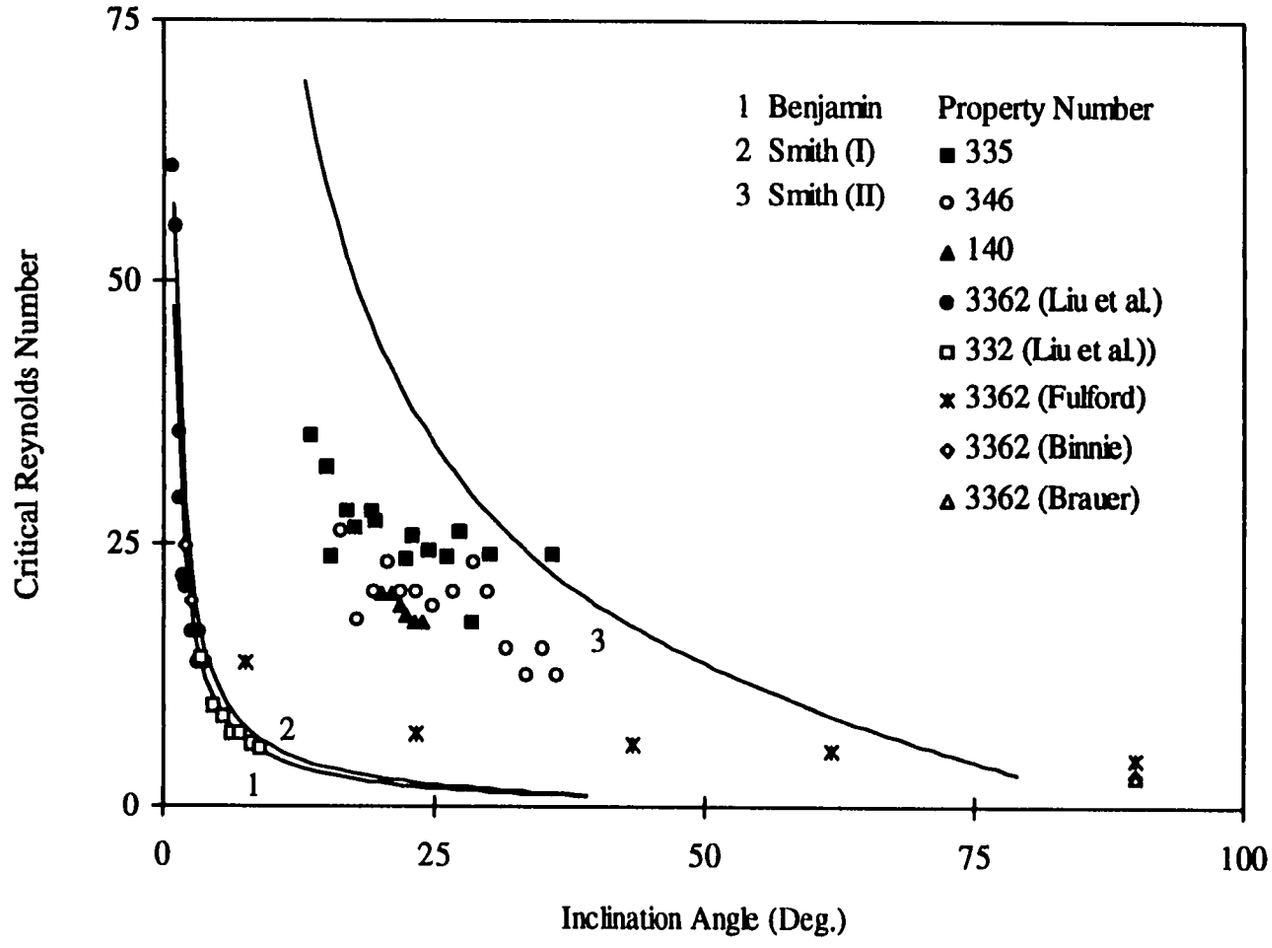

Figure 2-3 Stability Criteria

2.2.2 Transit Distance

Observation of surface waves running down the inclined plane from the inception point X=0, led us to record the distance downstream from X = 0 at which the wave has completely damped. This distance normalized to the average film thickness is called the transit distance. Figure 2-4 shows the transit distance for the flow of a glycerol solution with property number $\gamma = 613$, for different angles of inclination. Surface waves which appear at lager flow rates travel a longer distance before they are dampened. The angle of inclination does not seem to have a noticeable effect on the transit distance. The same trends (Figure 2-5, 2-6) were exhibited by two other glycerol solutions with property numbers $\gamma = 215$ and 92. The higher the property number, the longer is the transit distance of surface waves (Figure 2-7).

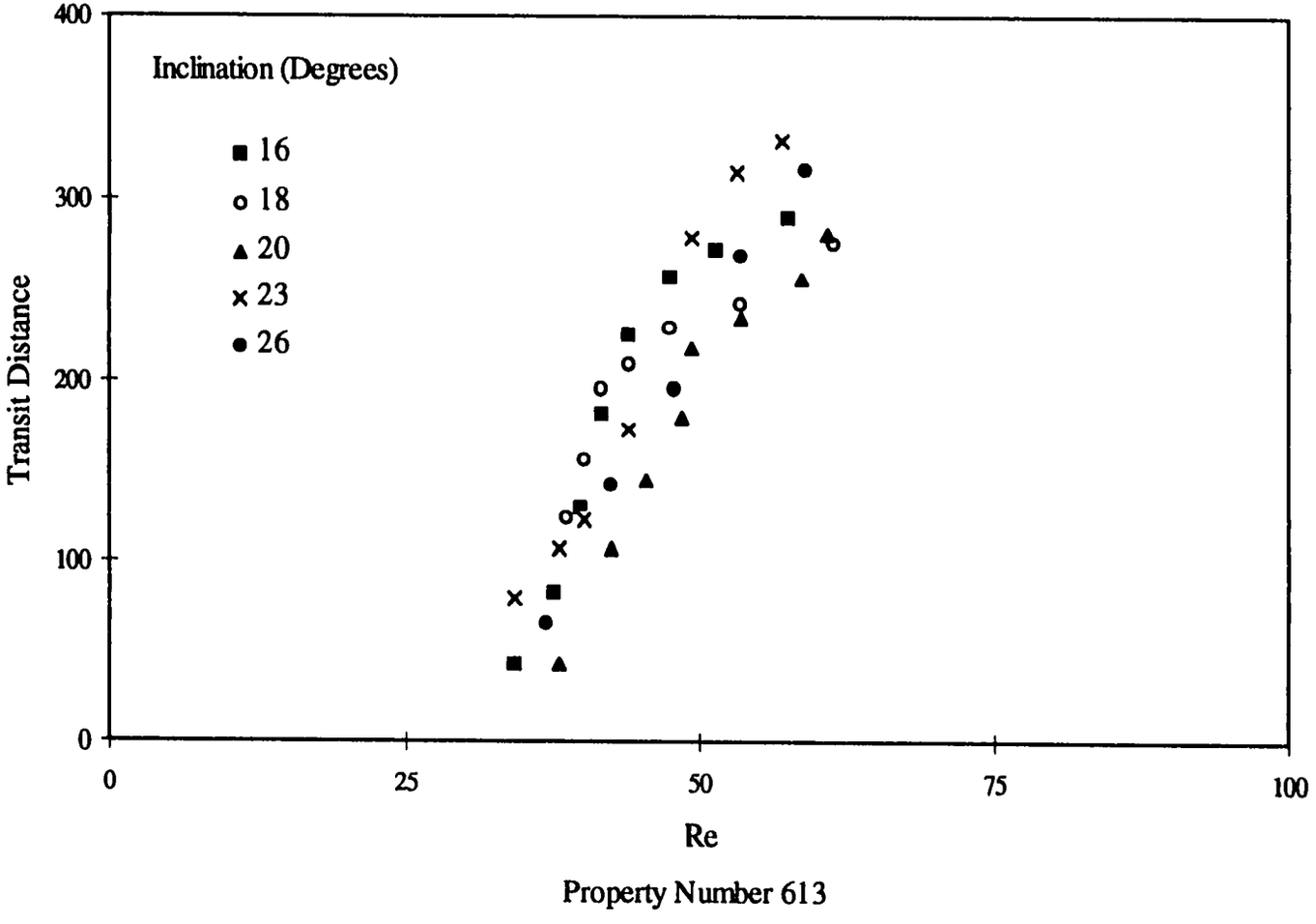

Figure 2-4 Transit Distance, $\gamma = 613$

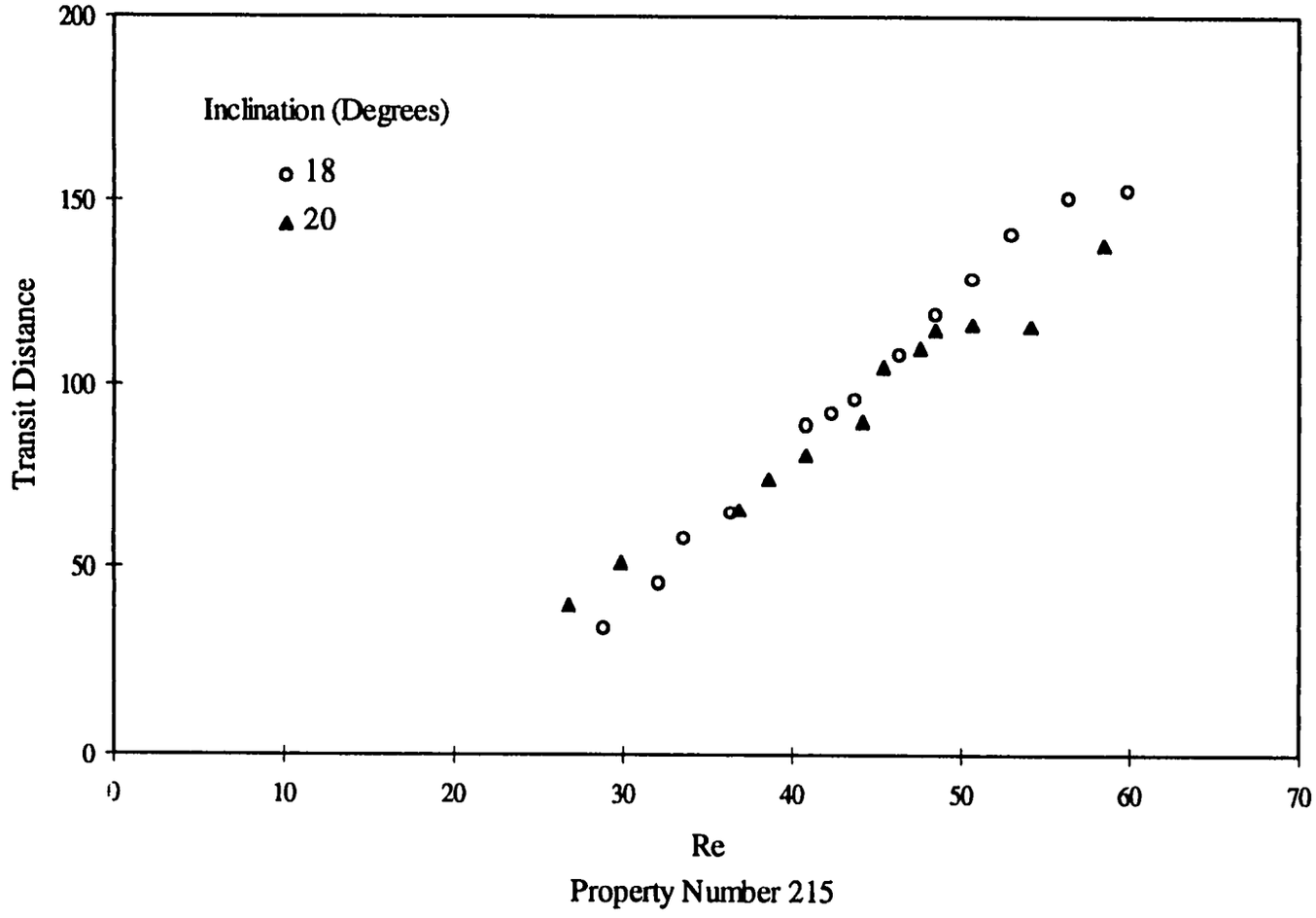

Figure 2-5 Transit Distance, $\gamma = 215$

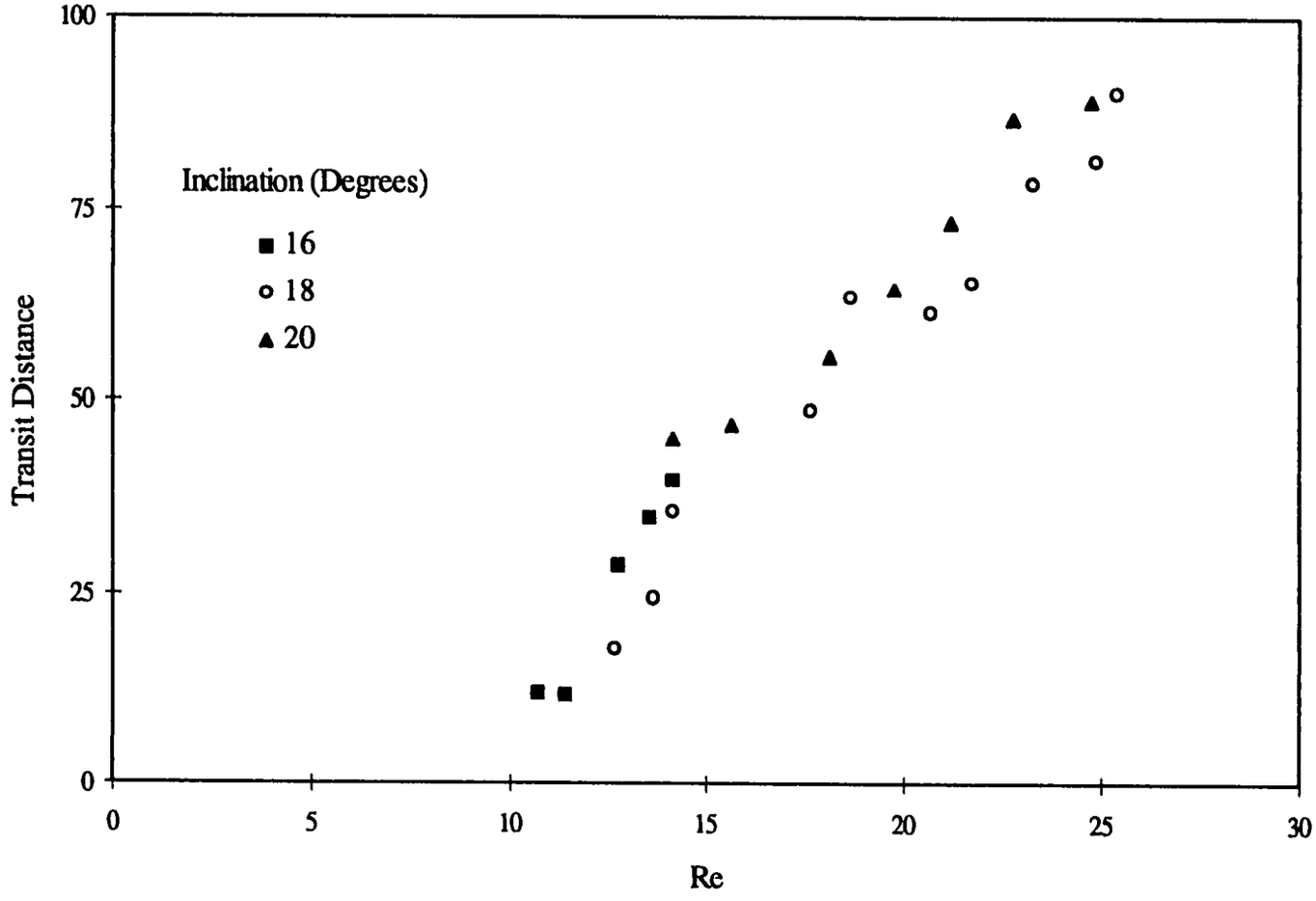

Figure 2-6 Transit Distance, $\gamma = 92$

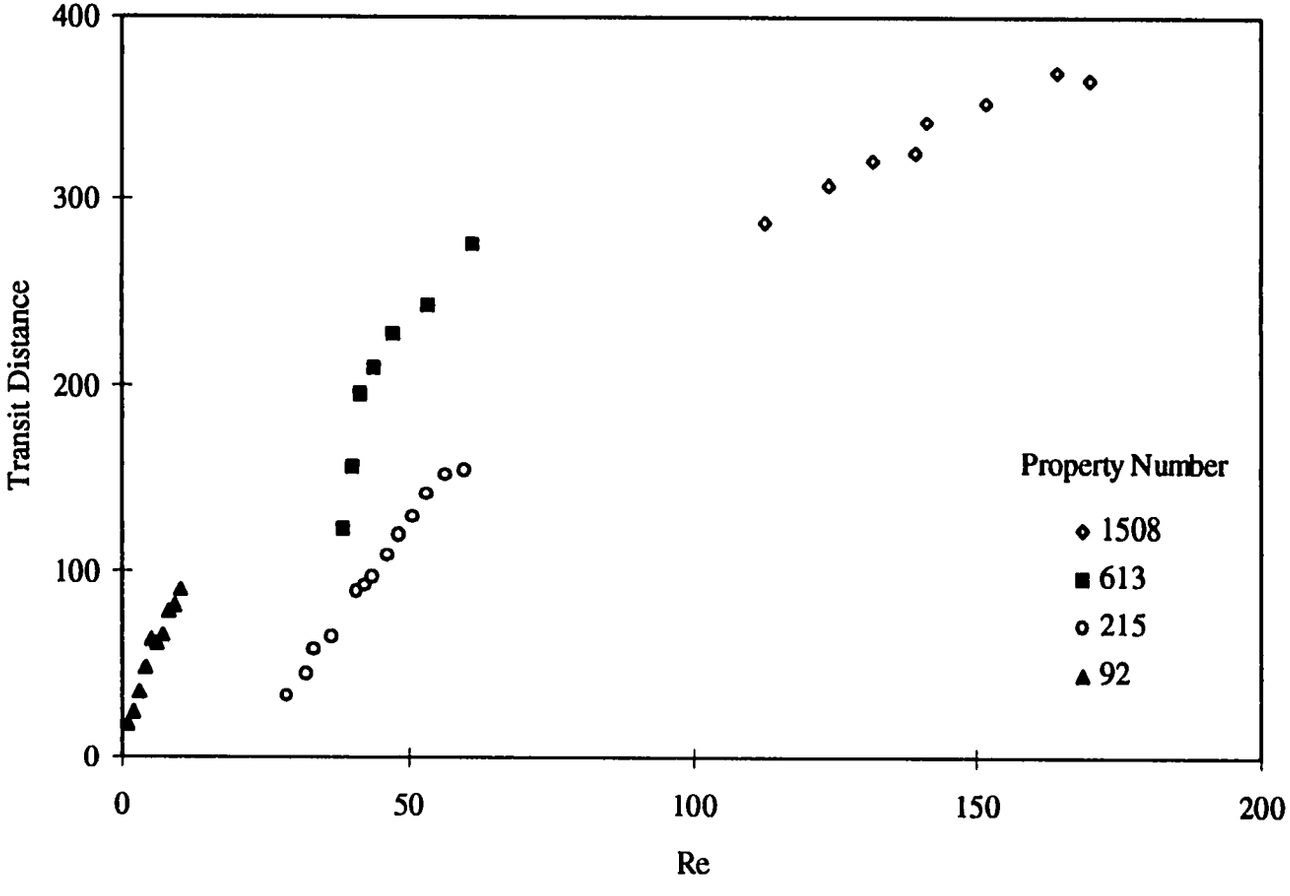

Inclination 18 (Degrees)

Figure 2-7 Transit Distance, 18° Degrees

2.2.3 Wave Frequencies

Experimental Results

Several glycerol-water solutions were tested in this work. Measurements were made at different flow rates for various combination of the inclination angle (11° - 30°) and the measurement positions (5 - 17 cm from the starting point of the inclined flat surface).

The optical signal registered at anyone of these positions was reduced to three components, the upper limit frequency (ULF) which corresponds to the shortest wavelength disturbances, the lower limit frequency (LLF) which corresponds to the longest wavelength disturbances, and dominant frequency (DF), corresponding to highest relative energy level.

Lower Limit Frequency

The lower limit frequency is pretty much constant for all positions, flow rates, and angles of inclination (Figure 2-8, 2-9). The upper limit frequency varies with flow rate, inclination angle, and liquid properties. Increases in flow rate lead to the appearance of shorter wavelength disturbances (Figure 2-8). Smaller angles of inclination lead to larger upper limit frequencies. These are ripples which flow over the surface of layers with higher velocities and smaller gravitational effects.

Surface tension plays an important role in wave formations over the free surface of thin liquid films. Its action is to minimize the surface area of the air/liquid interface. The wave-free surface of a thin liquid film is the smallest possible surface. Therefore, it is expected that surface tension force will exert a stabilizing influence on the laminar flow of a film with uniform thickness. Figure 2-9 shows the lower and upper limit frequencies plotted against the Weber number, which is a measure of inertia to surface tension forces. Increases in the Weber number lead to appearance of higher upper limit frequency disturbances. In terms of surface tension an increase in the Weber number corresponds to lower surface tension energy.

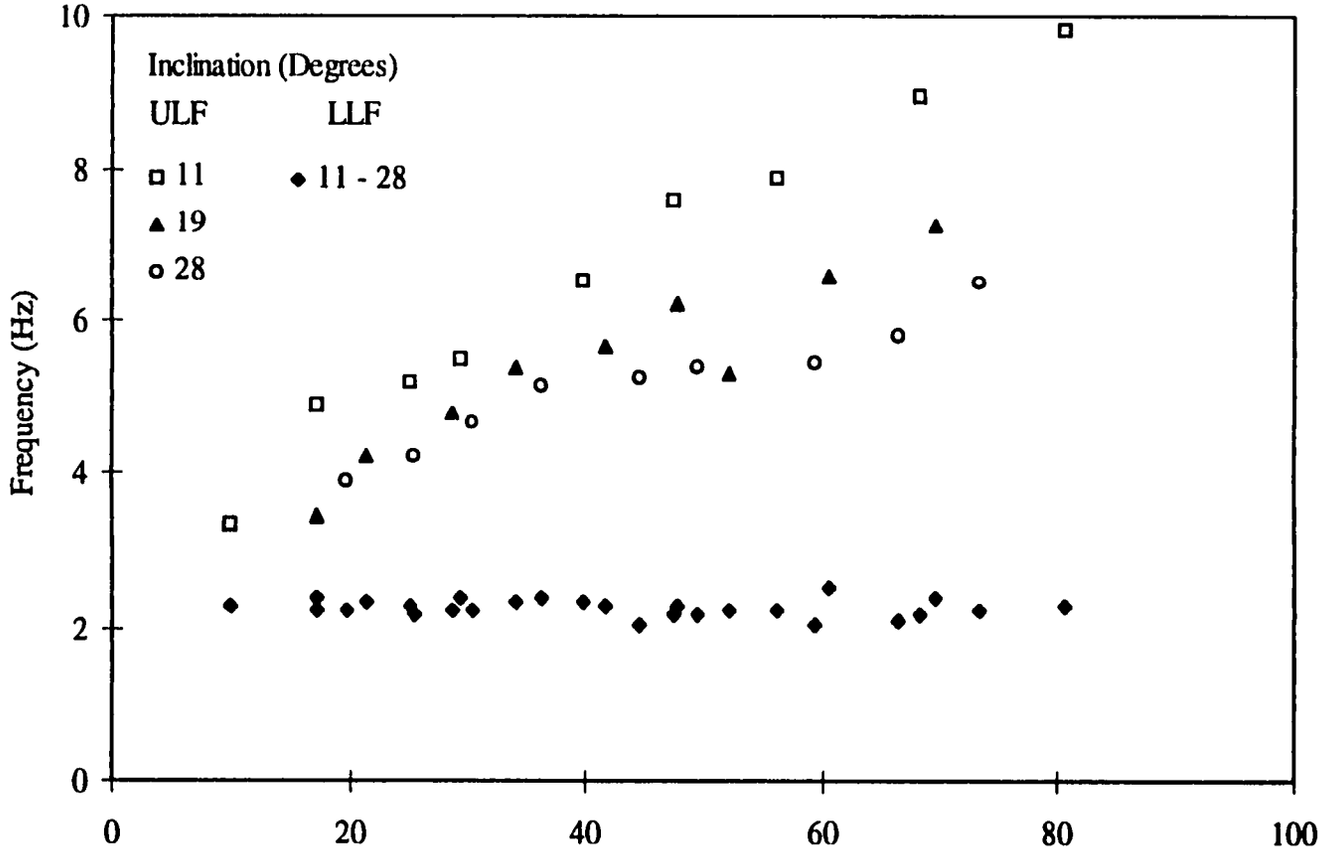

Property Number 344, Position 5 cm

Figure 2-8 Frequencies Over Flowrates, $\gamma = 344$

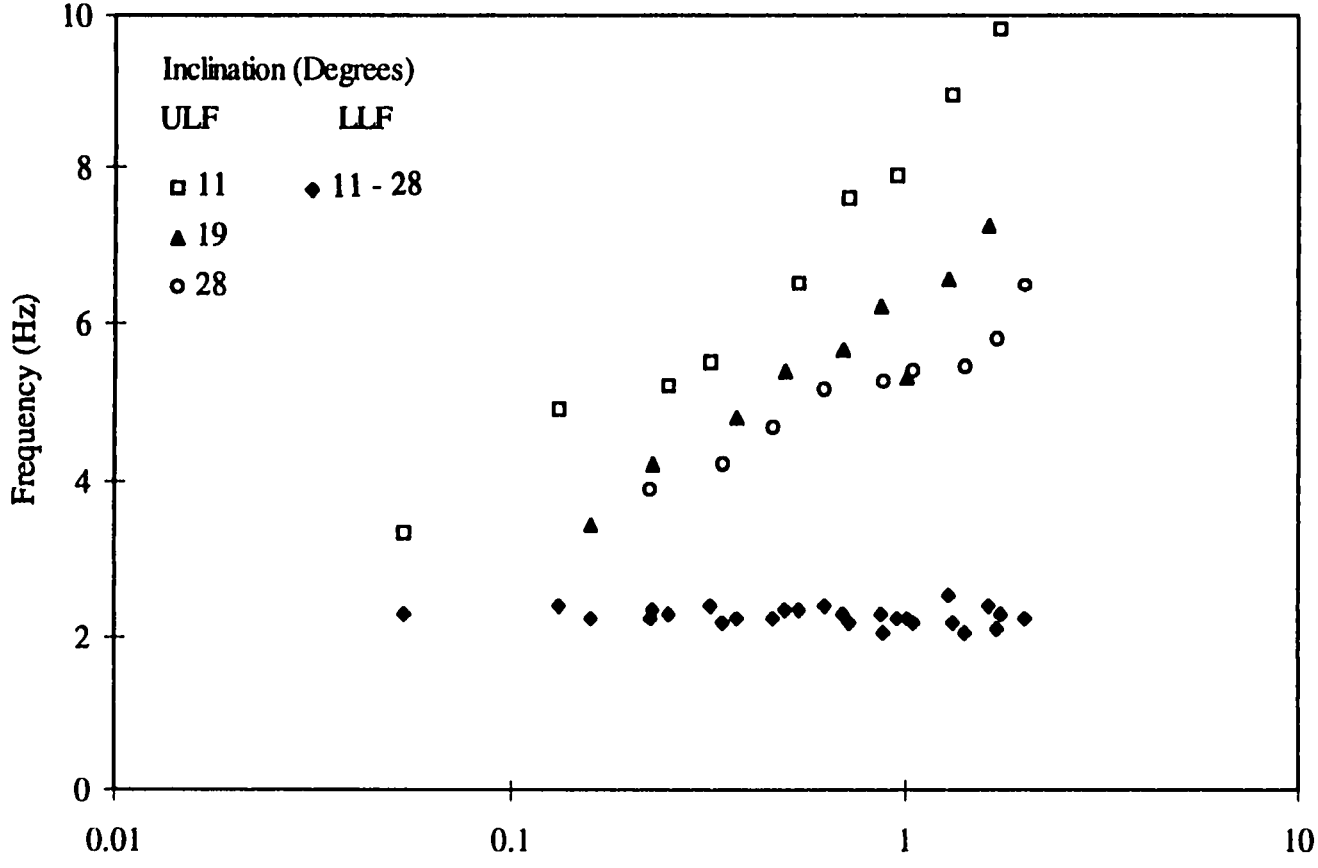

Property Number 344, Position 5 cm

Figure 2-9 Frequencies Over Surface Tensions, $\gamma = 344$

Upper Limit Frequency

The upper limit frequency of a disturbance is affected by the distance downstream. Figure 2-10 shows that closer to inception (5 cm) the disturbance has a higher upper limit frequency. However at longer distances (9 and 13 cm) the upper limit frequency does not seem to change with distance. More viscous liquids tend to develop higher upper limit frequencies. Figure 2-11 shows that higher frequencies rise rapidly with small flow rates for the most viscous solution ($\gamma = 25$). The rise in the upper limit frequency is much slower and much less significant for the solution with the smallest viscosity. The rise in the frequencies with decreasing surface tension is apparent from Figure 2-12 for all tested solutions.

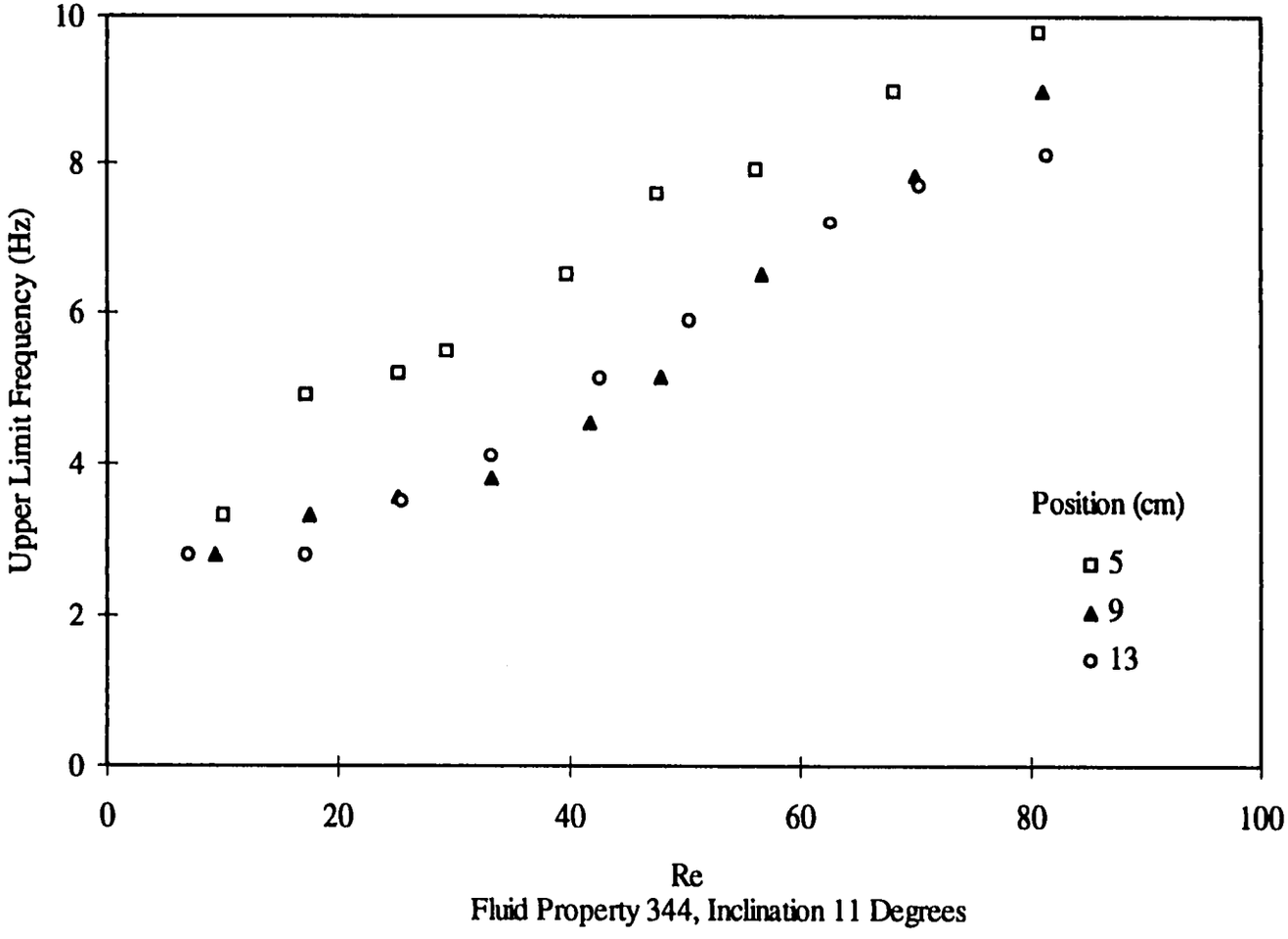

Fluid Property 344, Inclination 11 Degrees

Figure 2-10 Upper Limit Frequency Over Flowrates, Different Positions

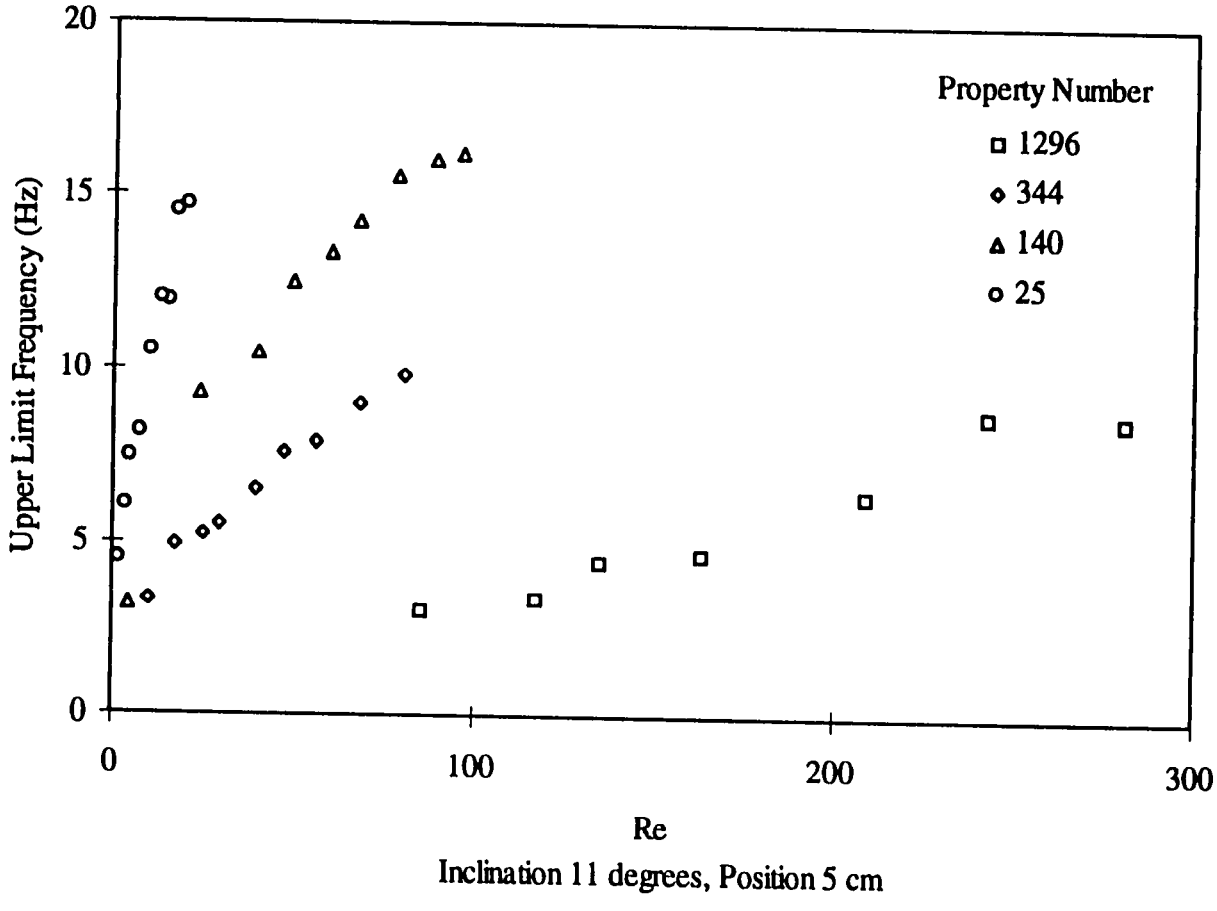

Figure 2-11 Upper Limit Frequency Over Flowrates, Different Liquids

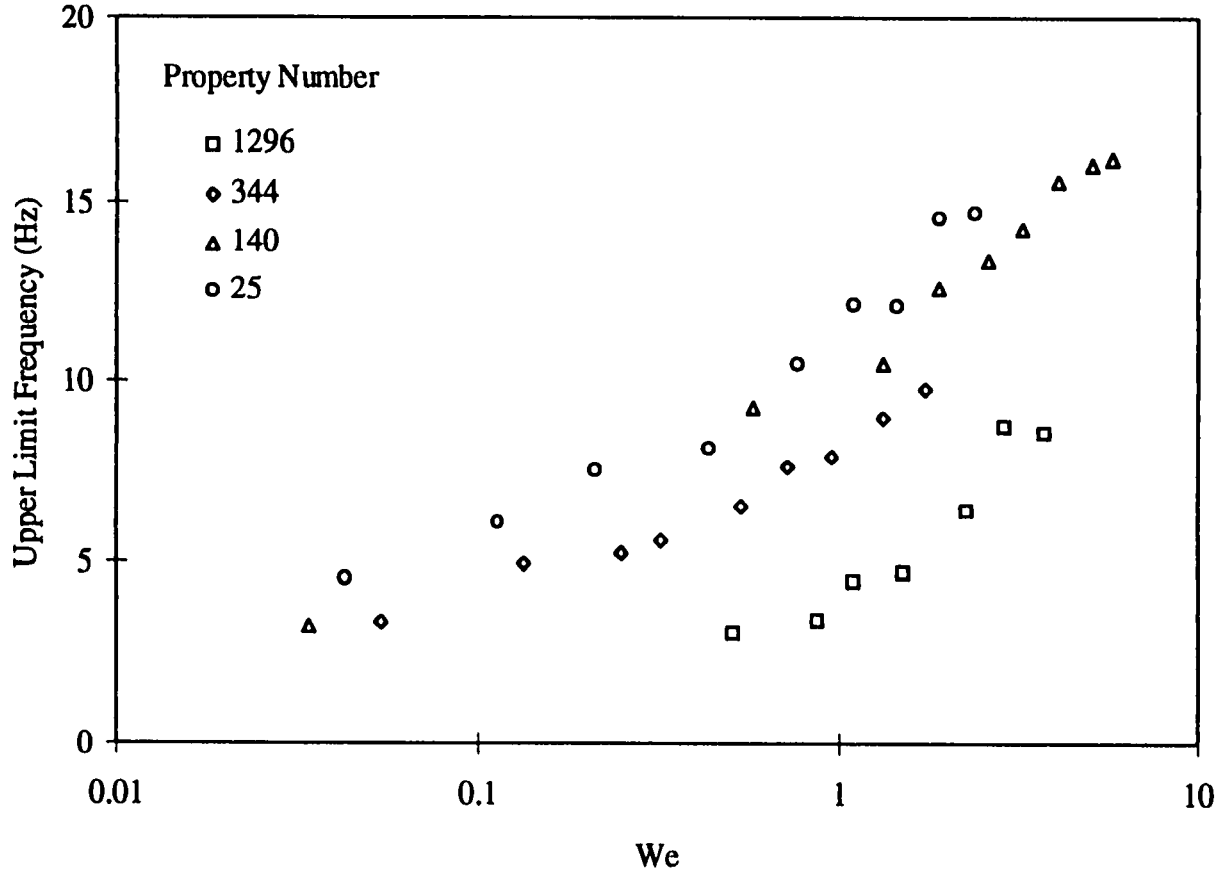

Inclination 11 degrees, Position 5 cm

Figure 2-12 Upper Limit Frequency Over Surface Tensions, Different Liquids

Dominant Frequency

The dominant frequency represents the wavelength with the highest energy in the spectrum of all wavelengths. In general it rises with flow rate. Liquids with high property number (low viscosity) tend to have a more constant dominant frequency with flow rates (Figure 2-13). However, even for such a liquid (γ = 1296) the dominant frequency rises slightly with high flow rates. More significant increases in the dominant frequency are experienced by more viscous liquids such as the glycerol solutions with property numbers γ = 344, 140, 25 (Figure 2-13). The effect of surface tension is shown through the Weber number in Figure 2-14. More viscous liquids experience higher values of the dominant frequency. Higher Weber numbers, corresponding to decreasing surface tension energy, lead to higher dominant frequencies, i.e. the dominant wavelength is shorter.

There is a noticeable effect of inclination angle on the dominant frequency. The effect becomes more noticeable for moderate Reynolds numbers Re > 40 (Figure 2-15). Higher inclination angles θ = 19°, 28° were associated with higher dominant frequencies that were rising with the Reynolds number. No noticeable effect on the dominant frequency was associated with the distance downstream from inception. Figure 2-16 shows a set of results for the same conditions as those presented in Figure 2-13 except that the measurements are recorded at a position 13 cm downstream compared to 5 cm in Figure 2-13. Essentially the results are the same.

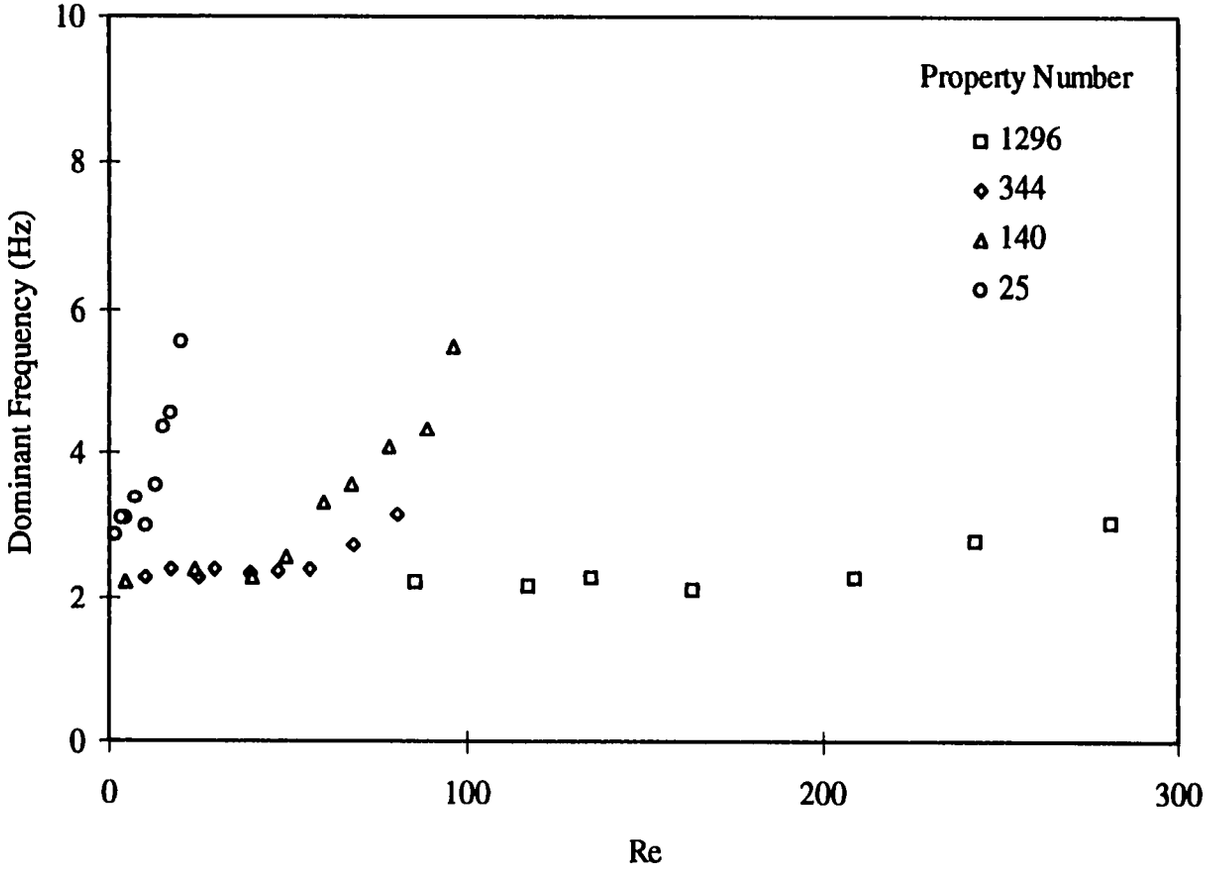

Inclination 11 degrees, Position 5 cm

Figure 2-13 Dominant Frequency Over Flowrates, Different Liquids

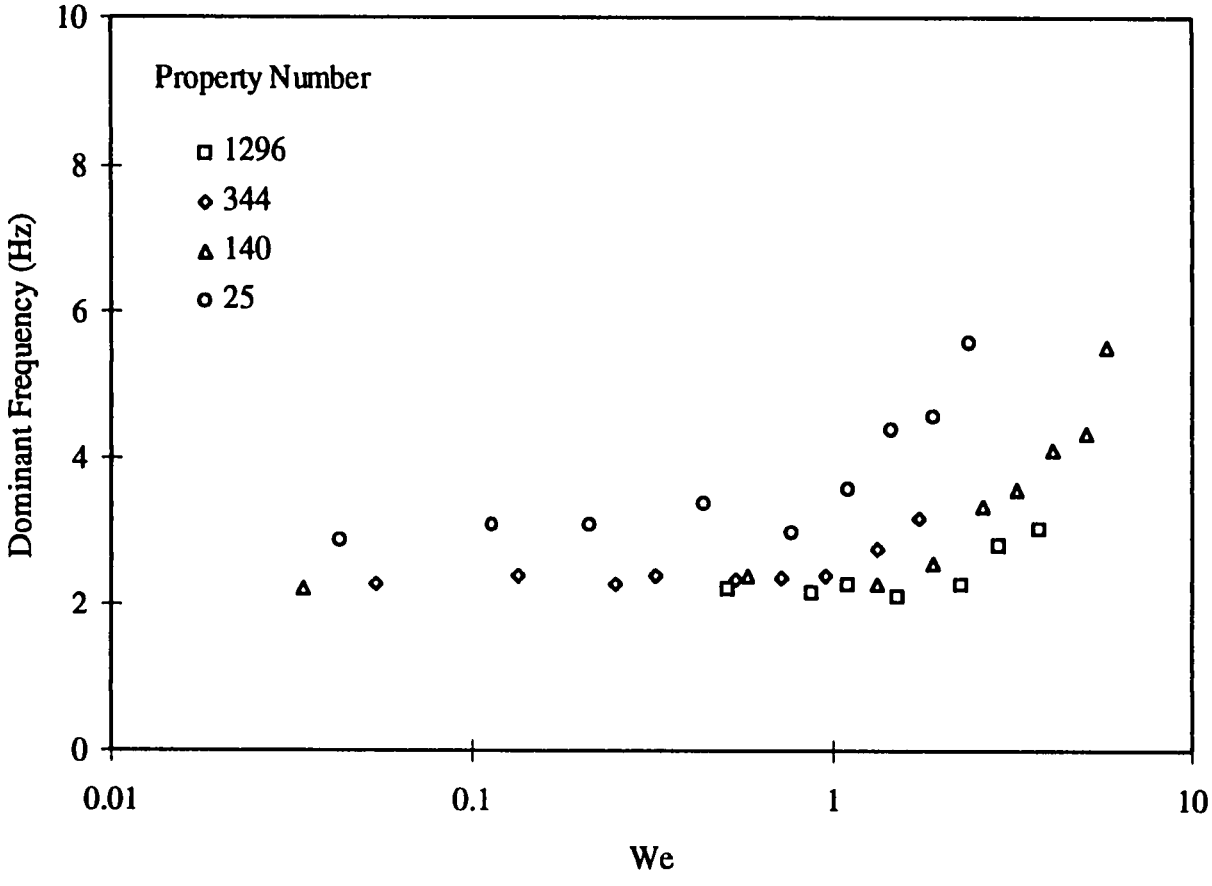

Inclination 11 degrees, Position 5 cm

Figure 2-14 Dominant Frequency Over Surface Tensions, Different Liquids

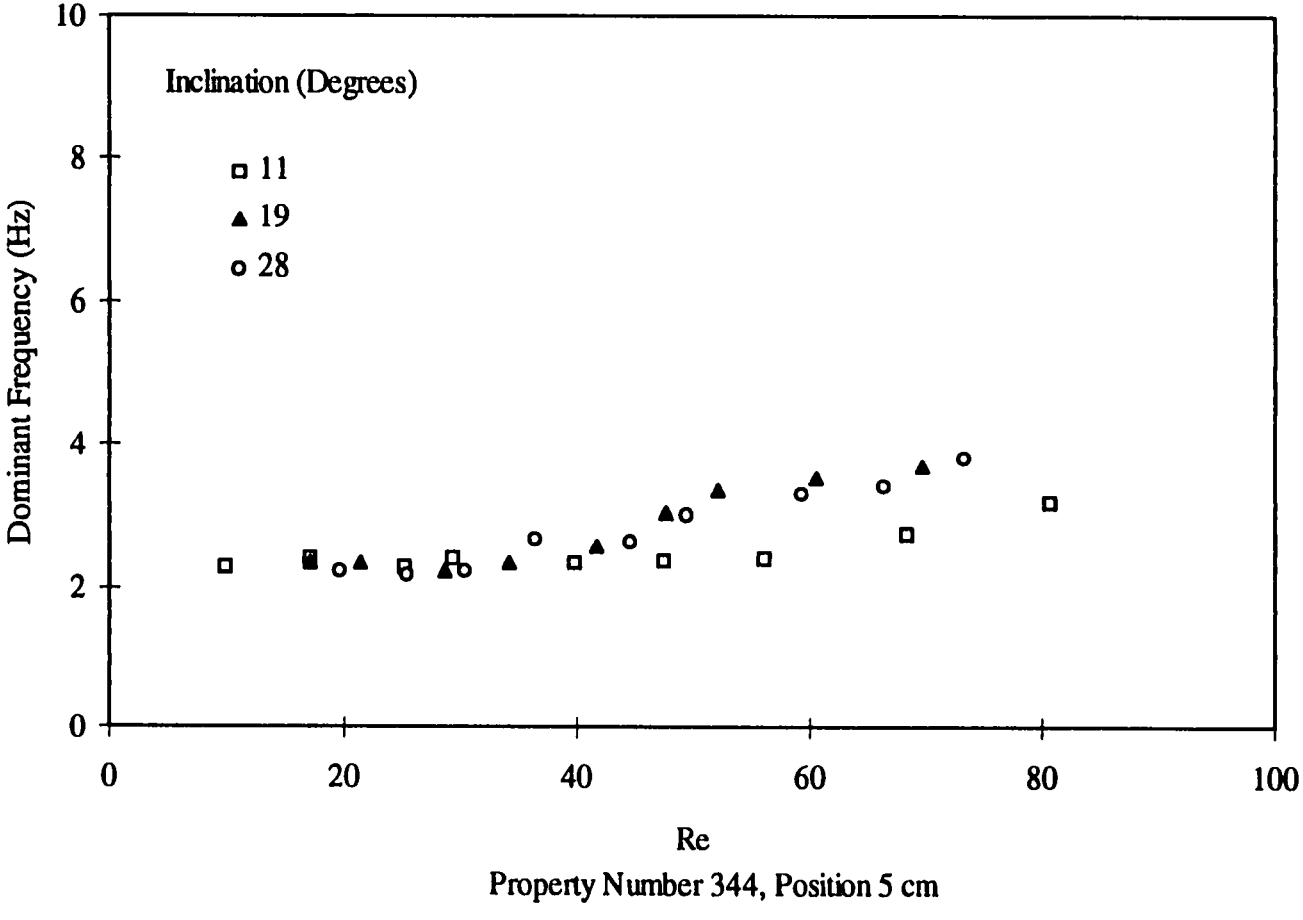

Property Number 344, Position 5 cm

Figure 2-15 Dominant Frequency Over Flowrates, Different Angles

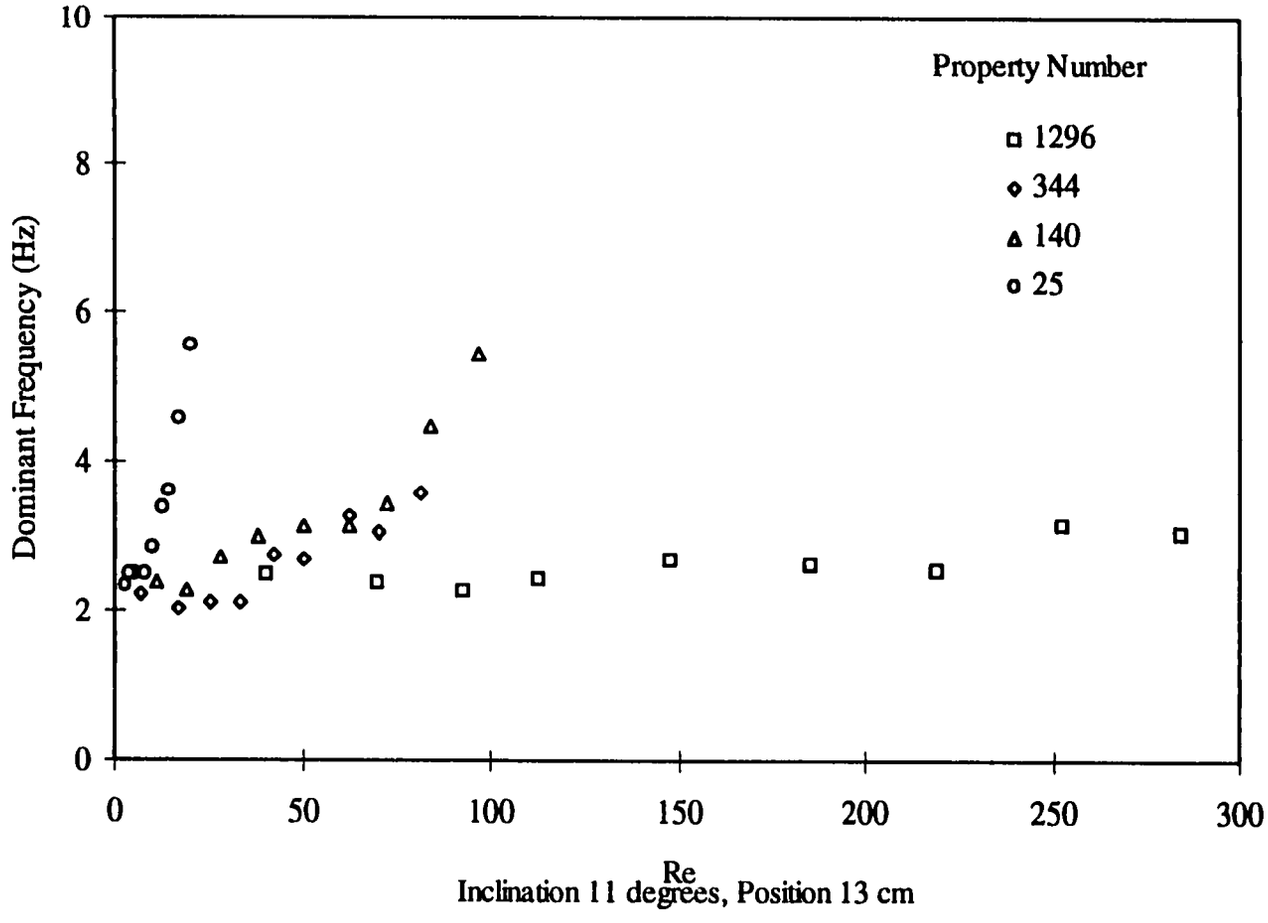

Figure 2-16 Dominant Frequency Over Flowrates, X=13 cm

Comparison With Previous Experiments

There are very few published experimental works about the frequency characteristics of free surface waves of thin liquid film flows. Javdani (1976) argued that for a given flow condition, the frequency of most highly amplified waves on falling films remains constant in all the stages of growth, starting from the initial state where the wave is in the form of an infinitesimal disturbance to the final state of equilibrium in which the wave attains a finite amplitude and constant properties. This most highly amplified frequency was measured by optical reflective technique.

Figures 2-17 to 2-19 show our upper limit and dominant frequencies compared to Javdani's most highly amplified frequency over the dimensionless number N. The comparison is made between our glycerol solution with the property number $\gamma = 25$, and Javdani's mineral oil $\gamma = 12$. Our solution has a density $\rho = 1190$ kg/m^3; viscosity $\mu =$ 23 mPa.s; and surface tension coefficient $\sigma = 32.3$ mN/m. The properties of Javdani's mineral oil were $\rho = 880$ kg/m^3; $\mu = 33.6$ mPa.s; and $\sigma = 29.5$ mN/m. Figure 2-17 to 2-19 compare the results for three different combinations of almost the same inclination angles, 11° and 11.8° in Figure 2-17, 19° and 20.9° in Figure 2-18, and 28° and 29.9° in Figure 2-19 for our and Javdani's work, respectively. The fundamental difference between the results is the rise in Javdani's highly amplified frequency for smaller N numbers. This range corresponds to smaller Reynolds numbers. The frequencies in our experiment were generally rising with the Reynolds number.

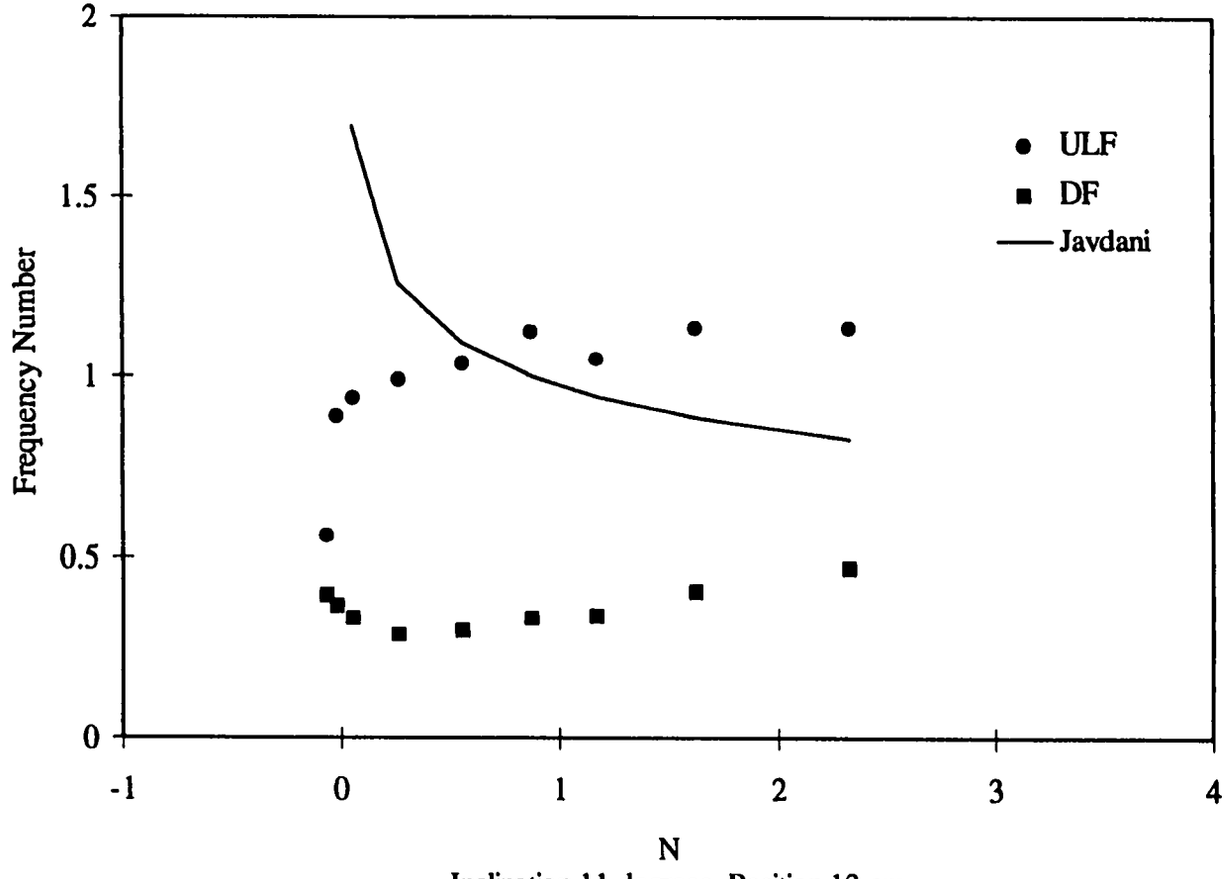

Figure 2-17 Upper Limit, Dominant, and Most Amplified Frequencies

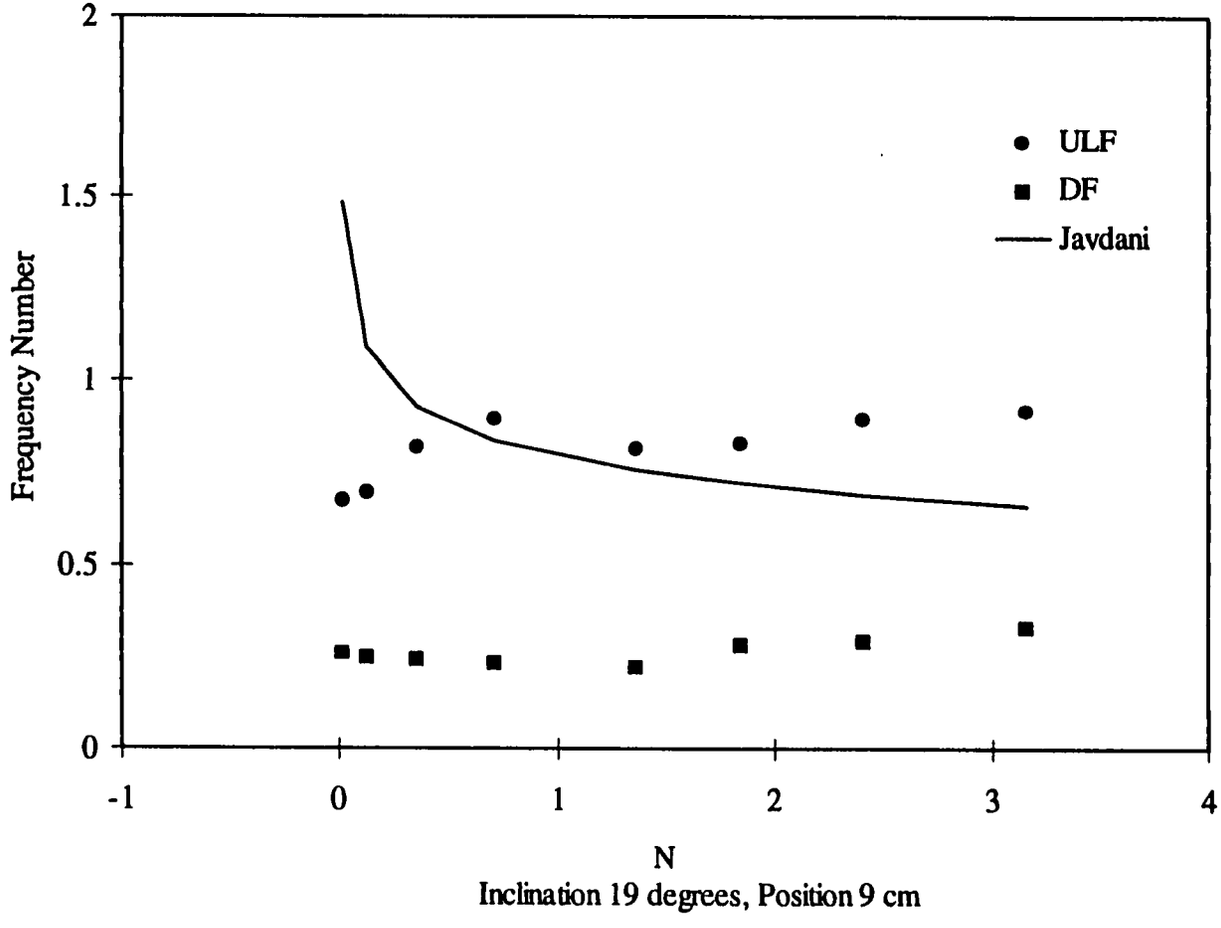

Inclination 19 degrees, Position 9 cm

Figure 2-18 Upper Limit, Dominant, and Most Amplified Frequencies

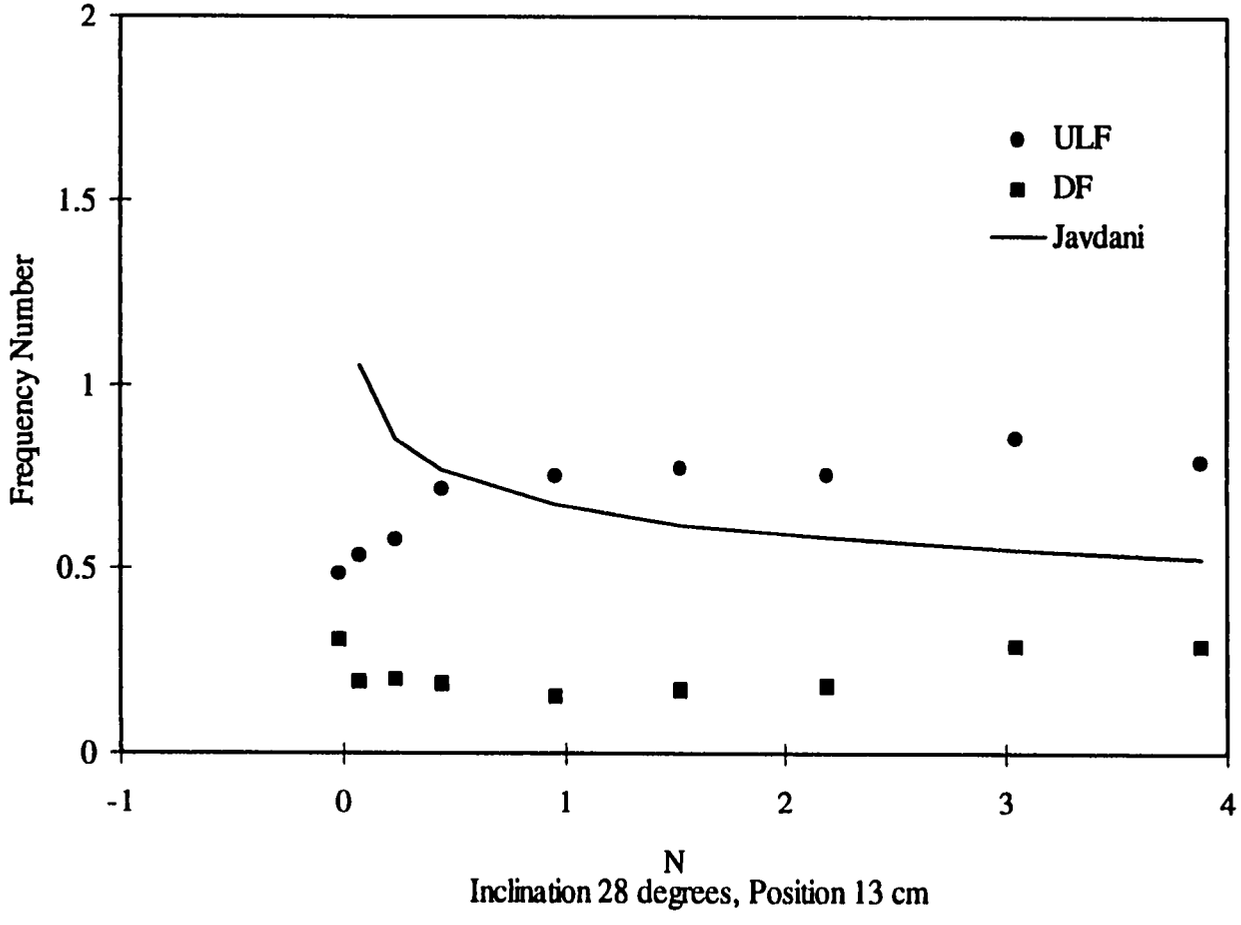

Figure 2-19 Upper Limit, Dominant, and Most Amplified Frequencies

More recent experiments were reported by Brauner and Maron (1982). Actually, they measured the spectra of the mass transfer rate of a chemical species from the liquid to the solid bottom. However, they experimentally demonstrated that these spectra are close to the wave spectra. Figure 2-20 shows our dominant frequency for a glycerol solution $\gamma = 1296$ compared with the dominant frequency reported by Brauner and Maron for water $\gamma = 3362$. The comparison is made for different inclination angles. There seem to be a general agreement in the trend and to some extent the values of frequency behavior.

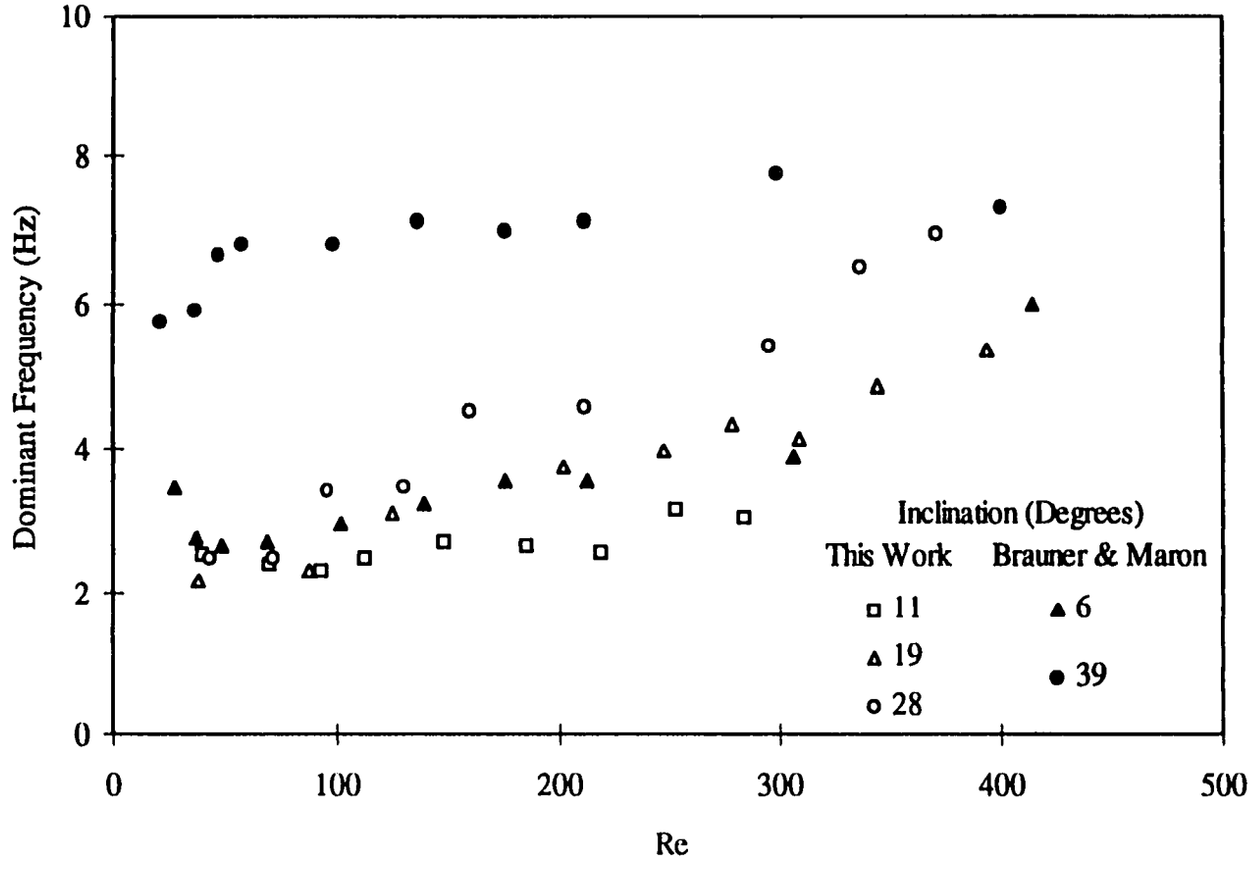

Property Number 1296 (this work), 3362 (Brauner & Maron)

Figure 2-20 Dominant Frequencies, Different Angles

2.3 DOUBLE LAYER FLOW SYSTEMS

In these experiments two thin layers of the same glycerol solution were allowed to flow down the inclined plane. Each of the layers had its own flow rate. Therefore, two Reynolds numbers were defined for a single experiment, the bottom layer and upper layer Reynolds numbers. The bottom layer Reynolds number is denoted by Re_b. The upper layer Reynolds number is denoted simply by Re. The Weber number We is based on the flow rate of the upper layer. Measurements were taken at various combinations of top and bottom flow rates, for different angles of inclination 11^0 to 28^0, and at different measurement positions X=5-17 cm from the starting point on the inclined plane. It is expected that the effect of issuing two separate layers down the plane will extend a certain distance, after which the flow should completely turn into a flow of a single layer with the combined flow rate. The investigation in these experiments centered on wave frequencies, and their comparison with frequencies arising in single layer systems.

The optical signal registered at anyone of these positions was reduced to three components, the upper limit frequency (ULF) which corresponds to the shortest wavelength disturbances, the lower limit frequency (LLF) which corresponds to the longest wavelength disturbances, and dominant frequency (DF), corresponding to highest relative energy level.

2.3.1 Comparison With Single Layer Systems

Figures 2-21 to 2-23 show the upper limit frequencies measured for a single and double layer systems as functions of the Reynolds number. Figures 2-21 and 2-22 show a comparison of the upper limit frequencies at a position 5 cm downstream from the starting point over the inclined plane. This position is not sufficiently far from the point for the flow to fully exhibit the features of a combined single layer system in the case of double layers. The velocity profiles of the two layers, originally separated by a solid plane, where no-slip conditions apply, have not yet fully recovered from the original separation. This should be particularly true for flows with less inertia, flow rate, and

consequently less Reynolds numbers. Double layer flows with higher inertia forces should be able to recover a single velocity profile at a distance closer to the starting point. The upper limit frequencies of waves running down the free-surface of a double layer flow are lower than those for a single layer flow for Reynolds numbers approximately less than 500. This means that the spectrum of these waves has shorter wavelengths in the case of single layer systems. From Figure 2-21 it can be argued that these differences in the frequencies disappear for the position X=5 cm at Reynolds numbers higher than Re=500, for liquids with properties numbers γ=1296 and for an inclination angle 11^0. The inclination angle does not seem to have any effect on this conclusion. Figure 2-22 shows the same comparison for a different angle (19^0). For Reynolds numbers less than 500 the upper limit frequencies of a single layer flow are higher than those for a double layer flow. The situation noticeably changes in measurements at a position X=11 cm, that is further downstream (Figure 2-23). Upper frequencies for the double layer flow seem to blend with those for single layer flows. In addition the upper limit frequencies of the double layer flow are generally lower at higher Reynolds numbers in position X=11 cm, than those measured at X=5 cm.

Figures 2-24 to 2-26 show a comparison of the dominant frequencies measured for a single layer flow with those measured for a double layer flow. There does not seem to be a distinct deviation in the results at lower Reynolds numbers as is the case for upper limit frequencies. One can argue from Figures 2-24 to 2-26 that in general the dominant frequency of waves running down the free-surface of double and single layer systems are practically the same. There is no noticeable change with position (X=5 and 11 cm), with the inclination angle (11^0 and 19^0), or with the Reynolds number.

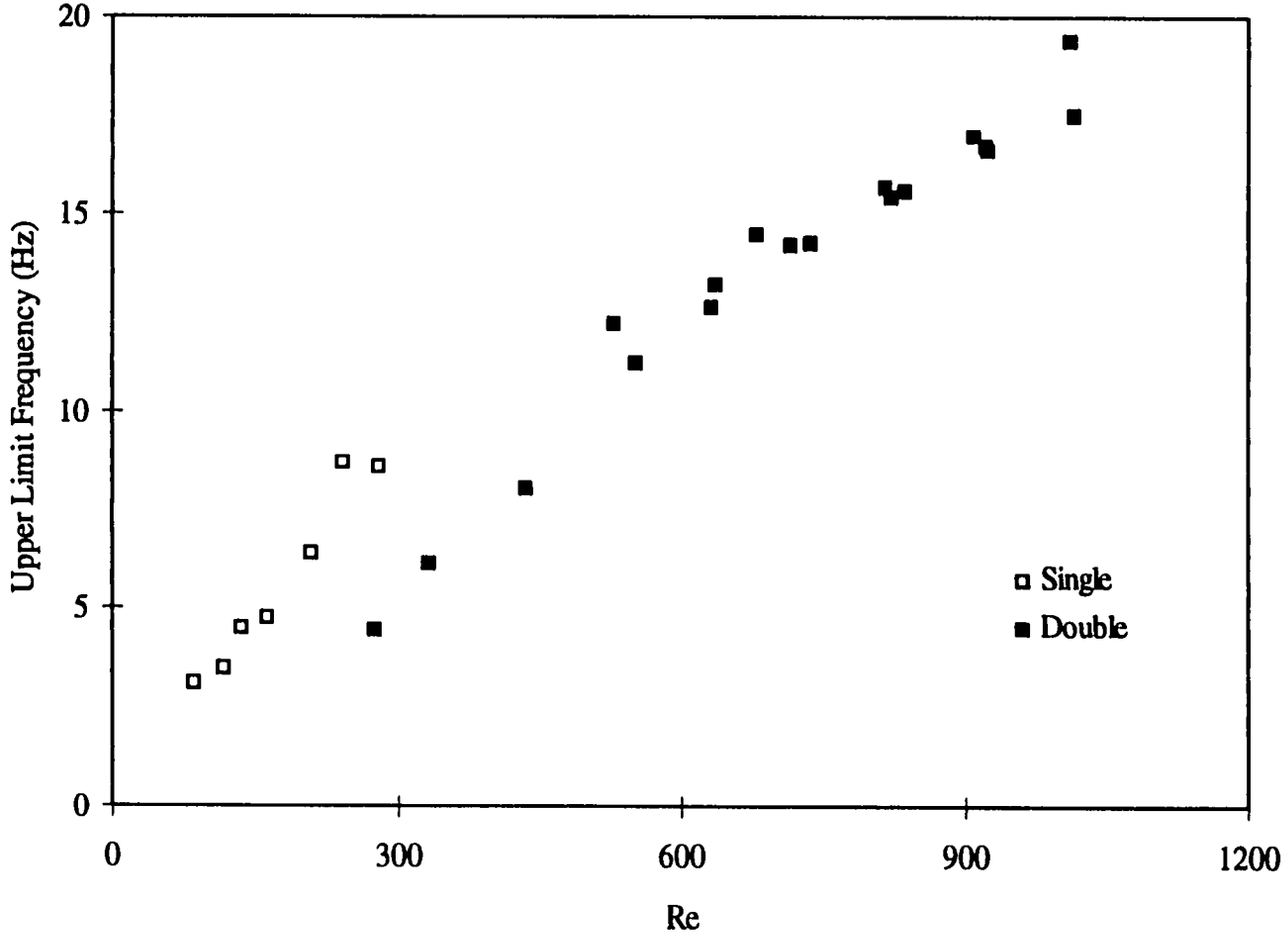

Property 1296, Inclination 11 degrees, Position 5 cm

Figure 2-21 Upper Limit Frequency

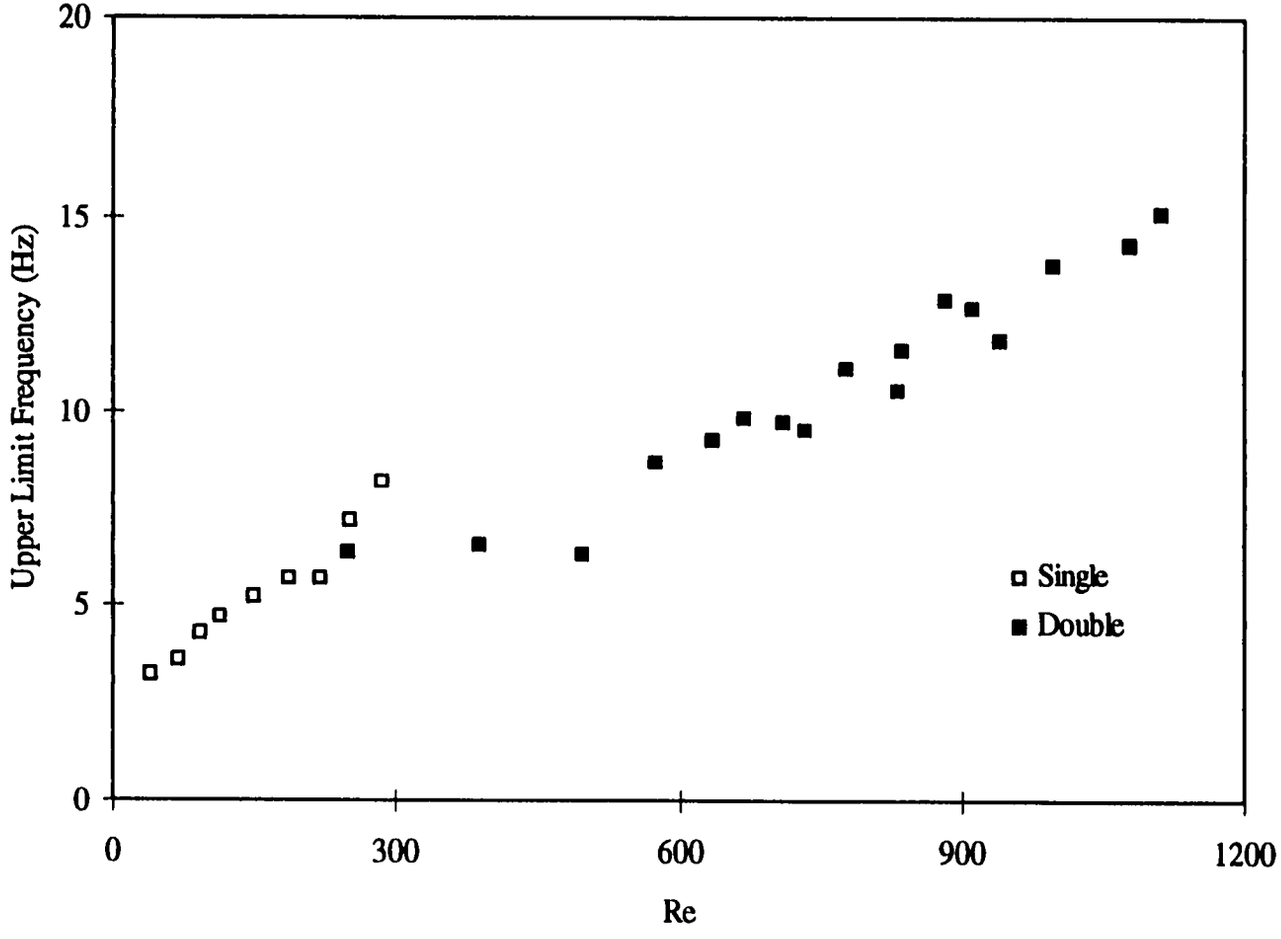

Property 1296, Inclination 11 degrees, Position 11 cm

Figure 2-22 Upper Limit Frequency

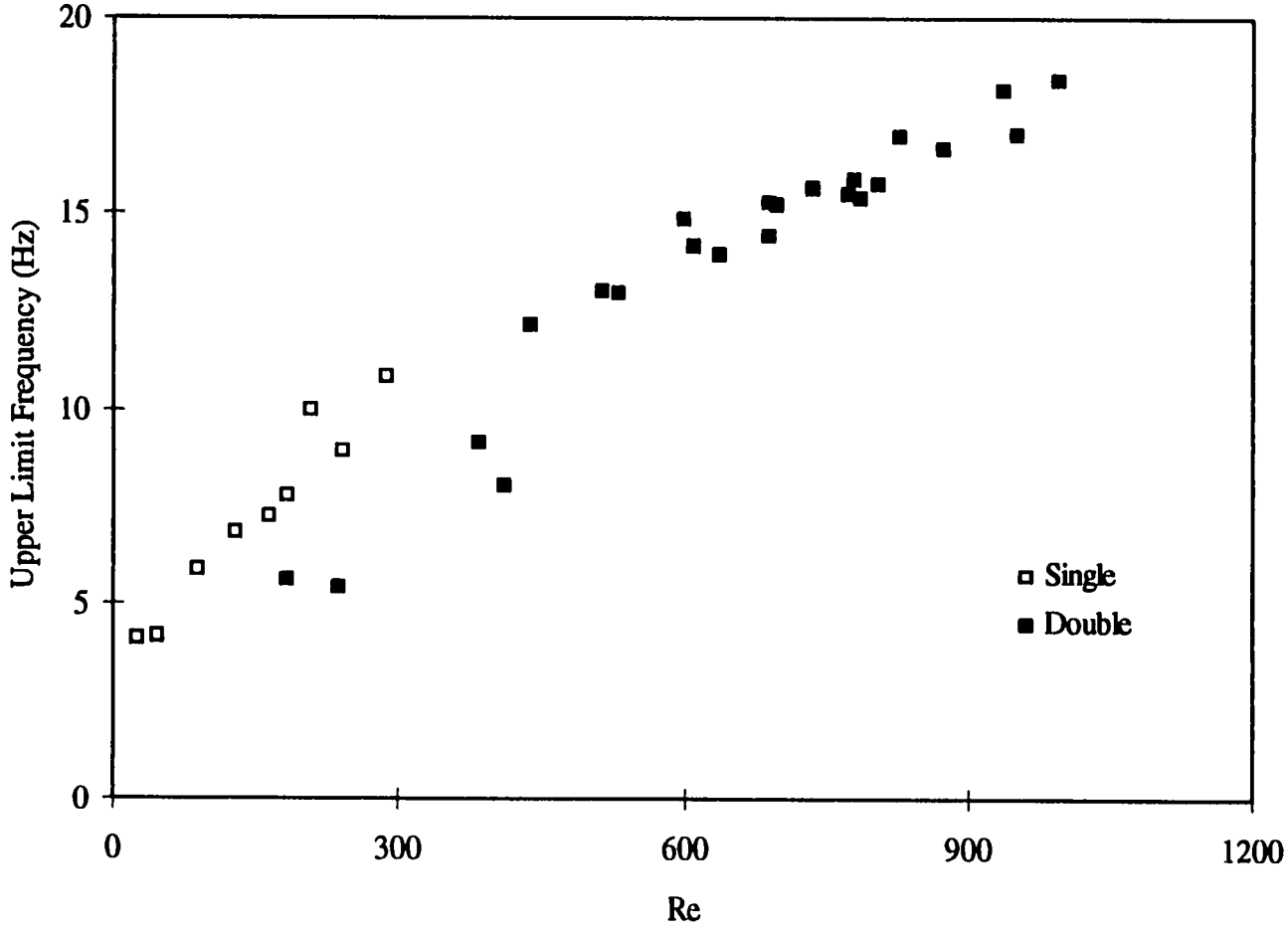

Property 1296, Inclination 19 degrees, Position 5 cm

Figure 2-23 Upper Limit Frequency

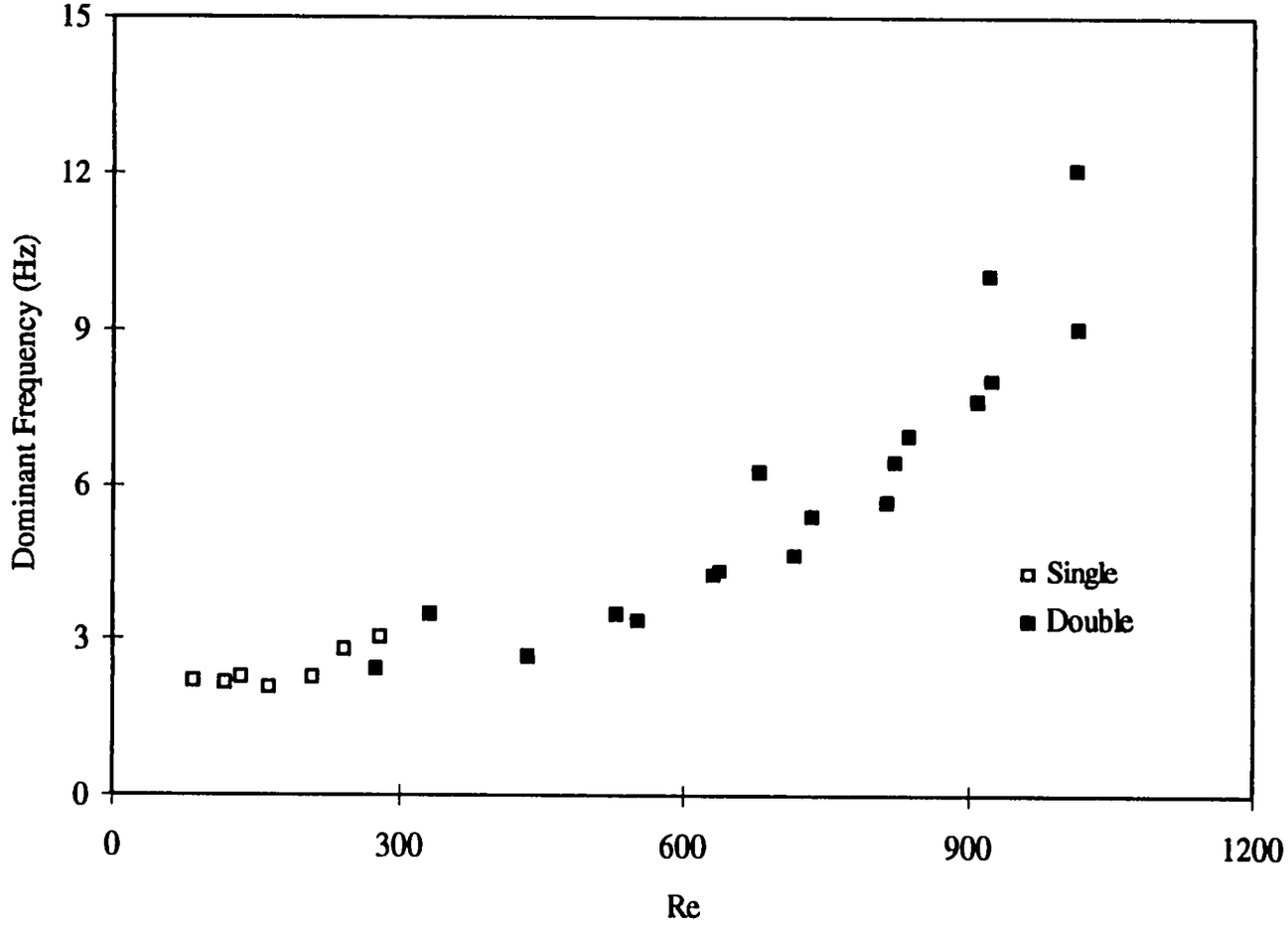

Property 1296, Inclination 11 degrees, Position 5 cm

Figure 2-24 Dominant Frequency

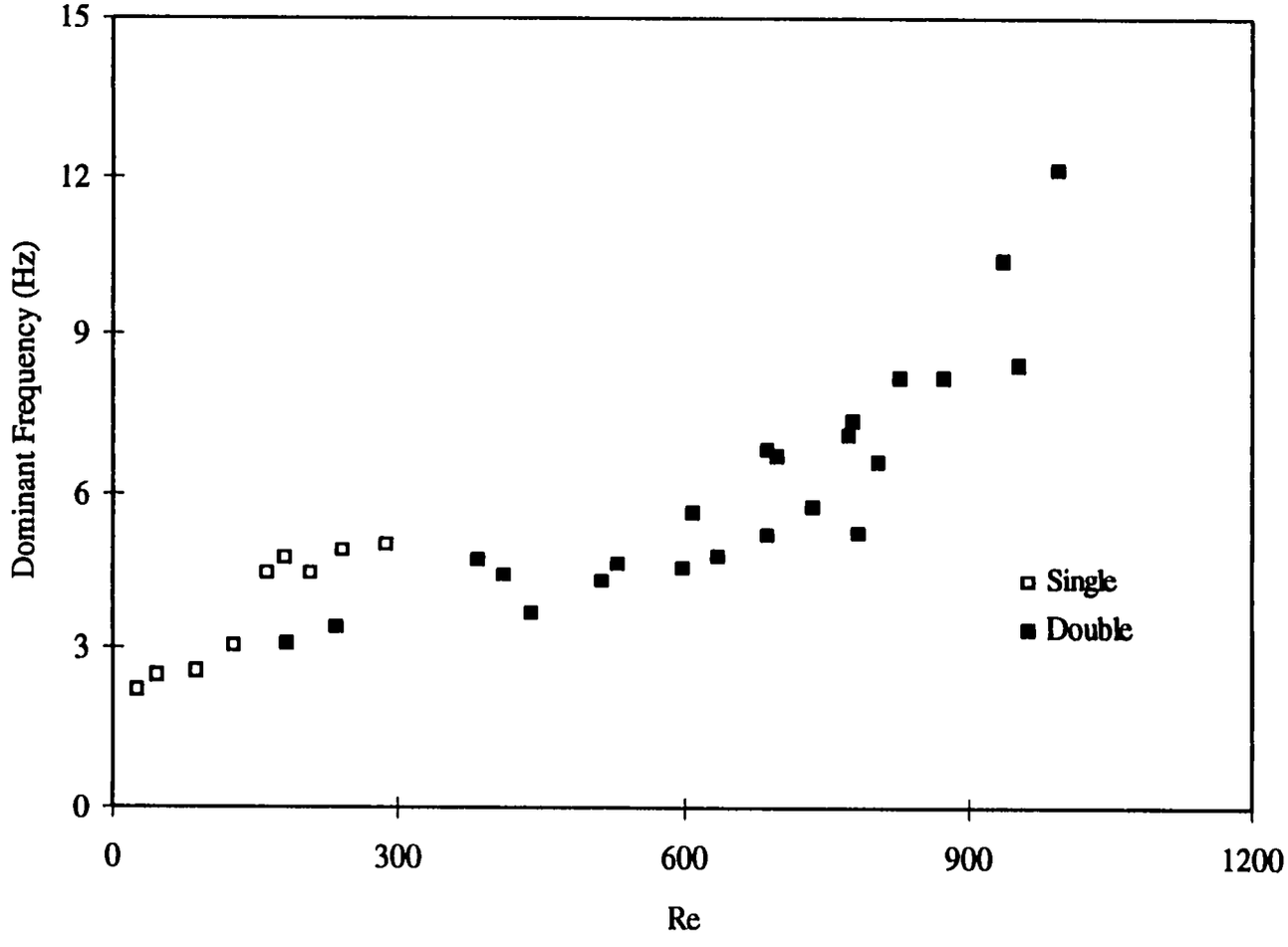

Property 1296, Inclination 19 degrees, Position 5 cm

Figure 2-25 Dominant Frequency

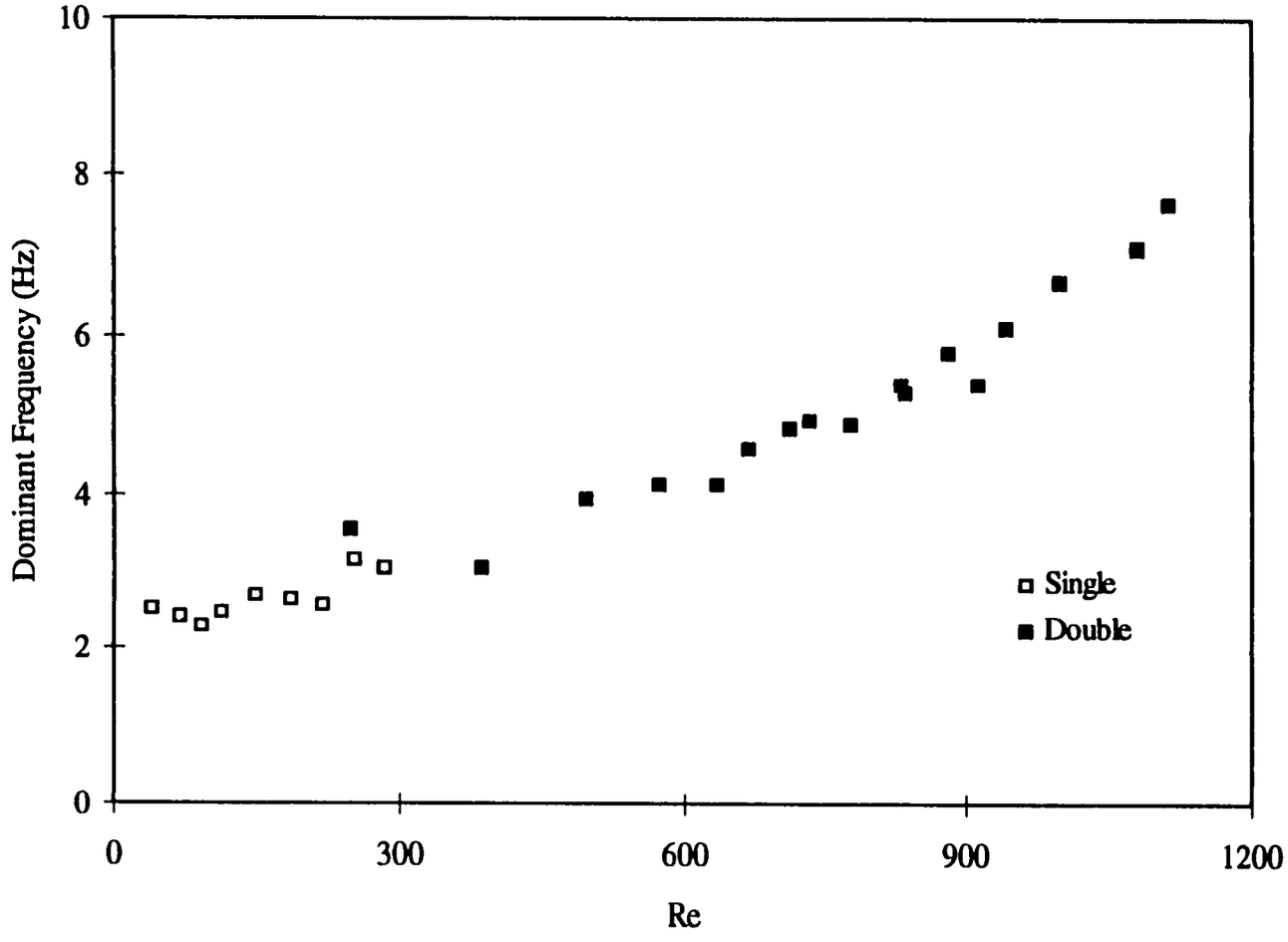

Property 1296, Inclination 11 degrees, Position 11 cm

Figure 2-26 Dominant Frequency

2.3.2 Frequencies

The lower limit frequency was pretty much constant for all positions of measurements, flow rates, and angles of inclination (Figures 2-27, 2-28). The upper limit frequency varies with flow rate, inclination angle, and liquid properties. Increases in the bottom flow rate lead to the appearance of shorter wavelength disturbances (Figure 2-27), even as the upper flow rate remains constant. However, this effect is significant only (Figure 2-28) in the region close to the inlet since the interface between the two fluid films disappears very quickly downstream (Figure 2-28). At lower flow rates of the upper layer, the upper limit frequency is still dependent on the bottom Reynolds number up to an upper Reynolds number of about Re=100 for a liquid γ=198 at 11^0 inclination and X=9 cm.

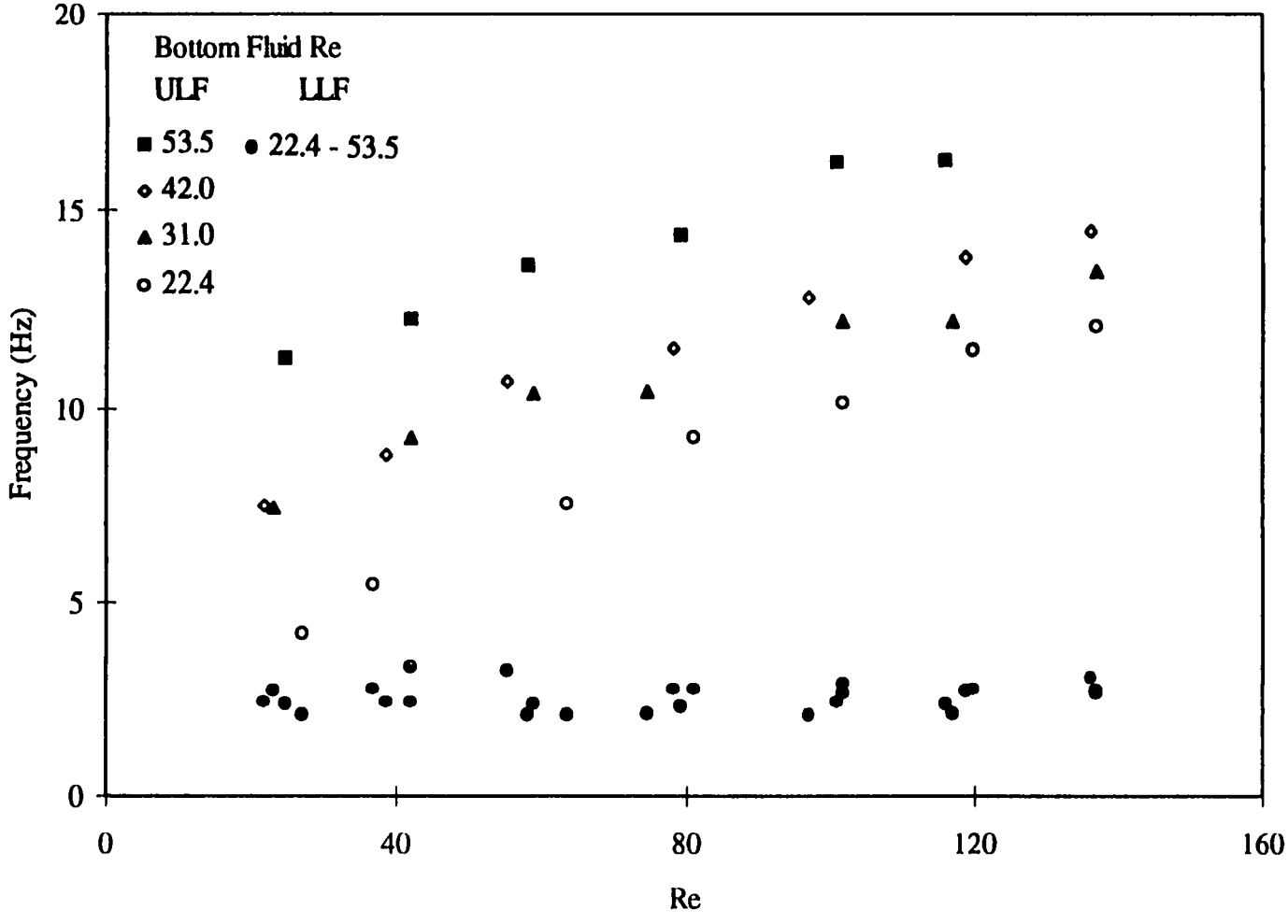

Property Number 198, Inclination 11 degrees, Position 5 cm

Figure 2-27 Frequencies

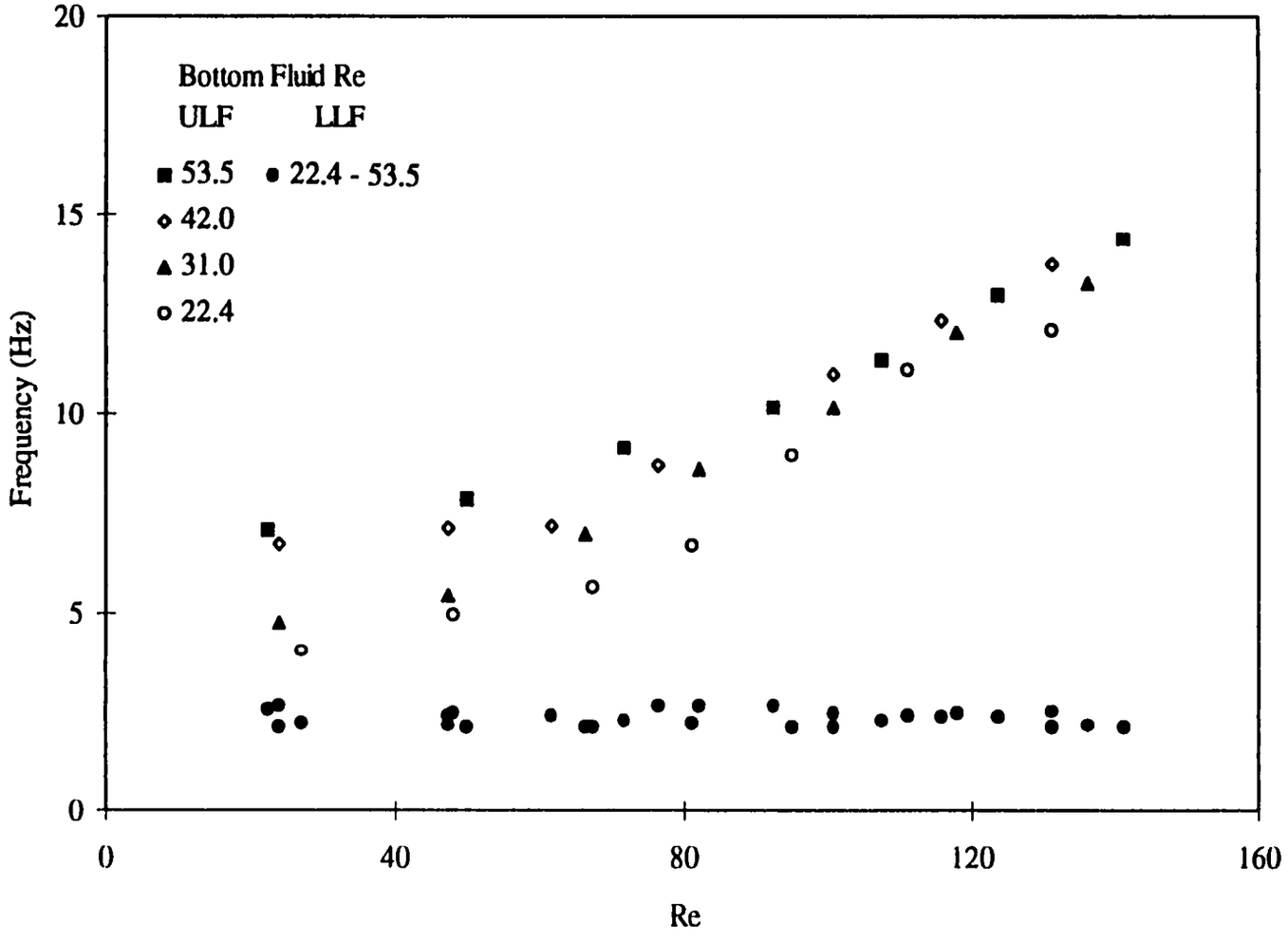

Property Number 198, Inclination 11 degrees, Position 9 cm

Figure 2-28 Frequencies

2.3.3 Upper Limit Frequencies

The upper limit frequency varies with flow rates, the angle of inclination, and liquid properties. The shorter wavelength disturbances depend more on the inclination angle (Figure 2-29) at lower flow rates in the upper layer. For higher upper flow rates this dependence seems to disappear. Liquid properties have a significant effect (Figure 2-30) on the possibility of higher frequencies in the spectrum of surface disturbances. This possibility is shifted towards lower flow rates of the upper layer for more viscous liquids (lower properties number γ). The influence of the position of measurements from the starting point of the inclined plane is shown in Figure 2-31. It is quite clear that the upper limit frequency is more dependent on this position closer to the point of inception. Downstream at positions X=9 and 13, there hardly seems to be any change in the upper limit frequencies. Figures 2-32 and 2-33 show the upper limit frequency versus the Weber number of the upper layer for different bottom Reynolds numbers (Figure 2-32), and different liquids (Figure 2-33). Increases in the bottom flow rate lead to the appearance of shorter wavelength disturbances (Figure 2-32) close to the upper limit of the frequency spectrum. Figure 2-33 illustrates that increased surface tension energy leads to disturbances with longer wavelengths. Surface tension is a stabilizing factor for short wavelength disturbances.

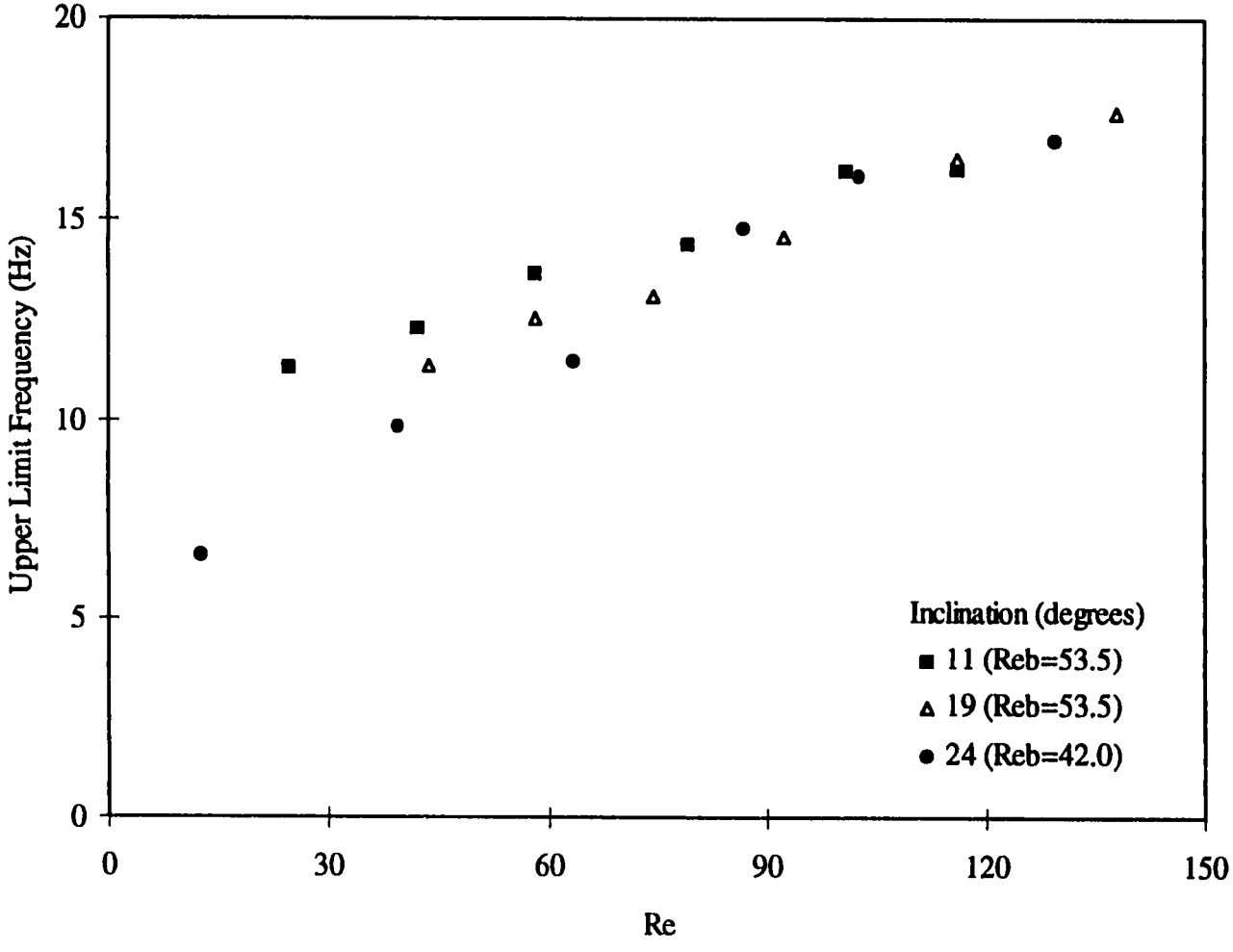

Property Number 198, Position 5 cm

Figure 2-29 Upper Limit Frequency (Different Inclinations)

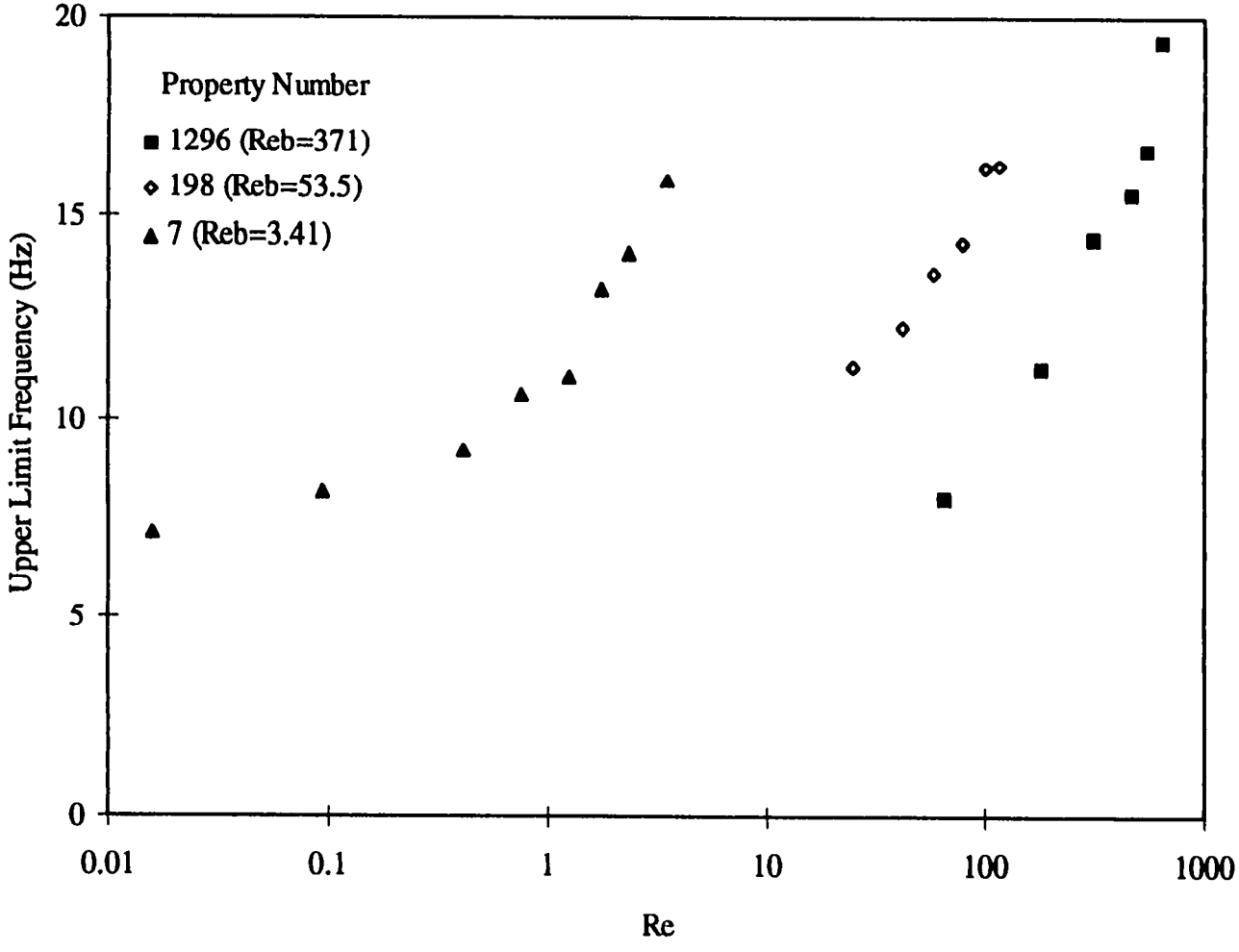

Inclination 11 degrees, Position 5 cm

Figure 2-30 Upper Limit Frequency (Different Fluids)

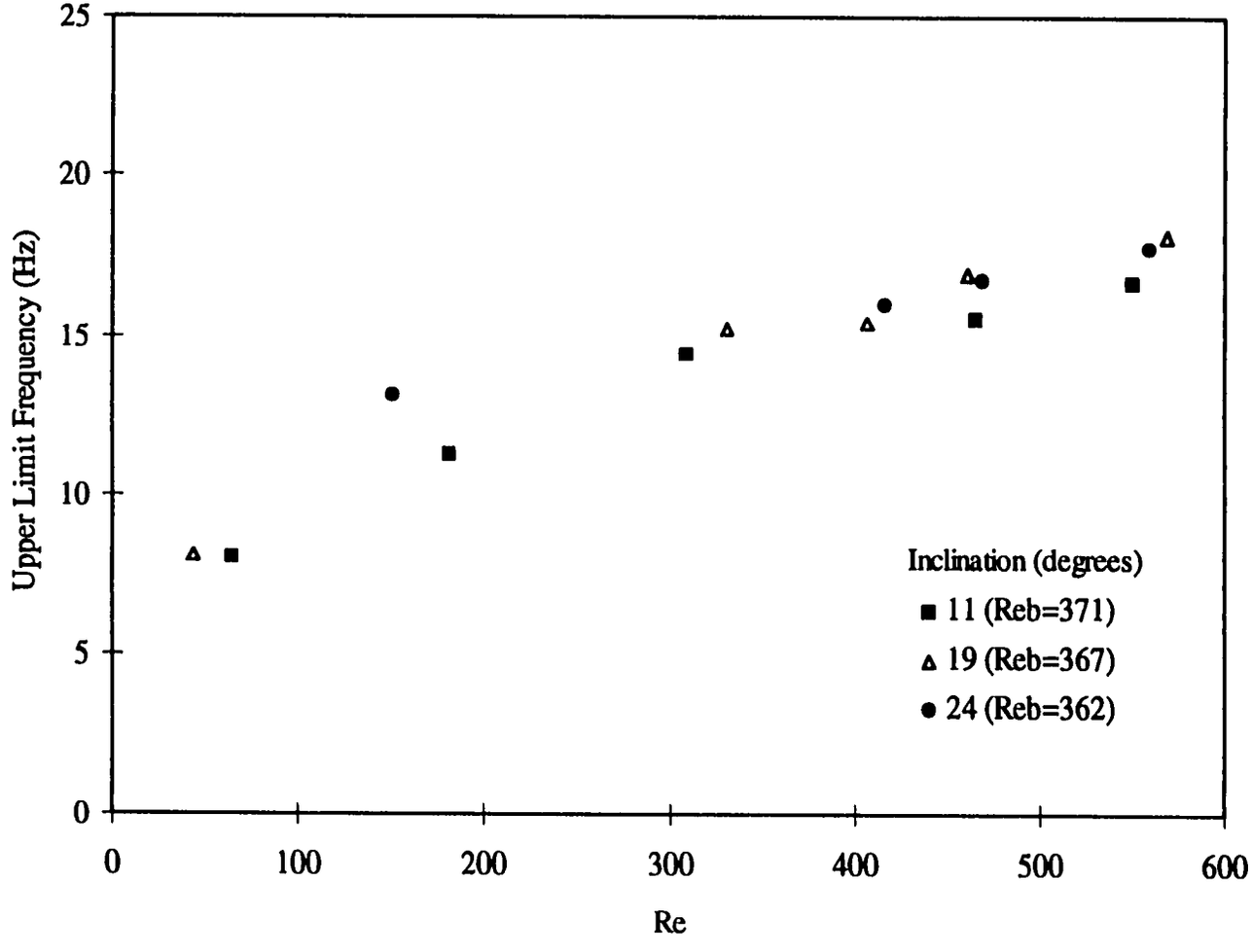

Property Number 1296, Position 5 cm

Figure 2-31 Upper Limit Frequency (Different Position)

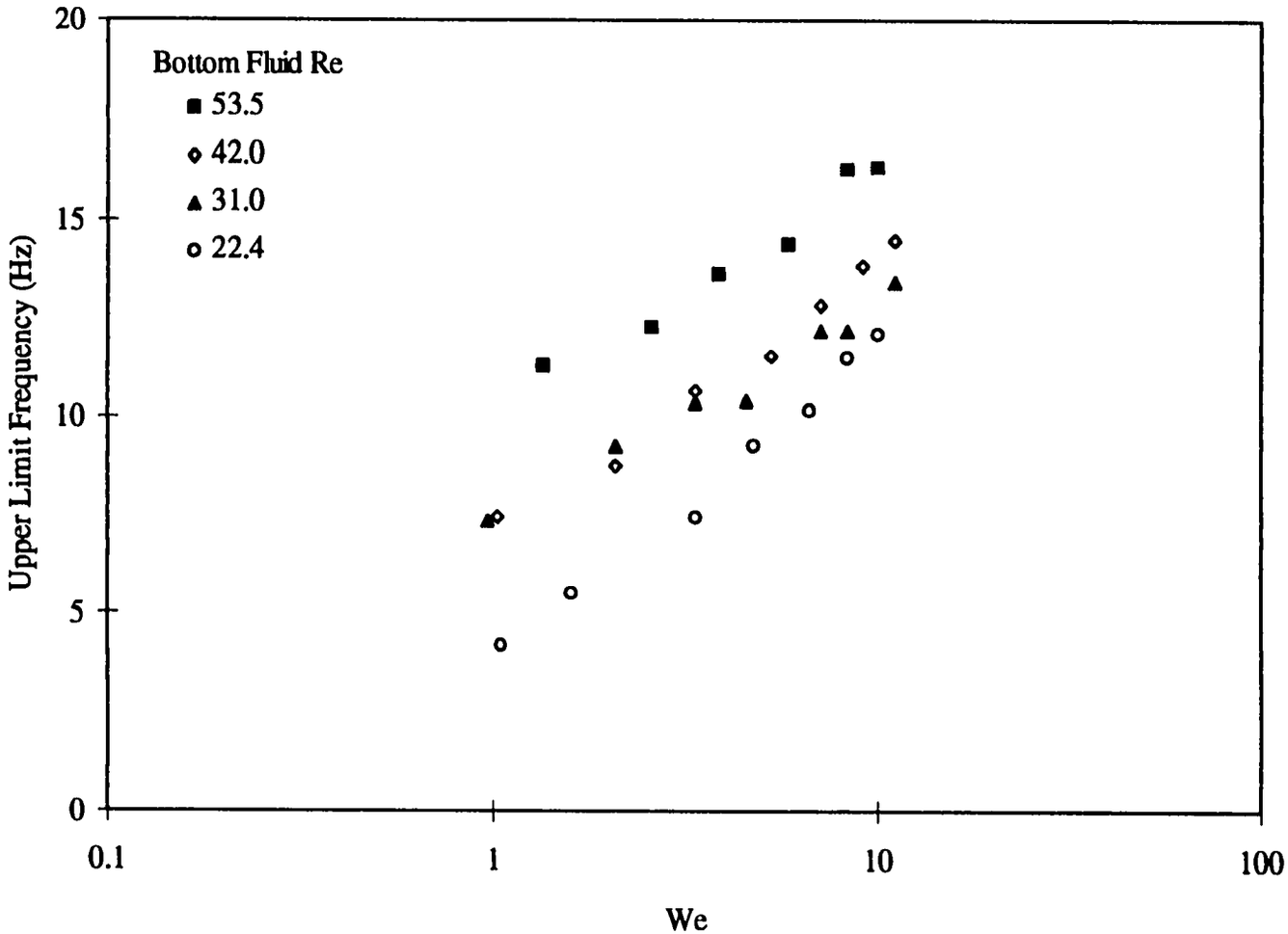

Property Number 198, Inclination 11 degrees, Position 5 cm

Figure 2-32 Upper Limit Frequency (Different Bottom Re)

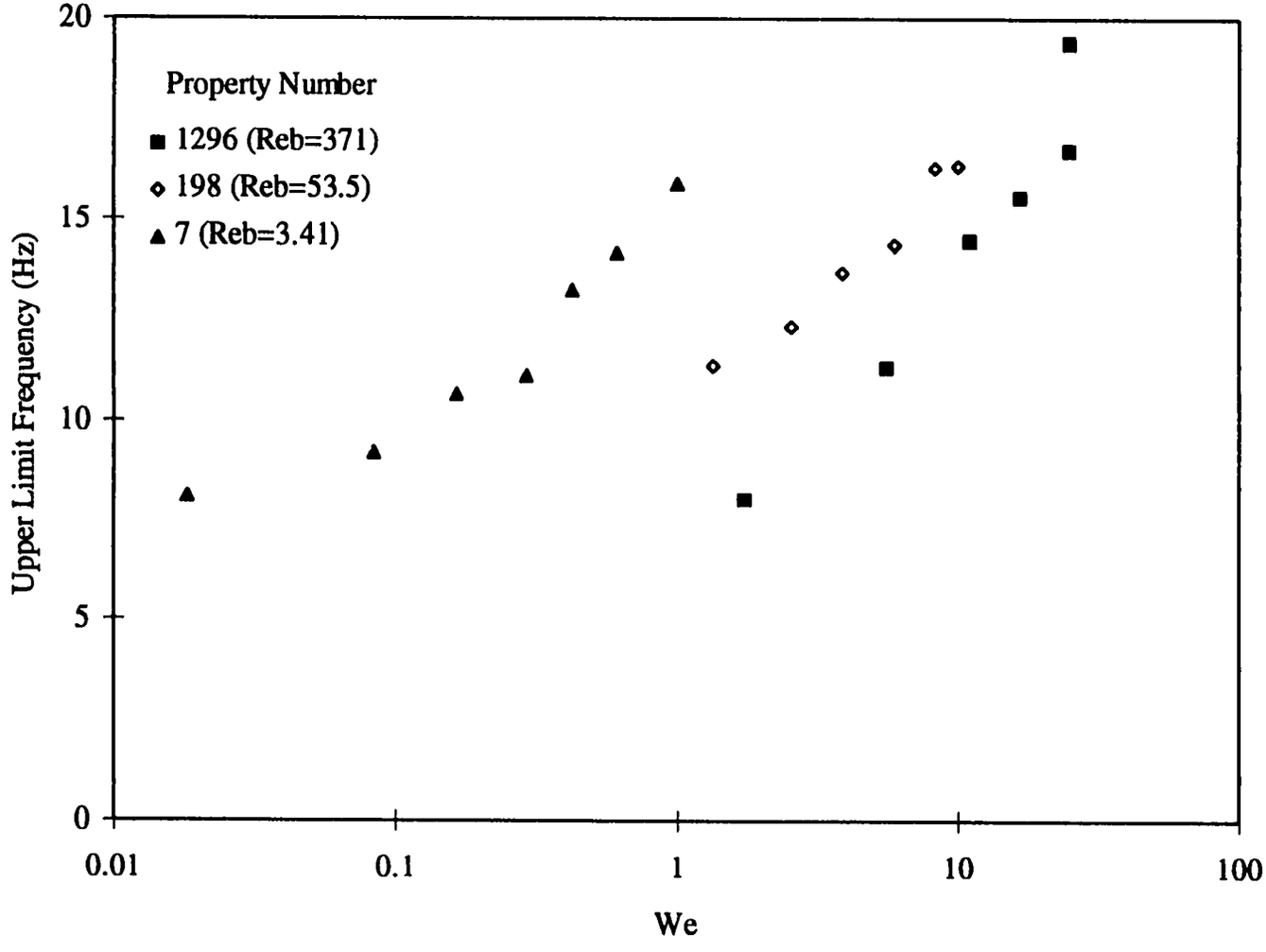

Inclination 11 degrees, Position 5 cm

Figure 2-33 Upper Limit Frequency (Different Fluids)

2.3.4 Dominant Frequencies

Higher upper flow rates correspond to higher values of the dominant frequency for all flow rates of the bottom layer (Figures 2-34, 2-35). This means that higher flow rates are associated with shorter wavelength waves

An increase in Weber number corresponds to lower surface tension energy, and consequently leads to the appearance of higher frequency disturbances (Figure 2-34). Surface tension effect is more significant for the dominant frequency than for the upper limit frequency.

Liquid physical properties have a significant influence on the type of dominant waves running over their free-surfaces. Figures 2-36 and 2-37 show this dependence versus the upper Reynolds number (Figure 2-36), and the upper Weber number (Figure 2-37). Shorter wavelength waves are dominant at lower flow rates for more viscous liquids.

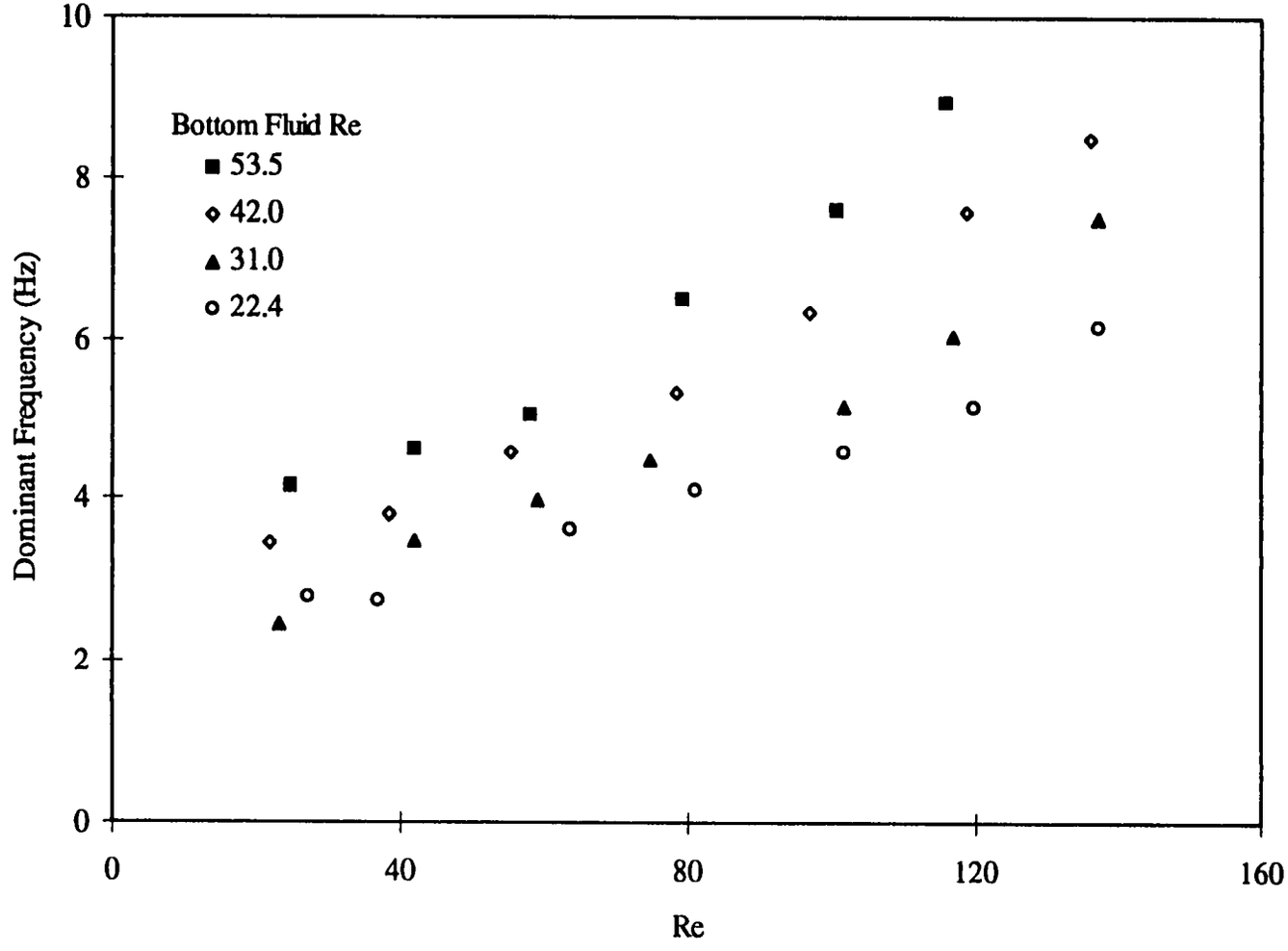

Property Number 198, Inclination 11 degrees, Position 5 cm

Figure 2-34 Dominant Frequency (Different Bottom Re)

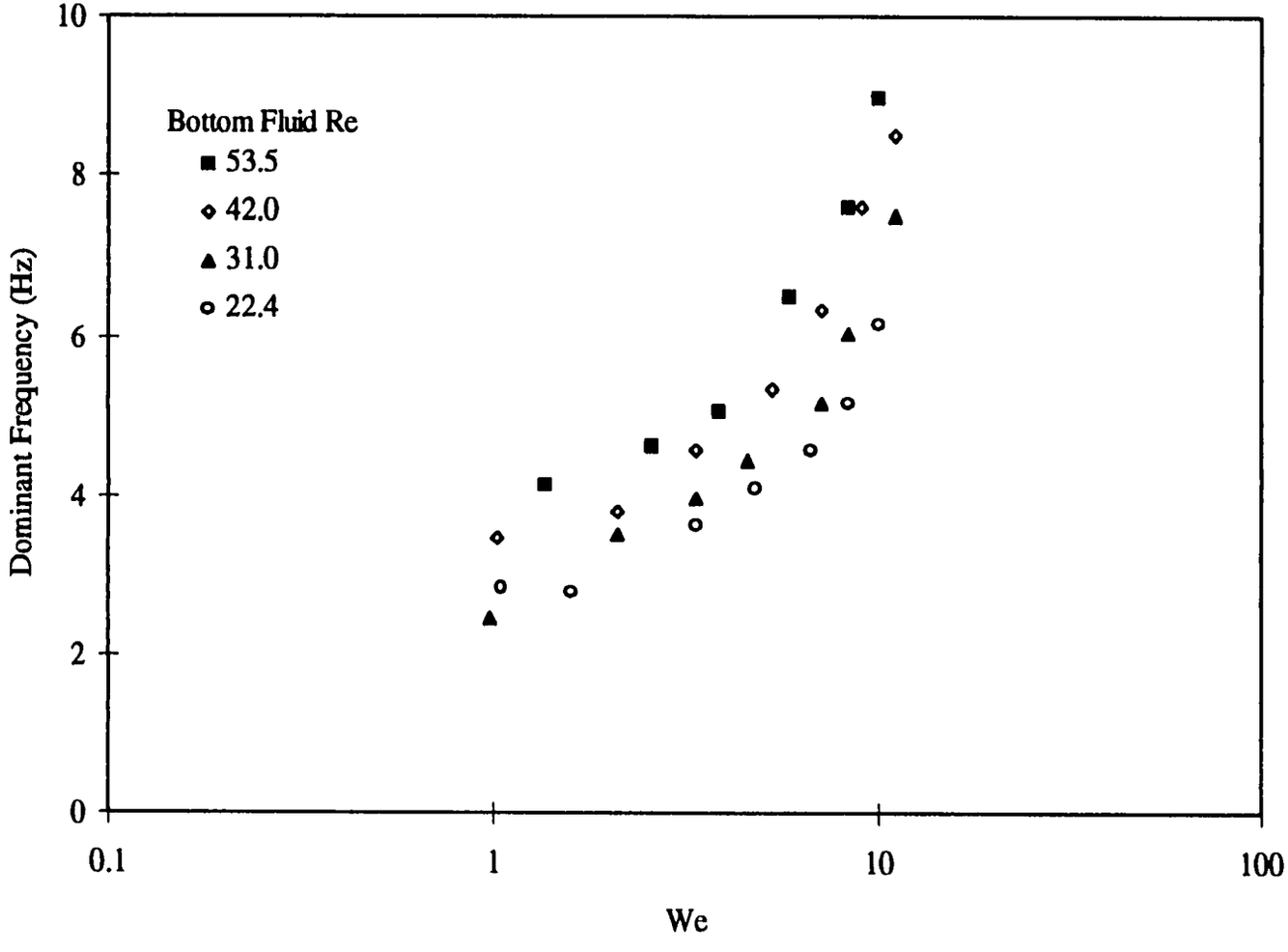

Property Number 198, Inclination 11 degrees, Position 5 cm

Figure 2-35 Dominant Frequency (Different Bottom Re)

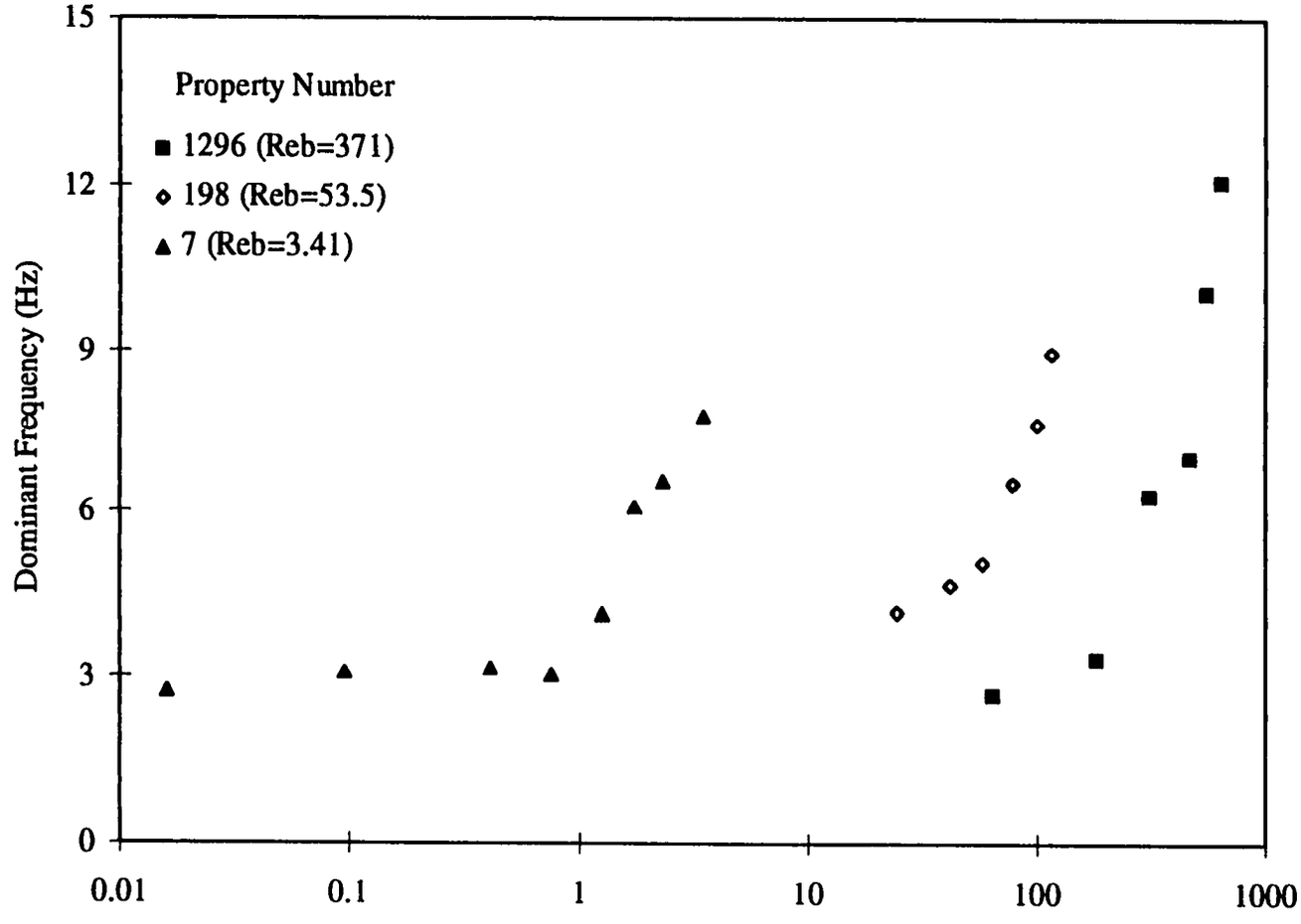

Inclination 11 degrees, Position 5 cm

Figure 2-36 Dominant Frequency (Different Fluids)

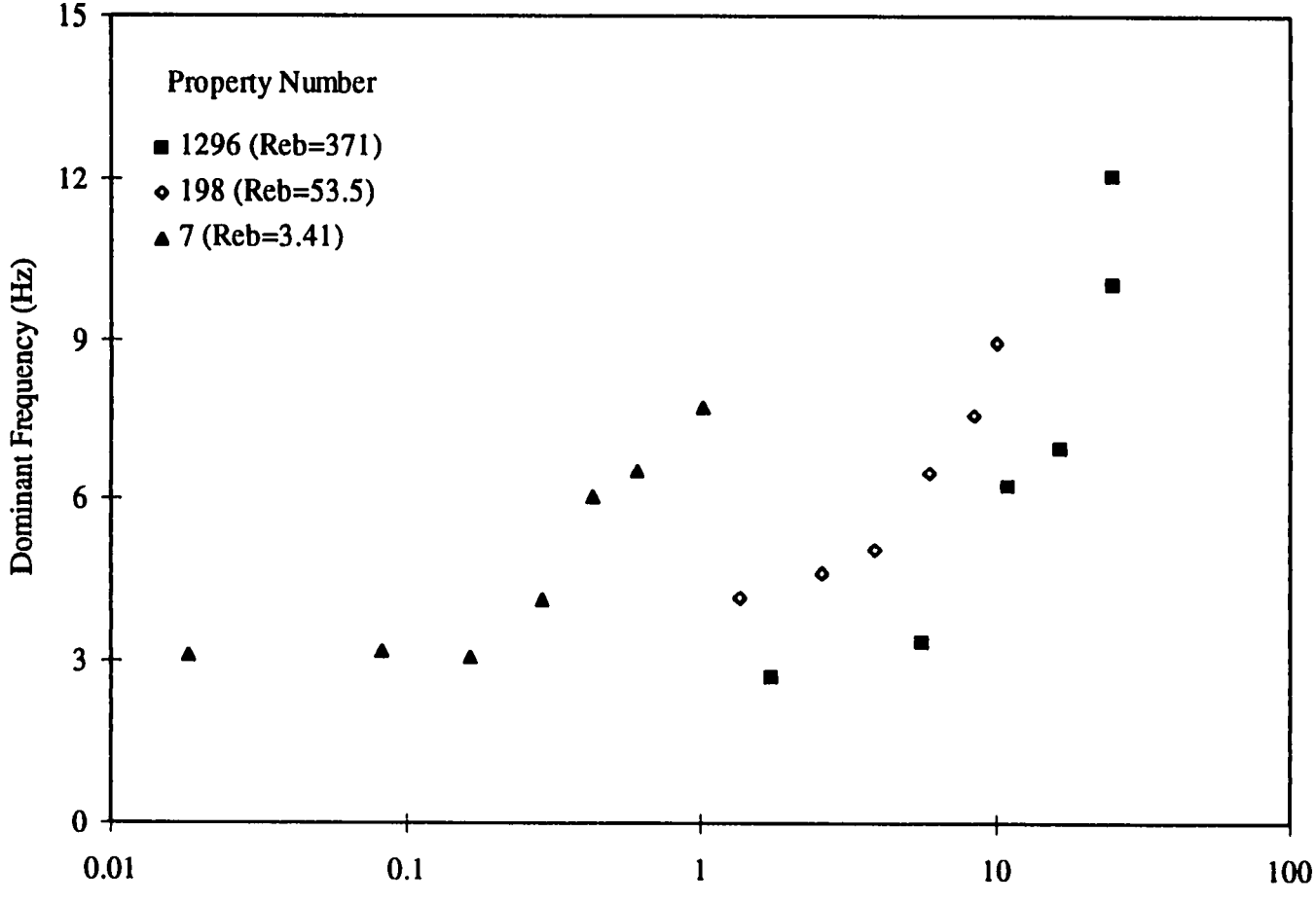

Inclination 11 degrees, Position 5 cm

Figure 2-37 Dominant Frequency (Different Fluids)

2.3.5 Maximum Relative Amplitudes

The maximum relative amplitude (MRA) of a measured wave is the maximum amplitude relative to the average signal drop from the reference signal. In this section we describe some of the results we processed for the MRA relative to the main parameters of the flow. The maximum relative amplitude remains constant for lower flow rates of the upper layer (Figures 2-38, 2-39). For the liquid $\gamma = 198$ this approximately corresponds to the range of upper Reynolds numbers Re<100 (Figure 2-39). In terms of the Weber number of the upper layer, the maximum relative amplitude remains (Figure 2-38) constant for We<5. MRA increases with higher upper Reynolds or Weber numbers.

We also notice that there is no apparent dependence of MRA on liquid properties (Figure 2-38). The angle of inclination does not seem to affect the maximum relative amplitude (Figure 2-39 to 2-41), except in one sets of data for angle 11^0 of liquid γ=198 (Figure 2-39). At position X=9 cm, which is further downstream from all previously mentioned results, the MRA remains constant past the limit Re=100 (Figure 2-39) to about Re=150 (Figure 2-40), for liquid γ=198. A better comparison of measurements at different positions X is given in Figure 2-42. It shows maximum relative amplitudes measured from three positions X=5, 11, and 17 cm from the point of inception. Only measurements from the position X=5 cm, which is the closest to inception, show an increase in MRA past Re=100.

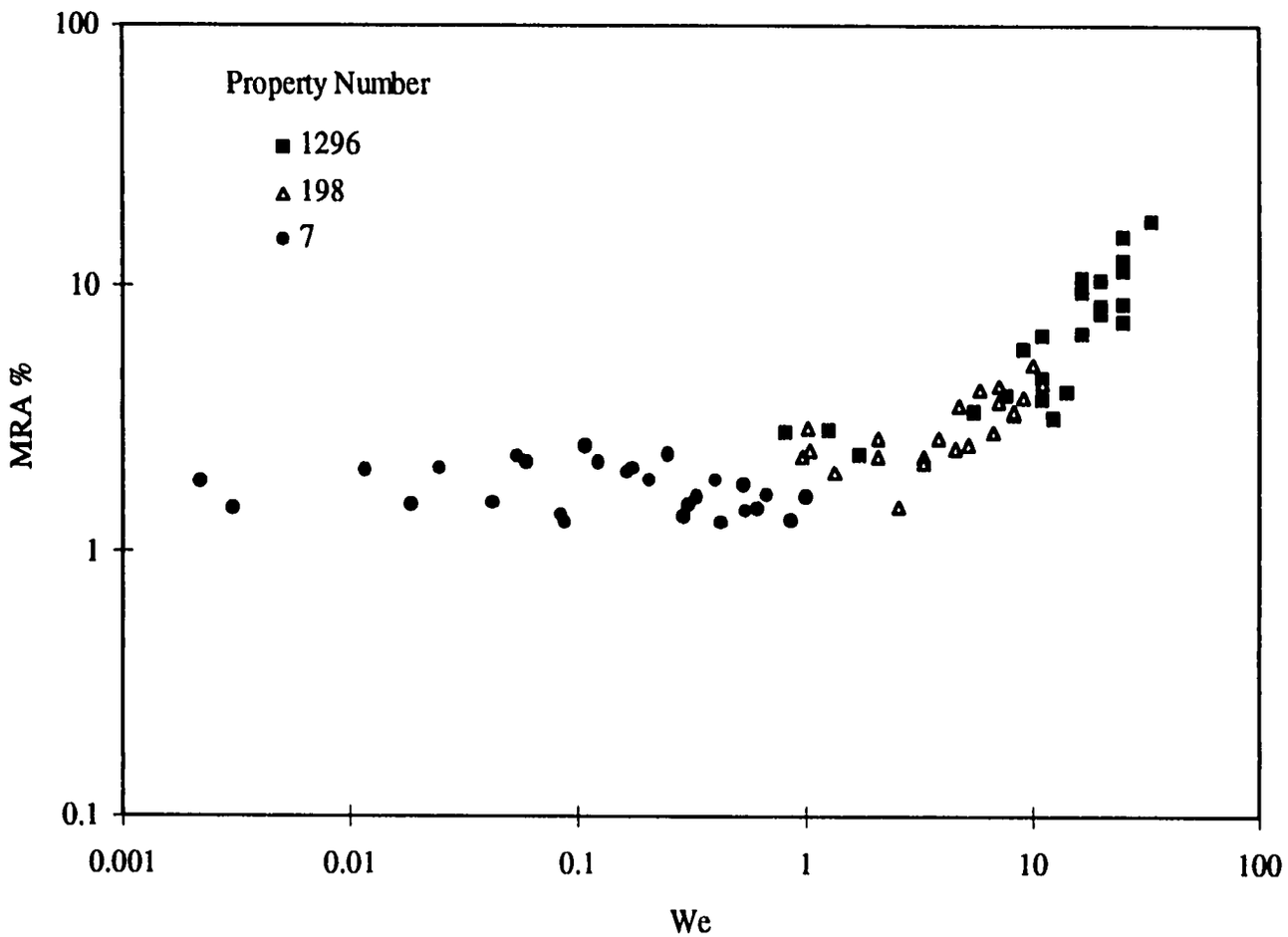

Inclination 11 degrees, Position 5 cm

Figure 2-38 Maximum Relative Amplitude (Diffrent Fluids)

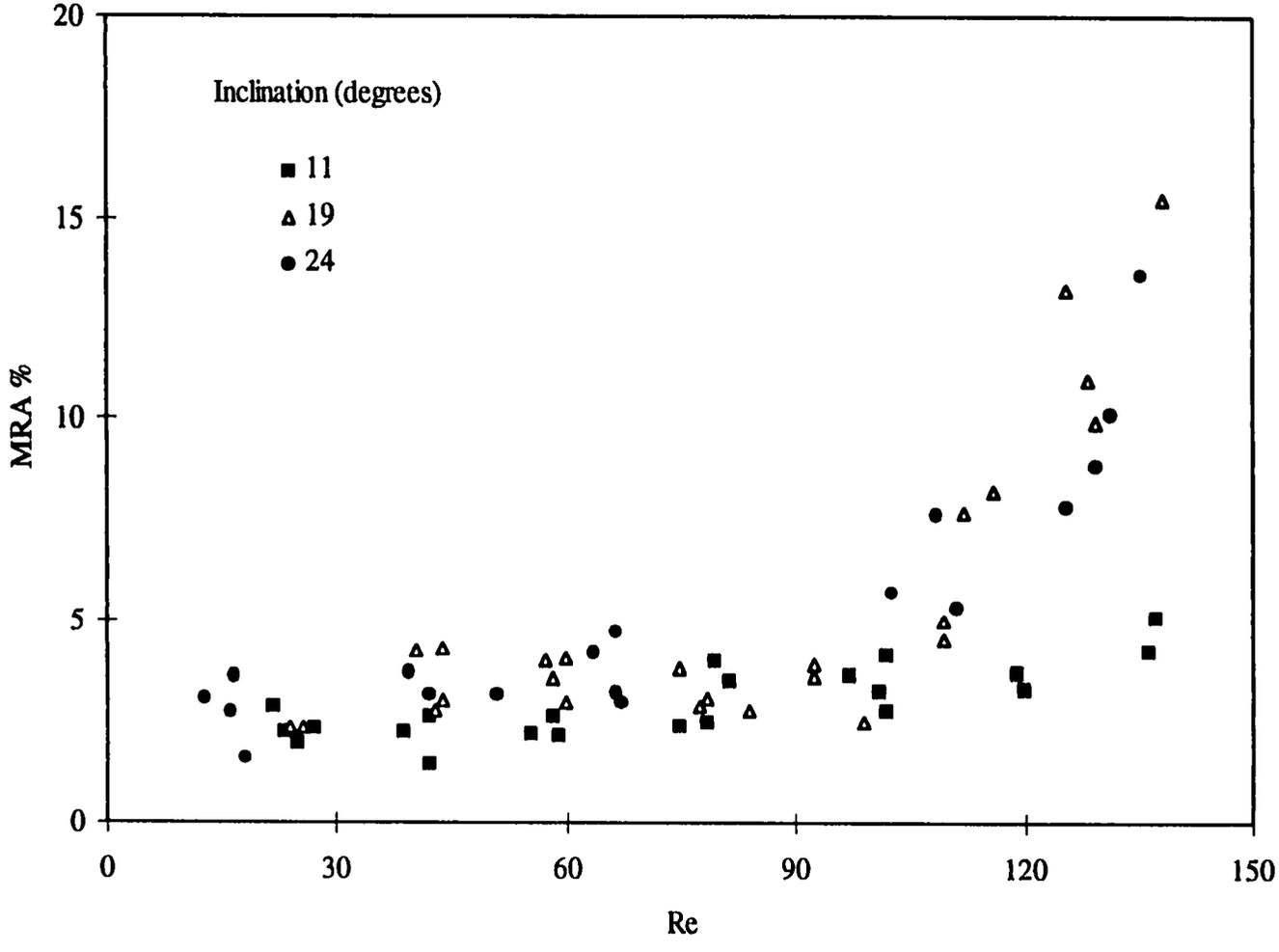

Property Number 198, Position 5 cm

Figure 2-39 Maximum Relative Amplitude

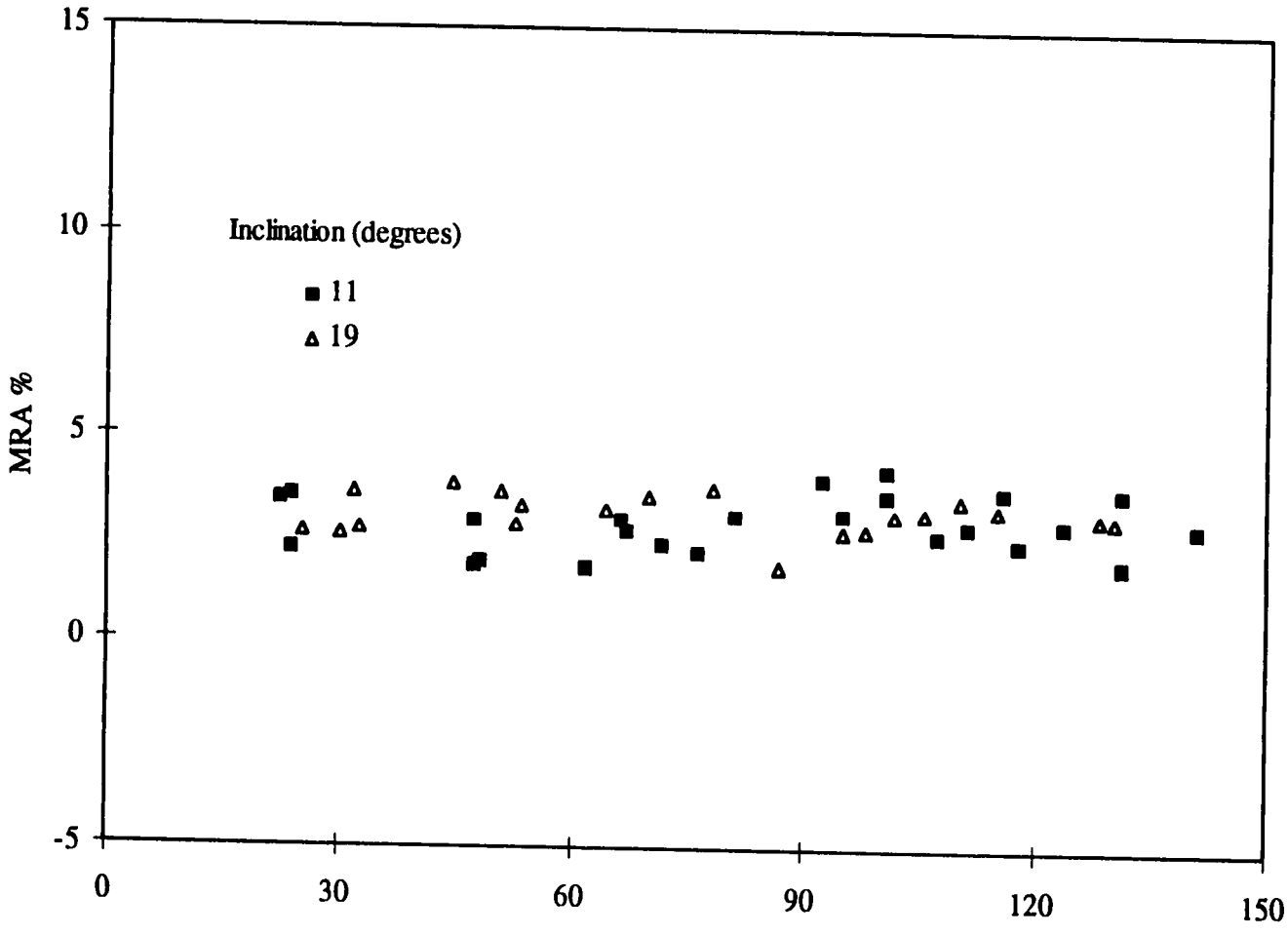

Property Number 198, Position 9 cm

Figure 2-40 Maximum Relative Amplitude

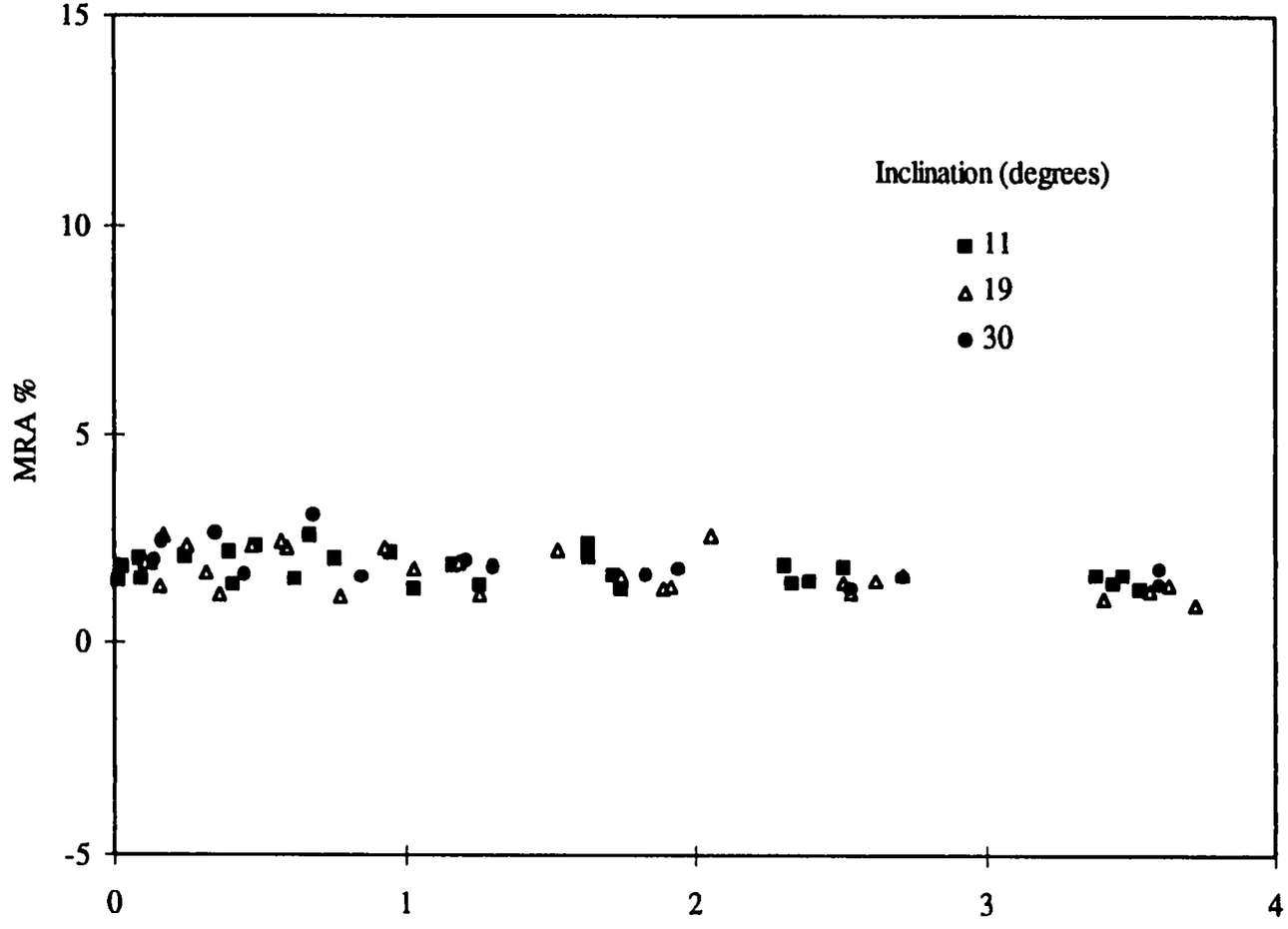

Property Number 7, Position 5 cm

Figure 2-41 Maximum Relative Amplitude

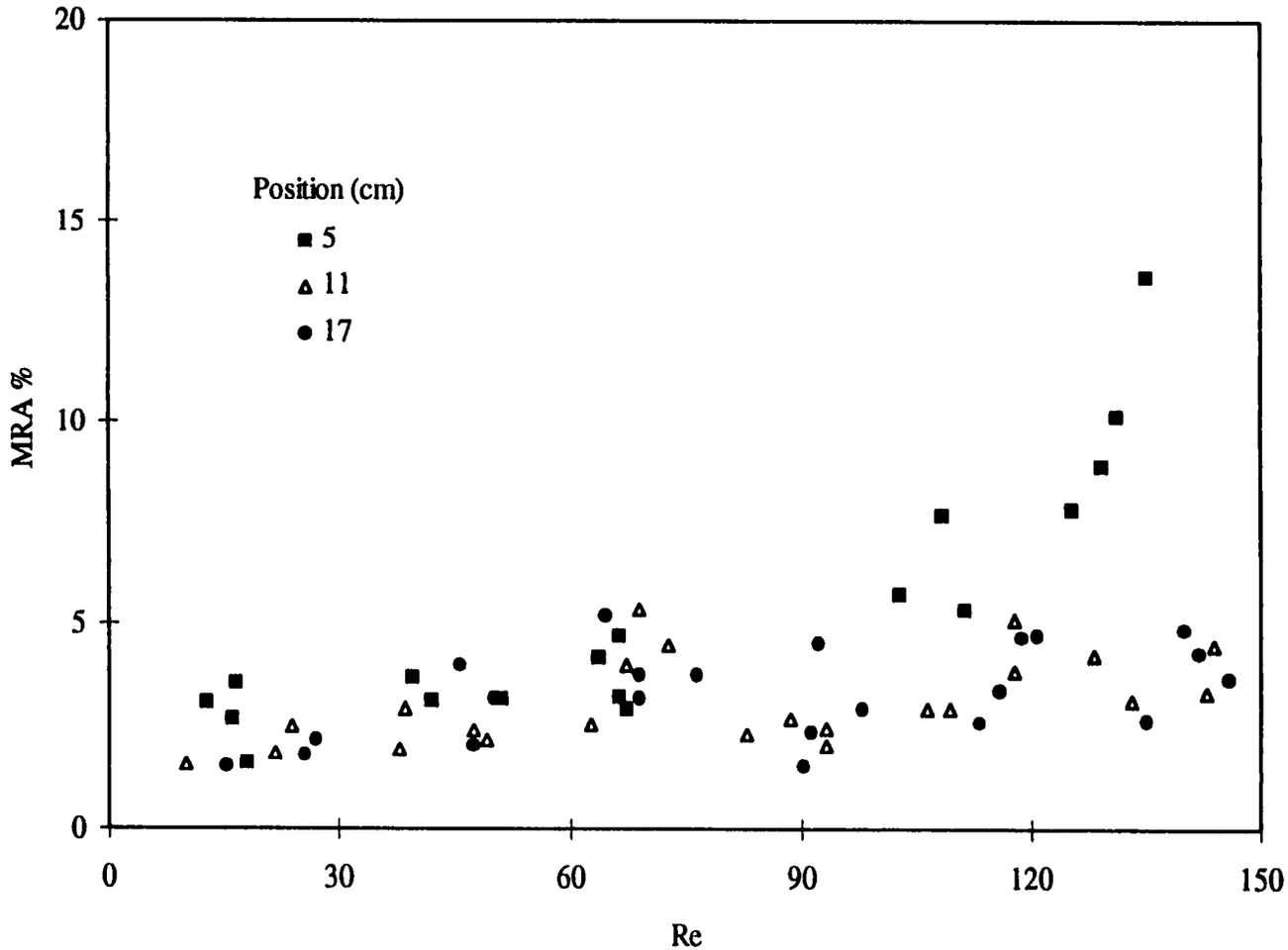

Property Number 198, Inclination 24 degrees

Figure 2-42 Maximum Relative Amplitude (Different Positions)

CHAPTER III
THE DEVELOPMENT OF COMPUTATIONAL METHOD

Time-accurate velocity and pressure distributions in the flow field is essential information for properly addressing the instability behavior of the flow system considered in this work. To do this we need to solve the unsteady state governing equations with adequate boundary conditions based on a grid system.

The existence of the free surface in our flow system creates some difficulties for the numerical simulation. At every time increment in time-propagation we need to know the free surface position for the sake of imposing the boundary conditions. However, this position is actually unknown before we get the velocity field for that time moment. The free surface as a boundary is one of the unknowns. The deformation of the free surface continuously alters the shape of the physical domain. Applying boundary fitted numerical grid generation techniques is one way to resolve this question. The method maps an irregular physical domain to a rectangular computational domain, on which finite difference formulations will be applied. The boundary lines become coordinate lines with one constant coordinate value for each section of the boundary.

Using the governing equations in primary velocity and pressure variables is necessary to properly describe the free surface and related boundary conditions. These boundary conditions are dominated by the pressure on the surface, and the alternative vorticity-streamfunction formulation of the Navier-Stokes equations could not adequately describe the pressure variable. Most of the available numerical methods for solving the Navier-Stokes equations in the velocity-pressure formulation are based on staggered grid systems (Figure 3-1). Such systems do not prescribe the pressure at the boundaries

of the computational cell. This contributes difficulties and inaccuracies in the application of the pressure-dependent boundary conditions on the free surface. In addition to this, the methods based on staggered grid systems are usually plagued by the so called numerical or false diffusion (Patankar, 1980). This is particularly so in the simulation of the flows with streamlines that do not closely conform to the grid lines. Calculation of free surface lines on staggered grids is complicated and inaccurate.

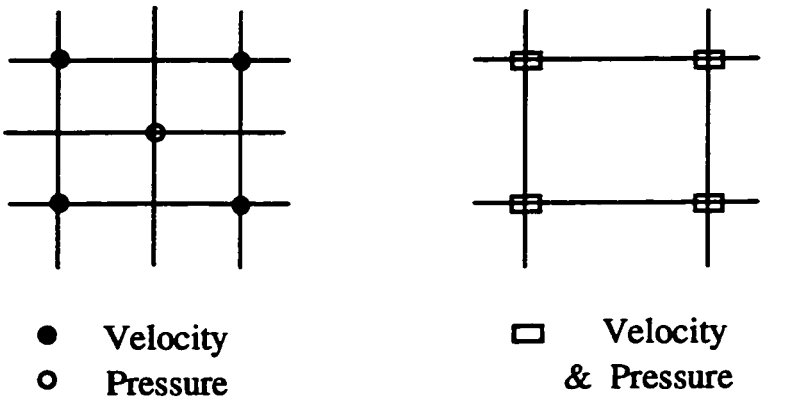

(a) staggered grid (b) non-staggered grid

Figure 3-1 Staggered Grid and non-Staggered Grid

Although the unsteady state Navier-Stokes equations are commonly used in the simulation of steady state system, the methods used in these cases usually do not give physically meaningful results for intermediate time intervals before the steady state is reached, and are not suitable for producing the real physical results of a transient state.

In this chapter the basic method of numerical grid generation will be discussed in detail. After this, the development of a new computational method, which can give physically meaningful solutions for all physical time levels, and some test results will be presented.

3.1 Grid Generation

3.1.1 Boundary-Fitted Coordinate Systems

Boundaries of flow regions that are primarily boundaries between solid and fluid are generally dominant in determining the character of the solution. So, it is imperative to accurately represent the boundary conditions in the finite difference formulation. For problems with regular straight boundaries finite-difference schemes are not a difficult task. However, for problems with irregular curved boundaries this will be difficult. The difficulty is that the boundary conditions are usually applied in these cases by interpolation between the grid points of the rectangular mesh, through which a curved boundary is passing.

The use of interpolation methods may lead to poor application of the boundary conditions. Besides, the large number of grid points involved will complicate computer codes. The situation can be alleviated by using boundary-fitted coordinate systems. This procedure eliminates the shape of the boundaries as a complicating factor and allows the problems with arbitrary boundaries to be treated essentially in the same way as that with simple boundaries. All computation can be done on a rectangular transformed field with a square mesh regardless of the shape or configuration of boundaries in the physical domain.

The technique of boundary-fitted coordinate systems is based on the transformation that maps the physical Cartesian coordinates to a general curvilinear coordinate system that has a coordinate line coincident with each boundary of a general multi-connected region involving any number of arbitrarily shaped boundaries. The transformation can be done by algebraic transformations, by differential equation transformations, and by conformal mapping techniques based on complex variables.

Algebraic transformations are difficult to apply if some sections of the physical boundaries cannot be expressed by algebraic equations. Besides, the smoothness of grids generated is heavily dependent on the shape of the physical boundaries.

Conformal mappings based on complex variables are limited to 2-D problems. In addition, the determination of the mapping function is sometimes a difficult task. The differential equation methods have better flexibility in their application to arbitrary boundaries, and yield better smoothness of the grid generated. Differential equation methods can be classified as parabolic, elliptic, and hyperbolic methods according to the form of the equations used. For closed boundary domains, elliptic transformations are usually used.

3.1.2 Basic Concepts

If the Cartesian coordinates in the physical domain are denoted by x and y, and the general curvilinear coordinates by ζ and η, then the basic problem of numerical grid generation is finding the transformation from x and y to ζ and η.

$$\zeta=\zeta(x,y) \tag{3-1a}$$
$$\eta=\eta(x,y) \tag{3-1b}$$

From these two equations we can obtain the following differential expressions:

$$d\zeta=\frac{\partial\zeta}{\partial x}dx+\frac{\partial\zeta}{\partial y}dy \tag{3-2a}$$
$$d\eta=\frac{\partial\eta}{\partial x}dx+\frac{\partial\eta}{\partial y}dy \tag{3-2b}$$

which are written in a compact form as

$$\begin{vmatrix} d\zeta \\ d\eta \end{vmatrix}=\begin{vmatrix} \frac{\partial\zeta}{\partial x} & \frac{\partial\zeta}{\partial y} \\ \frac{\partial\eta}{\partial x} & \frac{\partial\eta}{\partial y} \end{vmatrix}\begin{vmatrix} dx \\ dy \end{vmatrix} \tag{3-3}$$

Reversing the role of independent variables in Equation (3-1), we can write

$$x=x(\zeta,\eta) \tag{3-4a}$$
$$y=y(\zeta,\eta) \tag{3-4b}$$

Similarly, for the above equations we can have the following differential expressions in a compact form.

$$\begin{vmatrix} dx \\ dy \end{vmatrix} = \begin{vmatrix} \frac{\partial x}{\partial \zeta} & \frac{\partial x}{\partial \eta} \\ \frac{\partial y}{\partial \zeta} & \frac{\partial y}{\partial \eta} \end{vmatrix} \begin{vmatrix} d\zeta \\ d\eta \end{vmatrix} \tag{3-5}$$

Comparing Equation (3-3) and (3-5), it can be concluded that

$$\begin{vmatrix} \frac{\partial \zeta}{\partial x} & \frac{\partial \zeta}{\partial y} \\ \frac{\partial \eta}{\partial x} & \frac{\partial \eta}{\partial y} \end{vmatrix} = \begin{vmatrix} \frac{\partial x}{\partial \zeta} & \frac{\partial x}{\partial \eta} \\ \frac{\partial x}{\partial \zeta} & \frac{\partial x}{\partial \eta} \end{vmatrix}^{-1} \tag{3-6}$$

from which $$\frac{\partial \zeta}{\partial x} = \frac{1}{J}\frac{\partial y}{\partial \eta} \qquad \frac{\partial \zeta}{\partial y} = -\frac{1}{J}\frac{\partial x}{\partial \eta} \tag{3-7a}$$

$$\frac{\partial \eta}{\partial x} = -\frac{1}{J}\frac{\partial y}{\partial \zeta} \qquad \frac{\partial \eta}{\partial y} = \frac{1}{J}\frac{\partial x}{\partial \zeta} \tag{3-7b}$$

where, $$J = \frac{\partial x}{\partial \zeta}\frac{\partial y}{\partial \eta} - \frac{\partial x}{\partial \eta}\frac{\partial y}{\partial \zeta} \tag{3-8}$$

The Jacobian, J, is interpreted as the ratio of the area (volume in 3-D) in the computational space to that of the physical space.

The desired transformation (3-1) will turn an irregular physical space into a rectangular computational space. Figure 3-2 is a graphical illustration of the transformation between the coordinate systems. The physical space bounded by the curve abcda corresponds to the computational space bounded by ABCDA. The boundary segments ab, bc, cd, da correspond to the segments AB, BC, CD, and DA, respectively. The grid point p in physical space corresponds to the grid point P in computational space.

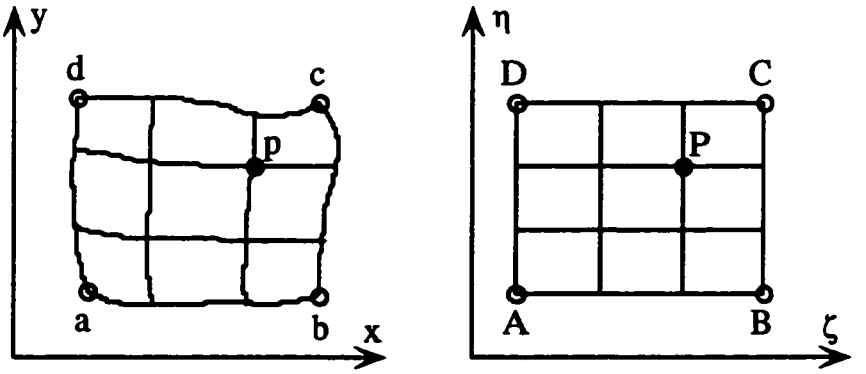

(a) physical space (b) Computational space

Figure 3-2 Grid Transformation

In determining the grid points, a few constraints must be imposed. First, the transformation must be single-valued, i.e. grid lines of the same family must not cross each other. Secondly, from a numerical point of view, a smooth distribution of grid points is required.

3.1.3 Elliptic Grid Generation

In this method a system of elliptic equations in the form of a Laplace equation or Poisson equation is solved for the location of the grid points in the physical space, whereas the computational domain is a rectangular shape with uniform grid spacing. For domains where all the physical boundaries are specified, elliptic grid generation works very well. It is commonly used for 2-D problems and has been extended to 3-D problems (Hoffmann, 1989).

For a closed domain, the distribution of grid points on the boundaries are specified and a set of elliptic partial differential equations is solved to locate the coordinates of the interior grid points.

$$\frac{\partial^2 \zeta}{\partial x^2} + \frac{\partial^2 \zeta}{\partial y^2} = 0 \qquad (3\text{-}9a)$$

$$\frac{\partial^2 \eta}{\partial x^2} + \frac{\partial^2 \eta}{\partial y^2} = 0 \qquad (3\text{-}9b)$$

The above equations can be easily solved by some iterative techniques, such as, Gauss-Seidel, point Successive Over Relaxation. However, computations must take place in a rectangular domain with uniform grid spacing. So the dependent and independent variables in Equation (3-9) have to be interchanged by using Equation (3-7). This leads to the equations

$$\alpha\frac{\partial^2 x}{\partial\zeta^2}-2\beta\frac{\partial^2 x}{\partial\zeta\partial\eta}+\gamma\frac{\partial^2 x}{\partial\eta^2}=0 \qquad (3\text{-}10a)$$

$$\alpha\frac{\partial^2 y}{\partial\zeta^2}-2\beta\frac{\partial^2 y}{\partial\zeta\partial\eta}+\gamma\frac{\partial^2 y}{\partial\eta^2}=0 \qquad (3\text{-}10b)$$

where

$$\alpha=(\frac{\partial x}{\partial\eta})^2+(\frac{\partial y}{\partial\eta})^2 \qquad (3\text{-}11a)$$

$$\beta=\frac{\partial x}{\partial\zeta}\frac{\partial y}{\partial\eta}+\frac{\partial x}{\partial\eta}\frac{\partial y}{\partial\zeta} \qquad (3\text{-}11b)$$

$$\gamma=(\frac{\partial x}{\partial\zeta})^2+(\frac{\partial y}{\partial\zeta})^2 \qquad (3\text{-}11c)$$

The system of elliptic equations (3-10) is solved in the computational domain (ζ, η) in order to provide the grid point locations in the physical domain (x, y). The equations are nonlinear. They can be linearized by a simple procedure. Usually, the coefficients α, β and γ are lagged one step, i.e. evaluated at the previous iteration level.

Finite difference equations are simplified by using a uniform grid spacing in the computational domain. In our calculations $\Delta\zeta = \Delta\eta = 1$ is used. Applying a central finite difference scheme to Equation (3-10) and rearranging the resulting equation we have

$$x_{i,j}=[\alpha(x_{i+1,j}+x_{i-1,j})+\gamma(x_{i,j+1}+x_{i,j-1})-\frac{1}{2}\beta(x_{i+1,j+1}+x_{i-1,j-1}-x_{i+1,j-1}-x_{i-1,j+1})]/[2(\alpha+\gamma)] \qquad (3\text{-}12a)$$

$$y_{i,j}=[\alpha(y_{i+1,j}+y_{i-1,j})+\gamma(y_{i,j+1}+y_{i,j-1})-\frac{1}{2}\beta(y_{i+1,j+1}+y_{i-1,j-1}-y_{i+1,j-1}-y_{i-1,j+1})]/[2(\alpha+\gamma)] \qquad (3\text{-}12b)$$

Successive Over Relaxation method is employed in this work to the resulting linear algebraic equations. In order to accelerate convergence, an over-relaxation factor ω is introduced. The common optimal value, ω=1.7, is used in our calculations. Then we have

$$x^{k+1}_{i,j} = (1-\omega)x^{k}_{i,j} + \omega[\alpha(x_{i+1,j} + x_{i-1,j}) + \gamma(x_{i,j+1} + x_{i,j-1}) - \frac{1}{2}\beta(x_{i+1,j+1} + x_{i-1,j-1} - x_{i+1,j-1} - x_{i-1,j+1})]/[2(\alpha+\gamma)] \qquad (3\text{-}13a)$$

$$y^{k+1}_{i,j} = (1-\omega)y^{k}_{i,j} + \omega[\alpha(y_{i+1,j} + y_{i-1,j}) + \gamma(y_{i,j+1} + y_{i,j-1}) - \frac{1}{2}\beta(y_{i+1,j+1} + y_{i-1,j-1} - y_{i+1,j-1} - y_{i-1,j+1})]/[2(\alpha+\gamma)] \qquad (3\text{-}13b)$$

where, k is the iteration index.

An example of a grid generated by this procedure is shown in Figure 3-3. The top boundary of the physical domain is specified by

$$y = 1 + 0.2\,x\sin(2\pi x) \qquad (3\text{-}14)$$

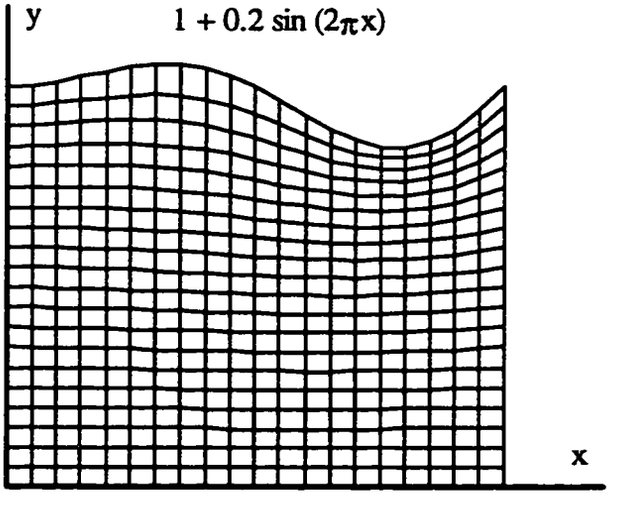

Figure 3-3 Grid Generated by Laplace Equation with Grid Points Evenly Distributed on The All Boundaries

Grid points are equally spaced on the boundaries. The grid generated is very smooth and more or less is equally spaced over the entire domain. When the grid points are not equally spaced on the boundaries, the grid generated by this procedure is not smooth

and has very large changes in the metric coefficients (3-8) and (3-11) near the boundaries. The large change in the metric coefficients of the grid will cause large errors in numerical calculation.

Figure 3-4 shows the grid generated by this procedure with unequally spaced boundary grid points. The physical domain is the same as that in Figure 3-3. The grid distribution along the left and right boundaries is described by

$$y_j = \frac{\log j}{\log jmax} \qquad (j = 1, 2, \ldots \ldots jmax\text{-}1, jmax) \qquad (3\text{-}15)$$

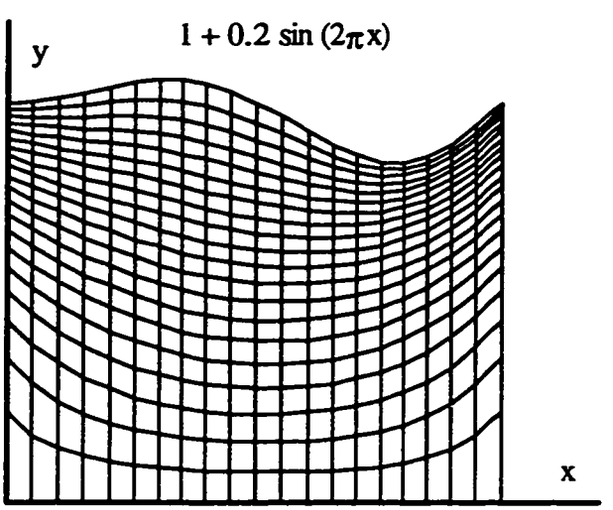

Figure 3-4 Grid Generated by Laplace Equation with Grid Points Concentrated toward The Top Boundary

It can be seen from Figure 3-4 that the space between grid lines in the field is not greatly affected by the distribution of the boundary points, except in the close neighborhood of the boundaries. In applications, flow parameters might change dramatically in certain regions. In order to catch these changes in detail and get the results in better accuracy, grid clustering in the region is desired and, sometimes necessary. Use of the Laplace Equation (3-9) without clustering will not satisfactory.

3.1.4 Control of Grid Distribution

The control functions, $P(\zeta,\eta)$ and $Q(\zeta,\eta)$ have to be introduced in the right hand side of Equation (3-9) for better control over grid-points distribution in the interior of the domain. Poisson's equation will be used

$$\frac{\partial^2\zeta}{\partial x^2}+\frac{\partial^2\zeta}{\partial y^2}=P(\zeta,\eta) \tag{3-16a}$$

$$\frac{\partial^2\eta}{\partial x^2}+\frac{\partial^2\eta}{\partial y^2}=Q(\zeta,\eta) \tag{3-16b}$$

Using Equation (3-7), they become

$$\alpha\frac{\partial^2 x}{\partial\zeta^2}-2\beta\frac{\partial^2 x}{\partial\zeta\partial\eta}+\gamma\frac{\partial^2 x}{\partial\eta^2}=-\frac{1}{J^2}\left(P\frac{\partial x}{\partial\zeta}+Q\frac{\partial x}{\partial\eta}\right) \tag{3-17a}$$

$$\alpha\frac{\partial^2 y}{\partial\zeta^2}-2\beta\frac{\partial^2 y}{\partial\zeta\partial\eta}+\gamma\frac{\partial^2 y}{\partial\eta^2}=-\frac{1}{J^2}\left(P\frac{\partial y}{\partial\zeta}+Q\frac{\partial y}{\partial\eta}\right) \tag{3-17b}$$

Thompson (1980) defined the control functions P and Q in the following form:

$$\begin{aligned}P(\zeta,\eta)=&-\sum_{i=1}^{n} a_i\,\mathrm{sgn}(\zeta-\zeta_i)\exp[-c_i|\zeta-\zeta_i|]\\&-\sum_{j=1}^{m} b_j\,\mathrm{sgn}(\zeta-\zeta_j)\exp[-d_j\sqrt{(\zeta-\zeta_j)^2+(\eta-\eta_j)^2}]\end{aligned} \tag{3-18a}$$

$$\begin{aligned}Q(\zeta,\eta)=&-\sum_{i=1}^{n} a_i\,\mathrm{sgn}(\eta-\eta_i)\exp[-c_i|\eta-\eta_i|]\\&-\sum_{j=1}^{m} b_j\,\mathrm{sgn}(\eta-\eta_j)\exp[-d_j\sqrt{(\zeta-\zeta_j)^2+(\eta-\eta_j)^2}]\end{aligned} \tag{3-18b}$$

They can be used to cluster the grid points towards the line $\zeta = \zeta_i$ and $\eta = \eta_i$, and towards a point (ζ_i, η_i). In Equation (3-18) 'a' and 'b' are the amplification factors and 'c' and 'd' the decay factors. Coefficients a, b, c, d and ζ_i, η_i are specified. The determination of these constant values can be achieved by trial and error for a specific problem. This procedure might be very complicated, or unacceptable in some cases.

A very efficient method is introduced by Thomas and Middlehoff (1980). They write Poisson's equation in the following form:

$$\frac{\partial^2\zeta}{\partial x^2}+\frac{\partial^2\zeta}{\partial y^2}=\phi(\zeta,\eta)[(\frac{\partial\zeta}{\partial x})^2+(\frac{\partial\zeta}{\partial y})^2] \qquad (3\text{-}19a)$$

$$\frac{\partial^2\eta}{\partial x^2}+\frac{\partial^2\eta}{\partial y^2}=\psi(\zeta,\eta)[(\frac{\partial\eta}{\partial x})^2+(\frac{\partial\eta}{\partial y})^2] \qquad (3\text{-}19b)$$

where ϕ and ψ are direct control parameters. The corresponding form in (ζ, η) is

$$\alpha(\frac{\partial^2 x}{\partial\zeta^2}+\phi\frac{\partial x}{\partial\zeta})-2\beta\frac{\partial^2 x}{\partial\zeta\partial\eta}+\gamma(\frac{\partial^2 x}{\partial\eta^2}+\psi\frac{\partial x}{\partial\eta})=0 \qquad (3\text{-}20a)$$

$$\alpha(\frac{\partial^2 y}{\partial\zeta^2}+\phi\frac{\partial y}{\partial\zeta})-2\beta\frac{\partial^2 y}{\partial\zeta\partial\eta}+\gamma(\frac{\partial^2 y}{\partial\eta^2}+\psi\frac{\partial y}{\partial\eta})=0 \qquad (3\text{-}20b)$$

If we demand that the grid lines are orthogonal at the boundaries, the ϕ and ψ on the boundaries can be written as

$$\phi=-(\frac{\partial x}{\partial\zeta}\frac{\partial^2 x}{\partial\zeta^2}+\frac{\partial y}{\partial\zeta}\frac{\partial^2 y}{\partial\zeta^2})\Big/[(\frac{\partial x}{\partial\zeta})^2+(\frac{\partial y}{\partial\zeta})^2] \qquad \text{on } \eta=\eta_b \qquad (3\text{-}21a)$$

$$\psi=-(\frac{\partial x}{\partial\eta}\frac{\partial^2 x}{\partial\eta^2}+\frac{\partial y}{\partial\eta}\frac{\partial^2 y}{\partial\eta^2})\Big/[(\frac{\partial x}{\partial\eta})^2+(\frac{\partial y}{\partial\eta})^2] \qquad \text{on } \zeta=\zeta_b \qquad (3\text{-}21b)$$

The values of ϕ and ψ at the interior grid-points can be obtained by a linear interpolation method along the lines of ζ= constant and η = constant, respectively. Equations (3-20) are then solved by the same method mentioned in the section 3.1.3. The role of ϕ and ψ is to bring the governing action of the boundary grid points deep inside the domain. The grid generated by this method has better smoothness and is orthogonal to the boundary at the boundaries.

Figure 3-5 shows the grid generated by this new method. The same physical domain and boundary grid points distribution are used. Clearly, it is much smoother than that generated by Equation (3-9). Good grid clustering in the entire domain can be achieved by a well designed grid distribution on the boundaries. The function used to define a grid-points distribution on the boundaries is called the stretching function.

The commonly used stretching functions are the power functions of order 2, 3, or higher, exponential and hyperbolic functions. In the domain of computational fluid mechanics exponential or hyperbolic functions are the best choices. Typical stretching functions for one-side clustering, two-side clustering, and center clustering can be found in Cao's work (Cao, 1993). By using these functions one can create any combination of grid points clustering in a physical domain.

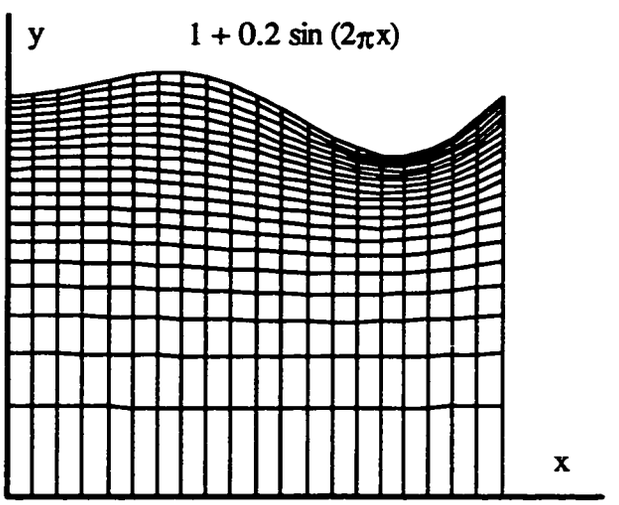

Figure 3-5 Grid Generated by Poisson Equation with Direct Control Method

3.2 Description of the Method

3.2.1 Governing Equations

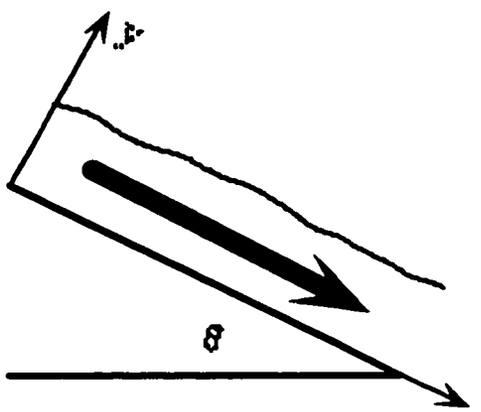

Figure 3-6 Inclined Falling Film Flow

The governing equations of the flow of an incompressible fluid are the Navier-Stokes (momentum) equations and continuity equation. For the flow system considered in this work (Figure 3-6), their dimensionless conservation forms in Cartesian coordinates (x, y) are

$$\frac{\partial u}{\partial t}+\frac{\partial u^2}{\partial x}+\frac{\partial uv}{\partial y}+\frac{\partial p}{\partial x}=\frac{1}{Re}\left(\frac{\partial^2 u}{\partial x^2}+\frac{\partial^2 u}{\partial y^2}\right)+F_x \qquad (3\text{-}22a)$$

$$\frac{\partial v}{\partial t}+\frac{\partial uv}{\partial x}+\frac{\partial v^2}{\partial y}+\frac{\partial p}{\partial y}=\frac{1}{Re}\left(\frac{\partial^2 v}{\partial x^2}+\frac{\partial^2 v}{\partial y^2}\right)+F_y \qquad (3\text{-}22b)$$

$$\frac{\partial u}{\partial x}+\frac{\partial v}{\partial y}=0 \qquad (3\text{-}22c)$$

where, x and y are the dimensionless coordinates of physical domain, u and v are the velocity components in x and y direction, respectively; p the pressure, Re the Reynolds number, t the physical dimensionless time, and F_x and F_y other force components in x and y direction, respectively.

The general curvilinear transformation from the physical domain to a computational domain can be performed by the transformation:

$$\zeta=\zeta(x, y, t) \qquad (3\text{-}23a)$$

$$\eta=\eta(x, y, t) \tag{3-23b}$$

Based on the transformations rule introduced by Vinokur (1974) and Steger (1978), in terms of the independent variables (ζ, η), we can rewrite these equations in the following form.

$$\frac{\partial u}{\partial t}+\frac{1}{J}[(\frac{\partial y}{\partial \zeta}\frac{\partial u}{\partial \eta}-\frac{\partial y}{\partial \eta}\frac{\partial u}{\partial \zeta})\frac{\partial x}{\partial t}+(\frac{\partial x}{\partial \eta}\frac{\partial u}{\partial \zeta}-\frac{\partial x}{\partial \zeta}\frac{\partial u}{\partial \eta})\frac{\partial y}{\partial t}]+$$
$$\frac{1}{J}[\frac{\partial y}{\partial \eta}\frac{\partial}{\partial \zeta}(u^2+p)-\frac{\partial y}{\partial \zeta}\frac{\partial}{\partial \eta}(u^2+p)+\frac{\partial x}{\partial \zeta}\frac{\partial}{\partial \eta}(uv)-\frac{\partial x}{\partial \eta}\frac{\partial}{\partial \zeta}(uv)]$$
$$=\frac{1}{ReJ}(\alpha\frac{\partial^2 u}{\partial \zeta^2}-2\beta\frac{\partial^2 u}{\partial \zeta\partial \eta}+\gamma\frac{\partial^2 u}{\partial \eta^2}+\tau\frac{\partial u}{\partial \zeta}+\varphi\frac{\partial u}{\partial \eta})+F_x \tag{3-24a}$$

$$\frac{\partial v}{\partial t}+\frac{1}{J}[(\frac{\partial y}{\partial \zeta}\frac{\partial v}{\partial \eta}-\frac{\partial y}{\partial \eta}\frac{\partial v}{\partial \zeta})\frac{\partial x}{\partial t}+(\frac{\partial x}{\partial \eta}\frac{\partial v}{\partial \zeta}-\frac{\partial x}{\partial \zeta}\frac{\partial v}{\partial \eta})\frac{\partial y}{\partial t}]+$$
$$\frac{1}{J}[\frac{\partial x}{\partial \zeta}\frac{\partial}{\partial \eta}(v^2+p)-\frac{\partial x}{\partial \eta}\frac{\partial}{\partial \zeta}(v^2+p)+\frac{\partial y}{\partial \eta}\frac{\partial}{\partial \zeta}(uv)-\frac{\partial y}{\partial \zeta}\frac{\partial}{\partial \eta}(uv)]$$
$$=\frac{1}{ReJ}(\alpha\frac{\partial^2 v}{\partial \zeta^2}-2\beta\frac{\partial^2 v}{\partial \zeta\partial \eta}+\gamma\frac{\partial^2 v}{\partial \eta^2}+\tau\frac{\partial v}{\partial \zeta}+\varphi\frac{\partial v}{\partial \eta})+F_y \tag{3-24b}$$

$$\frac{1}{J}[\frac{\partial y}{\partial \eta}\frac{\partial u}{\partial \zeta}-\frac{\partial y}{\partial \zeta}\frac{\partial u}{\partial \eta}+\frac{\partial x}{\partial \zeta}\frac{\partial v}{\partial \eta}-\frac{\partial x}{\partial \eta}\frac{\partial v}{\partial \zeta}]=0 \tag{3-24c}$$

A significant difficulty for incompressible flow calculations occurs since the continuity equation is given not in a time evolution form, but in the form of a divergence-free constraint. This is one of the major differences with compressible flow calculations. The pressure, which has no time term, is coupled implicitly with the divergence-free constraint on the velocity. This prohibits time integration of the incompressible flow equations in a straightforward manner.

The momentum equations, Equation (3-24a) and Equation (3-24b) will be used directly to solve the velocity field. In this stage the pressure field will be one step older than the velocity field. They explicitly involve the time derivative of the velocity components u and v, and are not difficult to solve. Then, based on the new velocity field, the pressure

field is updated by employing the pressure Poisson method. This method is introduced by Harlow and Welch (1965) and has different formulations in this work.

The Pressure Poisson equation is

$$\frac{\partial^2 p}{\partial x^2}+\frac{\partial^2 p}{\partial y^2}=-D_t+\frac{\partial}{\partial x}F_x+\frac{\partial}{\partial y}F_y-\frac{\partial}{\partial x}(u^2{}_x+uv_y)-\frac{\partial}{\partial y}(uv_x+v^2{}_y) \tag{3-25}$$

where, $D=\frac{\partial u}{\partial x}+\frac{\partial v}{\partial y}$

In general curvilinear coordinate system, it becomes

$$\begin{aligned}
&\frac{\partial}{\partial \zeta}\left(\frac{\alpha p_\zeta}{J}-\frac{\beta p_\eta}{J}\right)+\frac{\partial}{\partial \eta}\left(\frac{\gamma p_\eta}{J}-\frac{\beta p_\zeta}{J}\right)\\
&\quad=\frac{\partial y}{\partial \eta}\frac{\partial F_x}{\partial \zeta}-\frac{\partial y}{\partial \zeta}\frac{\partial F_x}{\partial \eta}+\frac{\partial x}{\partial \zeta}\frac{\partial F_y}{\partial \eta}-\frac{\partial x}{\partial \eta}\frac{\partial F_y}{\partial \zeta}\\
&\quad-\frac{\partial}{\partial \zeta}\frac{1}{J}\left[\left(\frac{\partial y}{\partial \eta}\right)^2\frac{\partial u^2}{\partial \zeta}-\frac{\partial y}{\partial \eta}\frac{\partial y}{\partial \zeta}\frac{\partial u^2}{\partial \eta}+2\frac{\partial x}{\partial \zeta}\frac{\partial y}{\partial \eta}\frac{\partial uv}{\partial \eta}\right.\\
&\quad\left.-2\frac{\partial x}{\partial \eta}\frac{\partial y}{\partial \eta}\frac{\partial uv}{\partial \zeta}-\frac{\partial x}{\partial \zeta}\frac{\partial x}{\partial \eta}\frac{\partial v^2}{\partial \eta}+\left(\frac{\partial x}{\partial \eta}\right)^2\frac{\partial v^2}{\partial \zeta}\right]\\
&\quad-\frac{\partial}{\partial \eta}\frac{1}{J}\left[\left(\frac{\partial y}{\partial \zeta}\right)^2\frac{\partial u^2}{\partial \eta}-\frac{\partial y}{\partial \eta}\frac{\partial y}{\partial \zeta}\frac{\partial u^2}{\partial \zeta}+2\frac{\partial x}{\partial \eta}\frac{\partial y}{\partial \zeta}\frac{\partial uv}{\partial \zeta}\right.\\
&\quad\left.-2\frac{\partial x}{\partial \zeta}\frac{\partial y}{\partial \zeta}\frac{\partial uv}{\partial \eta}-\frac{\partial x}{\partial \zeta}\frac{\partial x}{\partial \eta}\frac{\partial v^2}{\partial \zeta}+\left(\frac{\partial x}{\partial \zeta}\right)^2\frac{\partial v^2}{\partial \eta}\right]\\
&\quad-J\frac{\partial D}{\partial t}+\left(\frac{\partial y}{\partial \eta}\frac{\partial D}{\partial \zeta}-\frac{\partial y}{\partial \zeta}\frac{\partial D}{\partial \eta}\right)\frac{\partial x}{\partial t}+\left(\frac{\partial x}{\partial \zeta}\frac{\partial D}{\partial \eta}-\frac{\partial x}{\partial \eta}\frac{\partial D}{\partial \zeta}\right)\frac{\partial y}{\partial t}
\end{aligned} \tag{3-26}$$

where, $D=\frac{1}{J}\left[\frac{\partial y}{\partial \eta}\frac{\partial u}{\partial \zeta}-\frac{\partial y}{\partial \zeta}\frac{\partial u}{\partial \eta}+\frac{\partial x}{\partial \zeta}\frac{\partial v}{\partial \eta}-\frac{\partial x}{\partial \eta}\frac{\partial v}{\partial \zeta}\right]$

3.2.2 The Velocity-Solving Process

It is our objective to solve Equation (3-24) accurately in time and space. The standard Crank-Nicolson approximation is used to discretize the momentum equation with respect to time. For Equation (3-24a) we have

$$\frac{u^{n+1}-u^n}{\Delta t}+\frac{1}{2}[REST^{n+1}+REST^n]=0 \tag{3-27}$$

where Δt is the physical time increment, REST is a compact notation that represents all terms but the time derivative term of the Equation (3-24a). Superscripts n and n+1

refer to the physical time levels. The time difference Equation (3-27) has second-order accuracy in time. Next, we introduce the intermediate variables as follows

$$\bar{u}^{n+1}=u^{n+1}-u^{n} \tag{3-28a}$$

$$\bar{v}^{n+1}=v^{n+1}-v^{n} \tag{3-28b}$$

$$\bar{p}^{n+1}=p^{n+1}-p^{n} \tag{3-28c}$$

Substituting Equation (3-28) into Equation (3-27), dropping the superscript n and n+1 for convenience, and rearranging the resulted equation, we have

$$cu1\cdot\bar{u}+cv1\cdot\bar{v}+cux1\cdot\frac{\partial\bar{u}}{\partial\zeta}+cvx1\cdot\frac{\partial\bar{v}}{\partial\zeta}+cuy1\cdot\frac{\partial\bar{u}}{\partial\eta}+cvy1\cdot\frac{\partial\bar{v}}{\partial\eta}$$
$$+cxx\frac{\partial^2\bar{u}}{\partial\zeta^2}+cyy\frac{\partial^2\bar{u}}{\partial\eta^2}+UNL=UR \tag{3-29a}$$

where

$$cu1=1+\frac{\Delta t}{2J}[2(u_\zeta y_\eta-u_\eta y_\zeta)+v_\eta x_\zeta-v_\zeta x_\eta]$$

$$cv1=\frac{\Delta t}{2J}[u_\eta x_\zeta-u_\zeta x_\eta]$$

$$cux1=\frac{\Delta t}{2J}[(y_t-v)x_\eta-(x_t-2u)y_\eta-\frac{\tau}{ReJ}]$$

$$cvx1=-\frac{\Delta t}{2J}ux_\eta$$

$$cuy1=\frac{\Delta t}{2J}[(x_t-2u)y_\zeta-(y_t-v)x_\zeta-\frac{\delta}{ReJ}]$$

$$cvy1=\frac{\Delta t}{2J}ux_\zeta$$

$$cxx=-\frac{\Delta t}{2J}\frac{\alpha}{ReJ}$$

$$cyy=-\frac{\Delta t}{2J}\frac{\gamma}{ReJ}$$

$$UNL=\frac{\Delta t}{2J}[y_\eta(\bar{u}^2+\bar{p})_\zeta-y_\zeta(\bar{u}^2+\bar{p})_\eta+x_\zeta(\overline{uv})_\eta-x_\eta(\overline{uv})_\zeta+\frac{2\beta}{ReJ}\bar{u}_{\zeta\eta}]$$

$$UR=\Delta t\cdot F_x-2(cxx\cdot u_{\zeta\zeta}+cyy\cdot u_{\eta\eta}+\frac{\Delta t}{2}\frac{2\beta}{ReJ^2}u_{\zeta\eta})+\frac{\Delta t}{ReJ^2}(\tau u_\zeta+\delta u_\eta)$$

$$-\frac{\Delta t}{J}[(y_\zeta u_\eta - y_\eta u_\zeta)x_t - (x_\zeta u_\eta - x_\eta u_\zeta)y_t$$
$$+ y_\eta (u^2+p)_\zeta - y_\zeta (u^2+p)_\eta + x_\zeta (uv)_\eta - x_\eta (uv)_\zeta]$$

$$cu2\cdot\bar{u} + cv2\cdot\bar{v} + cux2\cdot\frac{\partial\bar{u}}{\partial\zeta} + cvx2\cdot\frac{\partial\bar{v}}{\partial\zeta} + cuy2\cdot\frac{\partial\bar{u}}{\partial\eta} + cvy2\cdot\frac{\partial\bar{v}}{\partial\eta}$$
$$+ cxx\frac{\partial^2\bar{v}}{\partial\zeta^2} + cyy\frac{\partial^2\bar{v}}{\partial\eta^2} + VNL = VR \qquad (3\text{-}29b)$$

where

$$cu2 = \frac{\Delta t}{2J}[v_\zeta y_\eta - v_\eta y_\zeta]$$

$$cv2 = 1 + \frac{\Delta t}{2J}[2(v_\eta x_\zeta - v_\zeta x_\eta) + u_\zeta y_\eta - u_\eta y_\zeta]$$

$$cux2 = \frac{\Delta t}{2J} vy_\eta$$

$$cvx2 = \frac{\Delta t}{2J}[(y_t - 2v)x_\eta - (x_t - u)y_\eta - \frac{\tau}{ReJ}]$$

$$cuy2 = -\frac{\Delta t}{2J} vy_\zeta$$

$$cvy2 = \frac{\Delta t}{2J}[(x_t - u)y_\zeta - (y_t - 2v)x_\zeta - \frac{\delta}{ReJ}]$$

$$VNL = \frac{\Delta t}{2J}[y_\eta(\overline{uv})_\zeta - y_\zeta(\overline{uv})_\eta + x_\zeta(\bar{v}^2+\bar{p})_\eta - x_\eta(\bar{v}^2+\bar{p})_\zeta + \frac{2\beta}{ReJ}\bar{u}_{\zeta\eta}]$$

$$VR = \Delta t\cdot F_y - 2(cxx\cdot v_{\zeta\zeta} + cyy\cdot v_{\eta\eta} + \frac{\Delta t}{2}\frac{2\beta}{ReJ^2}v_{\zeta\eta}) + \frac{\Delta t}{ReJ^2}(\tau v_\zeta + \delta v_\eta)$$
$$-\frac{\Delta t}{J}[(y_\zeta v_\eta - y_\eta v_\zeta)x_t - (x_\zeta v_\eta - x_\eta v_\zeta)y_t$$
$$+ y_\eta (uv)_\zeta - y_\zeta (uv)_\eta + x_\zeta (v^2+p)_\eta - x_\eta (v^2+p)_\zeta]$$

Equations (3-29) can be rewritten in the following compact form.

$$F\cdot E + A\cdot\frac{\partial E}{\partial\zeta} + B\cdot\frac{\partial E}{\partial\eta} + P\cdot\frac{\partial^2 E}{\partial\zeta^2} + Q\cdot\frac{\partial^2 E}{\partial\eta^2} + NL = R \qquad (3\text{-}30)$$

where

$E=(\bar{u},\ \bar{v})^T \qquad NL=(UNL,\ VNL)^T \qquad R=(UR,\ VR)^T$

$$F=\begin{vmatrix} cu1 & cv1 \\ cu2 & cv2 \end{vmatrix} \quad A=\begin{vmatrix} cux1 & cvx1 \\ cux2 & cvx2 \end{vmatrix} \quad B=\begin{vmatrix} cuy1 & cvy1 \\ cuy2 & cvy2 \end{vmatrix}$$

$$P=\begin{vmatrix} cxx & 0 \\ 0 & cxx \end{vmatrix} \quad Q=\begin{vmatrix} cyy & 0 \\ 0 & cyy \end{vmatrix}$$

At this point, an idea of Soh & Goodrich(1988) is adopted and a continuous auxiliary system in pseudo-time is introduced. Equation (3-30) changes its form to

$$\frac{\partial E}{\partial \tau}+F\cdot E+A\cdot\frac{\partial E}{\partial \zeta}+B\cdot\frac{\partial E}{\partial \eta}+P\cdot\frac{\partial^2 E}{\partial \zeta^2}+Q\cdot\frac{\partial^2 E}{\partial \eta^2}+NL=R \qquad (3\text{-}31)$$

where τ is the pseudo-time which is not physical. It is clear that the solution of the system (3-30) is equivalent to the steady state solution of the system (3-31) in the pseudo-time domain.

Now we apply an Euler implicit finite-difference scheme to the pseudo-time term,

$$\Delta E^k = E^{k+1} - E^k = \frac{\Delta\tau}{2}[(\frac{\partial E}{\partial \tau})^{k+1} + (\frac{\partial E}{\partial \tau})^k] + O(\Delta\tau^3) \qquad (3\text{-}32)$$

where, k is the pseudo-time index, and $\Delta\tau$ is the pseudo-time step. Substituting Equation (3-31) into Equation (3-32), rearranging the resulting equation, and denoting $\Delta NL^k = NL^{k+1} - NL^k$, we will get

$$\begin{aligned} &\Delta E^k+\frac{\Delta\tau}{2}[F\Delta E^k+A\frac{\partial \Delta E^k}{\partial \zeta}+B\frac{\partial \Delta E^k}{\partial \eta}+P\frac{\partial^2 \Delta E^k}{\partial \zeta^2}+Q\frac{\partial^2 \Delta E^k}{\partial \eta^2}+\Delta NL^k] \\ &\Delta\tau[FE^k+A\frac{\partial E^k}{\partial \zeta}+B\frac{\partial E^k}{\partial \eta}+P\frac{\partial^2 E^k}{\partial \zeta^2}+Q\frac{\partial^2 E^k}{\partial \eta^2}+NL^k] \\ &=\Delta\tau R \end{aligned} \qquad (3\text{-}33)$$

Dropping the superscript k of E^k, NL^k, and ΔNL^k terms for simplicity and setting,

$$T = I+\frac{\Delta\tau}{2}F$$

$$R^* = \Delta\tau[R-(FE+A\frac{\partial E}{\partial \zeta}+B\frac{\partial E}{\partial \eta}+P\frac{\partial E^2}{\partial \zeta^2}+Q\frac{\partial E^2}{\partial \eta^2}+NL)-\frac{1}{2}\Delta NL]$$

where, $I=\begin{vmatrix} 1 & 0 \\ 0 & 1 \end{vmatrix}$

Equation (3-33) will be in the following form:

$$[T+\frac{\Delta\tau}{2}(A\frac{\partial}{\partial\zeta}+B\frac{\partial}{\partial\eta}+P\frac{\partial^2}{\partial\zeta^2}+Q\frac{\partial^2}{\partial\eta^2})]\Delta E^k = R^* \tag{3-34}$$

Applying the Factored Approximation method to Equation (3-34) as Beam and Warming (1978) did in their work, and ignoring the error terms, we have

$$[T+\frac{\Delta\tau}{2}(A\frac{\partial}{\partial\zeta}+P\frac{\partial^2}{\partial\zeta^2})][I+\frac{\Delta\tau}{2}(T^{-1}B\frac{\partial}{\partial\eta}+T^{-1}Q\frac{\partial^2}{\partial\eta^2})]\Delta E^k = R^* \tag{3-35}$$

Finally, the velocity-solving procedure consists of three steps. They are

$$[T+\frac{\Delta\tau}{2}(A\frac{\partial}{\partial\zeta}+P\frac{\partial^2}{\partial\zeta^2})]\Delta E^* = R^* \tag{3-36a}$$

$$[I+\frac{\Delta\tau}{2}(T^{-1}B\frac{\partial}{\partial\eta}+T^{-1}Q\frac{\partial^2}{\partial\eta^2})]\Delta E^k = \Delta E^* \tag{3-36b}$$

$$E^{k+1} = E^k + \Delta E^k \tag{3-36c}$$

The finite difference approximations of second-order accuracy are used in the computations. In the computational domain (Figure 3-7) they are

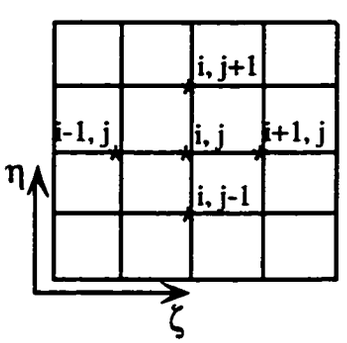

Figure 3-7 The Computational Domain

$$(\frac{\partial E}{\partial\zeta})_{ij} = 0.5(E_{i+1,j} - E_{i-1,j}) \tag{3-37a}$$

$$(\frac{\partial E}{\partial\eta})_{ij} = 0.5(E_{i,j+1} - E_{i,j-1}) \tag{3-37b}$$

$$(\frac{\partial^2 E}{\partial\zeta^2})_{ij} = E_{i+1,j} + E_{i-1,j} - 2E_{i,j} \tag{3-37c}$$

$$(\frac{\partial^2 E}{\partial\eta^2})_{ij} = E_{i,j+1} + E_{i,j-1} - 2E_{i,j} \tag{3-37d}$$

$$(\frac{\partial^2 E}{\partial\zeta\partial\eta})_{ij} = 0.25(E_{i+1,j+1} + E_{i-1,j-1} - E_{i+1,j-1} - E_{i-1,j+1}) \qquad (3\text{-}37e)$$

The partial difference equations (3-36) will be reduced to finite-difference equations using the finite-difference formulas (3-37). The resulted finite difference equations are solved line by line, first in ζ-direction then in η-direction. For each line we end up with a system of block-tridiagonal linear algebraic equations. For Equation (3-36a) we will have

$$\begin{vmatrix} L_2 & M_2 & U_2 & & & & & \\ & L_3 & M_3 & U_3 & & & & \\ & & \bullet & \bullet & \bullet & & & \\ & & & \bullet & \bullet & \bullet & & \\ & & & & L_{LX-2} & M_{LX-2} & U_{LX-2} & \\ & & & & & L_{LX-1} & M_{LX-1} & U_{LX-1} \end{vmatrix} \begin{vmatrix} \Delta E_1^* \\ \Delta E_2^* \\ \Delta E_3^* \\ \bullet \\ \bullet \\ \Delta E_{LX-2}^* \\ \Delta E_{LX-1}^* \\ \Delta E_{LX}^* \end{vmatrix} = \begin{vmatrix} R_2^* \\ R_3^* \\ \bullet \\ \bullet \\ R_{LX-2}^* \\ R_{LX-1}^* \end{vmatrix} \qquad (3\text{-}38a)$$

for each of j = 2, 3, ... LY-2, LY-1;

and for Equation (3-36b)

$$\begin{vmatrix} L'_2 & M'_2 & U'_2 & & & & & \\ & L'_3 & M'_3 & U'_3 & & & & \\ & & \bullet & \bullet & \bullet & & & \\ & & & \bullet & \bullet & \bullet & & \\ & & & & L'_{LY-2} & M'_{LY-2} & U'_{LY-2} & \\ & & & & & L'_{LY-1} & M'_{LY-1} & U'_{LY-1} \end{vmatrix} \begin{vmatrix} \Delta E_1^k \\ \Delta E_2^k \\ \Delta E_3^k \\ \bullet \\ \bullet \\ \Delta E_{LX-2}^k \\ \Delta E_{LX-1}^k \\ \Delta E_{LX}^k \end{vmatrix} = \begin{vmatrix} \Delta E_2^* \\ \Delta E_3^* \\ \bullet \\ \bullet \\ \Delta E_{LX-2}^* \\ \Delta E_{LX-1}^* \end{vmatrix} \qquad (3\text{-}38b)$$

for each of i = 2, 3, ... LX-2, LX-1. Each of L, M, U, and L', M', U' is a 2 by 2 matrix; and each ΔE^*, ΔE^k, and R^* is a the vector of length 2, where

$$L_i = \frac{\Delta\pi}{2}(P - \frac{1}{2}A)_{i,j} \qquad (3\text{-}39a)$$

$$M_i = (T - \Delta\pi P)_{i,j} \qquad (3\text{-}39b)$$

$$U_i = \frac{\Delta\pi}{2}\left(P + \frac{1}{2}A\right)_{i,j} \qquad (3\text{-}39c)$$

$$(i = 2, 3, \ldots \text{ LX-1 for } 2 < j < \text{LY-1})$$

$$L'_i = \frac{\Delta\pi}{2}\left(T^{-1}Q - \frac{1}{2}T^{-1}B\right)_{i,j} \qquad (3\text{-}39d)$$

$$M'_i = \left(I - \Delta\pi T^{-1}Q\right)_{i,j} \qquad (3\text{-}39e)$$

$$U'_i = \frac{\Delta\pi}{2}\left(T^{-1}Q + \frac{1}{2}T^{-1}B\right)_{i,j} \qquad (3\text{-}39f)$$

$$(j = 2, 3, \ldots \text{ LY-1 for } 2 < i < \text{LX-1})$$

Both systems are two equations short of the number of unknown vectors. The velocity boundary conditions will make up these two equations.

The solution procedure includes two steps at each pseudo-time level. First, Equation (3-36a), in which only the ζ-derivative terms are involved, is solved line by line in the ζ-direction along the line of every η = constant for ΔE^*. Then the Equation. (3-36b), in which only the η-derivative terms are involved, is solved line by line in η-direction along the line of every ζ = constant for ΔE^k. For each step, a block-tridiagonal matrix system with a 2 by 2 matrix in each block is solved by the efficient method of Direct Factorization. Equation (3-36c) will carry the solution into the next pseudo-time step.

This process is repeated until the value of pseudo-time derivative is less than the given tolerance. A time-accurate solution at a new physical time level is then achieved by adding this ultimate steady state solution in pseudo-time to the solution at the current physical time level.

3.2.3 The Pressure-Solving Process

During the velocity-solving process, a pressure field that is one-pseudo-time-step older is used. Once we get the velocity field at a new pseudo-time level we will use it to update the current pressure field by employing the pressure Poisson method.

The pressure Poisson equation in the intermediate variables, $\bar{u}, \bar{v}$ and $\bar{p}$ can be easily obtained by substituting Equation (3-28) into Equation (3-26) and rearranging the resulting equation. It is

$$
\begin{aligned}
&\frac{\partial}{\partial\zeta}\left(\frac{\alpha p_\zeta}{J}-\frac{\beta p_\eta}{J}\right)+\frac{\partial}{\partial\eta}\left(\frac{\gamma p_\eta}{J}-\frac{\beta p_\zeta}{J}\right)= \\
&\quad \frac{\partial y}{\partial\eta}\frac{\partial F_x}{\partial\zeta}-\frac{\partial y}{\partial\zeta}\frac{\partial F_x}{\partial\eta}+\frac{\partial x}{\partial\zeta}\frac{\partial F_y}{\partial\eta}-\frac{\partial x}{\partial\eta}\frac{\partial F_y}{\partial\zeta} \\
&\quad -\frac{\partial}{\partial\zeta}\frac{1}{J}\left[\left(\frac{\partial y}{\partial\eta}\right)^2\frac{\partial(u^2+p)}{\partial\zeta}-\frac{\partial y}{\partial\eta}\frac{\partial y}{\partial\zeta}\frac{\partial(u^2+p)}{\partial\eta}+2\frac{\partial x}{\partial\zeta}\frac{\partial y}{\partial\eta}\frac{\partial uv}{\partial\eta}\right. \\
&\quad \left.-2\frac{\partial x}{\partial\eta}\frac{\partial y}{\partial\eta}\frac{\partial uv}{\partial\zeta}-\frac{\partial x}{\partial\zeta}\frac{\partial x}{\partial\eta}\frac{\partial(v^2+p)}{\partial\eta}+\left(\frac{\partial x}{\partial\eta}\right)^2\frac{\partial(v^2+p)}{\partial\zeta}\right] \\
&\quad -\frac{\partial}{\partial\eta}\frac{1}{J}\left[\left(\frac{\partial y}{\partial\zeta}\right)^2\frac{\partial(u^2+p)}{\partial\eta}-\frac{\partial y}{\partial\eta}\frac{\partial y}{\partial\zeta}\frac{\partial(u^2+p)}{\partial\zeta}+2\frac{\partial x}{\partial\eta}\frac{\partial y}{\partial\zeta}\frac{\partial uv}{\partial\zeta}\right. \\
&\quad \left.-2\frac{\partial x}{\partial\zeta}\frac{\partial y}{\partial\zeta}\frac{\partial uv}{\partial\eta}-\frac{\partial x}{\partial\zeta}\frac{\partial x}{\partial\eta}\frac{\partial(v^2+p)}{\partial\zeta}+\left(\frac{\partial x}{\partial\zeta}\right)^2\frac{\partial(v^2+p)}{\partial\eta}\right] \\
&\quad -J\frac{\partial D}{\partial t}+\left(\frac{\partial y}{\partial\eta}\frac{\partial D}{\partial\zeta}-\frac{\partial y}{\partial\zeta}\frac{\partial D}{\partial\eta}\right)\frac{\partial x}{\partial t}+\left(\frac{\partial x}{\partial\zeta}\frac{\partial D}{\partial\eta}-\frac{\partial x}{\partial\eta}\frac{\partial D}{\partial\zeta}\right)\frac{\partial y}{\partial t} \\
&\quad -\frac{\partial}{\partial\zeta}\frac{1}{J}\left[\left(\frac{\partial y}{\partial\eta}\right)^2\frac{\partial(\bar{u}^2+2u\bar{u})}{\partial\zeta}-\frac{\partial y}{\partial\eta}\frac{\partial y}{\partial\zeta}\frac{\partial(\bar{u}^2+2u\bar{u})}{\partial\eta}\right. \\
&\quad \left.+2\frac{\partial x}{\partial\zeta}\frac{\partial y}{\partial\eta}\frac{\partial(\bar{u}\bar{v}+u\bar{v}+\bar{u}v)}{\partial\eta}-2\frac{\partial x}{\partial\eta}\frac{\partial y}{\partial\eta}\frac{\partial(\bar{u}\bar{v}+u\bar{v}+\bar{u}v)}{\partial\zeta}\right. \\
&\quad \left.-\frac{\partial x}{\partial\zeta}\frac{\partial x}{\partial\eta}\frac{\partial(\bar{v}^2+2v\bar{v})}{\partial\eta}+\left(\frac{\partial x}{\partial\eta}\right)^2\frac{\partial(\bar{v}^2+2v\bar{v})}{\partial\zeta}\right] \\
&\quad -\frac{\partial}{\partial\eta}\frac{1}{J}\left[\left(\frac{\partial y}{\partial\zeta}\right)^2\frac{\partial(\bar{u}^2+2u\bar{u})}{\partial\eta}-\frac{\partial y}{\partial\eta}\frac{\partial y}{\partial\zeta}\frac{\partial(\bar{u}^2+2u\bar{u})}{\partial\zeta}\right. \\
&\quad \left.+2\frac{\partial x}{\partial\eta}\frac{\partial y}{\partial\zeta}\frac{\partial(\bar{u}\bar{v}+u\bar{v}+\bar{u}v)}{\partial\zeta}-2\frac{\partial x}{\partial\zeta}\frac{\partial y}{\partial\zeta}\frac{\partial(\bar{u}\bar{v}+u\bar{v}+\bar{u}v)}{\partial\eta}\right. \\
&\quad \left.-\frac{\partial x}{\partial\zeta}\frac{\partial x}{\partial\eta}\frac{\partial(\bar{v}^2+2v\bar{v})}{\partial\zeta}+\left(\frac{\partial x}{\partial\zeta}\right)^2\frac{\partial(\bar{v}^2+2v\bar{v})}{\partial\eta}\right] \\
&\quad -J\frac{\partial\bar{D}}{\partial t}+\left(\frac{\partial y}{\partial\eta}\frac{\partial\bar{D}}{\partial\zeta}-\frac{\partial y}{\partial\zeta}\frac{\partial\bar{D}}{\partial\eta}\right)\frac{\partial x}{\partial t}+\left(\frac{\partial x}{\partial\zeta}\frac{\partial\bar{D}}{\partial\eta}-\frac{\partial x}{\partial\eta}\frac{\partial\bar{D}}{\partial\zeta}\right)\frac{\partial y}{\partial t} \qquad (3\text{-}40)
\end{aligned}
$$

where, $\bar{D}=\frac{1}{J}\left[\frac{\partial y}{\partial\eta}\frac{\partial\bar{u}}{\partial\zeta}-\frac{\partial y}{\partial\zeta}\frac{\partial\bar{u}}{\partial\eta}+\frac{\partial x}{\partial\zeta}\frac{\partial\bar{v}}{\partial\eta}-\frac{\partial x}{\partial\eta}\frac{\partial\bar{v}}{\partial\zeta}\right]$

The boundary conditions for the pressure Poisson equation can be easily derived from the corresponding momentum equations by introducing the vorticity function ω into the

momentum equations (3-22a) and (3-22b). The pressure Neumann boundary conditions are:

in the Cartesian coordinate system

$$\frac{\partial u}{\partial t}+\frac{\partial u^2}{\partial x}+\frac{\partial uv}{\partial y}+\frac{\partial p}{\partial x}-\frac{1}{Re}\frac{\partial \omega}{\partial y}-F_x=0 \tag{3-41a}$$

$$\frac{\partial v}{\partial t}+\frac{\partial uv}{\partial x}+\frac{\partial v^2}{\partial y}+\frac{\partial p}{\partial y}+\frac{1}{Re}\frac{\partial \omega}{\partial x}-F_y=0 \tag{3-41b}$$

where, $\omega=\frac{\partial u}{\partial y}-\frac{\partial v}{\partial x}$

and in the general curvilinear coordinate system

$$\begin{aligned}&\frac{\partial u}{\partial t}+\frac{1}{J}[(\frac{\partial y}{\partial \zeta}\frac{\partial u}{\partial \eta}-\frac{\partial y}{\partial \eta}\frac{\partial u}{\partial \zeta})\frac{\partial x}{\partial t}+(\frac{\partial x}{\partial \eta}\frac{\partial u}{\partial \zeta}-\frac{\partial x}{\partial \zeta}\frac{\partial u}{\partial \eta})\frac{\partial y}{\partial t}]+\\&\quad\frac{1}{J}[\frac{\partial y}{\partial \eta}\frac{\partial}{\partial \zeta}(u^2+p)-\frac{\partial y}{\partial \zeta}\frac{\partial}{\partial \eta}(u^2+p)+\frac{\partial x}{\partial \zeta}\frac{\partial}{\partial \eta}(uv)-\frac{\partial x}{\partial \eta}\frac{\partial}{\partial \zeta}(uv)]\\&\quad-\frac{1}{ReJ}(\frac{\partial x}{\partial \zeta}\frac{\partial \omega}{\partial \eta}-\frac{\partial x}{\partial \eta}\frac{\partial \omega}{\partial \zeta})-F_x=0\end{aligned} \tag{3-42a}$$

$$\begin{aligned}&\frac{\partial v}{\partial t}+\frac{1}{J}[(\frac{\partial y}{\partial \zeta}\frac{\partial v}{\partial \eta}-\frac{\partial y}{\partial \eta}\frac{\partial v}{\partial \zeta})\frac{\partial x}{\partial t}+(\frac{\partial x}{\partial \eta}\frac{\partial v}{\partial \zeta}-\frac{\partial x}{\partial \zeta}\frac{\partial v}{\partial \eta})\frac{\partial y}{\partial t}]+\\&\quad\frac{1}{J}[\frac{\partial x}{\partial \zeta}\frac{\partial}{\partial \eta}(v^2+p)-\frac{\partial x}{\partial \eta}\frac{\partial}{\partial \zeta}(v^2+p)+\frac{\partial y}{\partial \eta}\frac{\partial}{\partial \zeta}(uv)-\frac{\partial y}{\partial \zeta}\frac{\partial}{\partial \eta}(uv)]\\&\quad+\frac{1}{ReJ}(\frac{\partial y}{\partial \eta}\frac{\partial \omega}{\partial \zeta}-\frac{\partial y}{\partial \zeta}\frac{\partial \omega}{\partial \eta})-F_y=0\end{aligned} \tag{3-42b}$$

where, $\omega=\frac{1}{J}(\frac{\partial x}{\partial \zeta}\frac{\partial u}{\partial \eta}-\frac{\partial x}{\partial \eta}\frac{\partial u}{\partial \zeta}-\frac{\partial y}{\partial \eta}\frac{\partial v}{\partial \zeta}+\frac{\partial y}{\partial \zeta}\frac{\partial v}{\partial \eta})$

Dropping the terms, $\frac{\partial u}{\partial t}$ and $\frac{\partial v}{\partial t}$ from the above equations, applying the Equation (3-28), and rearranging the resulting equations and dropping the superscript, we can get the pressure Neumann boundary conditions:

$$\begin{aligned}&\frac{\beta}{J}\frac{\partial \bar{p}}{\partial \eta}-\frac{\alpha}{J}\frac{\partial \bar{p}}{\partial \zeta}-p_1\frac{\partial \bar{u}}{\partial \zeta}-p_2\frac{\partial \bar{u}}{\partial \eta}+p_3\frac{\partial \bar{v}}{\partial \zeta}+p_4\frac{\partial \bar{v}}{\partial \eta}-\frac{1}{J}(\frac{\partial y}{\partial \eta})^2\frac{\partial(\bar{u}^2+2u\bar{u})}{\partial \zeta}\\&\quad+\frac{1}{J}\frac{\partial y}{\partial \zeta}\frac{\partial y}{\partial \eta}\frac{\partial(\bar{u}^2+2u\bar{u})}{\partial \eta}+\frac{2}{J}\frac{\partial x}{\partial \eta}\frac{\partial y}{\partial \eta}\frac{\partial(\bar{u}\bar{v}+u\bar{v}+\bar{u}v)}{\partial \zeta}\\&\quad+\frac{1}{J}\frac{\partial x}{\partial \zeta}\frac{\partial x}{\partial \eta}\frac{\partial(\bar{v}^2+2v\bar{v})}{\partial \eta}-\frac{1}{J}(\frac{\partial x}{\partial \eta}\frac{\partial y}{\partial \zeta}+\frac{\partial x}{\partial \zeta}\frac{\partial y}{\partial \eta})\frac{\partial(\bar{u}\bar{v}+u\bar{v}+\bar{u}v)}{\partial \eta}\end{aligned}$$

$$
\begin{aligned}
&-\frac{1}{J}\left(\frac{\partial x}{\partial \eta}\right)^2\frac{\partial(\bar{v}^2+2v\bar{v})}{\partial \zeta}+\frac{1}{Re}\frac{\partial \bar{\omega}}{\partial \eta}\\
&=p_1\frac{\partial u}{\partial \zeta}+p_2\frac{\partial u}{\partial \eta}-p_3\frac{\partial v}{\partial \zeta}-p_4\frac{\partial v}{\partial \eta}+\frac{1}{J}\left(\frac{\partial y}{\partial \eta}\right)^2\frac{\partial(u^2+p)}{\partial \zeta}-\frac{1}{J}\frac{\partial y}{\partial \zeta}\frac{\partial y}{\partial \eta}\frac{\partial(u^2+p)}{\partial \eta}\\
&\quad-\frac{2}{J}\frac{\partial x}{\partial \eta}\frac{\partial y}{\partial \eta}\frac{\partial uv}{\partial \zeta}+\frac{1}{J}\left(\frac{\partial x}{\partial \eta}\frac{\partial y}{\partial \zeta}+\frac{\partial x}{\partial \zeta}\frac{\partial y}{\partial \eta}\right)\frac{\partial uv}{\partial \eta}+\frac{1}{J}\left(\frac{\partial x}{\partial \eta}\right)^2\frac{\partial(v^2+p)}{\partial \zeta}\\
&\quad-\frac{1}{J}\frac{\partial x}{\partial \zeta}\frac{\partial x}{\partial \eta}\frac{\partial(v^2+p)}{\partial \eta}-\frac{1}{Re}\frac{\partial \omega}{\partial \eta}+\frac{\partial x}{\partial \eta}F_y-\frac{\partial y}{\partial \eta}F_x
\end{aligned}
\tag{3-43a}
$$

$$
\begin{aligned}
&\frac{\gamma}{J}\frac{\partial \bar{p}}{\partial \eta}-\frac{\beta}{J}\frac{\partial \bar{p}}{\partial \zeta}-p_7\frac{\partial \bar{u}}{\partial \zeta}-p_8\frac{\partial \bar{u}}{\partial \eta}+p_5\frac{\partial \bar{v}}{\partial \zeta}+p_6\frac{\partial \bar{v}}{\partial \eta}-\frac{1}{J}\frac{\partial y}{\partial \zeta}\frac{\partial y}{\partial \eta}\frac{\partial(\bar{u}^2+2u\bar{u})}{\partial \zeta}\\
&\quad+\frac{1}{J}\left(\frac{\partial y}{\partial \zeta}\right)^2\frac{\partial(\bar{u}^2+2u\bar{u})}{\partial \eta}-\frac{2}{J}\frac{\partial x}{\partial \zeta}\frac{\partial y}{\partial \zeta}\frac{\partial(\bar{u}\bar{v}+u\bar{v}+\bar{u}v)}{\partial \eta}\\
&\quad-\frac{1}{J}\frac{\partial x}{\partial \zeta}\frac{\partial x}{\partial \eta}\frac{\partial(\bar{v}^2+2v\bar{v})}{\partial \zeta}+\frac{1}{J}\left(\frac{\partial x}{\partial \eta}\frac{\partial y}{\partial \zeta}+\frac{\partial x}{\partial \zeta}\frac{\partial y}{\partial \eta}\right)\frac{\partial(\bar{u}\bar{v}+u\bar{v}+\bar{u}v)}{\partial \eta}\\
&\quad+\frac{1}{J}\left(\frac{\partial x}{\partial \zeta}\right)^2\frac{\partial(\bar{v}^2+2v\bar{v})}{\partial \eta}+\frac{1}{Re}\frac{\partial \bar{\omega}}{\partial \zeta}\\
&=p_7\frac{\partial u}{\partial \zeta}+p_8\frac{\partial u}{\partial \eta}-p_5\frac{\partial v}{\partial \zeta}-p_6\frac{\partial v}{\partial \eta}+\frac{1}{J}\frac{\partial y}{\partial \zeta}\frac{\partial y}{\partial \eta}\frac{\partial(u^2+p)}{\partial \zeta}-\frac{1}{J}\left(\frac{\partial y}{\partial \zeta}\right)^2\frac{\partial(u^2+p)}{\partial \eta}\\
&\quad+\frac{2}{J}\frac{\partial x}{\partial \zeta}\frac{\partial y}{\partial \zeta}\frac{\partial uv}{\partial \eta}-\frac{1}{J}\left(\frac{\partial x}{\partial \eta}\frac{\partial y}{\partial \zeta}+\frac{\partial x}{\partial \zeta}\frac{\partial y}{\partial \eta}\right)\frac{\partial uv}{\partial \zeta}+\frac{1}{J}\frac{\partial x}{\partial \zeta}\frac{\partial x}{\partial \eta}\frac{\partial(v^2+p)}{\partial \zeta}\\
&\quad-\frac{1}{J}\left(\frac{\partial x}{\partial \zeta}\right)^2\frac{\partial(v^2+p)}{\partial \eta}-\frac{1}{Re}\frac{\partial \omega}{\partial \zeta}+\frac{\partial x}{\partial \zeta}F_y-\frac{\partial y}{\partial \zeta}F_x
\end{aligned}
\tag{3-43b}
$$

where, $\bar{\omega}=\frac{1}{J}\left(\frac{\partial x}{\partial \zeta}\frac{\partial \bar{u}}{\partial \eta}-\frac{\partial x}{\partial \eta}\frac{\partial \bar{u}}{\partial \zeta}-\frac{\partial y}{\partial \eta}\frac{\partial \bar{v}}{\partial \zeta}+\frac{\partial y}{\partial \zeta}\frac{\partial \bar{v}}{\partial \eta}\right)$

$$
p_1=\frac{1}{J}\left(\frac{\partial x}{\partial \eta}\frac{\partial y}{\partial t}-\frac{\partial y}{\partial \eta}\frac{\partial x}{\partial t}\right)\frac{\partial y}{\partial \eta}\qquad
p_2=\frac{1}{J}\left(\frac{\partial y}{\partial \zeta}\frac{\partial x}{\partial t}-\frac{\partial x}{\partial \zeta}\frac{\partial y}{\partial t}\right)\frac{\partial y}{\partial \eta}
$$

$$
p_3=\frac{1}{J}\left(\frac{\partial x}{\partial \eta}\frac{\partial y}{\partial t}-\frac{\partial y}{\partial \eta}\frac{\partial x}{\partial t}\right)\frac{\partial x}{\partial \eta}\qquad
p_4=\frac{1}{J}\left(\frac{\partial y}{\partial \zeta}\frac{\partial x}{\partial t}-\frac{\partial x}{\partial \zeta}\frac{\partial y}{\partial t}\right)\frac{\partial x}{\partial \eta}
$$

$$
p_5=\frac{1}{J}\left(\frac{\partial x}{\partial \eta}\frac{\partial y}{\partial t}-\frac{\partial y}{\partial \eta}\frac{\partial x}{\partial t}\right)\frac{\partial x}{\partial \zeta}\qquad
p_6=\frac{1}{J}\left(\frac{\partial y}{\partial \zeta}\frac{\partial x}{\partial t}-\frac{\partial x}{\partial \zeta}\frac{\partial y}{\partial t}\right)\frac{\partial x}{\partial \zeta}
$$

$$
p_7=\frac{1}{J}\left(\frac{\partial x}{\partial \eta}\frac{\partial y}{\partial t}-\frac{\partial y}{\partial \eta}\frac{\partial x}{\partial t}\right)\frac{\partial y}{\partial \zeta}\qquad
p_8=\frac{1}{J}\left(\frac{\partial y}{\partial \zeta}\frac{\partial x}{\partial t}-\frac{\partial x}{\partial \zeta}\frac{\partial y}{\partial t}\right)\frac{\partial y}{\partial \zeta}
$$

In simple notation, they are

$$
\frac{\beta}{J}\frac{\partial \bar{p}}{\partial \eta}-\frac{\alpha}{J}\frac{\partial \bar{p}}{\partial \zeta}=\mathrm{REST1}
\tag{3-44a}
$$

$$
\frac{\gamma}{J}\frac{\partial \bar{p}}{\partial \eta}-\frac{\beta}{J}\frac{\partial \bar{p}}{\partial \zeta}=\mathrm{REST2}
\tag{3-44b}
$$

If the grid is orthogonal at the boundaries, we will have ß = 0. Then the above equations can be used directly. Otherwise, they can be written as

$$\frac{\partial \bar{p}}{\partial \zeta} = \frac{\beta / J \cdot REST2 - \gamma / J \cdot REST1}{\alpha / J \cdot \gamma / J - (\beta / J)^2} \tag{3-45a}$$

$$\frac{\partial \bar{p}}{\partial \eta} = \frac{\alpha / J \cdot REST2 - \beta / J \cdot REST1}{\alpha / J \cdot \gamma / J - (\beta / J)^2} \tag{3-45b}$$

The important issue in the discretization of the pressure Poisson equation and its boundary conditions is consistency. Abdallah (1987) proved that only by consistent differencing for the pressure Poisson and its boundary conditions, could a solution for the pressure Poisson equation exist and be smooth. That is to say we have to apply the Neumann pressure boundary conditions at the position that is a half cell away from the physical boundaries. Otherwise, the iterative solution of pressure will drift slowly and endlessly. The computational procedure is shown in Figure 3-8.

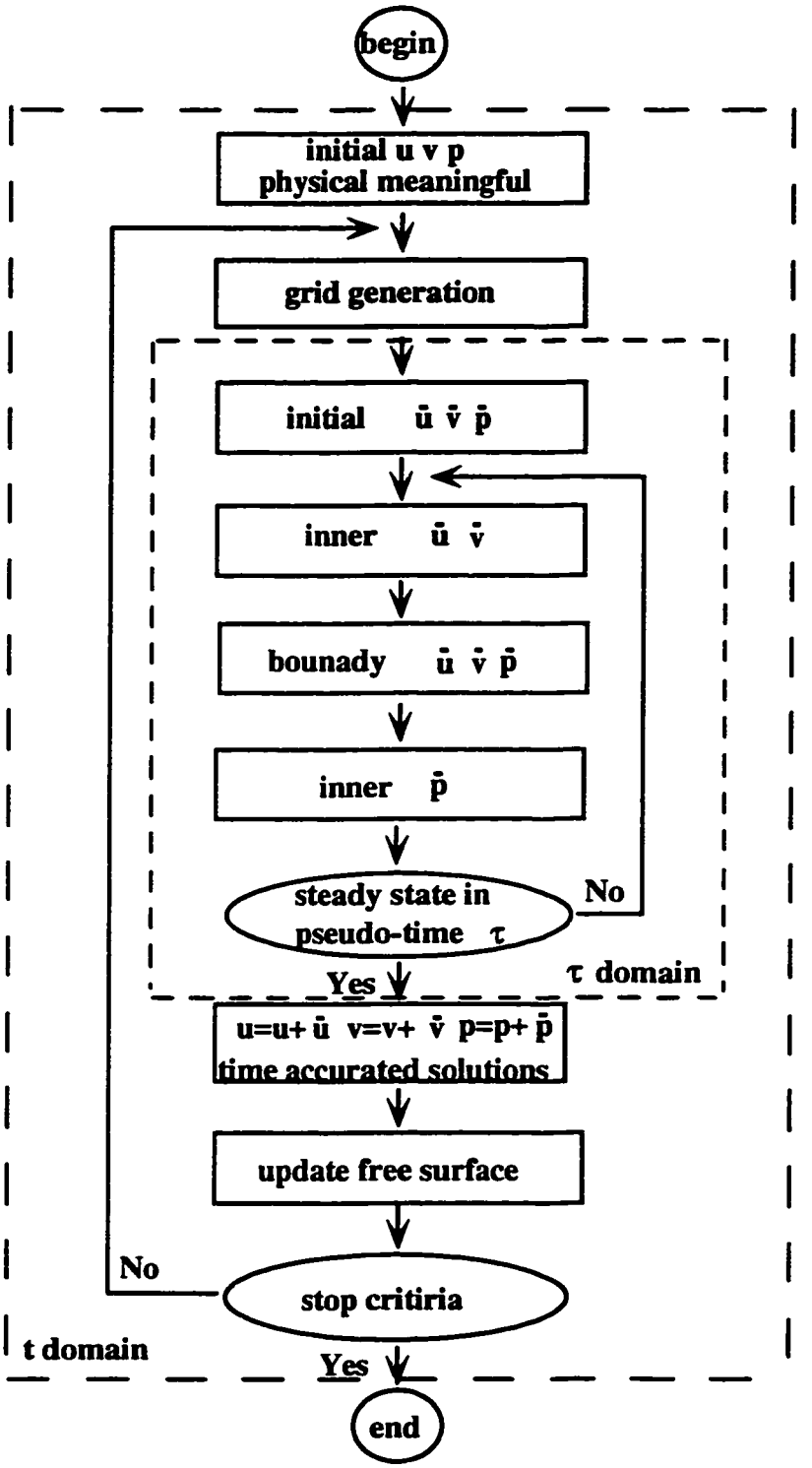

Figure 3-8 The Computational Procedures

3.3 Test Problem

Computational methods of fluid mechanics are usually tested and compared by applying them to one or more standard problems. Two test problems (Figure 3-9), the standard square driven cavity (SSDC) problem and oscillating square driven cavity (OSDC) problem, are used to test our method.

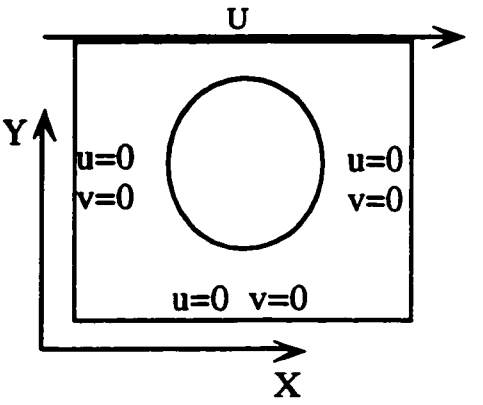

Figure 3-9 Test Problems ($U = U_0$ for SSDC, $U = U_0\cos(\omega t)$ for OSDC)

3.3.1 Standard Square Driven Cavity

For this problem the velocity distribution (in the form of stream function and vorticity function) and the pressure distribution inside the cavity are readily available in many publications for different Reynolds numbers.

For the sake of consistency the Neumann pressure boundary conditions have to be applied at the position that is on half cell away from the physical boundaries. For instance, the pressure boundary condition on the top wall will be applied at the point * (refer to Figure 3-10). The formulations for ζ-derivative and η–derivative at the point * will be

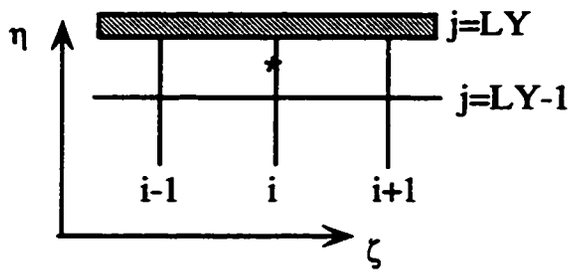

Figure 3-10 Top Wall Boundary

$$\frac{\partial E}{\partial \eta} = E_{i,LY} - E_{i,LY-1} \tag{3-46a}$$

$$\frac{\partial E}{\partial \zeta} = 0.25(E_{i+1,LY} + E_{i+1,LY-1} - E_{i-1,LY} - E_{i-1,LY-1}) \tag{3-46b}$$

The results show that immediately after beginning to move the lid, a large vortical structure appears inside the cavity. The vortex center is located at about x = 0.5 and is very close to the lid in the beginning. As time advances the vortex center gradually moves towards the right and the bottom wall, and the flow pattern gradually approaches the steady state. Figure 3-11 to Figure 3-13 show the steady state results of Re = 100, Re = 400, and Re = 1000, respectively. The results are very consistent with the results reported in literature (refer to Tuann and Mervyn, 1977).

The stream function is defined as

$$u = \frac{\partial \psi}{\partial y} \qquad v = -\frac{\partial \psi}{\partial x} \tag{3-47}$$

Then, we have

$$\frac{\partial^2 \psi}{\partial x^2} + \frac{\partial^2 \psi}{\partial y^2} = \frac{\partial u}{\partial y} - \frac{\partial v}{\partial x} = \omega \tag{3-48}$$

The boundary conditions for the stream function are very simple. On all boundaries, ψ=0.0. It must be noted that the Equation (3-48) has to be transferred into the general curvilinear coordinate system first. A point successive over-relaxation method is used in our calculations for the stream function over the entire domain.

The dimensionless pressure is presented in the term of a pressure coefficient, which is defined as

$$C_p = 2\,Re(P - P_r)/U^2 \qquad (3\text{-}49)$$

where, P_r is the reference pressure at the central bottom, and U the top wall velocity.

Table 3-1 The Summery of Standard Driven Cavity Problem

Re	Grid	Δt	$\Delta\tau$	Steady State Time
100	21 by 21	1/30	0.75	15.23
400	31 by 31	1/40	0.75	37.57
1000	41 by 41	1/200	0.4	40.70
1000	41 by 41	1/160	0.4	43.17

In order to address the accuracy of our method the u-velocity along the vertical center line and the v-velocity along the horizontal center line are illustrated in Figure 3-14 to Figure 3-16. The scattered data represent the results obtained by Ghia et al. (1982) using a 129 by 129 grid. Comparing these results and considering the grid used in our calculation (refer to Table 3-1) we can say that the accuracy of our method is good.

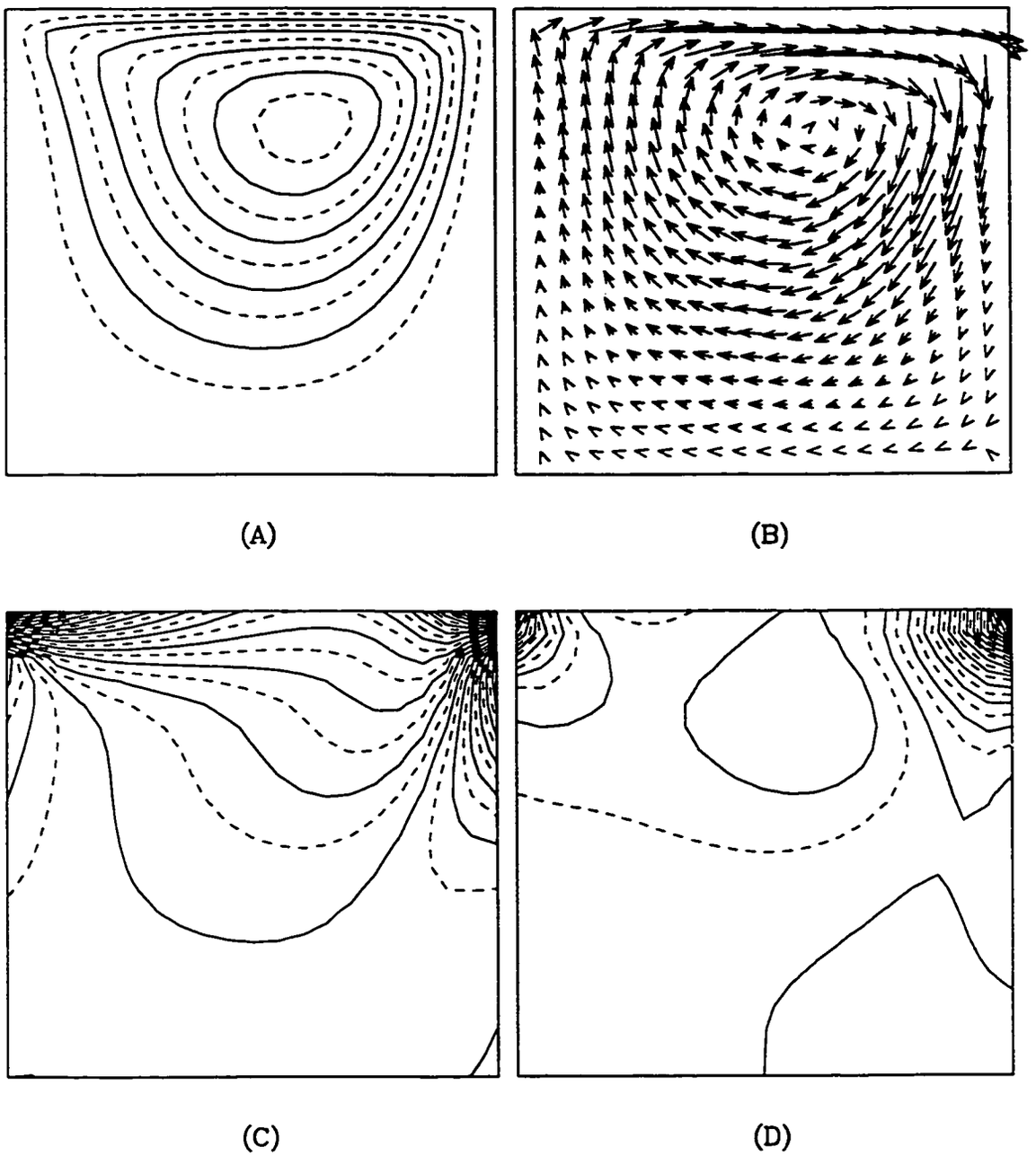

Figure 3-11 Flow Pattern in The Square Cavity of Re = 100
(A) Stream Contour Line
(B) Velocity Vectors
(C) Vorticity Contour
(D) Pressure Coefficient Contour

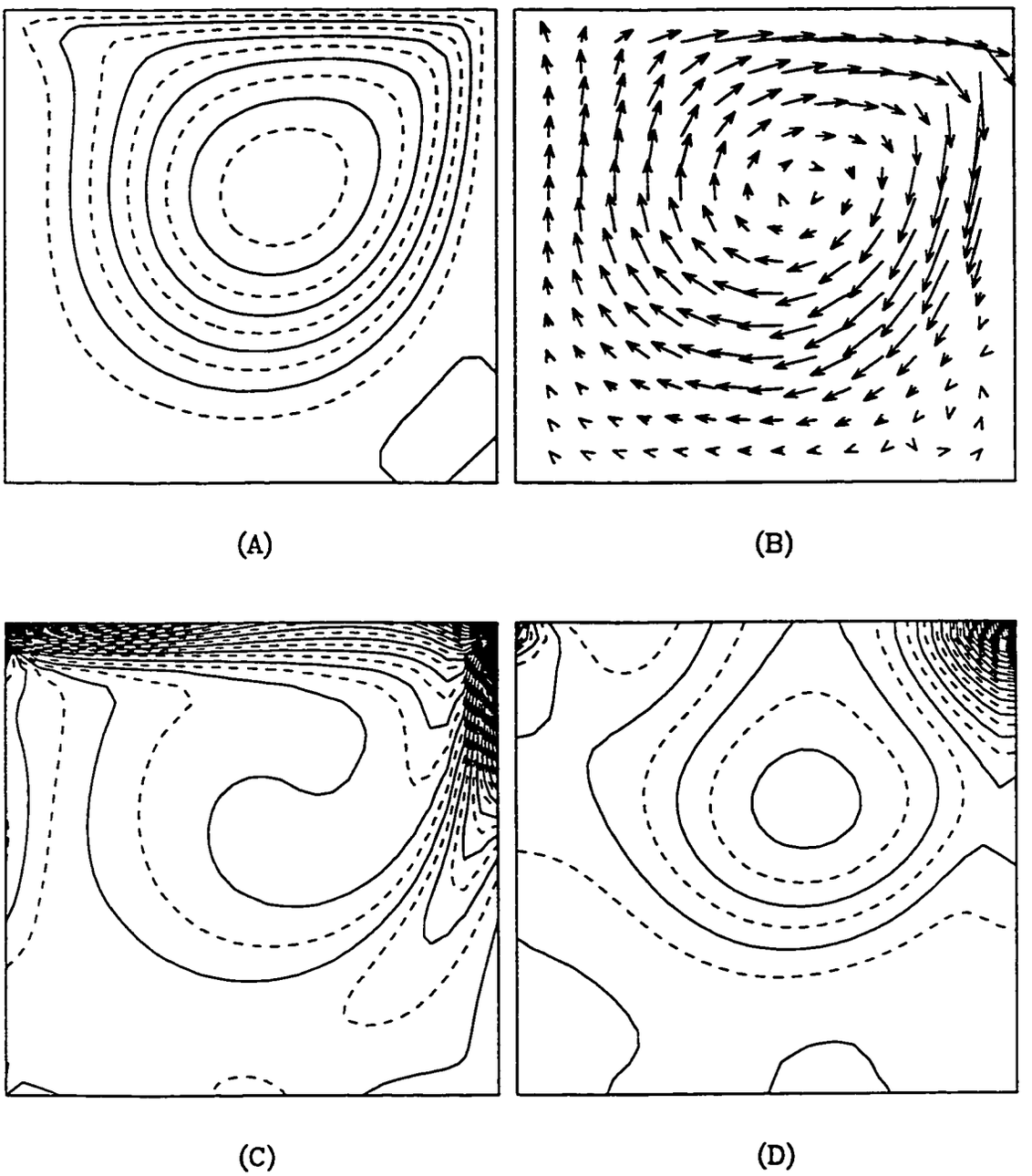

Figure 3-12 Flow Pattern in The Square Cavity of Re = 400
(A) Stream Contour Line
(B) Velocity Vectors
(C) Vorticity Contour
(D) Pressure Coefficient Contour

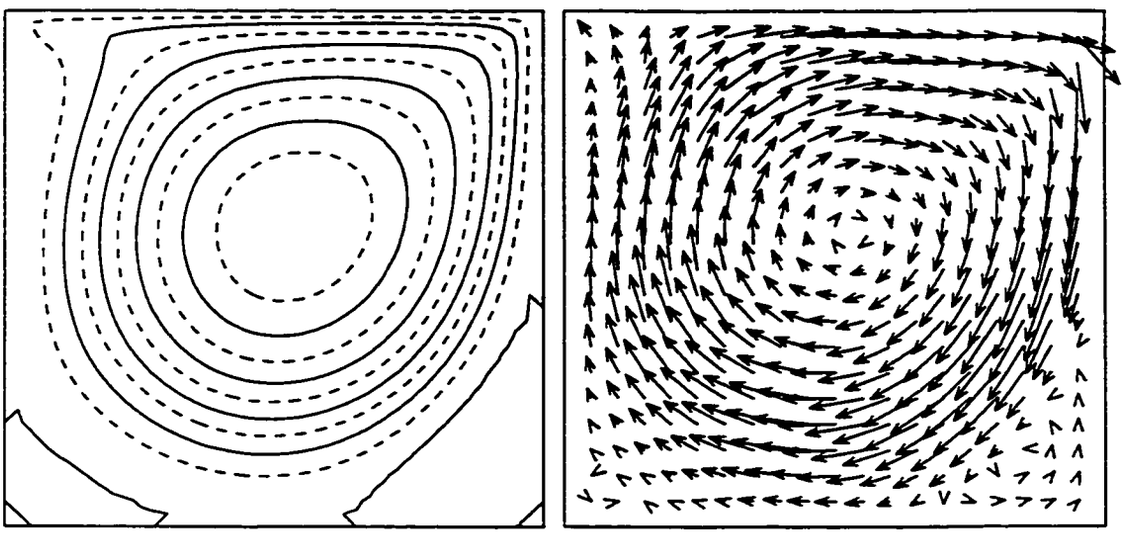

(A) (B)

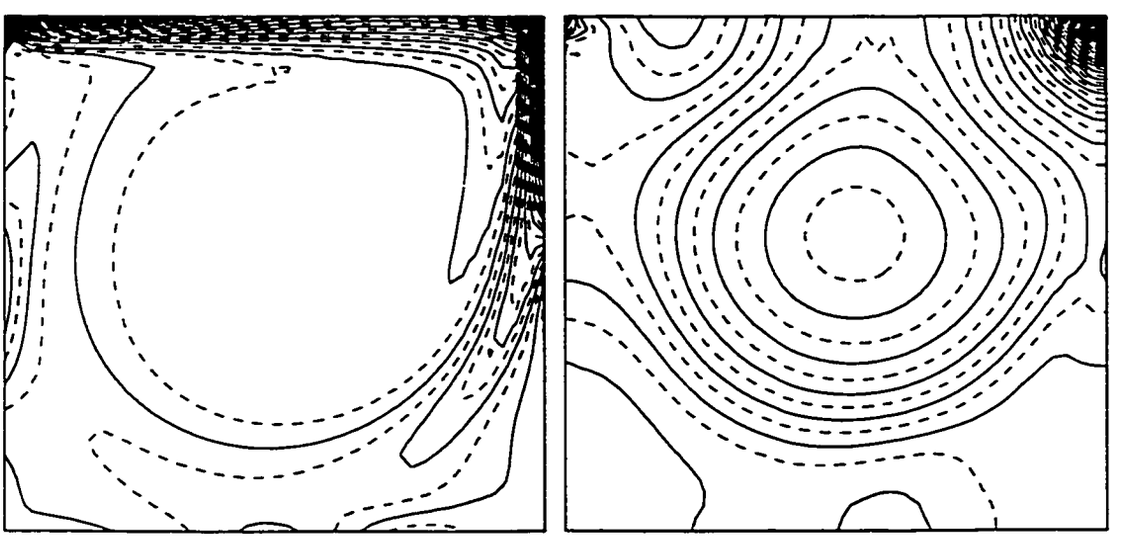

(C) (D)

Figure 3-13 Flow Pattern in The Square Cavity of Re = 1000
(A) Stream Contour Line
(B) Velocity Vectors
(C) Vorticity Contour
(D) Pressure Coefficient Contour

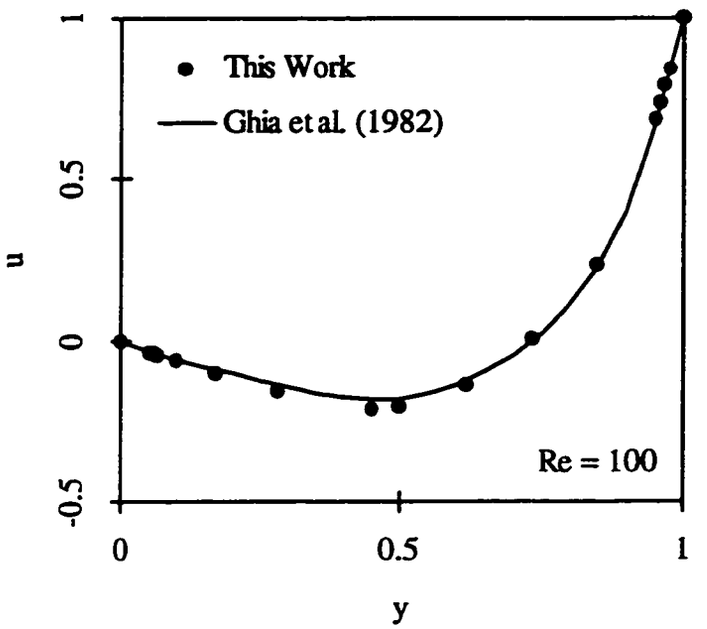

(a)

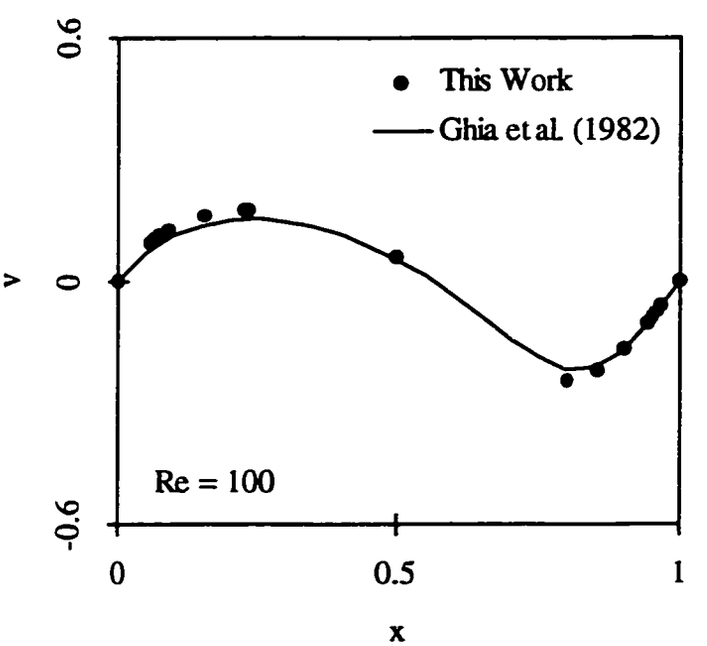

(b)

Figure 3-14 Central Line Velocity Distributions of Re = 100
(a) u-Velocity along Vertical Central Line
(b) v-Velocity along Horizontal Central Line

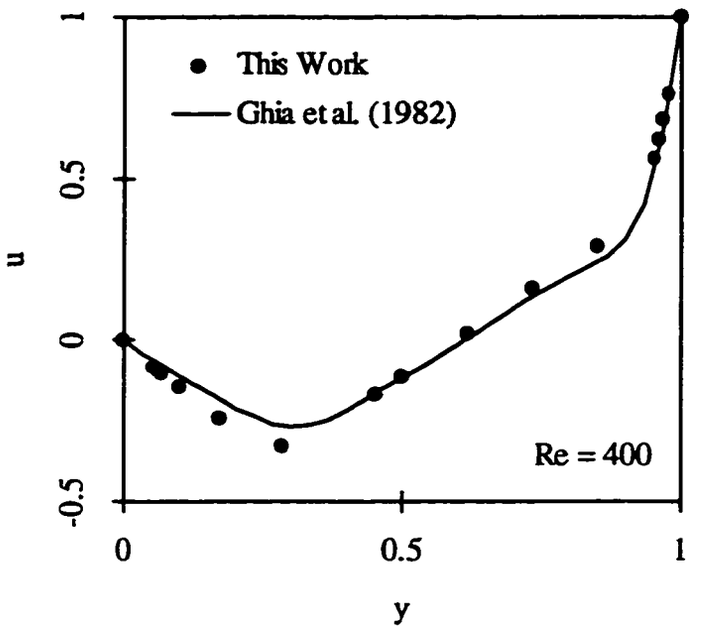

(a)

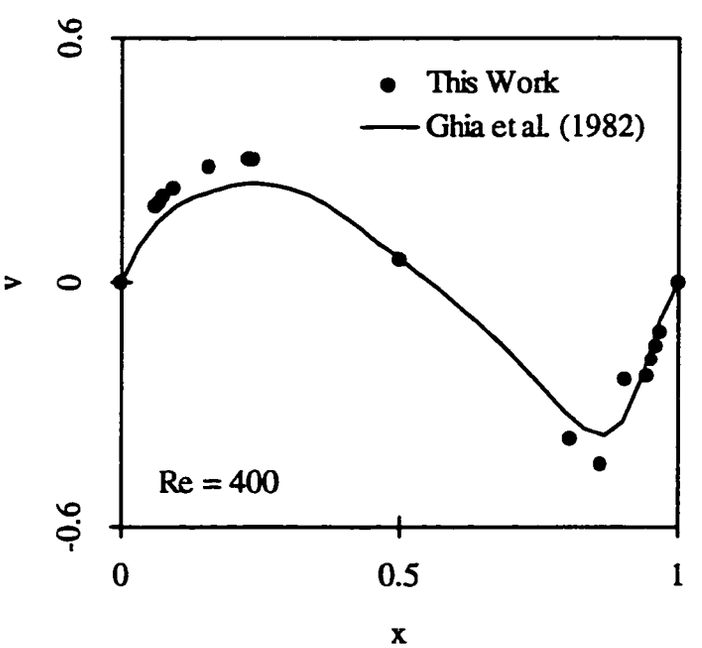

(b)

Figure 3-15 Central Line Velocity Distributions of Re = 400
(a) u-Velocity along Vertical Central Line
(b) v-Velocity along Horizontal Central Line

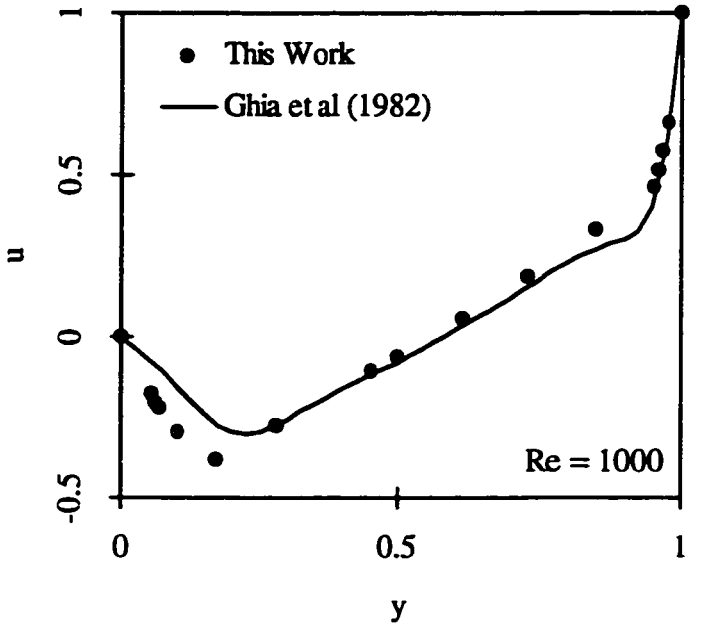

(a)

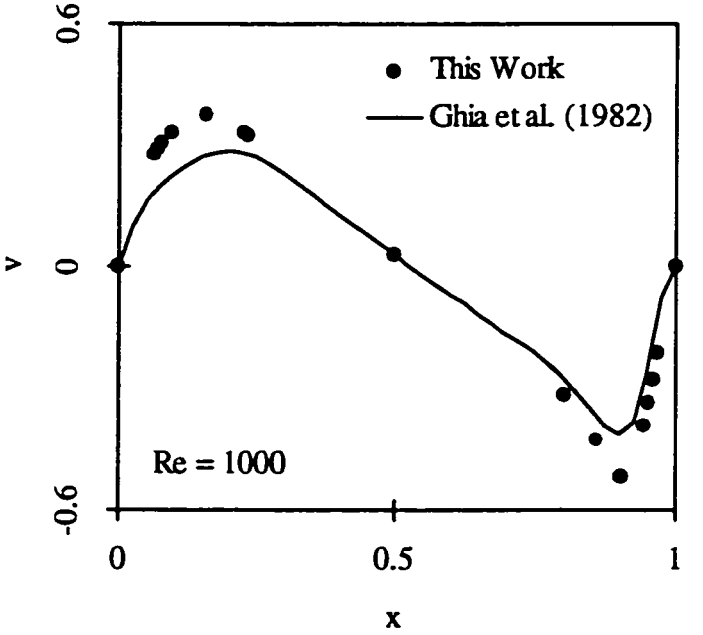

(b)

Figure 3-16 Central Line Velocity Distributions of Re = 1000
(a) u-Velocity along Vertical Central Line
(b) v-Velocity along Horizontal Central Line

This method has been tested by the standard square driven cavity problem, and is shown to be very accurate and efficient for the steady state solutions of an incompressible fluid flow on a general curvilinear non-staggered grid system. As we mentioned before our aim is to obtain the time-accurate solution of our flow system, including the intermediate state solution. This method has to be further tested for its accuracy and efficiency by a transient flow problem before it can be employed to our flow system.

3.3.2 Oscillating Square Driven Cavity

The square driven cavity with a periodically oscillating lid is a good test for testing the time factor in our procedure. The oscillating lid velocity is given as

$$U(t) = U_0 \cos \omega t \tag{3-50}$$

where, ω is the frequency, with the period $T = 2\pi/\omega$. In these calculations we will take $U_0 = 1.0$ and $\omega = 1.0$. The Reynolds number is 400 based on the maximum lid velocity U_0. The steady state solution for the standard square driven cavity problem of Re = 400 is taken as the initial velocity field and pressure field. The physical time-step in the calculation is $2\pi/40$, i.e. one period is divided into 40 uniform time intervals. The pseudo-time boundary condition on the top oscillating wall is

$$\bar{u} = U(t_{n+1}) - U(t_n) \tag{3-51}$$

There is no steady state solution for this problem, but after a certain period of time, the solution tends to a periodic state. That is to say, after certain time the flow pattern inside the cavity at time t is exactly the same as it is at time T+t, 2T+t, etc. The time needed to get to the periodic state is about 8 periods, in our calculations. Soh and Goodrich (1988) reported the same number for this case. The time history of the flow development is shown in Figure 3-17 to Figure 3-21 by presenting the stream function contours (top subplot), the vorticity contours (middle subplot), and the pressure coefficient contours (bottom subplot). The solution at t = 9T and t = 10T are identical to the solution at t = 8T. So the periodic state is obtained after 8 periods.

The solutions for the periodic steady state are presented in Figure 3-22 to Figure 3-26 at the 11th cycle for $10T < t < 11T$. A symmetry consideration leads us to expect that the flow pattern at times t and t+T/2 are mirror images of each other. Generally, our calculations support this point. Figure 3-22 to Figure 3-26 are an illustration of flow patterns inside the cavity for the times 10T and $10T+20\Delta t$, $10T+4\Delta t$ and $10T+24\Delta t$, $10T+8\Delta t$ and $10T+28\Delta t$, $10T+12\Delta t$ and $10T+32\Delta t$, and $10T+16\Delta t$ and $10T+36\Delta t$, respectively.

This numerical computational method based on a non-staggered grid has been tested by a steady state and transient problem for its efficiency, accuracy and correctness. In this method a pseudo-time system in the velocity and pressure primitive variables is adopted, and the pressure Poisson approach is employed in the pseudo-time system for smooth pressure field. It can provide physically meaningful results for all physical time steps, and can be used to analyze both steady state and dynamic problems. When our interest is limited to the steady state solution, the method can be simplified by limiting the number of iterations in pseudo-time loop.

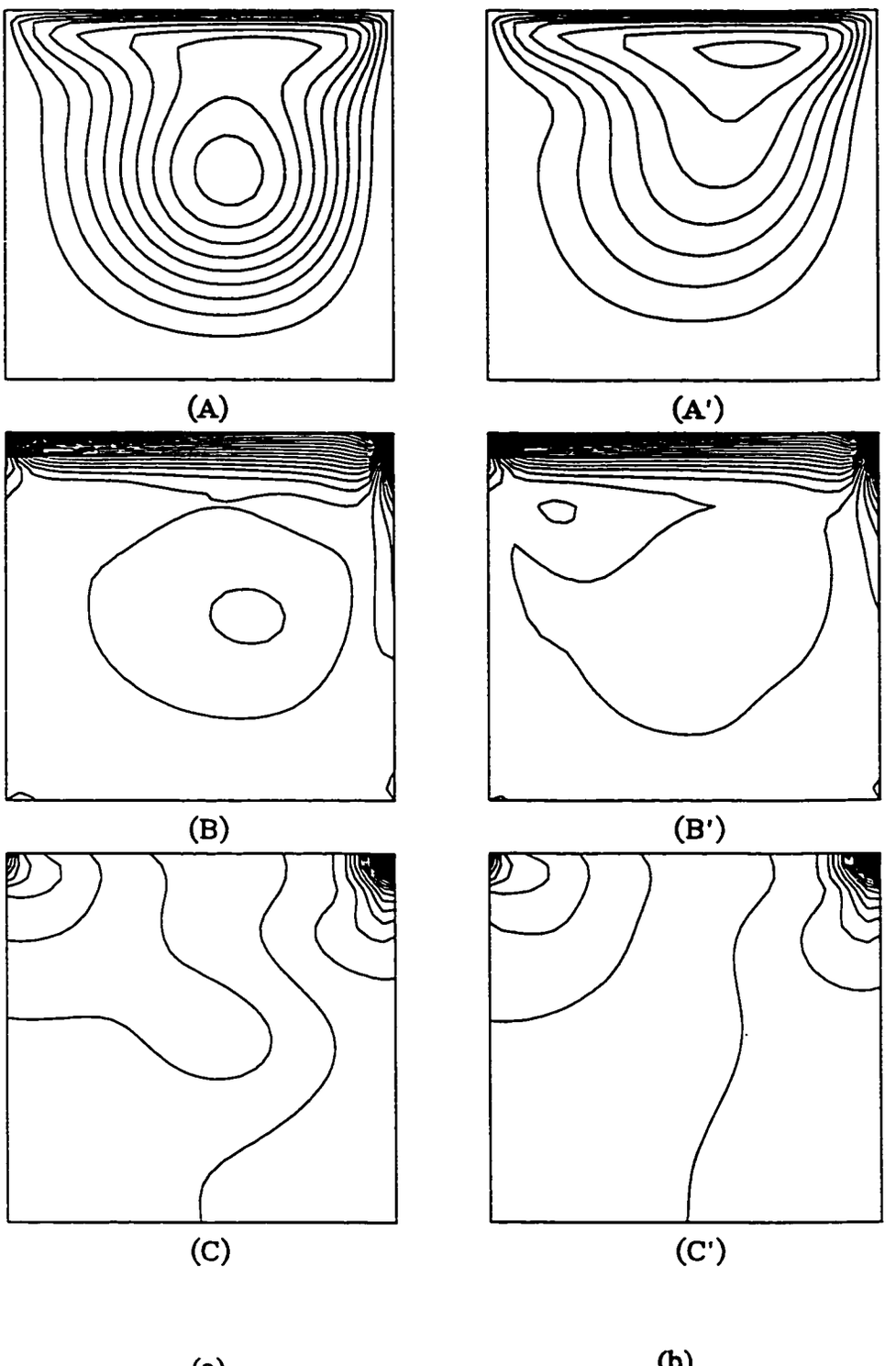

Figure 3-17 Flow Pattern inside The Square Cavity with An Oscillating Top Wall for (a) t = 1T and (b) t = 2T

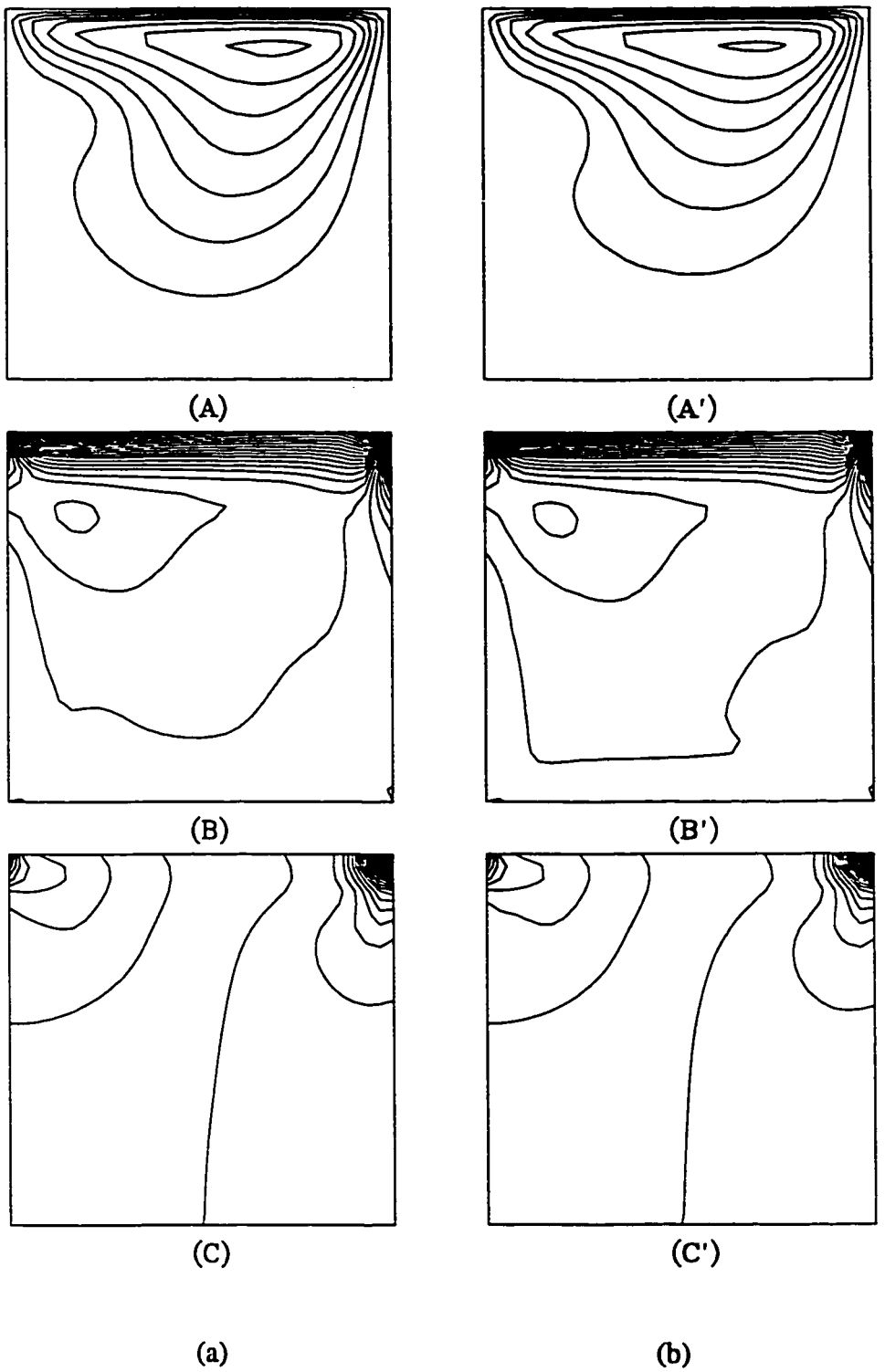

Figure 3-18 Flow Pattern inside The Square Cavity with An Oscillating Top Wall for (a) t = 3T and (b) t = 4T

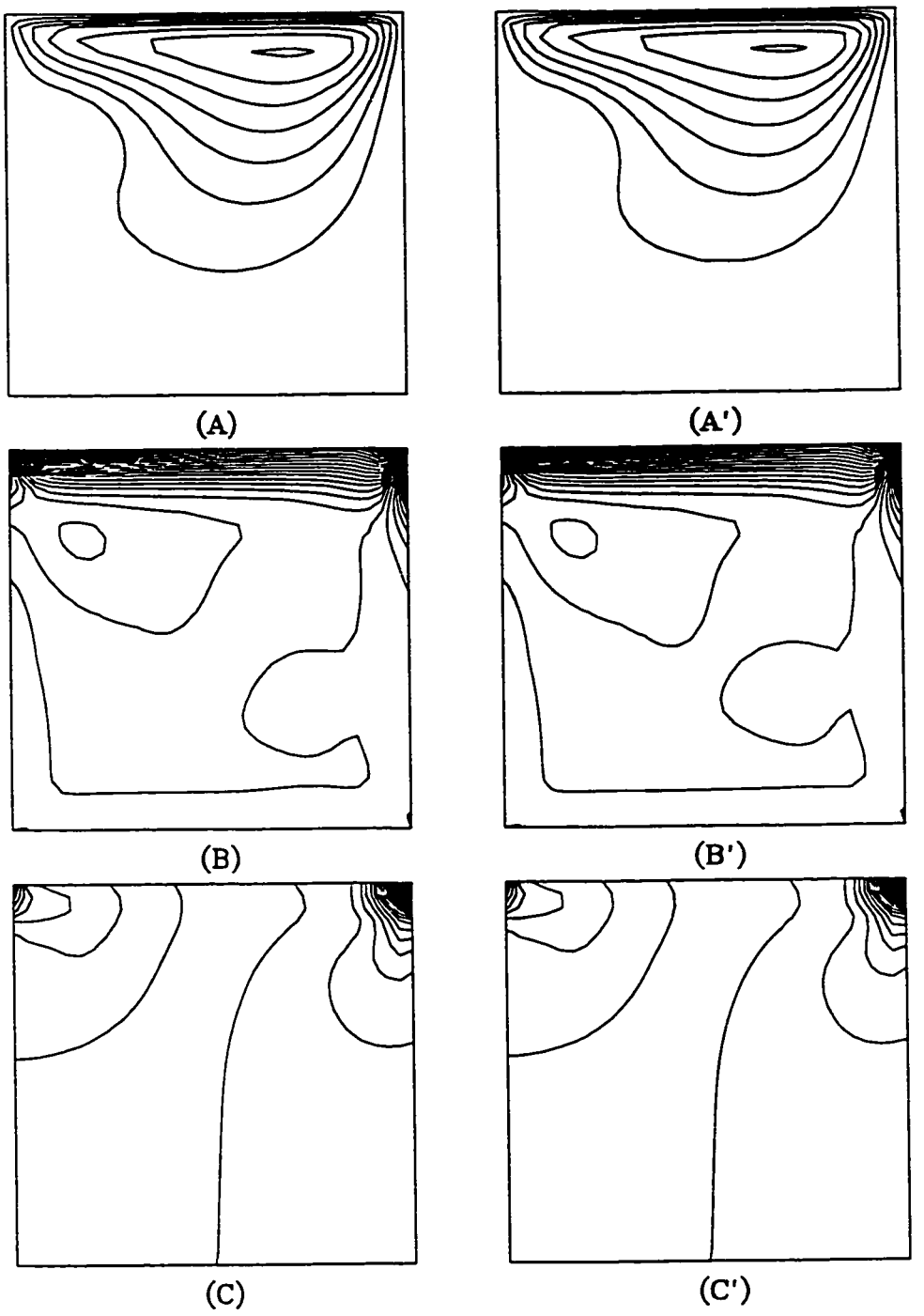

Figure 3-19 Flow Pattern inside The Square Cavity with An Oscillating Top Wall for (a) t = 5T and (b) t = 6T

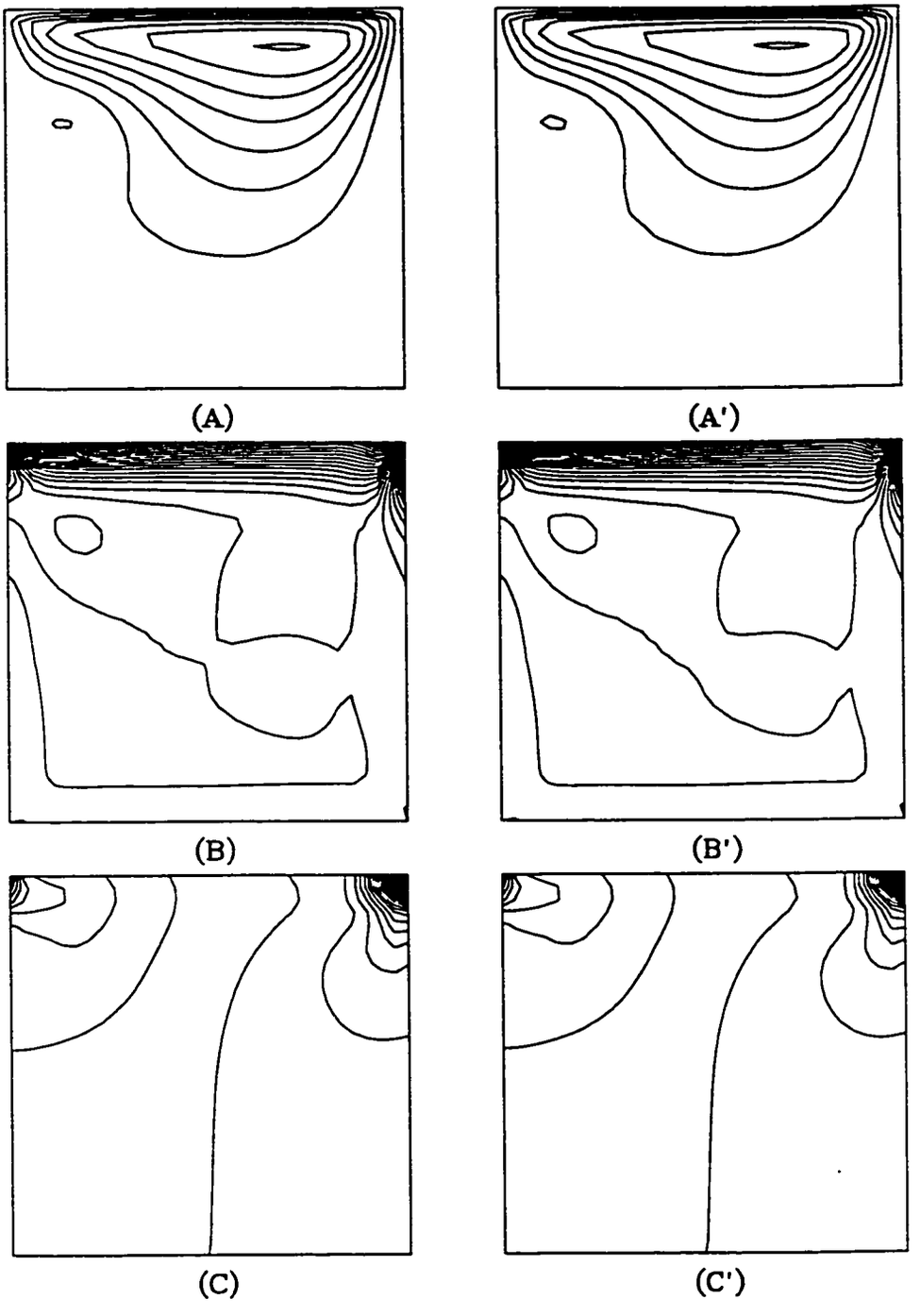

Figure 3-20 Flow Pattern inside The Square Cavity with An Oscillating Top Wall for (a) t = 7T and (b) t = 8T

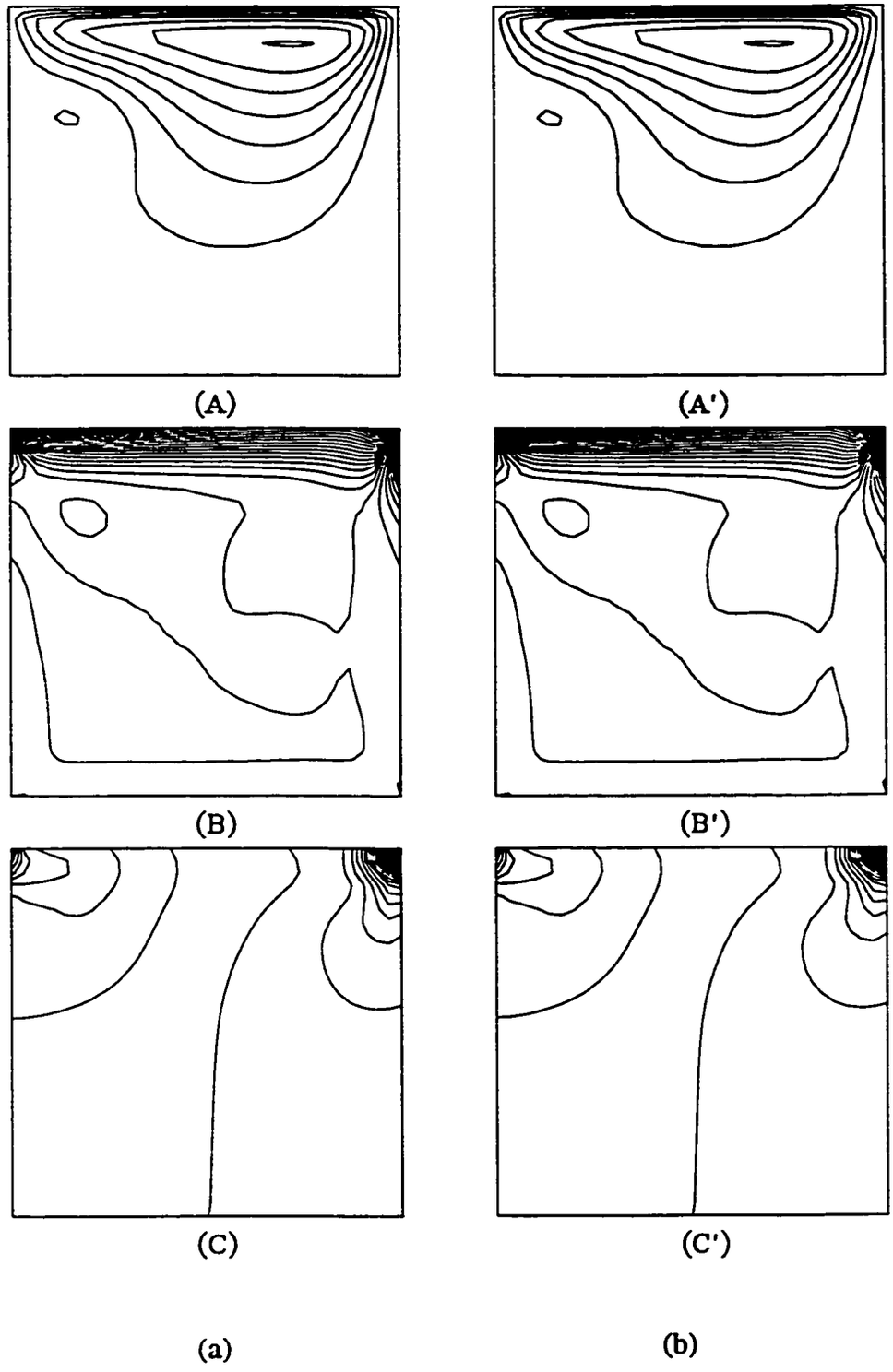

Figure 3-21 Flow Pattern inside The Square Cavity with An Oscillating Top Wall for (a) t = 9T and (b) t = 10T

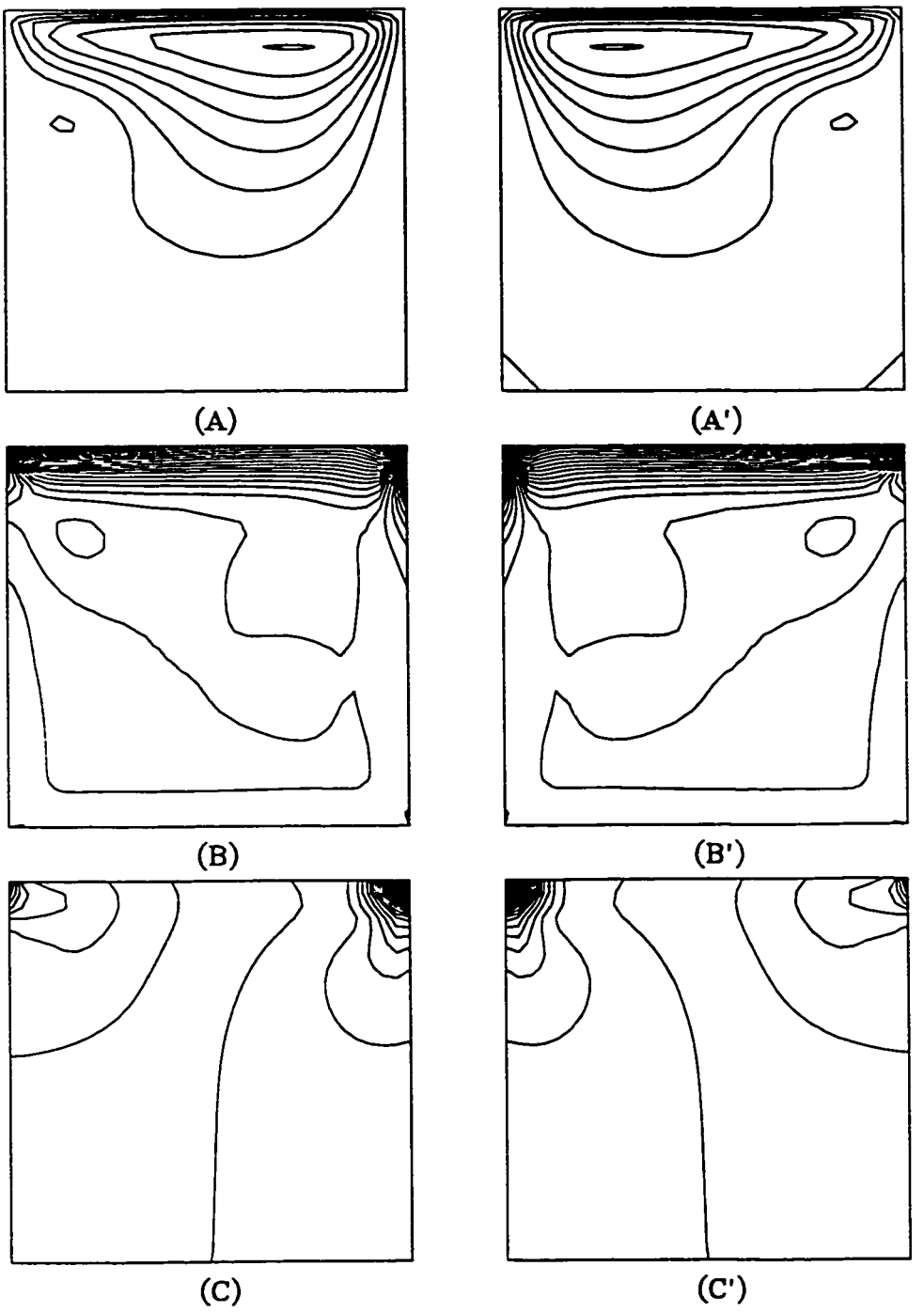

Figure 3-22 Flow Pattern inside The Square Cavity with An Oscillating Top Wall for (a) $t = 10T+0\Delta t$ and (b) $t = 10T+20\Delta t$

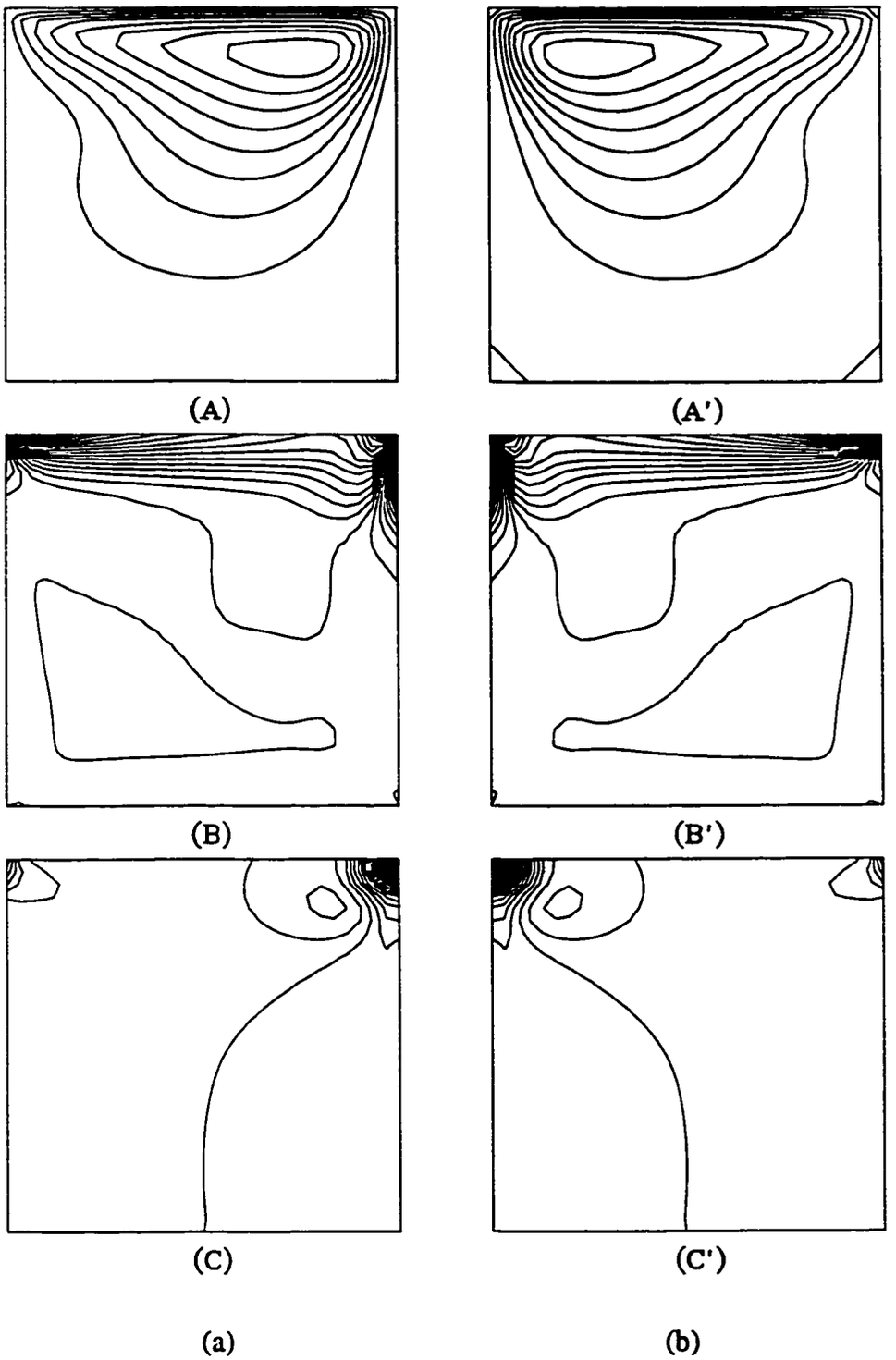

Figure 3-23 Flow Pattern inside The Square Cavity with An Oscillating Top Wall for (a) $t = 10T+4\Delta t$ and (b) $t = 10T+24\Delta t$

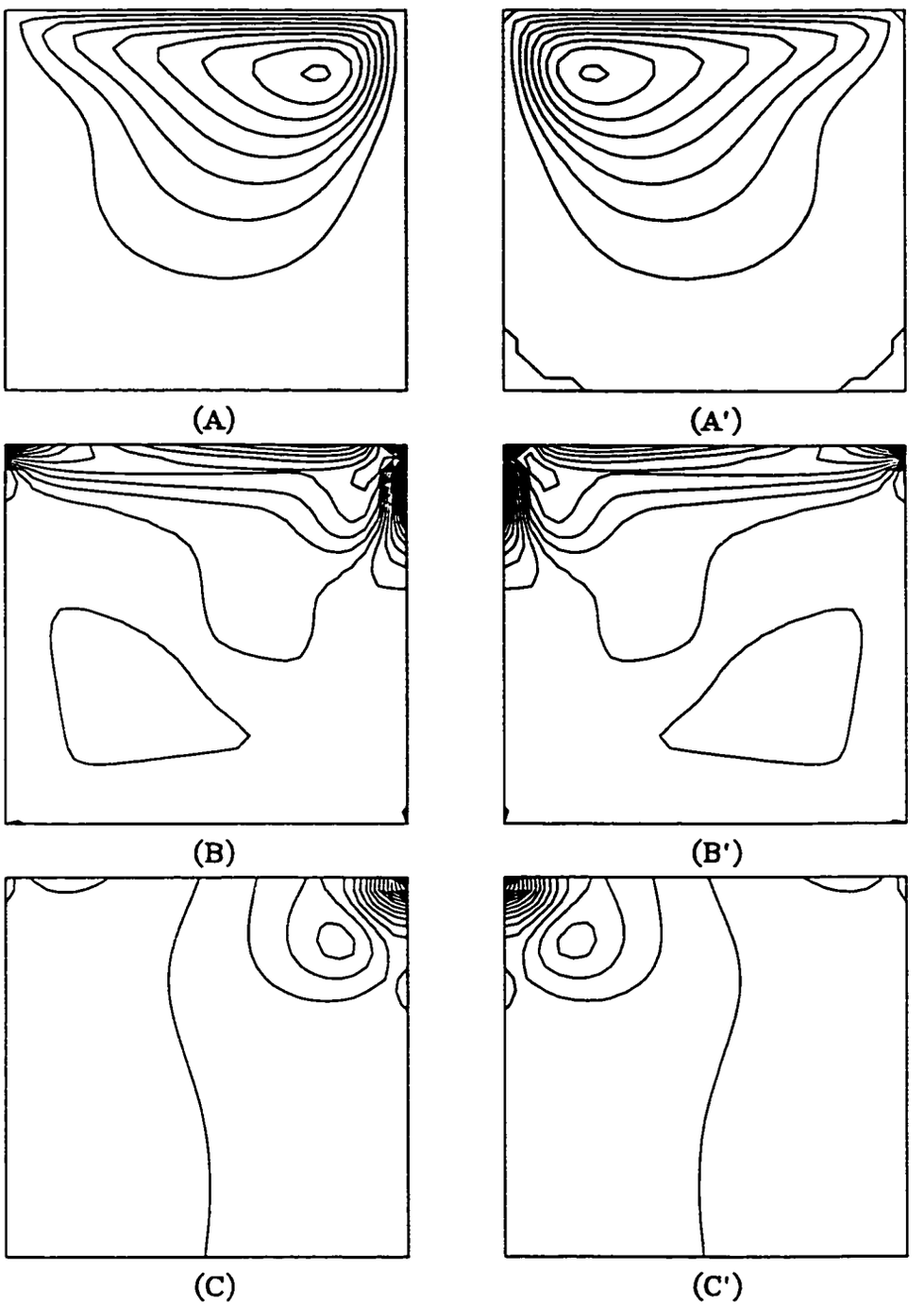

Figure 3-24 Flow Pattern inside The Square Cavity with An Oscillating Top Wall for (a) $t = 10T+8\Delta t$ and (b) $t = 10T+28\Delta t$

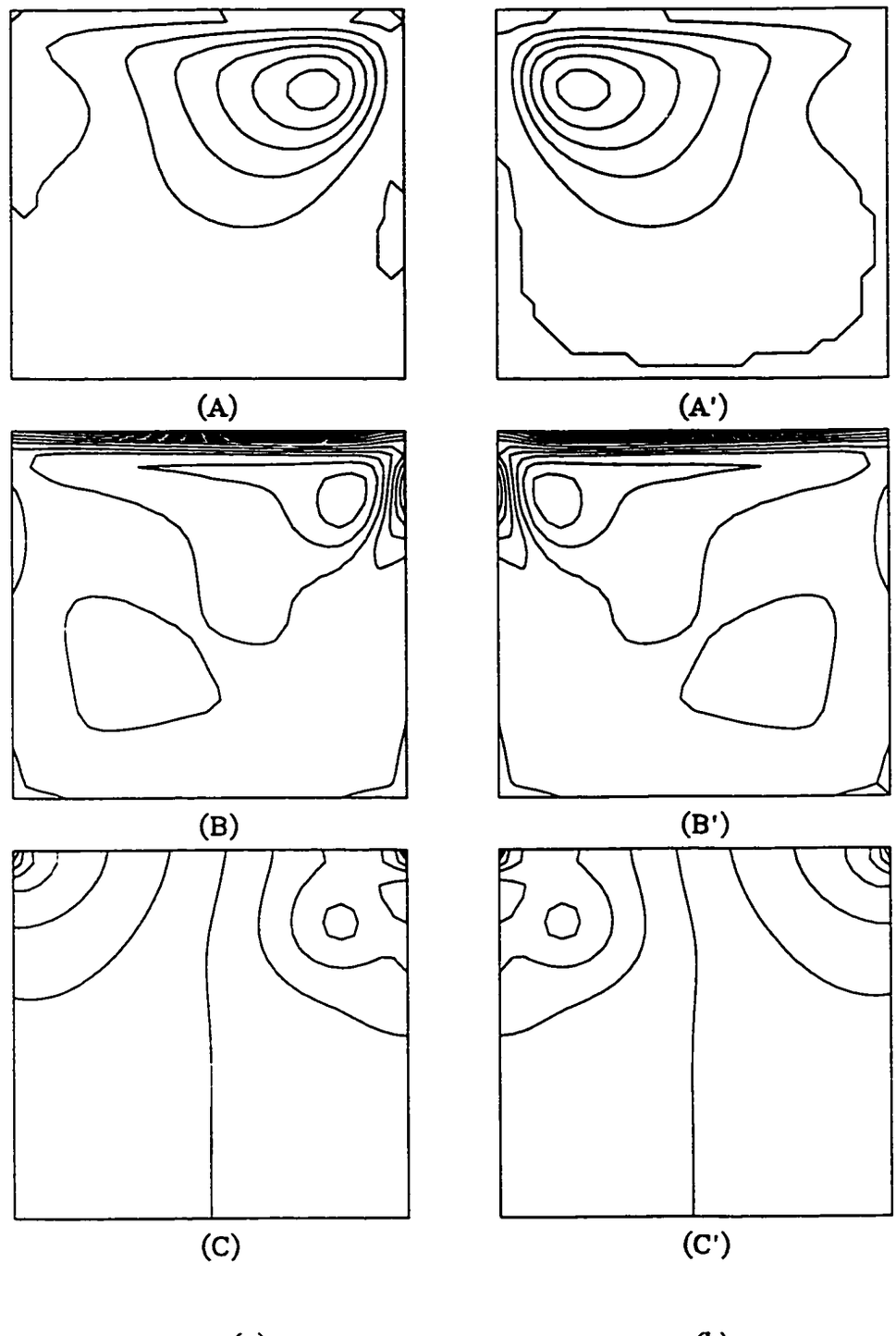

Figure 3-25 Flow Pattern inside The Square Cavity with An Oscillating Top Wall for (a) $t = 10T+12\Delta t$ and (b) $t = 10T+32\Delta t$

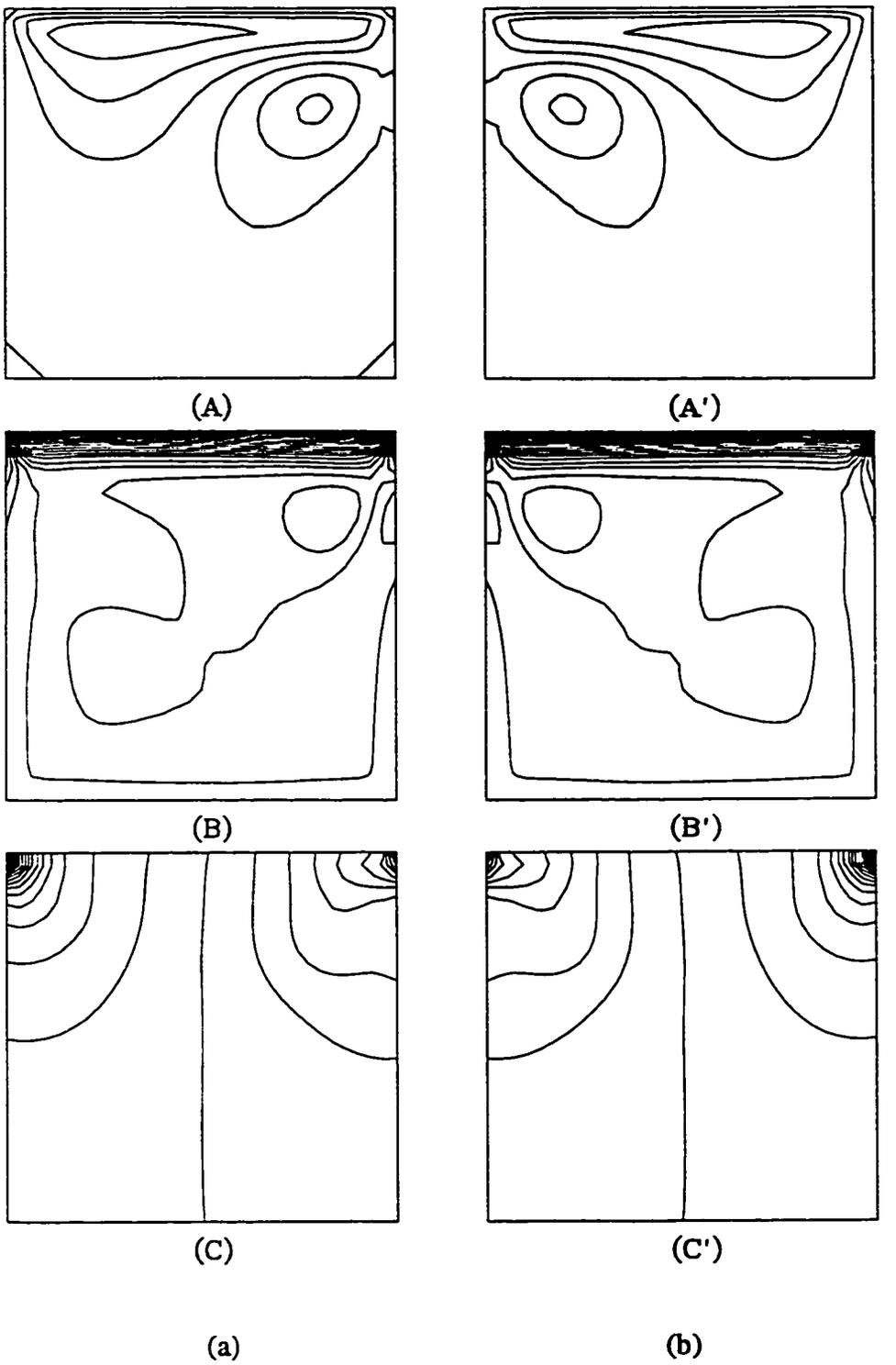

Figure 3-26 Flow Pattern inside The Square Cavity with An Oscillating Top Wall for (a) $t = 10T+16\Delta t$ and (b) $t = 10T+36\Delta t$

CHAPTER IV
NUMERICAL SIMULATION

A new computational scheme was developed in chapter III. Two known dynamic problems, namely, the standard square driven cavity (SSDC) problem and the oscillating square driven cavity (OSDC) problem, were used to test the method. The results suggested that the method is good for both steady and unsteady state fluid dynamic problems.

In this chapter the method will be used to simulate our flow system of a single layer. The complete boundary conditions of the flow system are given here. The formulation and implementation of these boundary conditions, especially the boundary conditions on the free surface, are addressed in detail. Then, a new approach is introduced to describe the imposed disturbance. Finally, results of the simulation are presented.

4.1 THE BOUNDARY CONDITIONS

The boundary of this flow system can be divided into three sections; solid bottom wall boundary, free surface boundary on the top, and inlet/outlet boundaries.

The velocity boundary condition on the solid wall is the no-slip condition.

$$u = 0,\ v = 0 \quad \text{for } y = 0,\ 0 \le x \le L \tag{4-1}$$

where L is the dimensionless length of the inclined plane. In pseudo-time domain, it is

$$\bar{u} = 0,\ \bar{v} = 0 \quad \text{for } y = 0,\ 0 \le x \le L \tag{4-2}$$

The velocity boundary condition at the inlet boundary is given by

$$u = U(y)[1 + u_{dis}(t)],\quad v = 0 \qquad \text{for} \quad x = 0,\ 0 \le y \le 1 \tag{4-3}$$

where U(y) is the steady state velocity of the flow system considered, which is in the form of a parabolic distribution; and $u_{dis}(t)$ is the imposed velocity disturbance.

$$U(y) = 2y - y^2 \tag{4-4}$$

$$u_{dis}(t) = A\sin(2\pi ft) \tag{4-5}$$

Here, A and f are the dimensionless amplitude and frequency of the disturbance.

In the pseudo-time domain the condition becomes

$$\bar{u} = U(y)\,A[\sin(2\pi f(t+\Delta t) - \sin(2\pi ft)] \quad \text{for} \quad x = 0,\ 0 \le y \le 1 \tag{4-6a}$$

$$\bar{v} = 0 \quad \text{for} \quad x = 0,\ 0 \le y \le 1 \tag{4-6b}$$

This boundary condition is consistent with the non-slip condition on the solid wall.

The velocity at the outlet is controlled by a condition that assumes continuity of the same velocity gradient (continuous flow),

$$\frac{\partial^2 u}{\partial x^2} = 0 \quad \text{for} \quad x = L,\ \ 0 \le y \le 1 \tag{4-7a}$$

and the continuity equation.

$$\frac{\partial u}{\partial x} + \frac{\partial v}{\partial y} = 0 \quad \text{for} \quad x = L,\ \ 0 \le y \le 1 \tag{4-7b}$$

In pseudo-time domain, they are

$$\frac{\partial^2 \bar{u}}{\partial x^2} = -\frac{\partial^2 u}{\partial x^2} \quad \text{for} \quad x = L,\ \ 0 \le y \le 1 \tag{4-8a}$$

$$\frac{\partial \bar{u}}{\partial x} + \frac{\partial \bar{v}}{\partial y} = -\left(\frac{\partial u}{\partial x} + \frac{\partial v}{\partial y}\right) \quad \text{for} \quad x = L,\ \ 0 \le y \le 1 \tag{4-8b}$$

It is noted that these conditions need to be transferred into the general curvilinear coordinate system, (ζ, η). The pressure conditions on the solid wall and inlet/outlet boundaries are the Neumann boundary conditions defined in the Chapter III.

At the free surface, there are four unknowns, u, v, p and the free surface position y(x). Four independent boundary conditions are needed. They are the normal and shear stress balance conditions, the continuity equation, and the kinematic condition.

The normal and shear stress balance on the free surface can be found in the work of Esmail and Hummel (1975). In dimensional form they are

$$2b\left(\frac{\partial u}{\partial x}-\frac{\partial v}{\partial y}\right)-(1-b^2)\left(\frac{\partial v}{\partial x}+\frac{\partial u}{\partial y}\right)=0 \tag{4-9a}$$

$$b\mu\left(\frac{\partial v}{\partial x}+\frac{\partial u}{\partial y}\right)-2\mu\frac{\partial v}{\partial y}+\left(p-p_0+\frac{\sigma}{R}\right)=0 \tag{4-9b}$$

where $b=\frac{dy}{dx}$; $R=\frac{db/dx}{(1+b^2)^{3/2}}$ are the free surface profile and the radius of curvature of the free surface; μ and σ the viscosity and the surface tension of the fluid, respectively. p_0 is the atmospheric pressure. In dimensionless form they are

$$-2b\frac{\partial u}{\partial x}+\frac{\partial u}{\partial y}+\frac{\partial v}{\partial x}+bRe\left(p-p_0+\frac{1}{RWe}\right)=0 \tag{4-10a}$$

$$2\frac{\partial v}{\partial y}-b\left(\frac{\partial u}{\partial y}+\frac{\partial v}{\partial x}\right)-bRe\left(p-p_0+\frac{1}{RWe}\right)=0 \tag{4-10b}$$

At the free surface, the continuity equation, Equation (4-7b), must be satisfied. Besides, the free surface by nature is a streamline. Therefore, the following kinematic condition, which expresses a mass balance across the liquid film, must be satisfied too.

$$\frac{dy}{dx}=\frac{v}{u} \tag{4-10c}$$

In order to impose these four boundary conditions on the free surface we have to transform them into the general curvilinear coordinate system. The transformations of Equation (4-7b) and (4-10c) are straightforward. The transformation of Equations (4-10a) and (4-10b) can be found in Thompson's work (Thompson, 1980). They are

$$\alpha^2\frac{\partial u}{\partial \zeta}=\left(\alpha\beta-J\frac{\partial x}{\partial \eta}\frac{\partial y}{\partial \eta}\right)\frac{\partial u}{\partial \eta}+J\left(\frac{\partial x}{\partial \eta}\right)^2\frac{\partial v}{\partial \eta}$$
$$+\frac{1}{2}ReJ\alpha\frac{\partial y}{\partial \eta}\left(p-p_0+\frac{1}{RWe}\right) \tag{4-11a}$$

$$\alpha^2\frac{\partial v}{\partial \zeta}=\left(\alpha\beta+J\frac{\partial x}{\partial \eta}\frac{\partial y}{\partial \eta}\right)\frac{\partial v}{\partial \eta}-J\left(\frac{\partial y}{\partial \eta}\right)^2\frac{\partial u}{\partial \eta}$$
$$-\frac{1}{2}ReJ\alpha\frac{\partial x}{\partial \eta}\left(p-p_0+\frac{1}{RWe}\right) \tag{4-11b}$$

The surface is a boundary defined by η = constant, so we can write

$$\frac{\partial u}{\partial \eta}=\frac{(\frac{\partial u}{\partial \zeta}\frac{\partial y}{\partial \eta}-\frac{\partial v}{\partial \zeta}\frac{\partial x}{\partial \eta})[J(\frac{\partial x}{\partial \eta})^3+(\alpha\beta+J\frac{\partial x}{\partial \eta}\frac{\partial y}{\partial \eta})\frac{\partial y}{\partial \eta}]+\alpha^2\frac{\partial x}{\partial \zeta}(\frac{\partial u}{\partial \zeta}\frac{\partial x}{\partial \eta}+\frac{\partial v}{\partial \zeta}\frac{\partial y}{\partial \eta})}{\frac{\partial y}{\partial \zeta}[J(\frac{\partial x}{\partial \eta})^3+(\alpha\beta+J\frac{\partial x}{\partial \eta}\frac{\partial y}{\partial \eta})\frac{\partial y}{\partial \eta}]-\frac{\partial x}{\partial \zeta}[J(\frac{\partial y}{\partial \eta})^3-(\alpha\beta-J\frac{\partial x}{\partial \eta}\frac{\partial y}{\partial \eta})\frac{\partial x}{\partial \eta}]} \tag{4-12a}$$

$$\frac{\partial v}{\partial \eta}=\frac{(\frac{\partial u}{\partial \zeta}\frac{\partial y}{\partial \eta}-\frac{\partial v}{\partial \zeta}\frac{\partial x}{\partial \eta})[J(\frac{\partial y}{\partial \eta})^3+(\alpha\beta-J\frac{\partial x}{\partial \eta}\frac{\partial y}{\partial \eta})\frac{\partial x}{\partial \eta}]+\alpha^2\frac{\partial y}{\partial \zeta}(\frac{\partial u}{\partial \zeta}\frac{\partial x}{\partial \eta}+\frac{\partial v}{\partial \zeta}\frac{\partial y}{\partial \eta})}{\frac{\partial y}{\partial \zeta}[J(\frac{\partial x}{\partial \eta})^3+(\alpha\beta+J\frac{\partial x}{\partial \eta}\frac{\partial y}{\partial \eta})\frac{\partial y}{\partial \eta}]-\frac{\partial x}{\partial \zeta}[J(\frac{\partial y}{\partial \eta})^3-(\alpha\beta-J\frac{\partial x}{\partial \eta}\frac{\partial y}{\partial \eta})\frac{\partial x}{\partial \eta}]} \tag{4-12b}$$

in which the continuity equation was used to eliminate the pressure term.

Equation (4-12) can be rewritten in the following compact form

$$A\frac{\partial E}{\partial \eta}+B\frac{\partial E}{\partial \zeta}=0 \tag{4-13}$$

where

$$A=\begin{vmatrix} t_1\frac{\partial y}{\partial \zeta}-t_2\frac{\partial x}{\partial \zeta} & 0 \\ 0 & t_1\frac{\partial y}{\partial \zeta}-t_2\frac{\partial x}{\partial \zeta} \end{vmatrix} \quad E=\begin{vmatrix} u \\ v \end{vmatrix}$$

$$B=\begin{vmatrix} -(t_1\frac{\partial y}{\partial \eta}+\alpha^2\frac{\partial x}{\partial \zeta}\frac{\partial x}{\partial \eta}) & t_1\frac{\partial x}{\partial \eta}-\alpha^2\frac{\partial x}{\partial \zeta}\frac{\partial y}{\partial \eta} \\ -(t_2\frac{\partial y}{\partial \eta}+\alpha^2\frac{\partial y}{\partial \zeta}\frac{\partial x}{\partial \eta}) & t_2\frac{\partial x}{\partial \eta}-\alpha^2\frac{\partial y}{\partial \zeta}\frac{\partial y}{\partial \eta} \end{vmatrix}$$

$$t_1=J(\frac{\partial x}{\partial \eta})^3+(\alpha\beta+J\frac{\partial x}{\partial \eta}\frac{\partial y}{\partial \eta})\frac{\partial y}{\partial \eta}$$

$$t_2=J(\frac{\partial y}{\partial \eta})^3-(\alpha\beta-J\frac{\partial x}{\partial \eta}\frac{\partial y}{\partial \eta})\frac{\partial x}{\partial \eta}$$

In pseudo-time domain Equation (4-13) becomes

$$A\frac{\partial \overline{E}}{\partial \eta}+B\frac{\partial \overline{E}}{\partial \zeta}=-(A\frac{\partial E}{\partial \eta}+B\frac{\partial E}{\partial \zeta}) \tag{4-14}$$

Applying the finite difference approximations to Equation (4-14) we will get a system of block-tridiagonal linear algebraic equations, which is then solved by direct factorization method for the surface velocities in the pseudo-time domain. The surface pressure in pseudo-time domain can be obtained from either Equation (4-11a) or Equation (4-11b), which has to be rewritten in the terms of pseudo-time velocities and pressure.

4.2 TWO APPROACHES TO DISTURBANCE

All disturbances, simple or complex, are described by several components with a single fundamental frequency. In the previous work mentioned in the Literature Review the disturbance concerned is said to be the perturbation of the position of the free surface (i.e. some sort of free surface wave motion) directly, and is described as:

$$\eta = A \exp [i(\alpha x - \omega t)] \qquad (4\text{-}15)$$

where, η is the displacement of the free surface; A is the initial perturbation amplitude; $\omega = 2\pi f\delta/u_0$ is the dimensionless angular frequency, where f is the wave frequency. This assumption implies that: at the time $t = 0^-$ there is no disturbance and the free surface is a straight line; and at time $t = 0^+$ the disturbance of Equation (4-15) is imposed directly on the free surface and the whole free surface is waved at once by this disturbance (Figure 4-1).

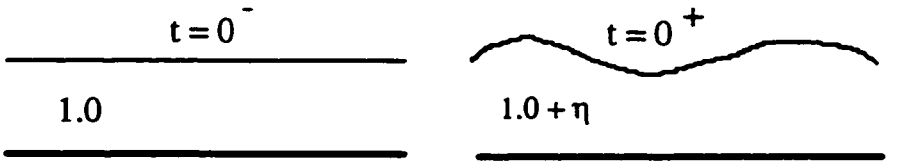

Figure 4-1 The Approach to Disturbance in Literature

In practice, disturbances usually originate from flowrate perturbation. Such disturbances take some time to reshape the velocity field and to disturb the whole free surface. That is, the wave motion on the free surface occurs gradually.

In our work we approach this issue in a different way. Again we use a single disturbance component. However, the disturbance is imposed at the upstream end in the form of a velocity perturbation. At the time $t = 0^-$ no disturbance is imposed and the free surface is a straight line. At the time $t = 0^+$ a minute velocity disturbance is imposed on the upstream end and the free surface will be gradually "waved" by this velocity perturbation (Figure 4-2).

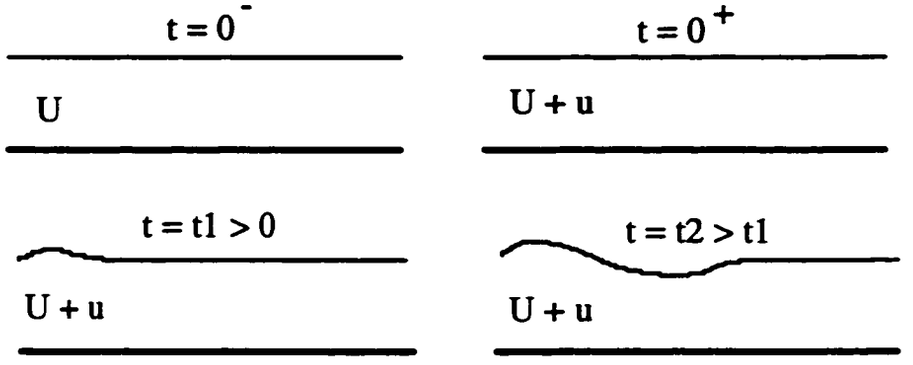

Figure 4-2 The New Approach in This Work

4.3 NUMERICAL RESULTS

The numerical techniques described in Chapter III were applied to viscous liquid flows in thin layers. The initial flow is Nusselt (1916) uniform thickness layer, with a laminar parabolic velocity distribution. This is the undisturbed wave-free flow. At the initial moment a disturbance is imposed at the upstream end of the flow region. This disturbance is in the form of a minute velocity perturbation:

$$u = UA \sin(2\pi ft) \qquad (4\text{-}16)$$

where U is the u-velocity at the steady state, A is the relative amplitude of the disturbance, f is the dimensionless frequency of the disturbance, and t is the dimensionless time. The initial amplitude of the disturbance is set at A = 0.0001. Flow systems were considered to be stable if numerical solutions for velocity and pressure were stable up to a dimensionless time t = 30.0.

In our work, the following simulation parameters are used (refer to Table).

Table 4-1 Simulation Parameters

Parameter	Value
Tolerence	10^{-6}
Precision	Double
Physical Time Increment, Δt	0.01
Pseudo Time Increment, $\Delta \tau$	0.4
Physical Domain, L/W	30
X Grid Size, Δx	0.2
Y Grid Size, Δy	0.1
Stop Time, T	30.0

The numerical method was also tested for much longer stop-time (T = 70.0), different physical domains (L/W = 40, 50, and 60), and different physical time increments (Δt = 0.005 and 0.0025) for its stability and robustness. For each of these test cases, at least 3 combinations of Reynolds number, the properties number of fluid, and the angle of inclination were simulated.

4.3.1 Wave Profiles

The unsteady state time-accurate computational model produced stable wavy regimes for a wide range of flow conditions. Solutions were obtained for different liquid properties $0.0467 < \gamma < 467$, different angles of inclination $0.1° < \theta < 89.9°$, and different Reynolds numbers $Re < 30$. Computations for vertical flow $\theta = 90°$ always diverged. However, any shift in angle from 90° produced stable solutions. Calculations for higher Reynolds numbers consumed increasingly more CPU time.

Figures 4-3 to 4-8 show sets of wave profiles produced for an angle of inclination θ=80°. The profiles shown are graphed for dimensionless distances (with respect to mean thickness), and dimensionless time (with respect to mean thickness, and surface velocity). Liquids with lower viscosity ($\gamma = 467$, Figure 4-3) experienced simple form stable waves running over their free-surfaces. This is in contrast to the more complicated forms of waves running over the free-surfaces of more viscous liquids. For example Figure 4-7 and 4-8 show the waves running over surfaces of a liquid with $\gamma = 0.0467$.

The wave developed at a Reynolds number Re=12.5 (Figure 4-8) seems to be dominated by a longer wavelength than the wave developed at a Reynolds number Re=4.17 (Figure 4-7). All disturbances (Figure 4-3 to 4-8) seem to die out some distance (transit distance) downstream. This computational description of the waves is supported by our experimental observations of Chapter II.

Figures (4-9 to 4-14) show wave profiles computed for an angle of inclination θ=10°. Figures 4-9 and 4-10 show that the transit distance for the smaller Reynolds Re=12.5 is much shorter than that for the higher Reynolds number Re=29.2. This underscores in comparison to Figure 4-3 and 4-4 for θ=80° that the result is independent of the angle of inclination. Although wave forms and amplitudes are different the general conclusions for the angle θ=80° (Figure 4-3 to 4-8) apply to the angle θ=10°.

Figures 4-15 to 4-20 show wave profiles computed for an angle of inclination θ=1°. The transit distances are appreciably longer for all liquids and Reynolds numbers. In fact for the liquid γ=0.0467 the disturbance persists throughout the entire computational region (Figures 4-19 and 4-20). These profiles are clearly dominated by a long wavelength wave. Simple form waves are shown for liquids with lower viscosity γ=46.7 and 467 (Figure 4-15 and 4-16). Figure 4-17 shows a case of a solitary wave that can be predicted by the nonlinear theory (Esmail 1980).

Figures 4-21 and 4-22 show wave profiles for the smallest angle of inclination θ=0.1°. Figure 4-22 shows a long wavelength disturbance which turns into complex ripples as time advances.

4.3.2 Wave Speed

In our calculations we monitored the front edge of the imposed disturbance and followed its development downstream. We established a wave speed reflecting the speed of disturbance propagation C over the free-surface. This wave speed was made dimensionless with respect to the steady state surface speed.

Figures 4-23 and 4-24 show the wave speeds C for the liquid with lower viscosity γ=467. The speed is recorded after a dimensionless time of 1.0, for several angles of inclination. In Figure 4-23 the dependence on the Reynolds number is shown. Wave speeds vary with angle of inclination. They generally decrease with the Reynolds number (Figure 4-23) and the Weber number (Figure 4-24). However, their dependence on the flow rate shows higher wave speeds for lower angles of inclination (close to horizontal). Disturbance propagation is approximately 4 to 6 times the material speed of particles on the surface. In the case of their dependence on the Weber number which represents surface tension, wave speeds collapse in one relationship for all angles of inclination (Figure 4-24).

Figures 4-25 and 4-26 show similar results for a liquid with larger viscosity γ=4.67, at a dimensionless time 2.0. In this set of results a smaller angle of inclination θ=1° show wave speeds that deviate (Figure 4-26) from the general relationship for all other angles of inclination. In general for this more viscous liquid wave speeds range from 2 to 5 times the material speed of particles on the surface.

For a rather viscous liquid γ=0.0467, and dimensionless time 2.0 wave speeds are shown in Figures 4-27 and 4-28. At an angle of inclination θ=1°, wave speeds show the same deviation from the general relationship over the Weber number (Figure 4-26). Wave speeds for this liquid also range from about 5 to 2 times the speed of surface particles.

Figure 4-29 shows a comparison of wave speeds over the Reynolds number for a wide range of liquids. For the same flow rate, wave speeds over the free surface of liquids with smaller property number are lower than their counterpart for liquids with higher property numbers. The same trend continued to a dimensionless time of 5.0 in Figure 4-30. Figures 4-29 and 4-30 are for an almost vertical layer θ=89°. Figure 4-31 to 4-33 show similar results for angles θ=45°, 10°, and 3°.

We compared our results for wave speeds with the experimental results of Chu & Dukler (1974), and the theoretical results of Benjamin (1957) and Yih (1963). Figure 4-34 shows this comparison. Our results, though lying slightly above the experimental measurements of Chu & Dukler (1974), are consistent with them. The linear theories of Benjamin (1957) and Yih (1963), are shown to be a rather rough estimation of actual wave propagation speeds.

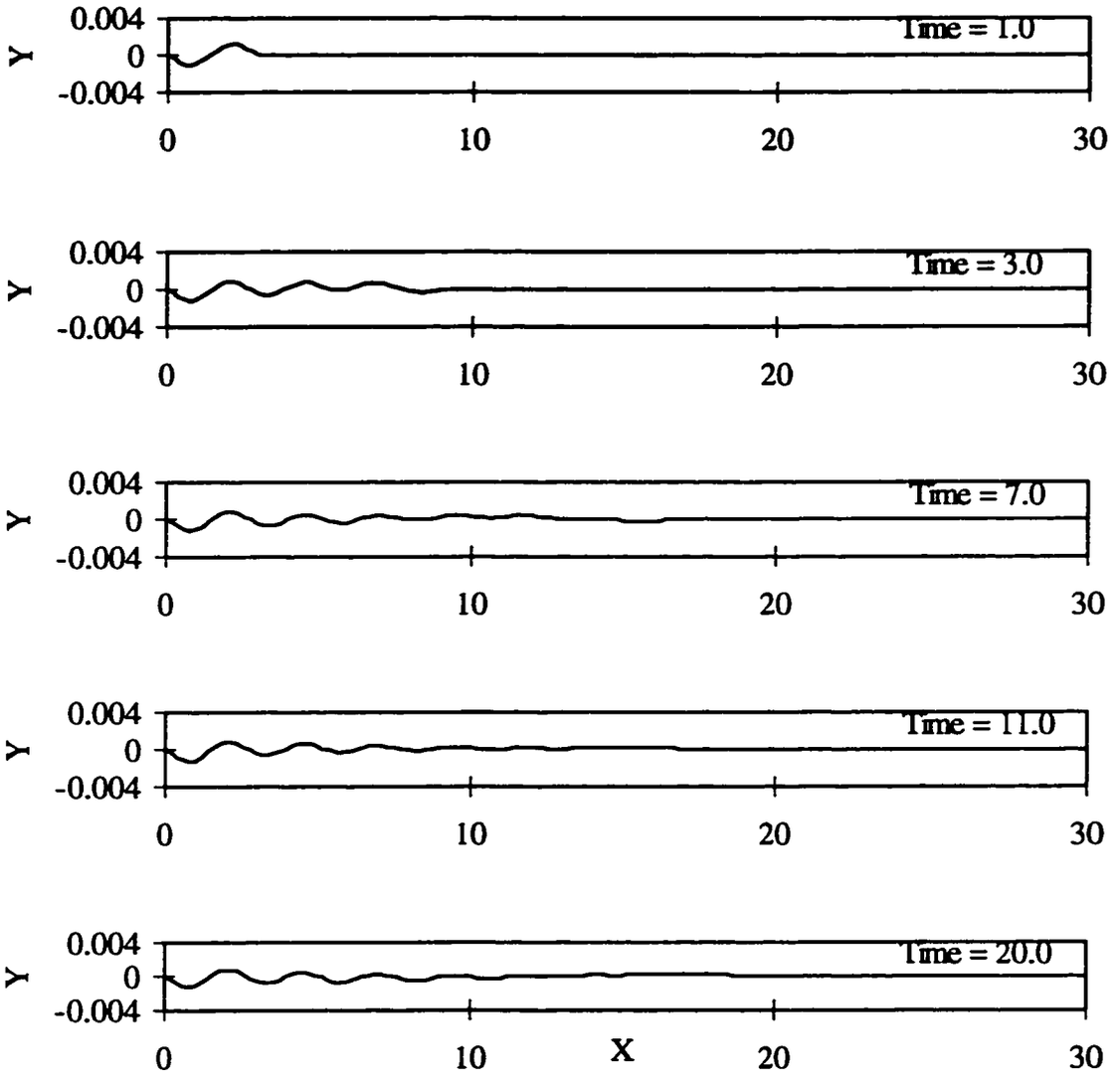

Figure 4-3 Wave Profile (Re=29.2, θ=80°, γ=467)

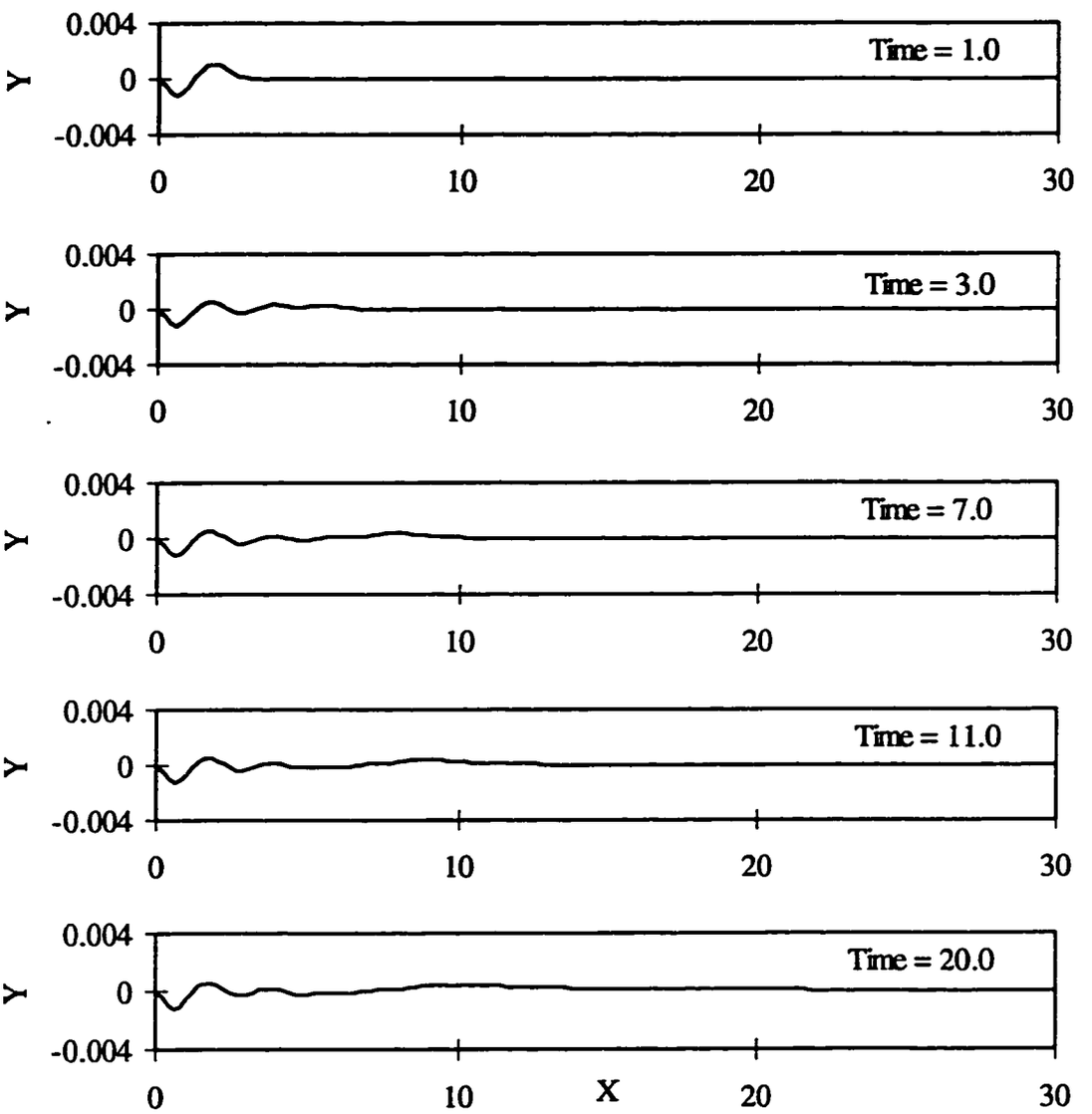

Figure 4-4 Wave Profile (Re=12.5, θ=80°, γ=46.7)

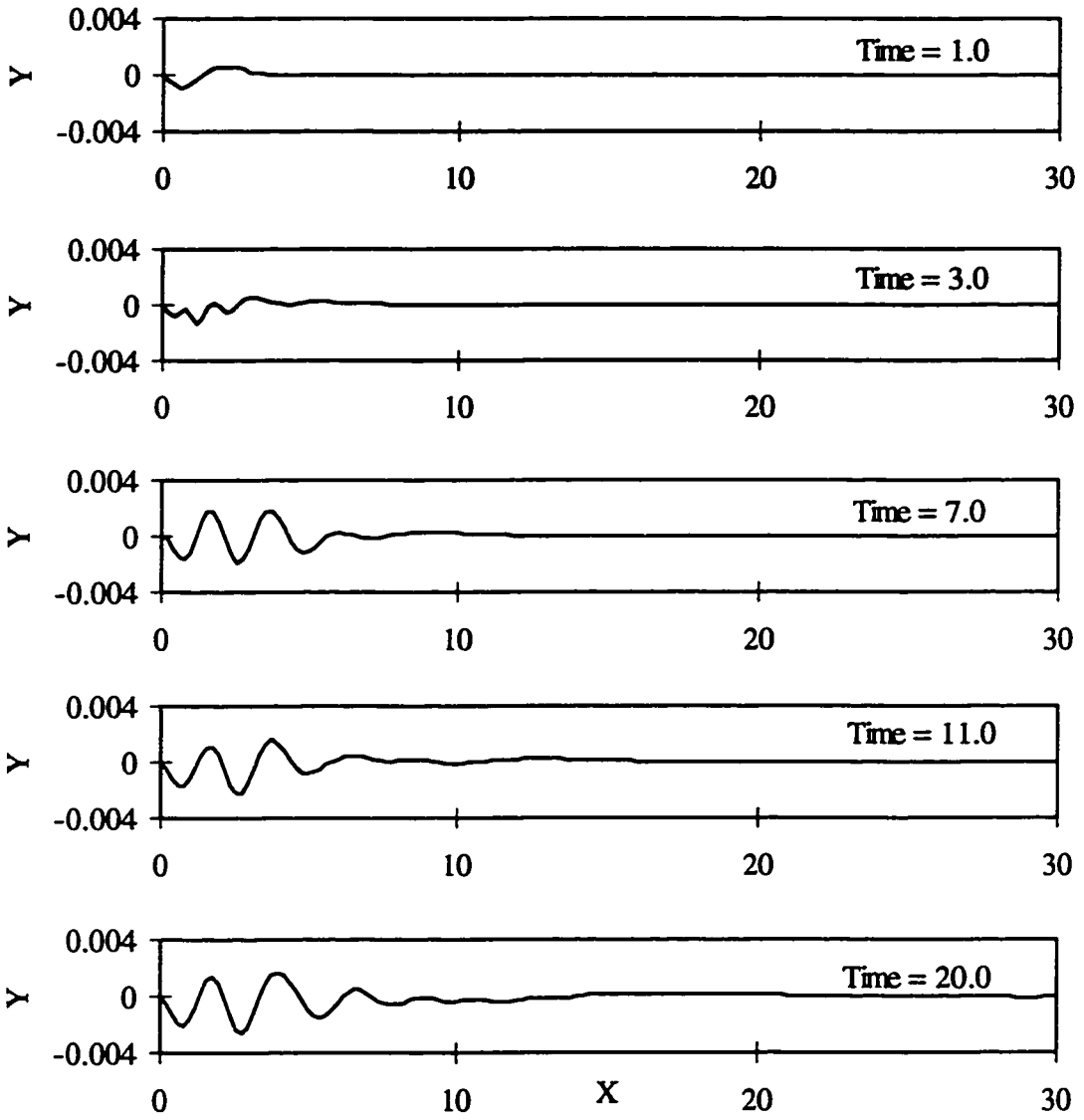

Re=4.17, Inclination=80.0 degree, Property 4.67

Figure 4-5 Wave Profile (Re=4.17, θ=80°, γ=4.67)

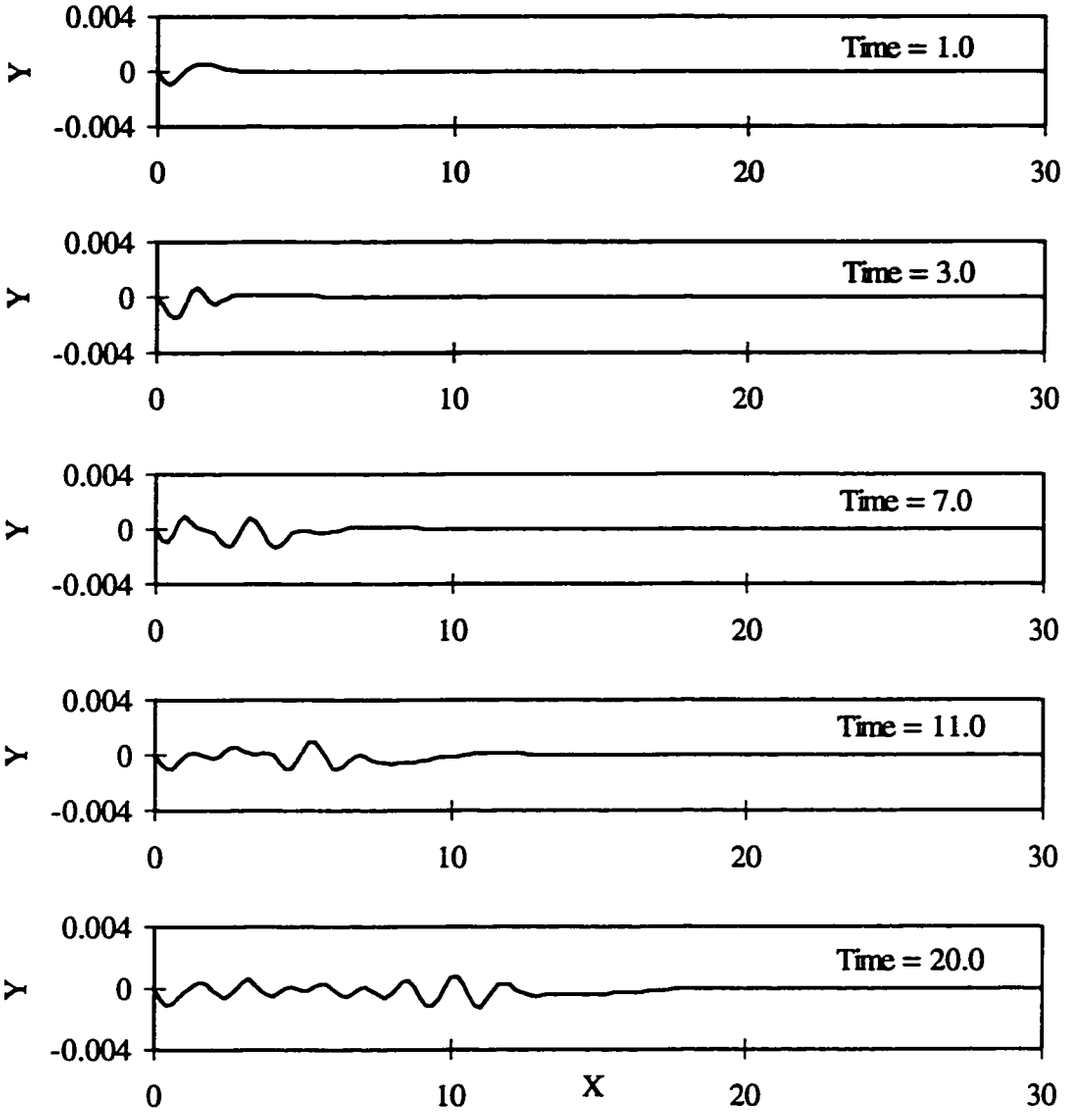

Figure 4-6 Wave Profile (Re=12.5, θ=80°, γ=4.67)

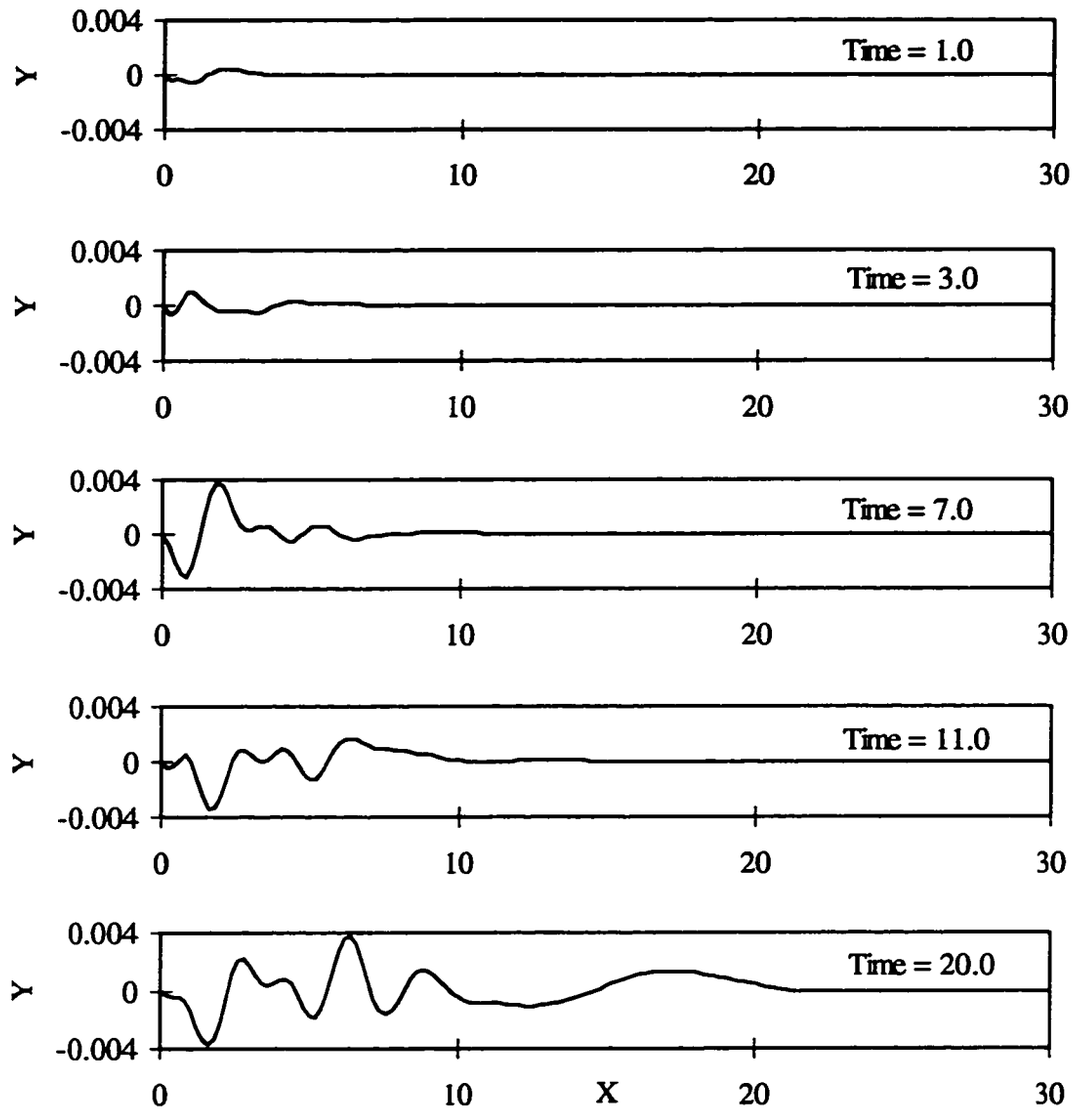

Figure 4-7 Wave Profile (Re=4.17, θ=80°, γ=0.0467)

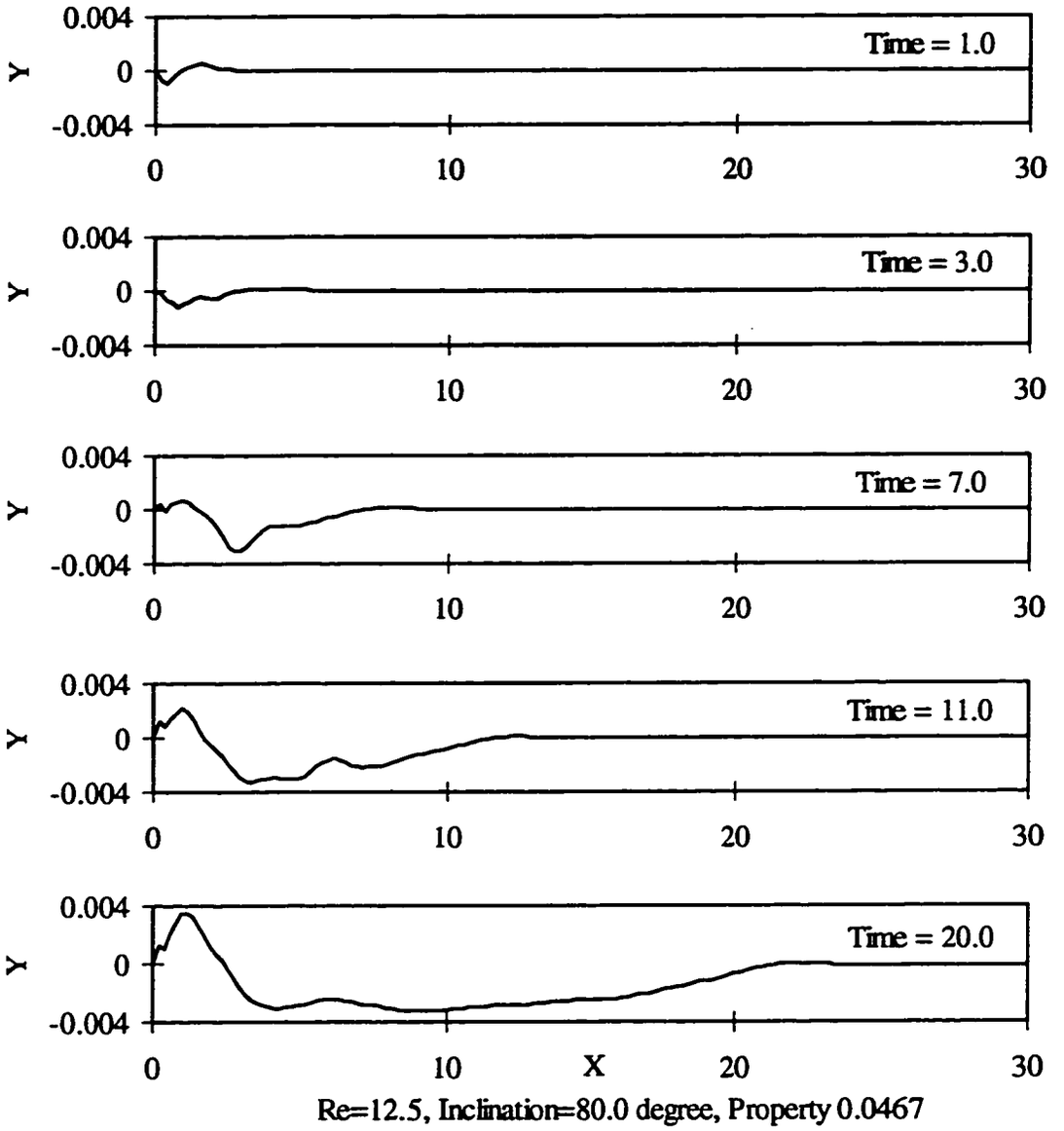

Figure 4-8 Wave Profile (Re=12.5, θ=80°, γ=0.0467)

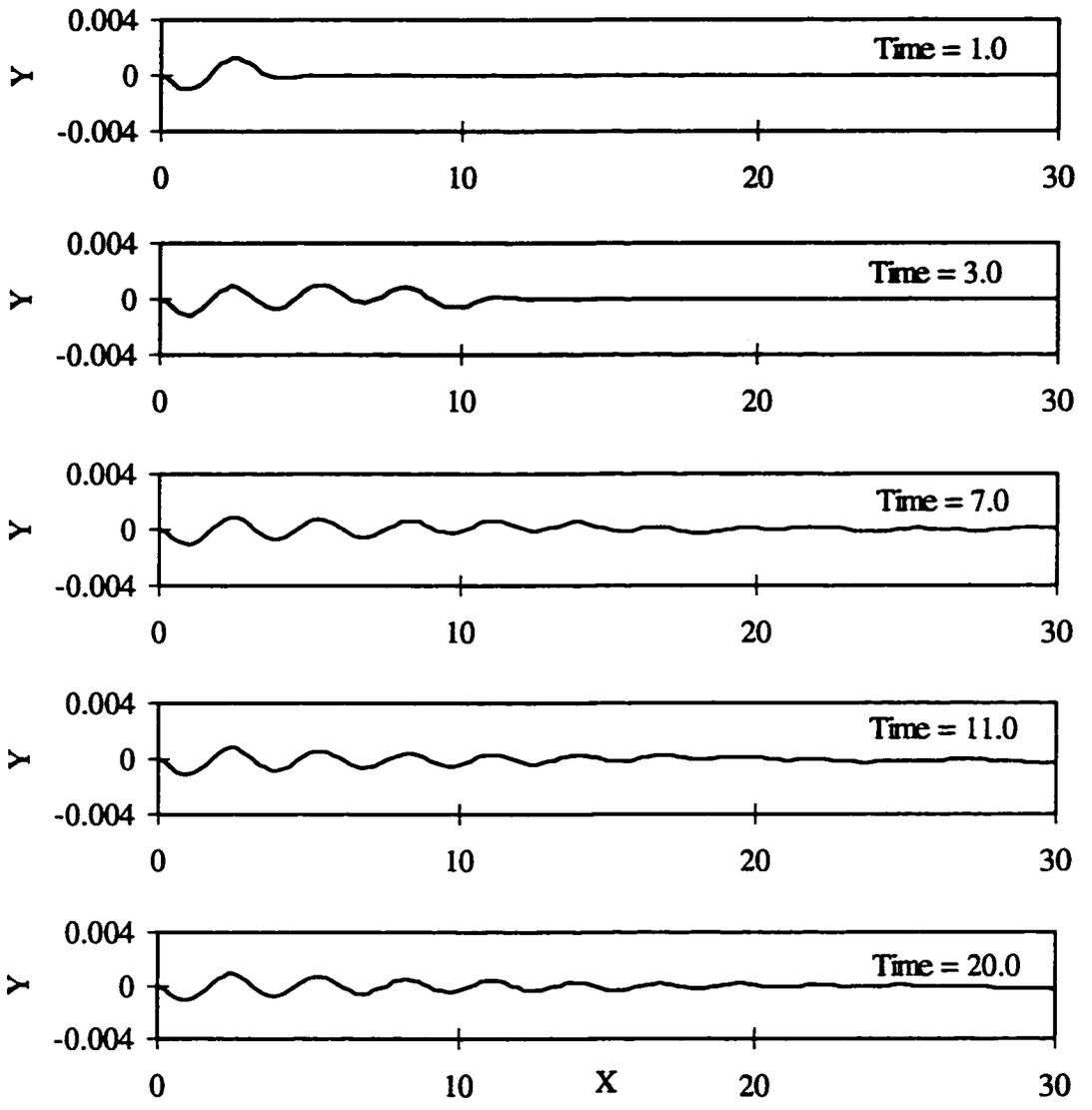

Figure 4-9 Wave Profile (Re=29.2, θ=10°, γ=467)

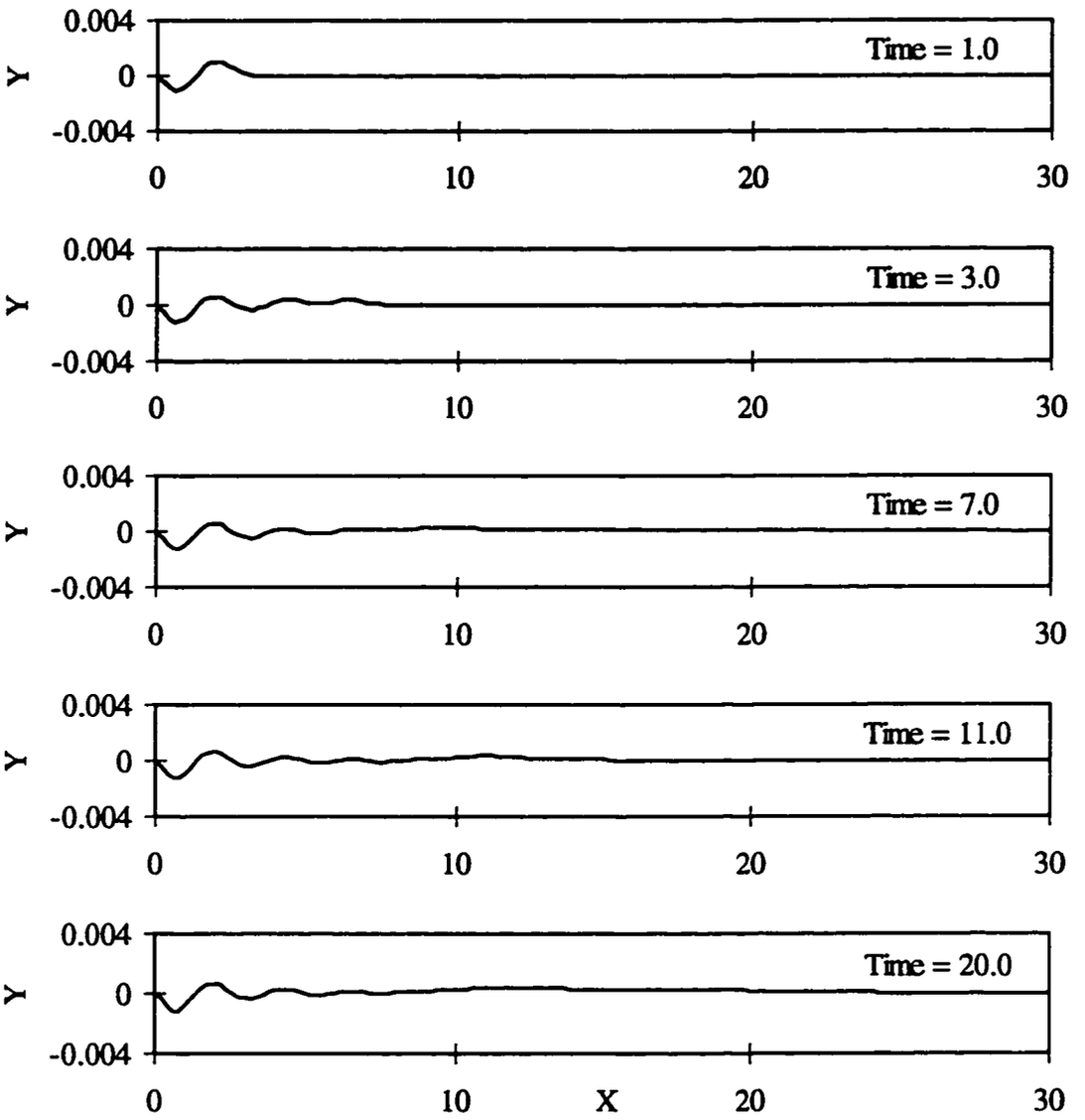

Figure 4-10 Wave Profile (Re=12.5, θ=10°, γ=46.7)

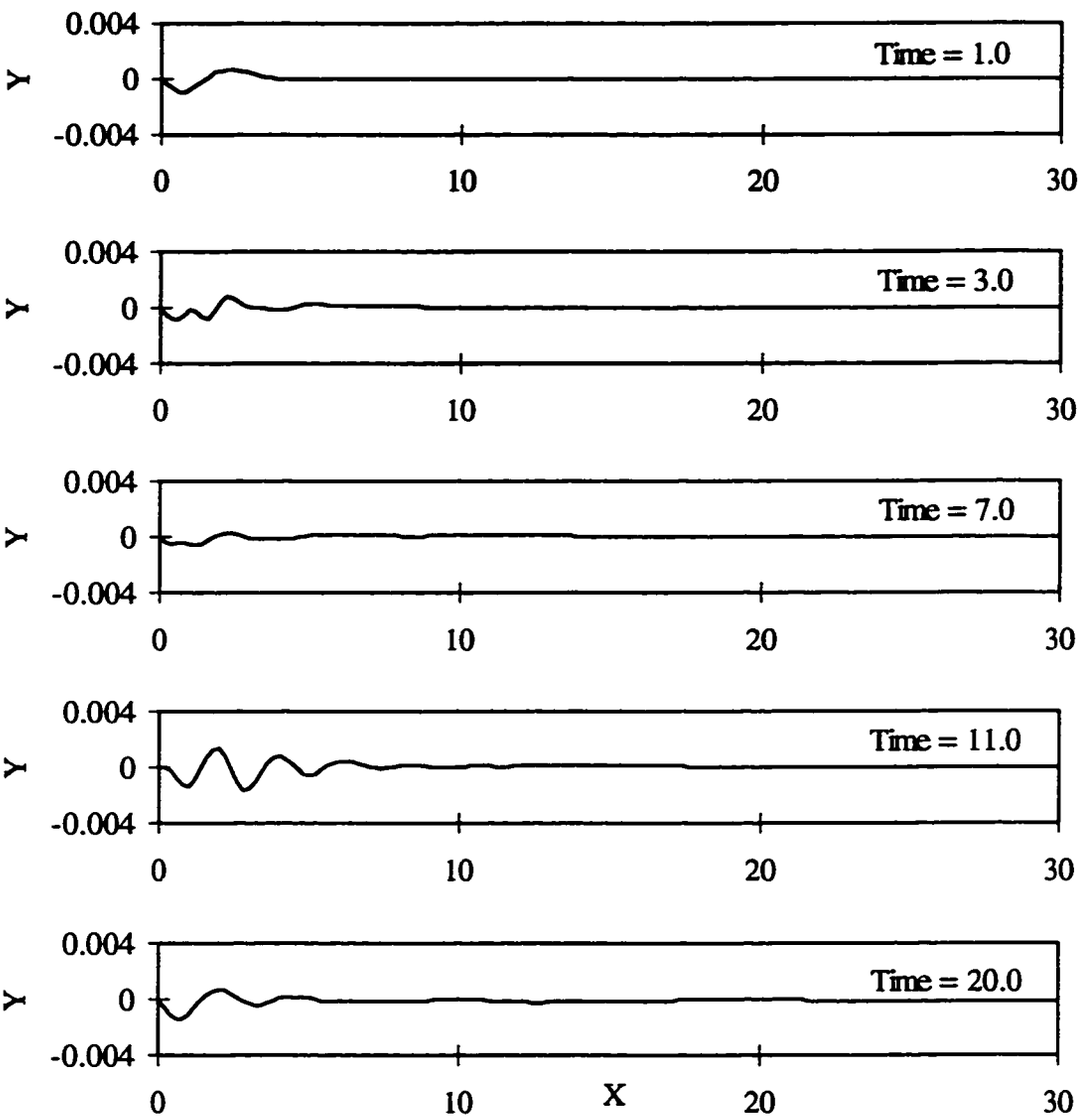

Figure 4-11 Wave Profile (Re=4.17, θ=10°, γ=4.67)

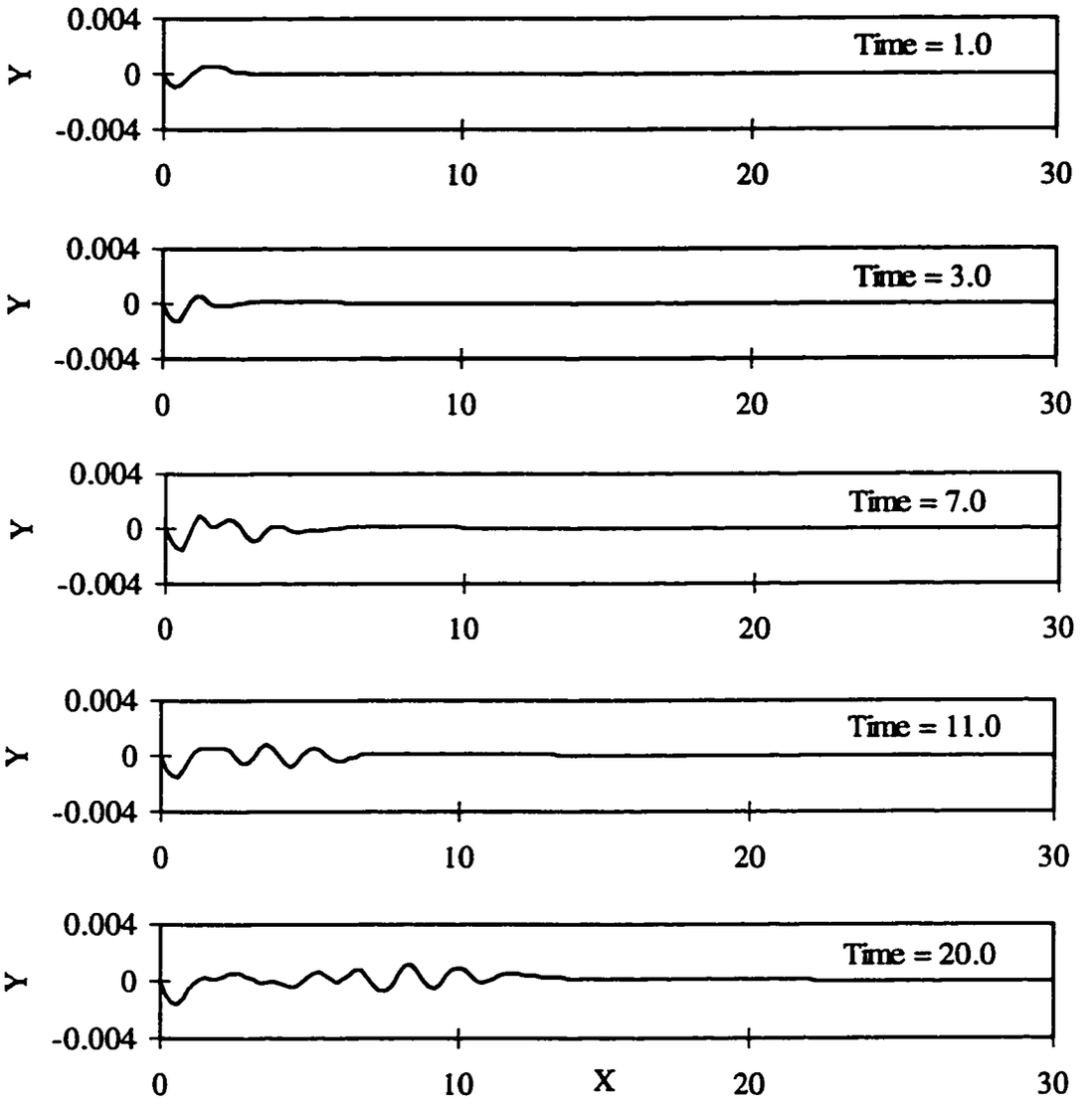

Re=12.5, Inclination=10.0 degree, Property 4.67

Figure 4-12 Wave Profile (Re=12.5, θ=10°, γ=4.67)

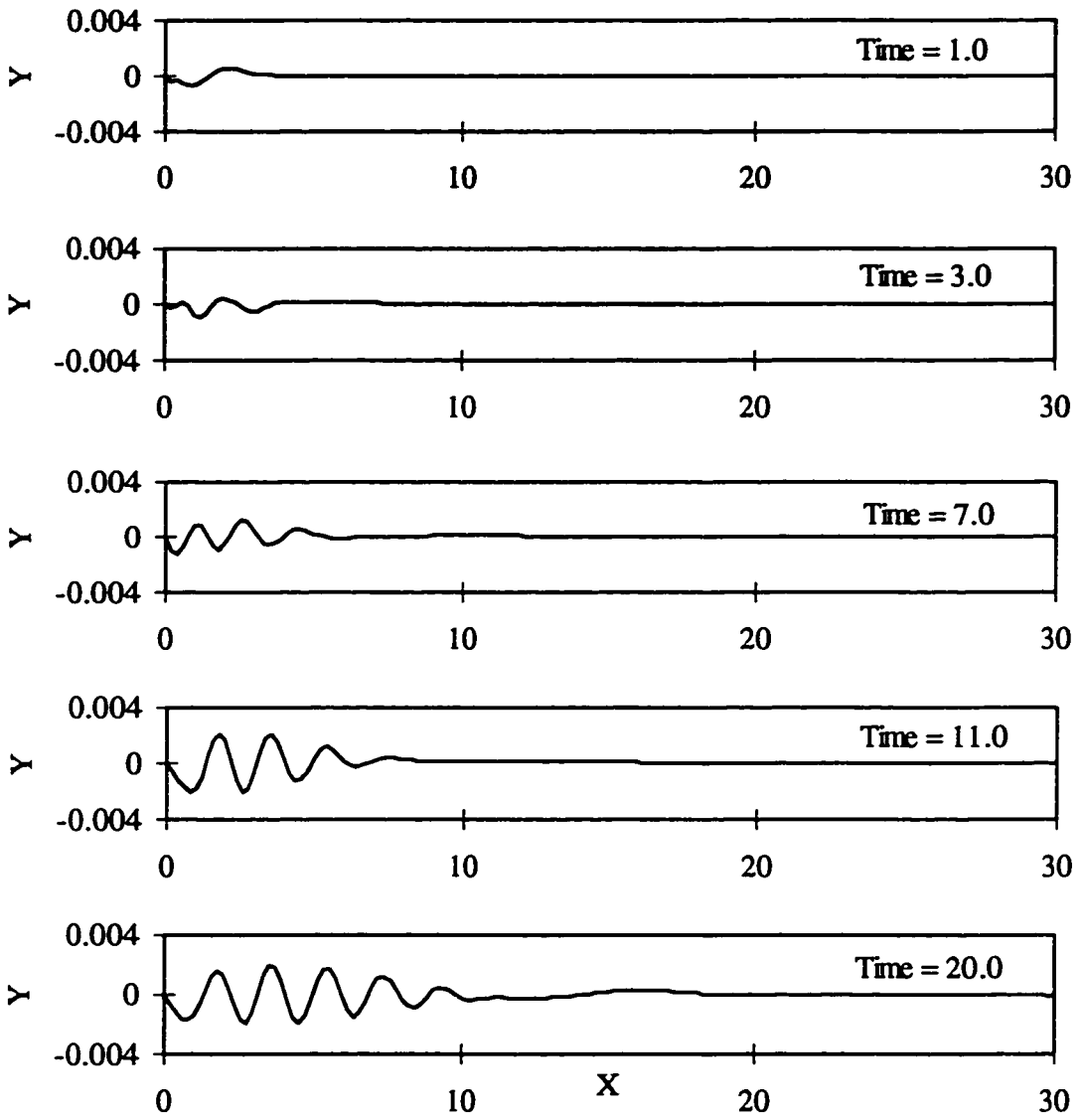

Re=4.17, Inclination=10.0 degree, Property 0.0467

Figure 4-13 Wave Profile (Re=4.17, θ=10°, γ=0.0467)

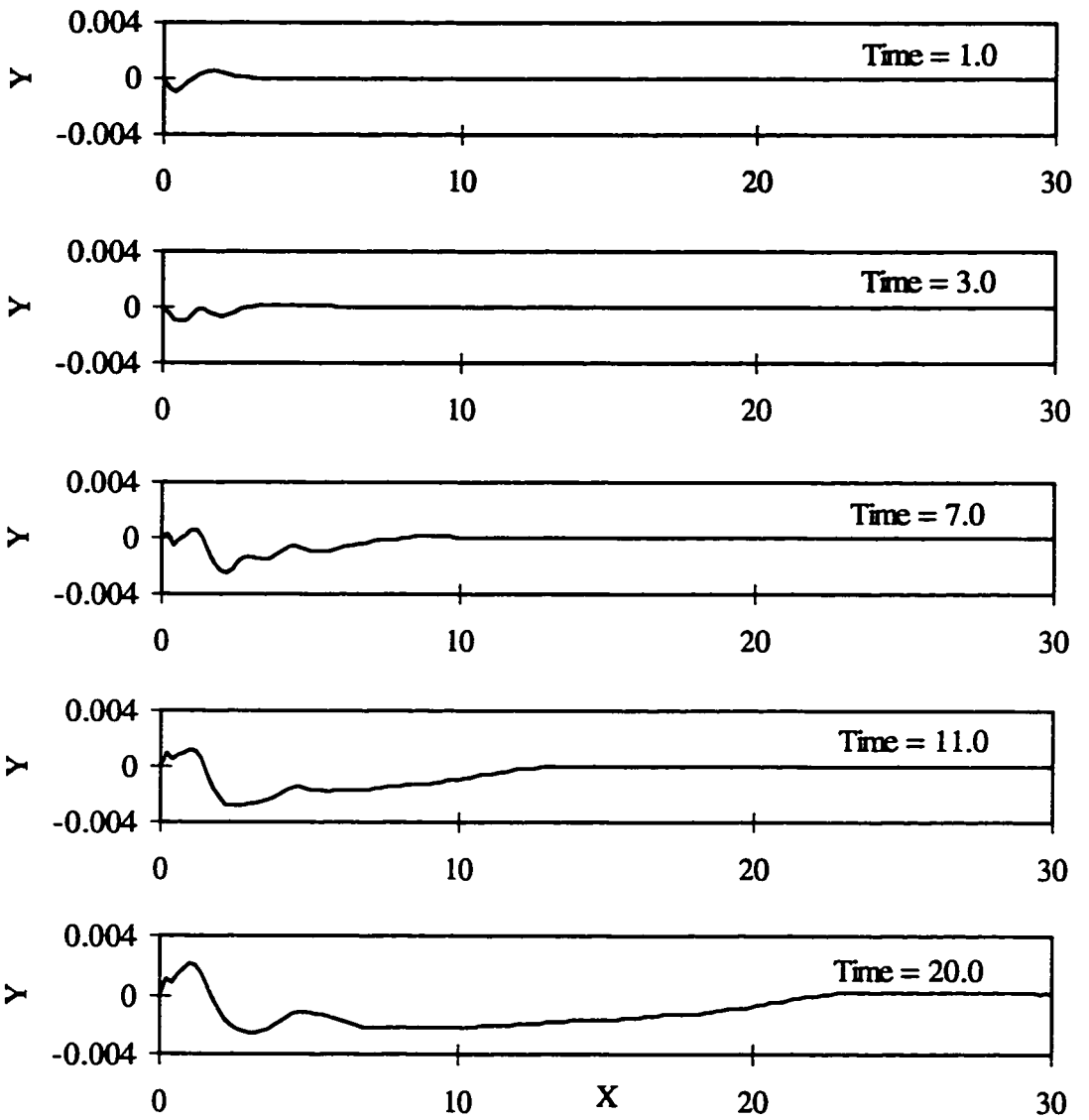

Figure 4-14 Wave Profile (Re=12.5, θ=10°, γ=0.0467)

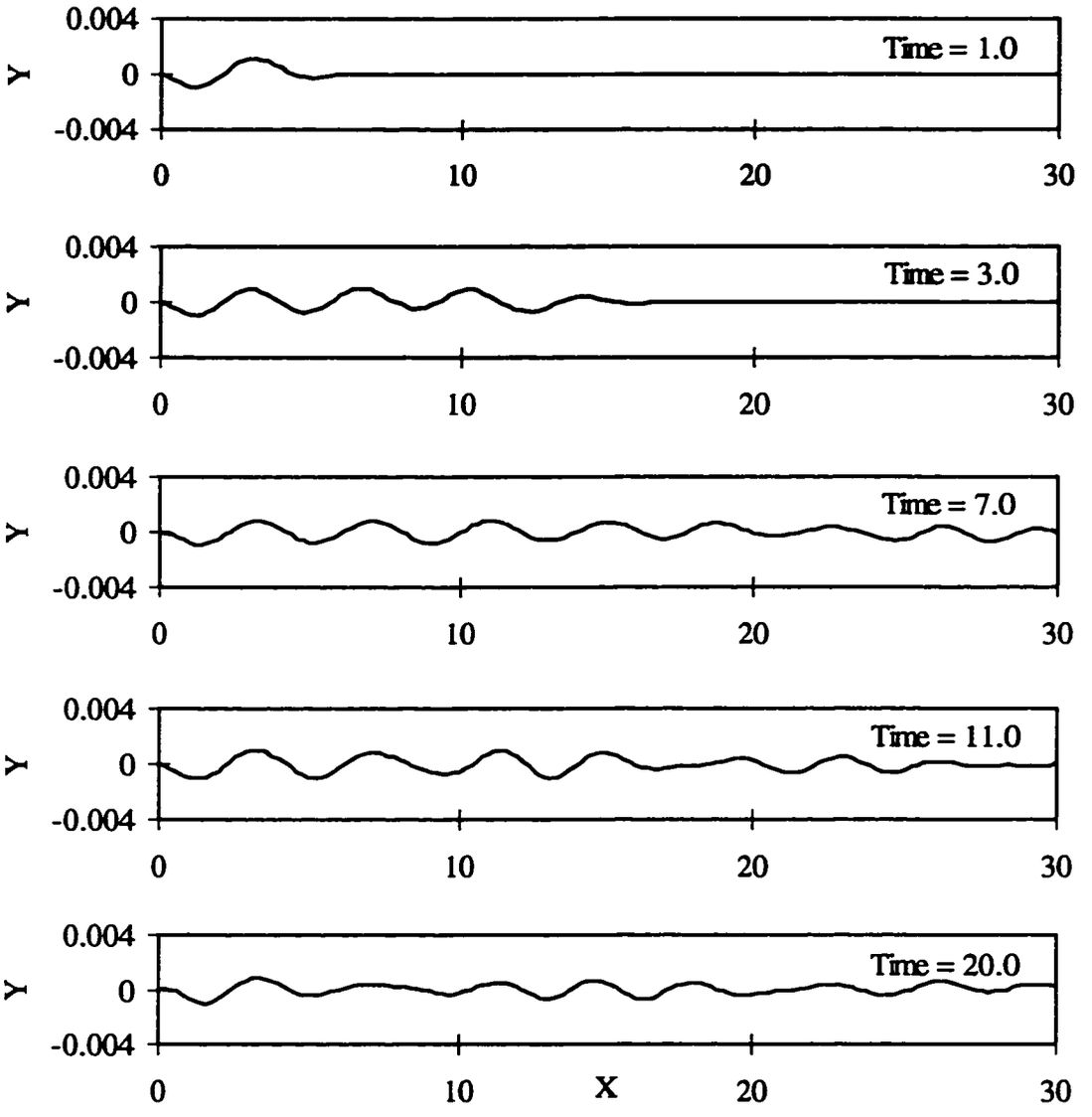

Figure 4-15 Wave Profile (Re=29.2, θ=1°, γ=467)

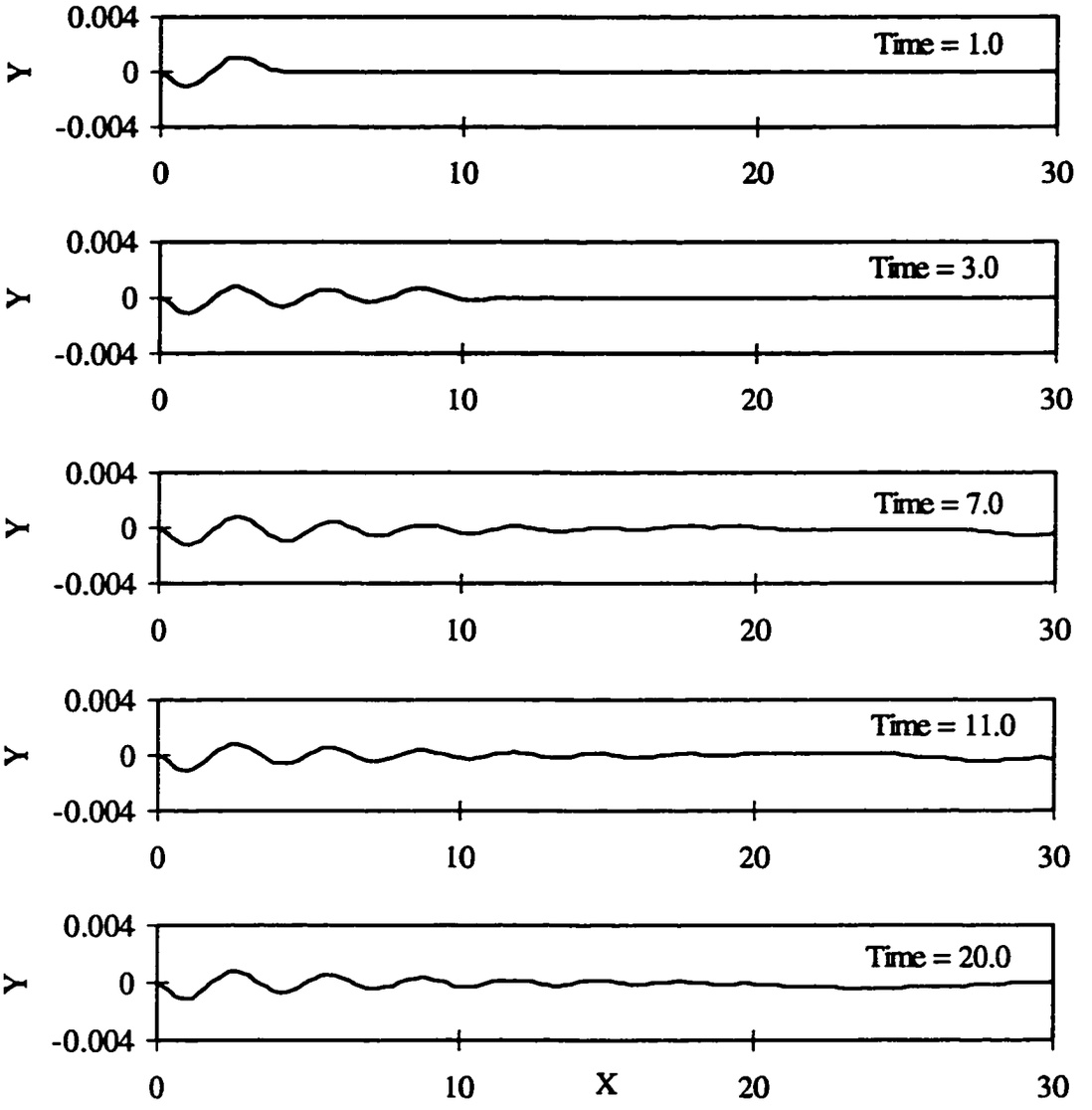

Figure 4-16 Wave Profile (Re=12.5, θ=1°, γ=46.7)

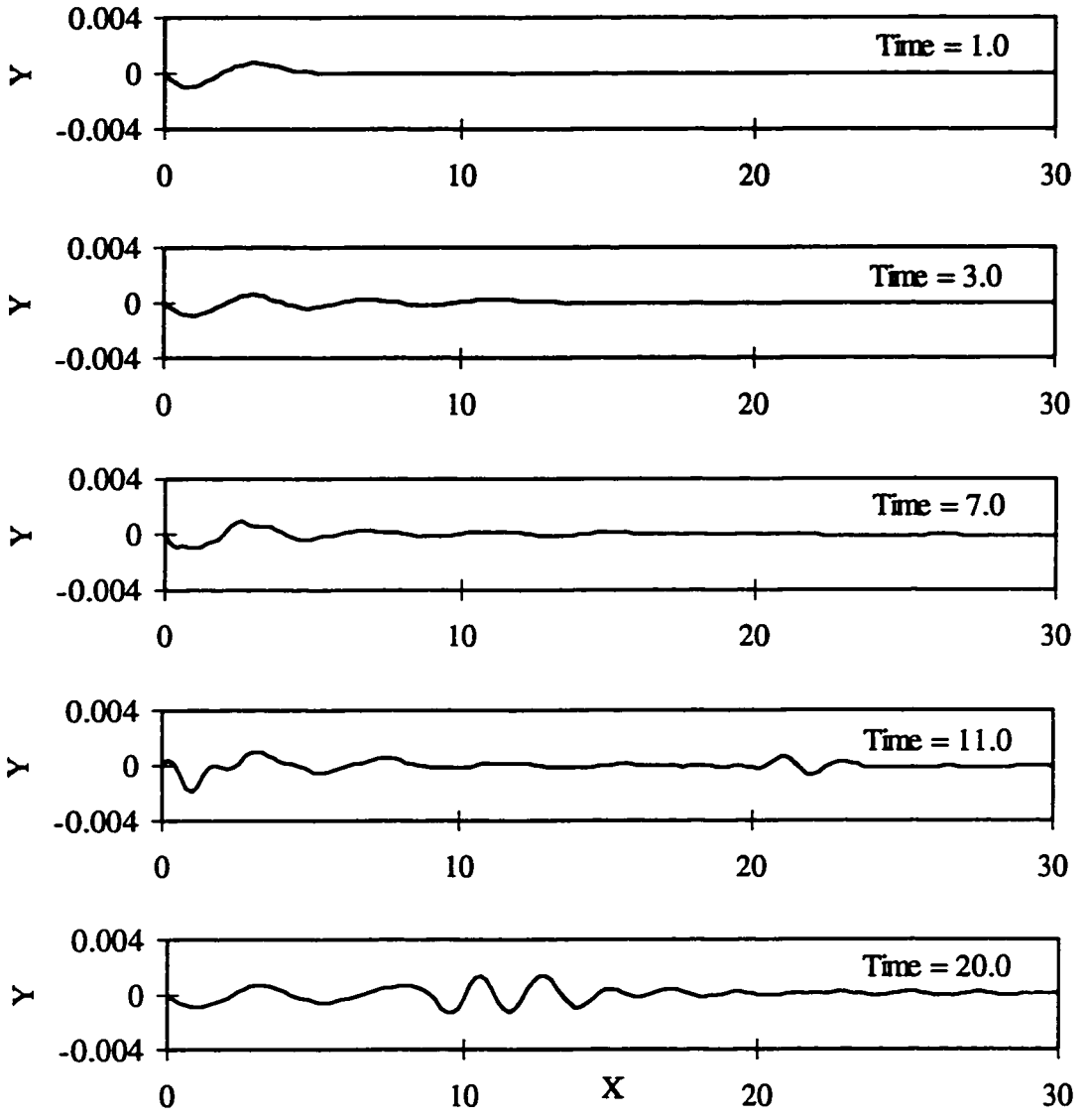

Re=4.17, Inclination=1.0 degree, Property 4.67

Figure 4-17 Wave Profile (Re=4.17, θ=1°, γ=4.67)

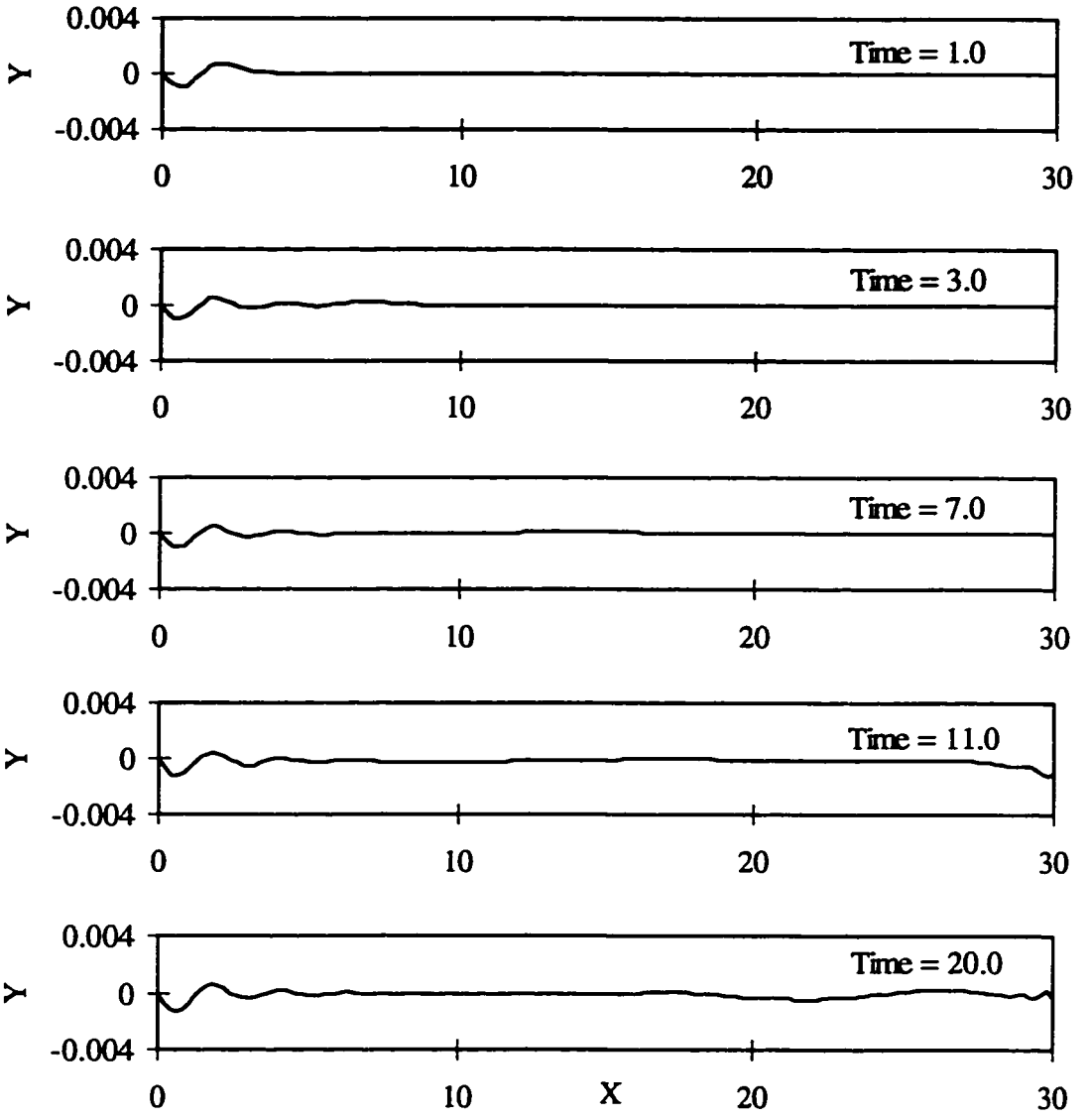

Re=12.5, Inclination=1.0 degree, Property 4.67

Figure 4-18 Wave Profile (Re=12.5, θ=1°, γ=4.67)

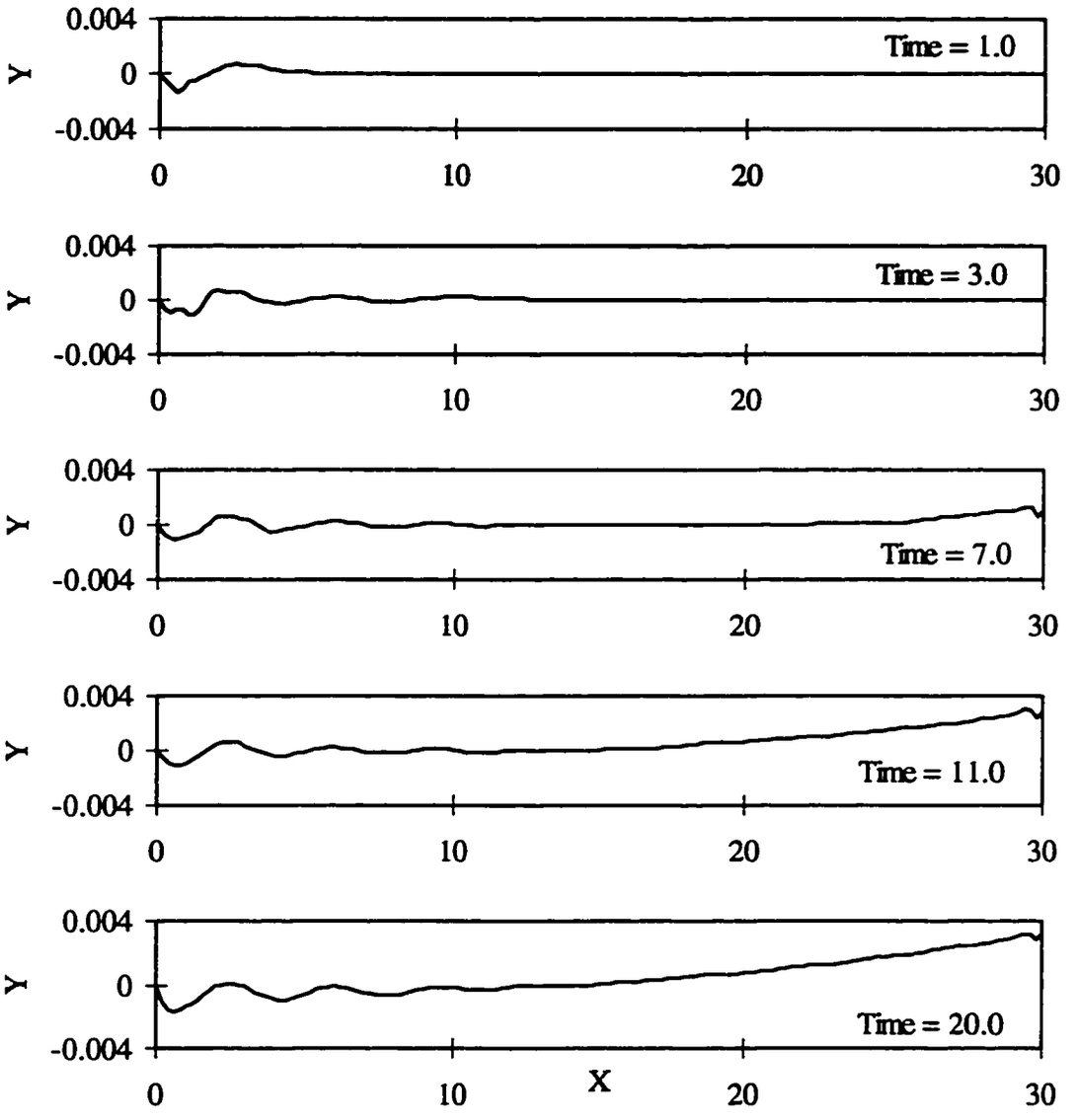

Figure 4-19 Wave Profile (Re=4.17, θ=1°, γ=0.0467)

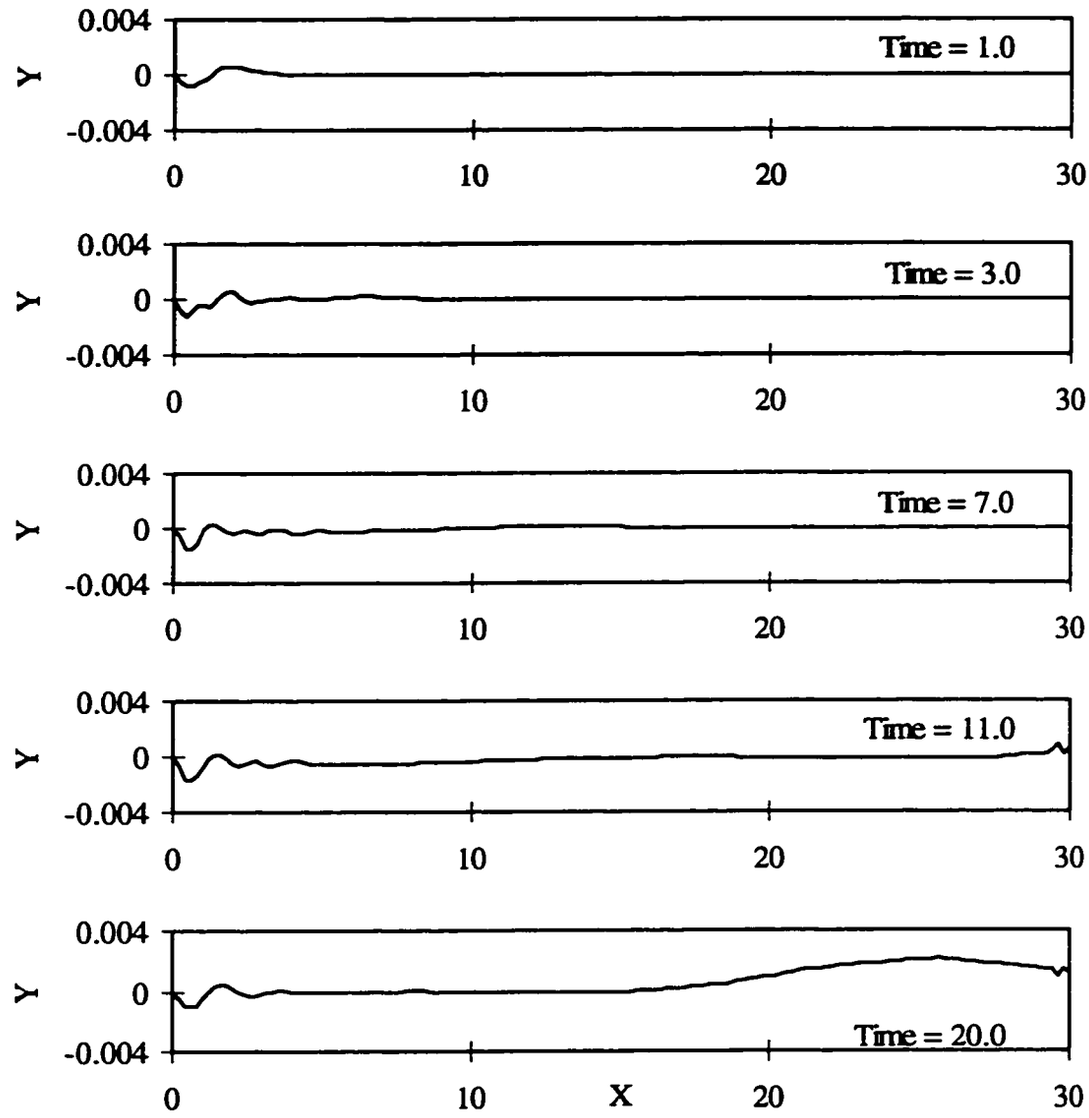

Figure 4-20 Wave Profile (Re=12.5, θ=1°, γ=0.0467)

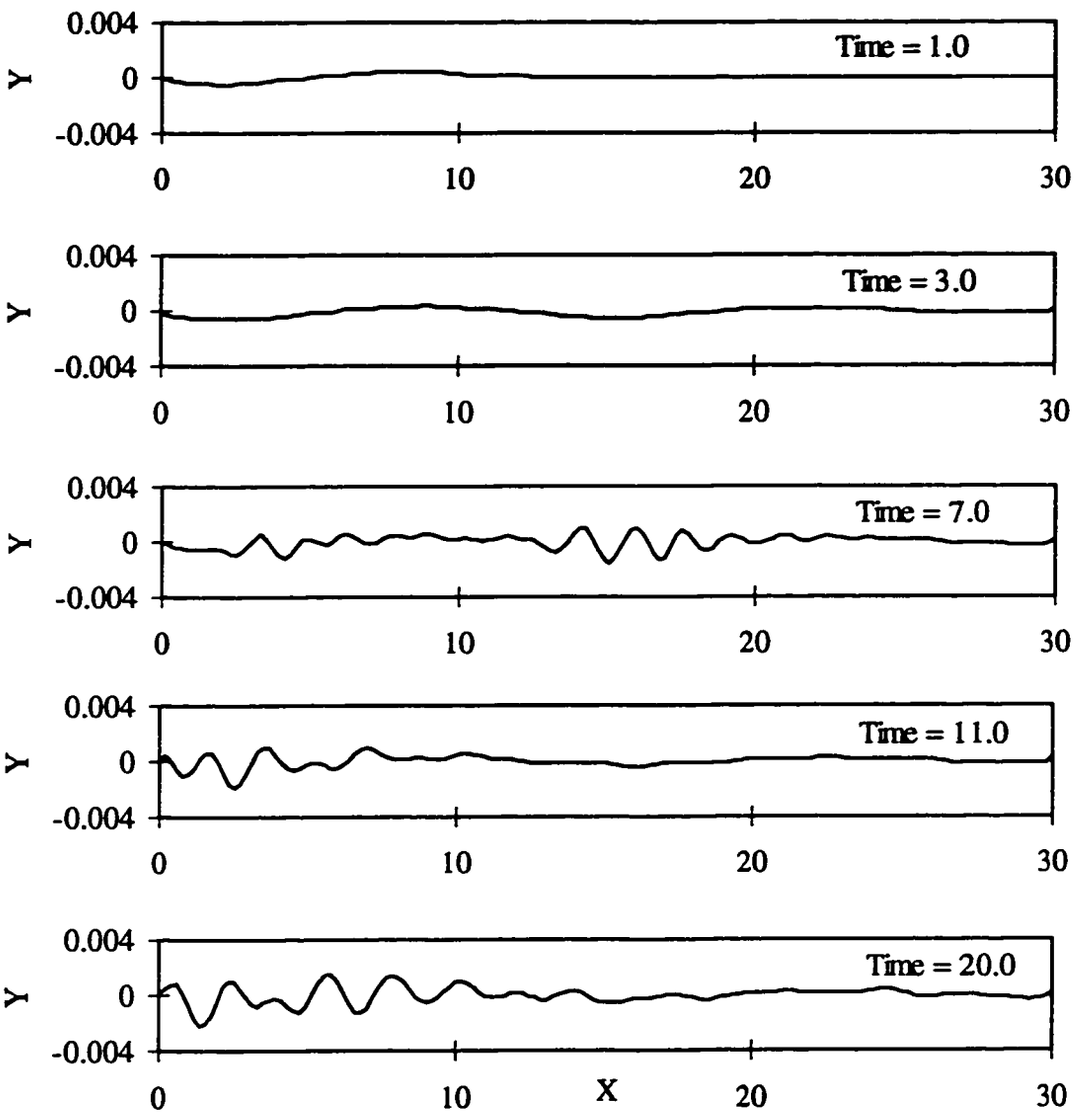

Re=4.17, Inclination=0.1 degree, Property 4.67

Figure 4-21 Wave Profile (Re=4.17, θ=0.1°, γ=4.67)

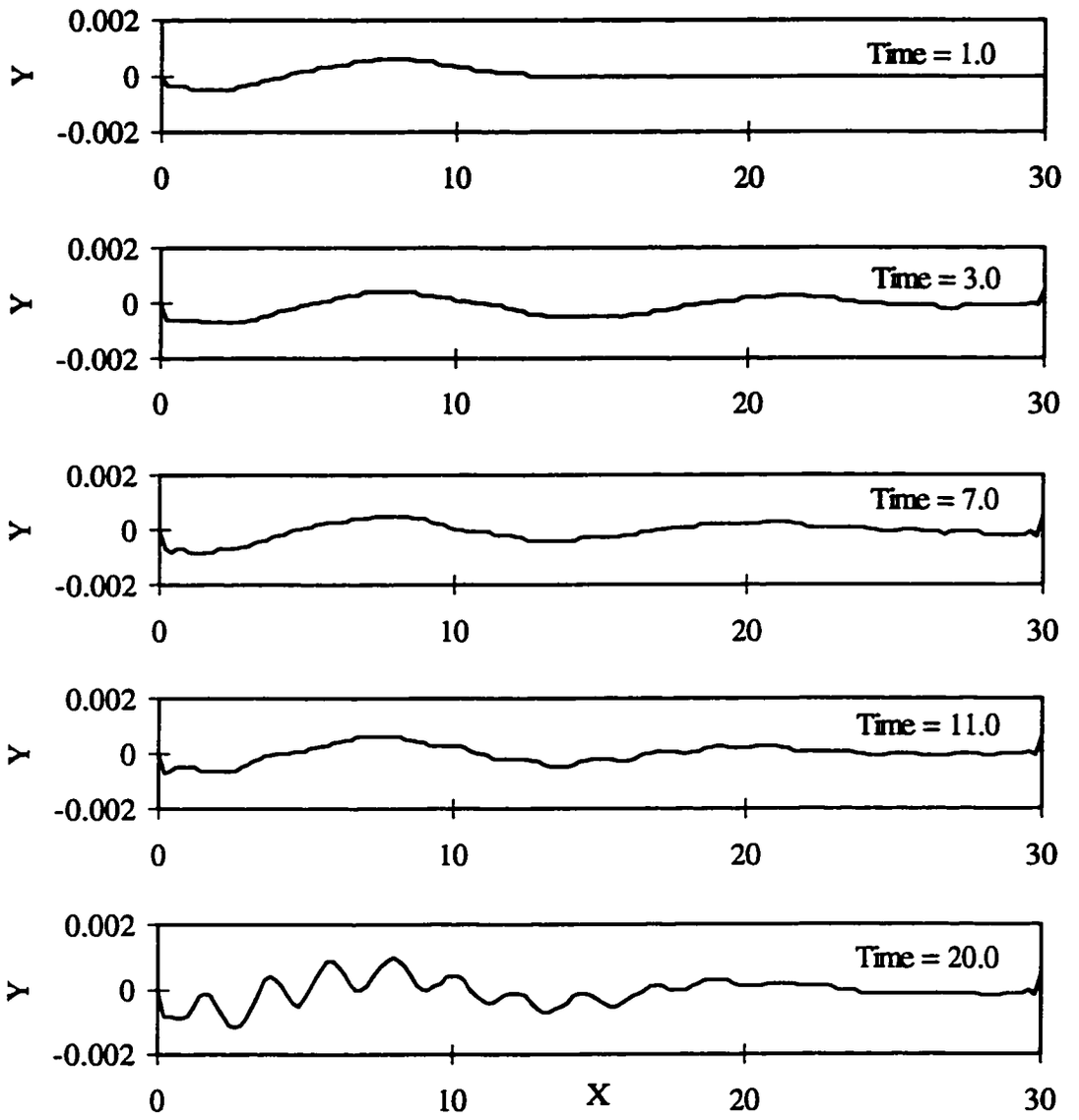

Re=4.17, Inclination=0.1 degree, Property 0.0467

Figure 4-22 Wave Profile (Re=4.17, θ=0.1°, γ=0.0467)

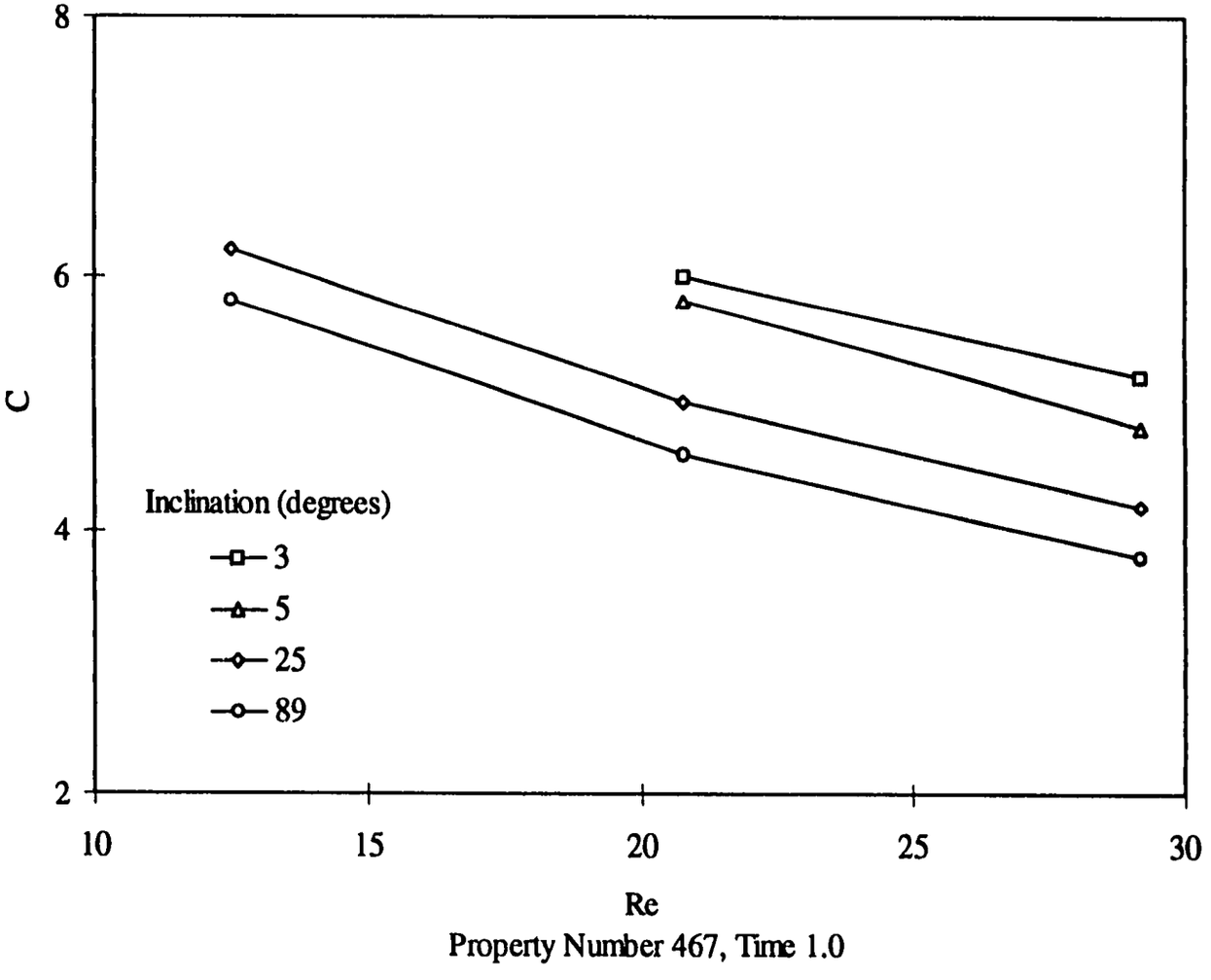

Figure 4-23 Wave Speed (γ=467, time=1.0)

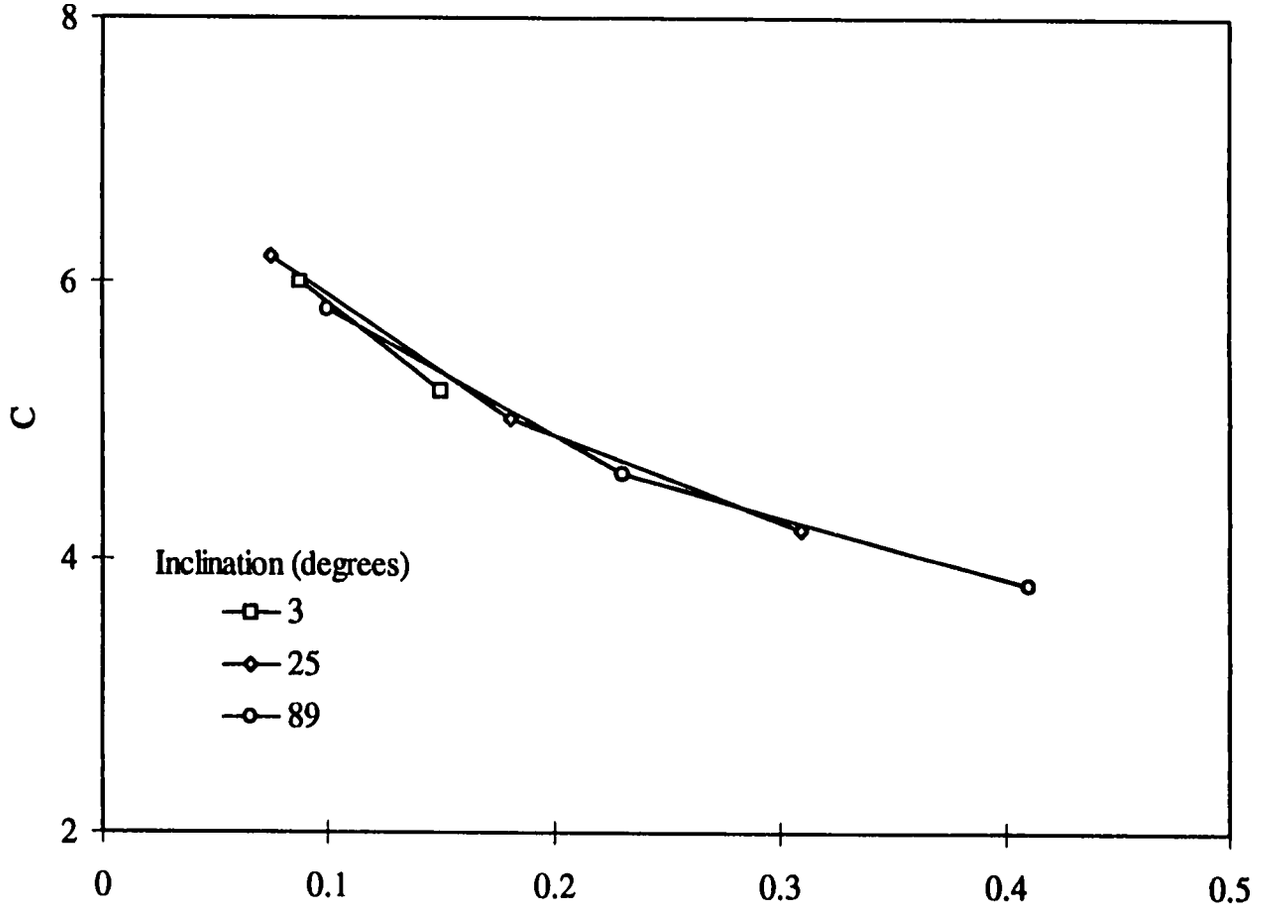

Property Number 467, Time 1.0

Figure 4-24 Wave Speed (γ=467, time=1.0)

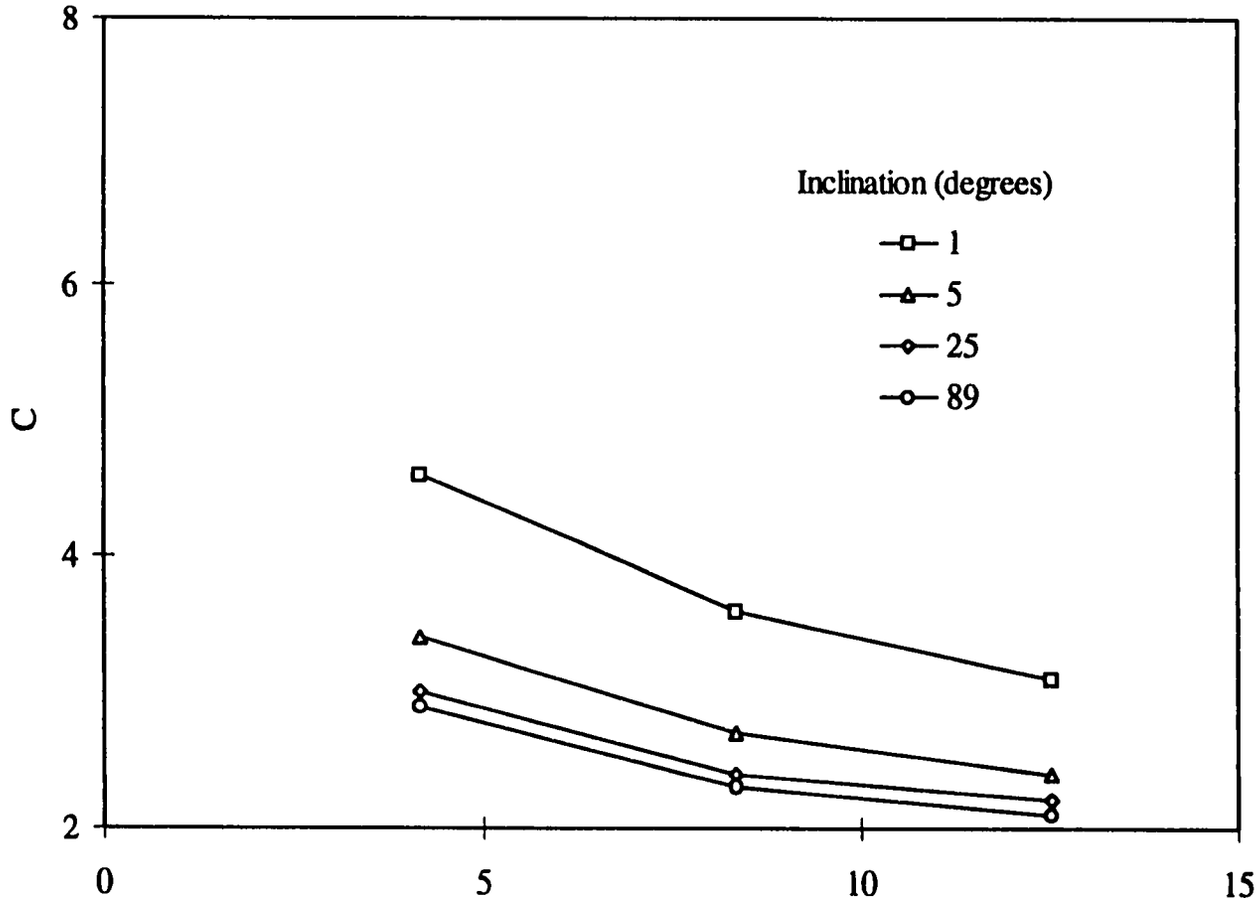

Property Number 4.67, Time 2.0

Figure 4-25 Wave Speed (γ=4.67, time=2.0)

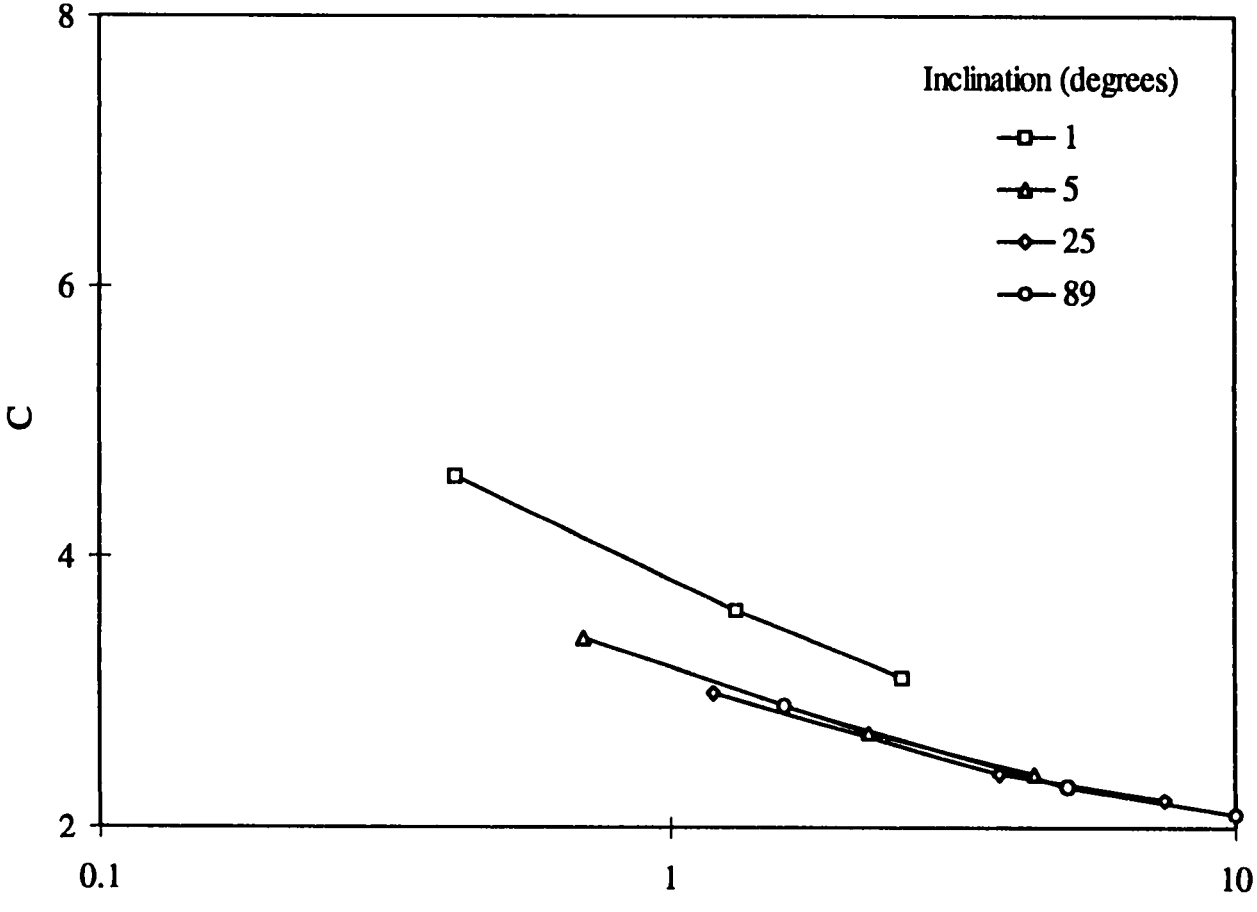

Property Number 4.67, Time 2.0

Figure 4-26 Wave Speed (γ=4.67, time=2.0)

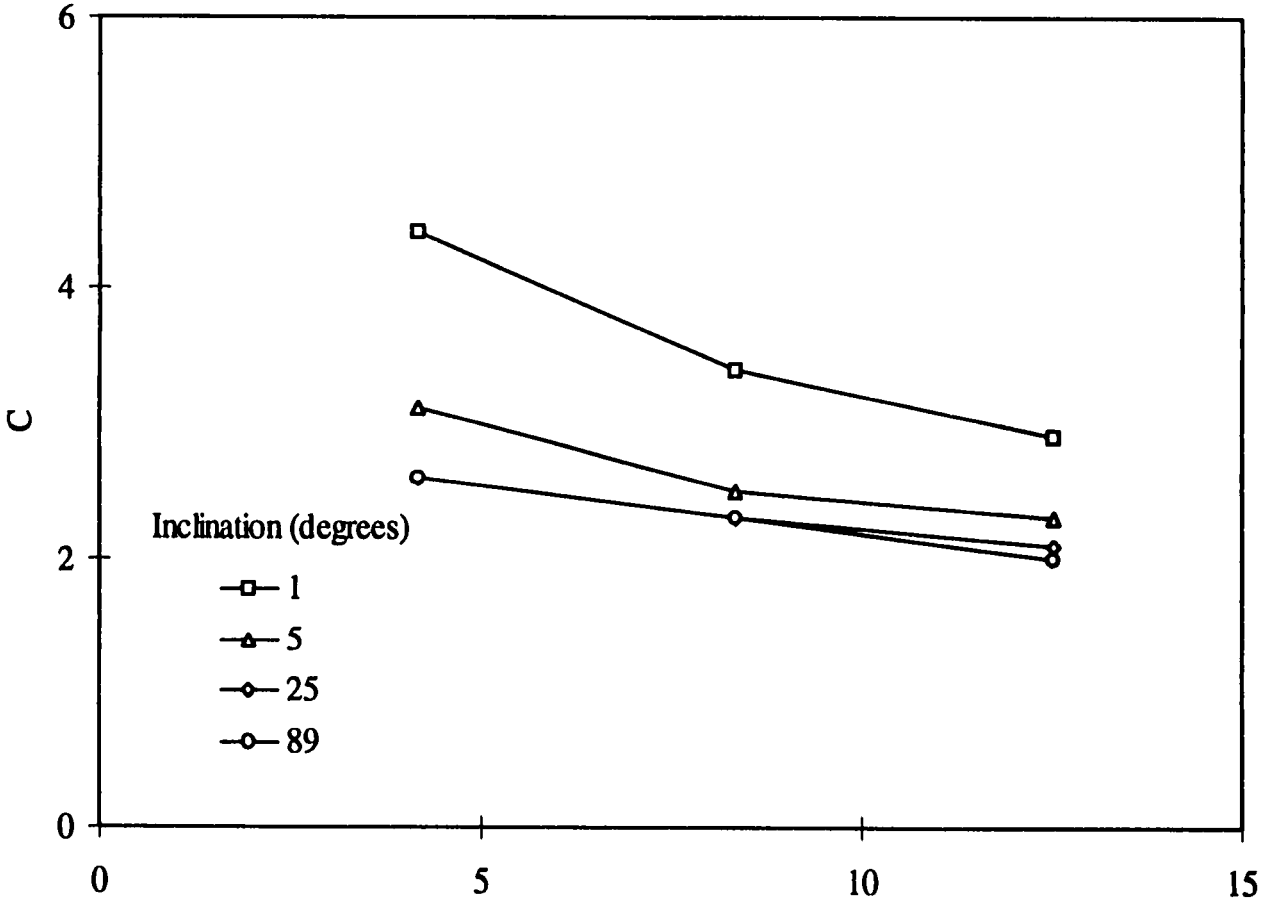

Property Number 0.0467, Time 2.0

Figure 4-27 Wave Speed (γ=0.0467, time=2.0)

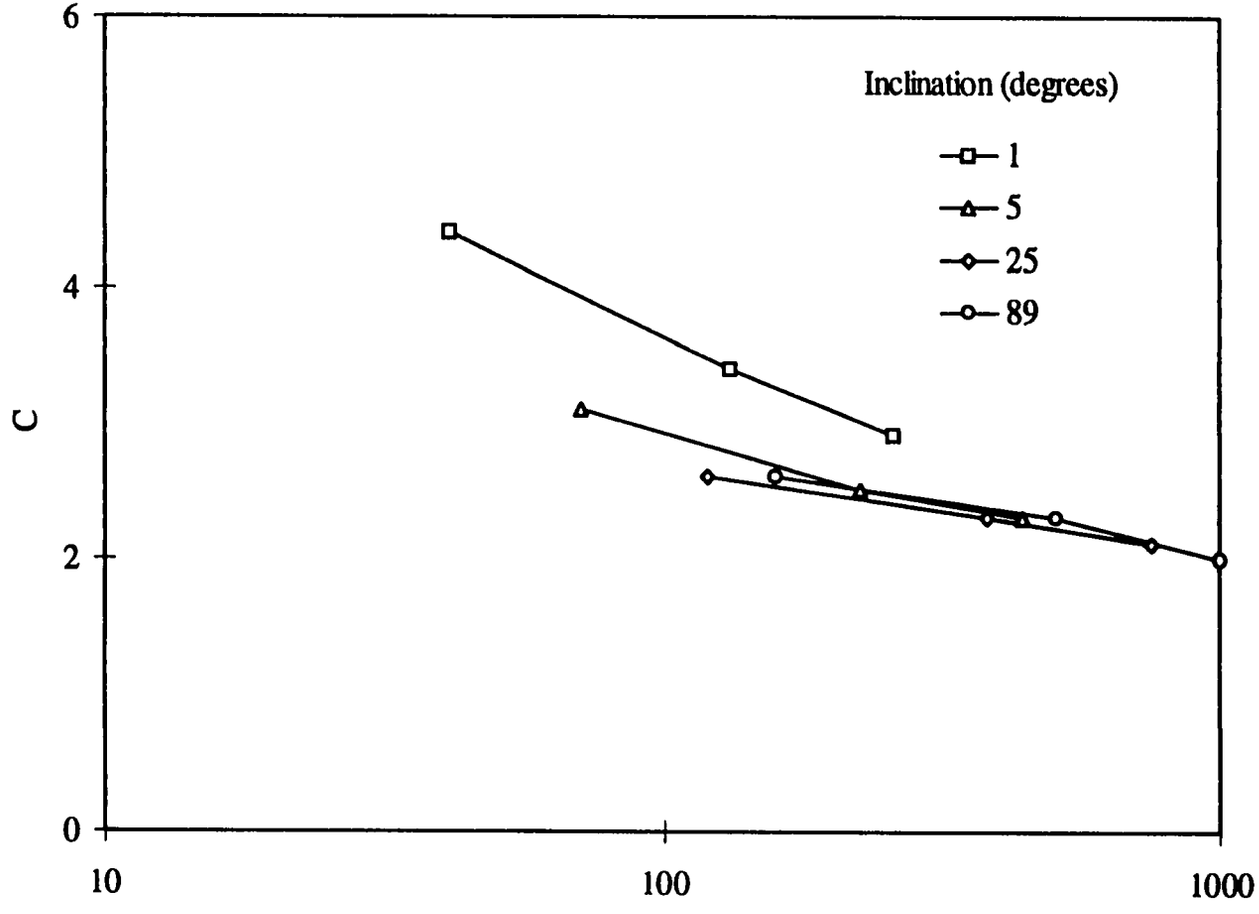

Property Number 0.0467, Time 2.0

Figure 4-28 Wave Speed (γ=0.0467, time=2.0)

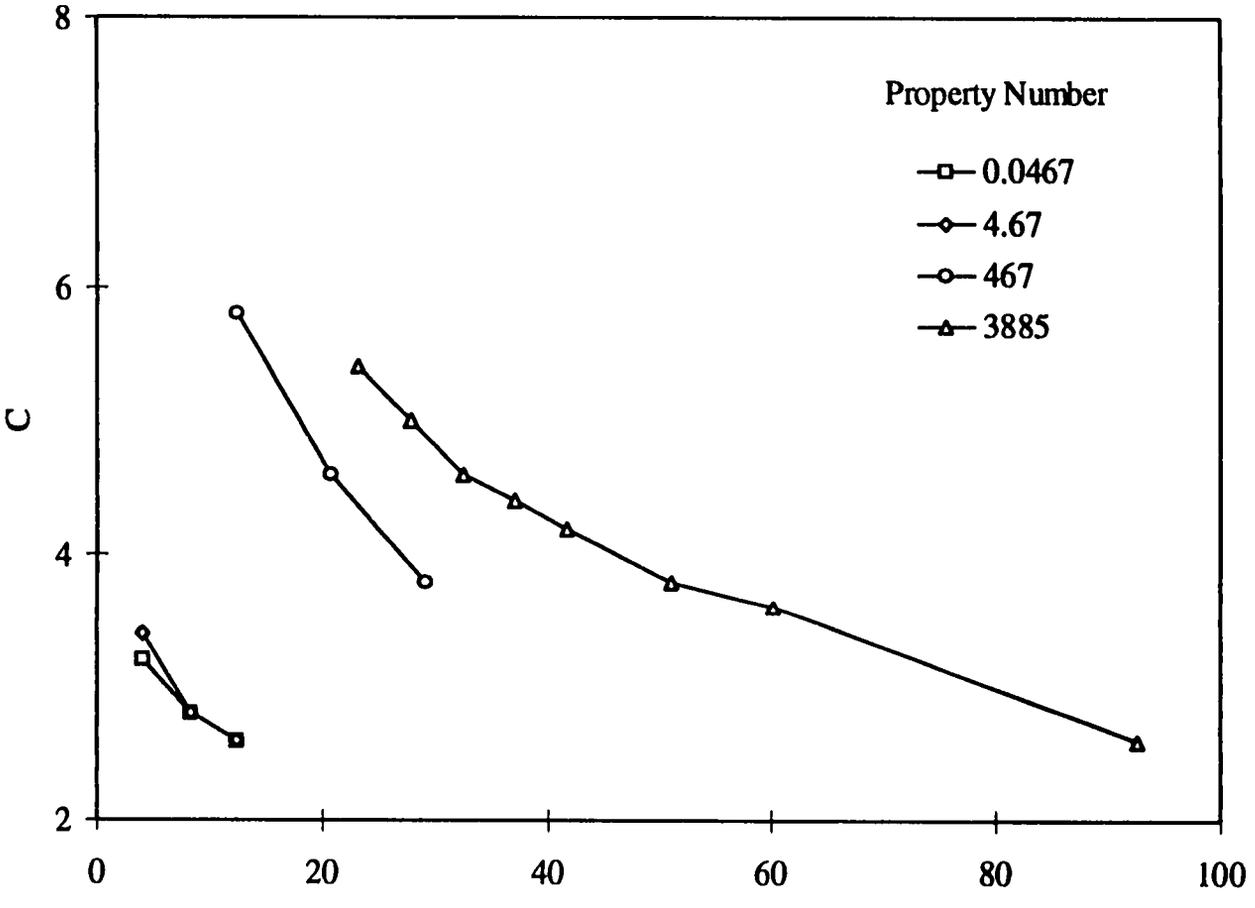

Inclination 89.0 Degree, Time 1.0

Figure 4-29 Wave Speed (θ=89°, time=1.0)

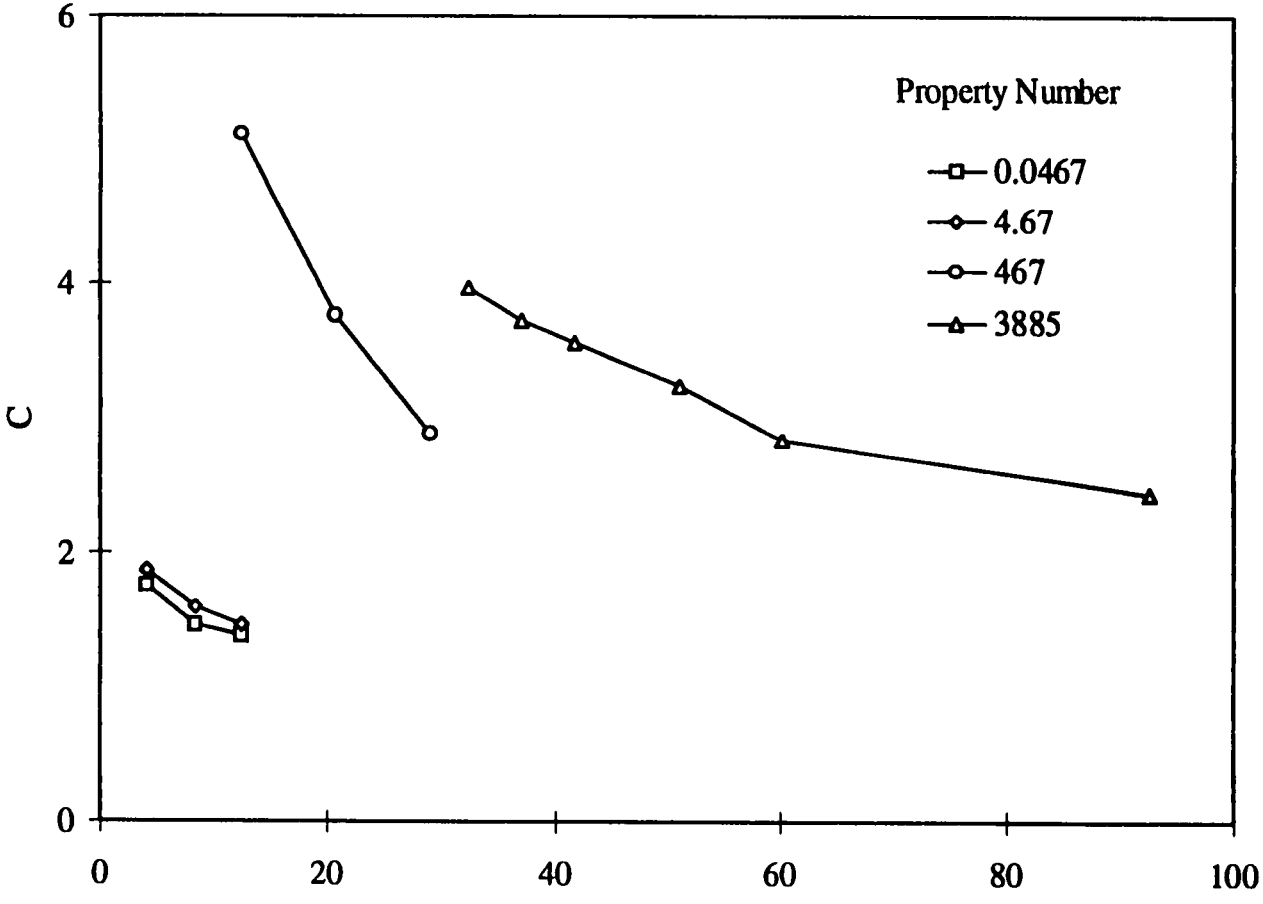

Inclination 89.0 Degree, Time 5.0

Figure 4-30 Wave Speed (θ=89°, time=5.0)

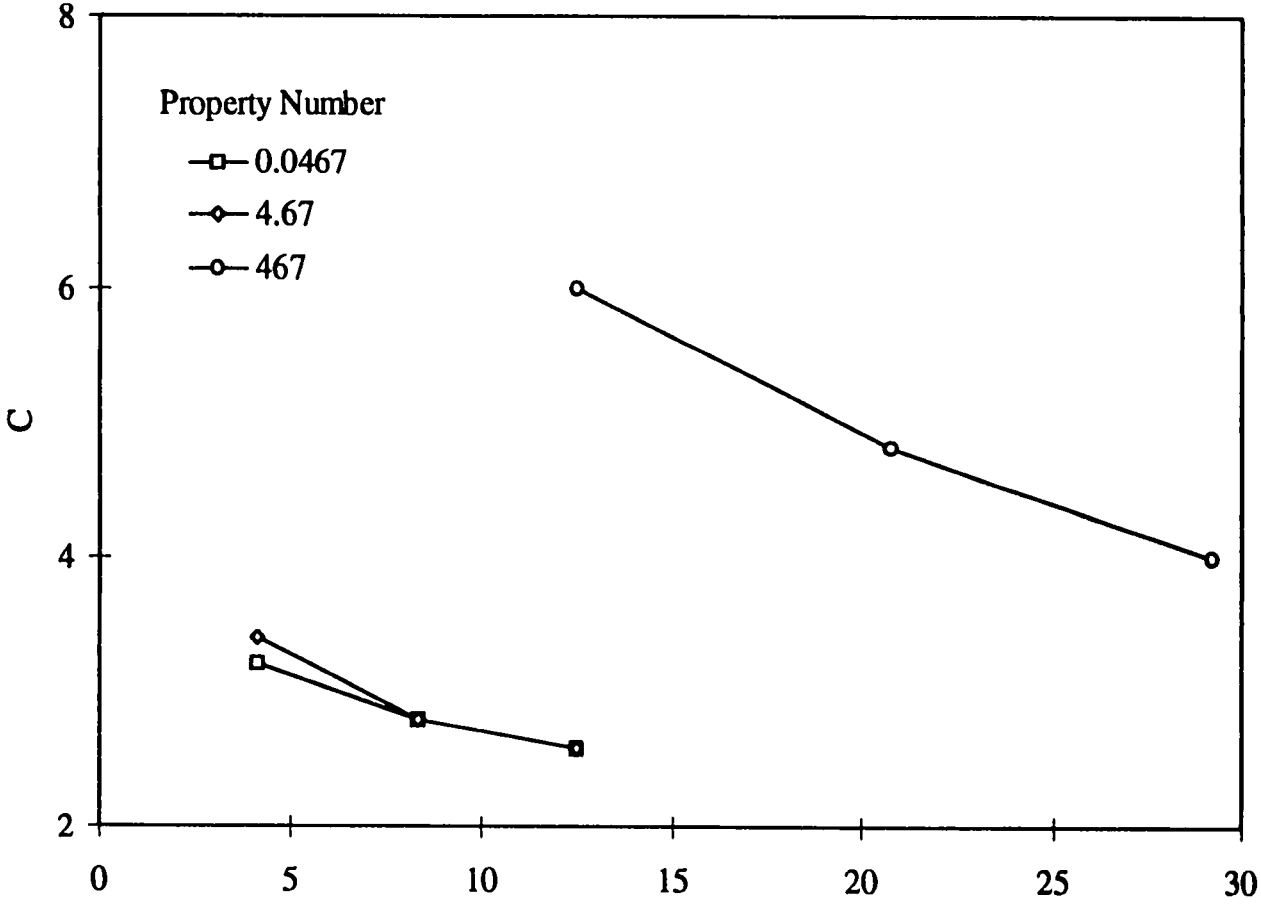

Inclination 45.0 Degree, Time 1.0

Figure 4-31 Wave Speed (θ=45.0°, time=1.0)

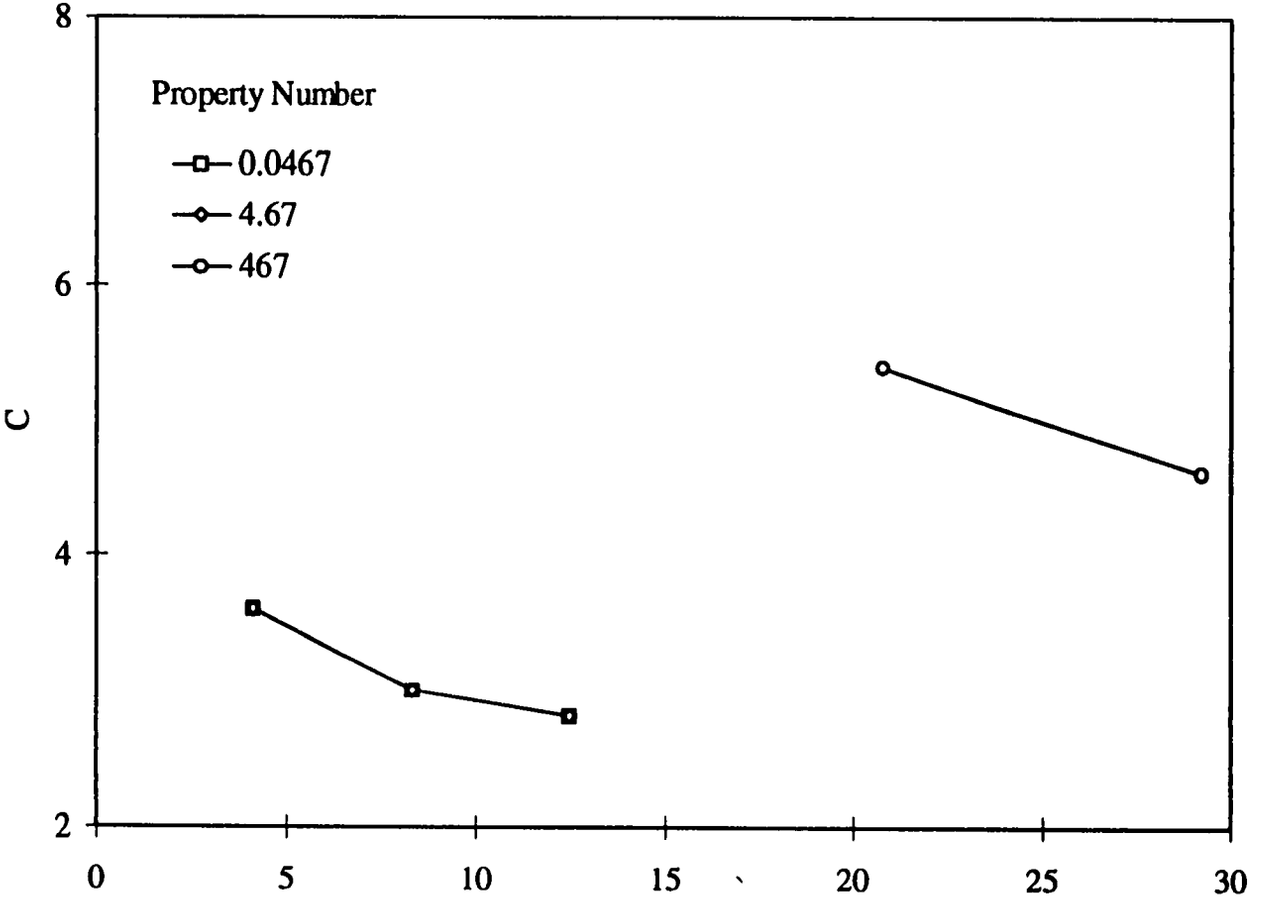

Inclination 10.0 Degree, Time 1.0

Figure 4-32 Wave Speed (θ=10.0°, time=1.0)

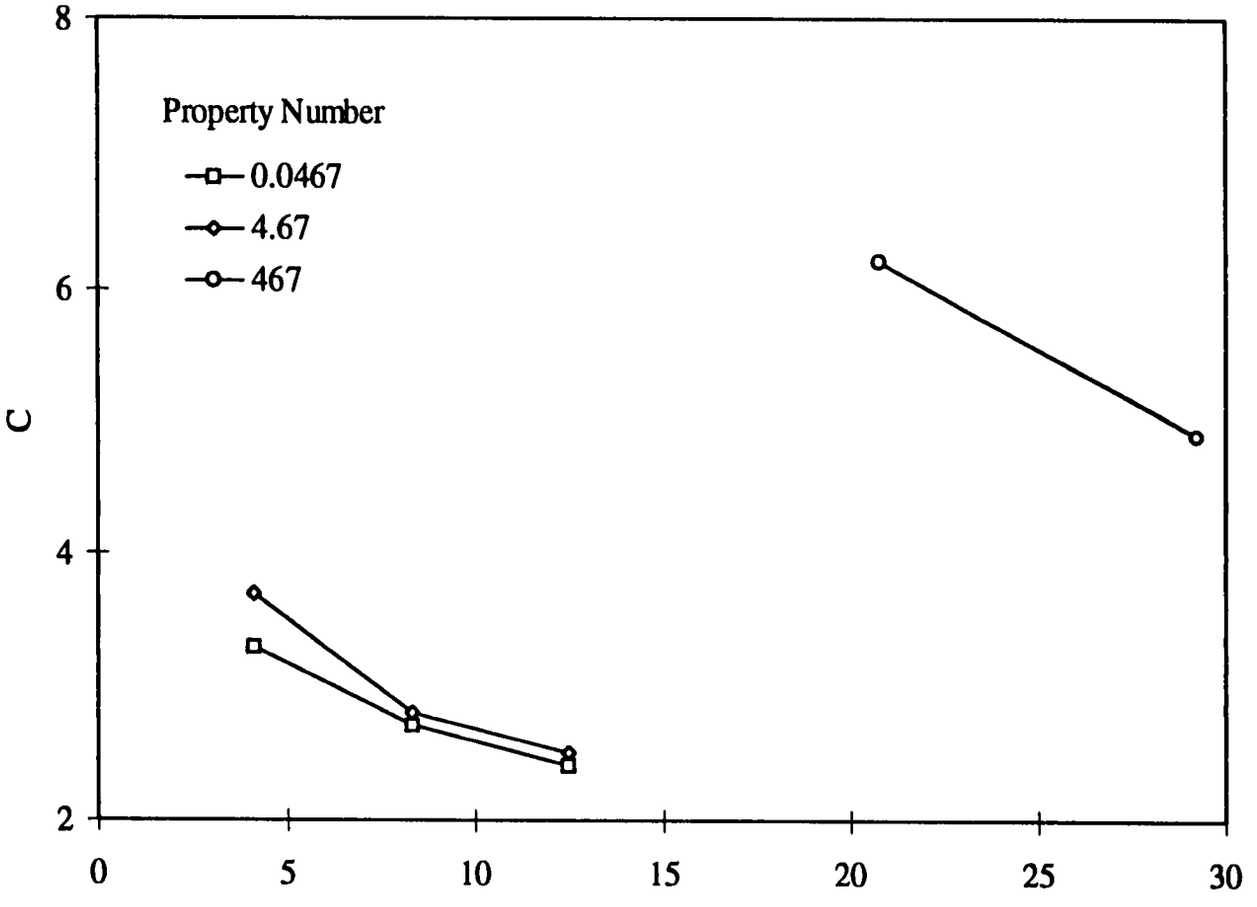

Inclination 3.0 Degree, Time 1.0

Figure 4-33 Wave Speed (θ=3.0°, time=1.0)

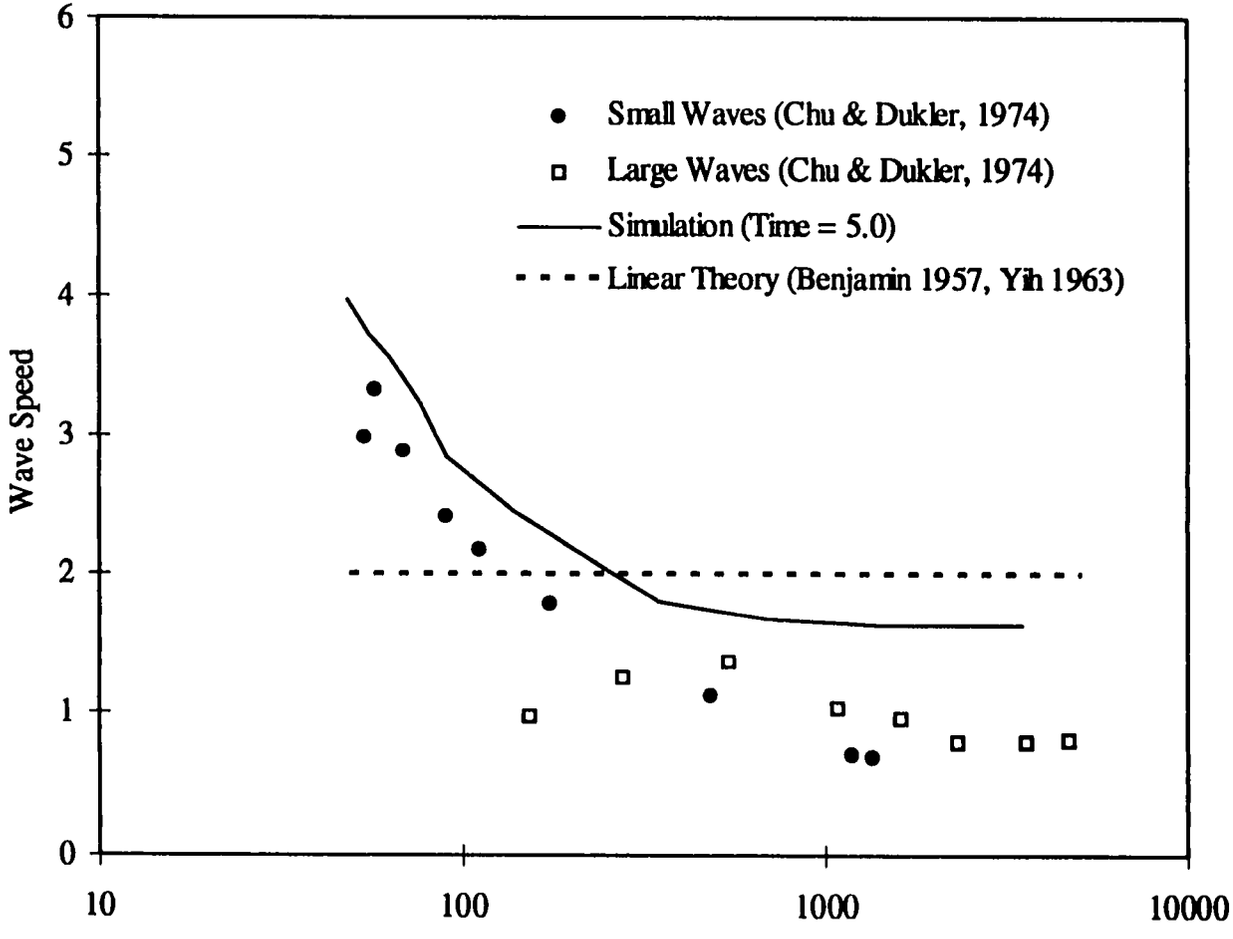

Water (90 Deg.)

Figure 4-34 Wave Speed (Water)

CONCLUSIONS AND RECOMMENDATIONS

CONCLUSIONS

Experiment

- A new method based on *optic-electric technique* is developed. The wave information carried by the final recorded signal can be extracted by digital signal processing techniques. They include signal sampling, noise filtration, mean removal and normalization, and energy spectral analysis using Fourier transformation.

Single Layer System

- Our measurements for *critical Reynolds number* that marks the onset of wave motions on the free surface show higher values than those in previous work, and are located well above the long-wave prediction of well accepted linear theory (Benjamin 1957, Yih 1963) but just below the inertia driven limiting case of Smith (1990).

- Observation of surface waves led us to record the distance downstream from X=0 (the inception point) at which the wave has completely damped. This distance normalized to the average film thickness is called the *transit distance*. Longer transit distances were observed for larger flow rates, and the fluids with higher property number.

- The *lower limit frequency* (LLF) is pretty much constant for all measurement positions, flow rates, angles of inclination, and liquid properties. The upper limit frequency (ULF) and the dominant frequency (DF) vary with measurement position, flow rate, inclination angle, and liquid properties.

- Larger flow rates and smaller angles of inclination lead to *larger upper limit frequencies*. These are ripples which flow over the surface of layers with higher velocities and smaller gravitational effects. Also, larger upper limit frequencies were observed for more viscous fluids, and the measurement position that is closer to inception.

- *Surface tension* plays an important role in wave formations over the free surface of thin liquid films, and exerts a stabilizing influence on the laminar flow of a film with uniform thickness. Increases in the Weber number (i.e. decreases in surface tension), which is a measure of inertia to surface tension forces, lead to appearance of higher upper limit frequency disturbances.

- The general conclusions about the upper limit frequency can be also applied to the *dominant frequency* representing the wavelength with the highest relative energy in the spectrum of all wavelengths.

- The fundamental difference with Javdani's (1976) results is the rise in Javdani's highly amplified frequency for smaller N numbers. This range corresponds to smaller Reynolds numbers. The *comparison* between our dominant frequency and the measurement of Brauner & Maron (1982) over the Reynolds number led to a general agreement in the trend and to some extent the values of frequency behavior.

Double Layer System

- The *lower limit frequency* (LLF) was pretty much constant for all positions of measurements, flow rates, and angles of inclination. The upper limit frequency (ULF) and the dominant frequency (DF) vary with flow rate, inclination angle, and liquid properties.

- Increases in the *bottom flow rate* lead to the appearance of shorter wavelength disturbances even as the upper flow rate remains constant. However, this effect is significant only in the region close to the inlet since the interface between the two fluid films disappears very quickly downstream. The shorter wavelength disturbances depend more on the *inclination angle* at lower flow rates in the upper layer. For higher upper flow rates this dependence seems to disappear.

- *Liquid properties* have a significant effect on the possibility of higher frequencies in the spectrum of surface disturbances. This possibility is shifted towards lower flow rates of the upper layer for more viscous liquids. *Surface tension* is a stabilizing factor for short wavelength disturbances, and the increase in surface tension leads to disturbances with longer wavelengths.

- *The maximum relative amplitude* (MRA) remains constant for lower flow rates of the upper layer. MRA increases with higher upper Reynolds or Weber numbers. There is no apparent dependence of MRA on liquid properties and angle of inclination.

Simulation

- Our *new numerical method* is good for simulating both steady and dynamic flow problems. This method is based on non-staggered grid system and developed in a general curvilinear coordinate system. It can handle the flow system with free surface and is able to produce physical meaningful velocity and pressure distributions for all physical time levels.

- Viscous liquid flows in thin layers were simulated by our numerical techniques for a wide range of flow conditions. Solutions were obtained for different liquid properties $0.0467 < \gamma < 467$, different angles of inclination $0.1° < \theta < 89.9°$, and

different Reynolds numbers Re < 30. Computations for vertical flow $\theta = 90°$ always diverged. However, any shift in angle from 90° produced stable solutions.

Wave Profile

- Generally speaking, liquids with lower viscosity *experienced simple form stable waves* running over their free-surfaces, and more complicated forms of waves running over the free-surfaces were found for more viscous liquids. Also, *solitary wave* forms predicted by the nonlinear theory (Esmail 1980) was obtained in this work.

- All disturbances seem to die out some distance downstream. This computational description of the waves is supported by our experimental observations. *Transit distance* is shorter for smaller Reynolds number than that for higher Reynolds number, and independent of the angle of inclination

Wave Speed

- A dimensionless wave speed (with respect to the steady state surface speed) was established to describe the speed of disturbance propagation over the free-surface. Generally speaking, disturbance propagation is approximately 2 to 6 times the material speed of particles on the surface.

- Wave speeds vary with angle of inclination, Reynolds number, Weber number which represents surface tension, and the property number of the fluid. Their dependence on the flow rate shows higher wave speeds for lower angles of inclination. In the case of their dependence on the Weber number wave speeds collapse in one relationship for all angles of inclination. Wave speeds over the free surface of liquids with smaller property number are lower than their counterpart for liquids with higher property numbers.

- Although our results for wave speeds are slightly larger than the experimental measurements of Chu & Dukler (1974), they are in good consistence with one another. The linear theories of Benjamin (1957) and Yih (1963) are shown to be a rather rough estimation of actual wave propagation speeds.

RECOMMENDATIONS

Experiment

- The experiments should be extended to cover double layer systems with viscosity and density stratification.
- The experiments should be extended to cover the behavior of surface waves over the free-surfaces of non Newtonian liquids.
- The experimental technique should be modified to cover wave formations on the interface between two layers.

Simulation

- Simulation techniques should be extended to cover double layer flows, and non Newtonian liquid flows.

REFERENCE

Abdallah S. J., Comput. Phys., Vol. 70, pp. 182 (1987)

Akhtaruzzaman A. F. M., Wang C. K. & Lin S. P.,
J. Appl Mech., Vol. 45, pp. 25 (1978)

Alekseenko S. V., Nakoryakov V. Ye. & Pokusaev B. G.,
AIChE J., Vol. 31, pp. 1446 (1985)

Anshus B. D. & Goren S. L., AIChE J., Vol. 12, pp. 1004 (1966)

Anturkar N. R., Papanastasiou T. C. & Wilkes J. O.,
Chem Eng Sci., Vol. 45, pp. 3271 (1990)

Beam R. M. & Warming R. F., AIAA J., Vol. 16, pp. 393 (1978)

Benjamin T. B., J Fluid Mech., Vol. 2, pp. 554 (1957)

Benjamin T. B., J Fluid Mech., Vol. 10, pp. 401 (1961)

Binnie A. M., J Fluid Mech., Vol. 2, pp. 551 (1957)

Binnie A. M., J Fluid Mech., Vol. 5, pp. 561 (1959)

Brauer H., VDI-Forschungsheft, Vol. 457 (1956)

Brauner N. & Maron D. M., Intl. J. Heat Mass Transfer, Vol. 25, pp. 99 (1982)

Cao Z. L., Ph. D Thesis, University of Saskatchewan, Canada (1993)

Charles M. E. & Lilleleht L.U., J Fluid Mech., Vol. 22, pp. 217 (1965)

Chen K., Phys Fluids A, Vol. 5, pp. 3038 (1993)

Chin R. W., Abernathy F. H. & Bertschy J. R.,
J Fluid Mech., Vol. 168, pp. 501 (1986)

Chu K. J. & Dukler A. E., AIChE J., Vol. 20, pp. 695 (1974)

Chu K. J. & Dukler A. E., AIChE J., Vol. 21, pp. 583 (1975)

Cooley J. W. & Tukey J. W., Math Computations, Vol. 19 (1965)

Dagan G., J Fluid Mech., Vol. 67, pp. 113 (1975)

Dandapat B. S. & Gupta A. S., Rheol Acta, Vol. 17, pp. 492 (1978)

De Bruin G. T., J Eng Maths, Vol. 8, pp. 259 (1974)

Dukler A. E., In Progress in Heat and Mass Transfer, Pergamon, pp. 207 (1972)

Esmail M. N., Can J Chem Eng., Vol. 58, pp. 145 (1980)

Esmail M. N. & Hummel R. L., AIChE J., Vol. 21, pp. 958 (1975)

Esmail, M. N. & Ghannam, M. T., Can. J. Chem. Eng., Vol. 68, pp. 197 (1990)

Fulford G. D., Ph. D Thesis, U. of Birmingham, England (1962)

Fulford G. D., Advances in Chemical Engineering, N.Y. pp. 151 (1964)

Ghia U., Ghia K. N. & Shin C. T., J. Comp. Phy., Vol. 48, pp.387 (1982)

Goussis D. A. & Kelly R. E., Bull Am Phys Soc., Vol. 30, pp. 1732 (1983)

Goussis D. A. & Kelly R. E., J. Fluid Mech., Vol. 223, pp. 25 (1991)

Graef M., Mitteilungen aus dem Max-Planck-Institut fur Stromungsforschung und der Aerodynamischen Verschsanstalt, Vol. 36, pp. 1 (1966)

Gupta A. S., J Fluid Mech., Vol. 28, pp. 17 (1967)

Gupta A. S. & Rai L., Proc Camb Phil Soc., Vol. 63, pp. 527 (1967)

Gupta A. S. & Rai L., J Fluid Mech., Vol. 33, pp. 87 (1968)

Harlow F. H. & Welch J. E., Phys Fluids, Vol. 8, pp. 2182 (1965)

Hoffman M. A. & Potts W. W., I &EC Fundam, Vol. 18, pp. 27 (1979)

Hoffmann K. A., Computational Fluid Dynamics for Engineers, Austin, Texas (1989)

Howard L. N., J Fluid Mech., Vol. 16, pp. 333 (1963)

Hsieh D. Y., Phys Fluids, Vol. 8, pp. 1785 (1965)

Hsieh D. Y., Phys Fluids A, Vol. 2, pp. 1145 (1990)

Jacobson R. E., Ray S. F. & Attridge G. G., The Manual of Photography, Focal Press, London (1988)

Javdani K., AIChE J., Vol. 22, pp. 867 (1976)

Jones L. O. & Whitaker S., AIChE J., Vol. 12, pp. 525 (1966)

Kao T. W., Phys Fluids, Vol. 8, pp. 812 (1965a)

Kao T. W., Phys Fluids, Vol. 8, pp. 2190 (1965b)

Kao T. W., J Fluid Mech., Vol. 33, pp. 561 (1968)

Kao T. W. & Park C., J Fluid Mech., Vol. 52, pp. 401 (1972)

Kapitsa P. L., Zh. Eksperim. i. Teor. Fiz., Vol. 18, pp. 3 (1948)

Kapitsa P. L. & Kapitsa S. P., Zh. Eksperim. i. Teor. Fiz., Vol. 19, pp. 105 (1949)

Kapitsa P. L., Collected papers of P. L. Kapitsa, MacMillan, New York (1964)

Kelly R. E., Goussis D. A., Lin S. P. & Hsu F. K., Phys Fluids A, Vol. 1, pp. 819 (1989)

Kobayashi C., Nohjo K. & Yoshimura Y., the Paper for AIChE's Spring National Meeting (1986)

Kobayashi C., the Paper for AIChE's Spring National Meeting (1990)

Krantz W. B. & Goren S. L., I &EC Fundam, Vol. 9, pp. 107 (1970)

Krantz W. B. & Goren S. L., AIChE J., Vol. 17, pp. 494 (1971a)

Krantz W. B. & Goren S. L., I & EC Fundam, Vol. 10, pp. 91 (1971b)

Krishna M. V. G. & Lin S. P., Phys Fluids, Vol. 20, pp. 1039 (1977)

Lacy C. E., Sheintuch M. & Dukler A. E., AIChE J., Vol. 37, pp. 481 (1991)

Lai W., Phys Fluids, Vol.10, pp. 844 (1967)

Levey M., the 35mm Film Source Book, Focal Press, pp. 29 (1992)

Li C. H., Phys Fluids, Vol. 13, pp. 1701 (1970)

Lin C. C., the Theory of Hydrodynamic Stability, Cambridge University Press (1955)

Lin S. P., Phys Fluids, Vol. 10, pp. 308 (1967a)

Lin S. P., Phys Fluids, Vol. 10, pp. 69 (1967b)

Lin S. P., J Fluid Mech., Vol. 36, pp. 113 (1969)

Lin S. P., J Fluid Mech., Vol. 40, pp. 307 (1970)

Lin S. P. & Krishna M. V. G., Phys Fluids, Vol. 20, pp. 2005 (1977)

Lin S. P. & Wang C. Y.,
Encyclopedia of Fluid Mechanics, Gulf., Vol. 1, pp. 931 (1985)

Liu J., Paul J. D. & Gollub J. P., J Fluid Mech, Vol. 250, pp. 69 (1993)

Liu J., Paul J. D. & Gollub J. P., J Fluid Mech., Vol. 250, pp. 69 (1993)

Nakaya C., Phys Fluids, Vol. 18, pp. 1407 (1975)

Nusselt W., VDI (Ver. Deut. Ingr) Z., Vol. 60, pp. 549 (1916)

Patankar S. V., Numerical Heat Transfer and Fluid Flow,
Hemisphere Publishing Corp. (1980)

Pierson R. W. & Whitaker S., I & EC Fundam., Vol. 16, pp. 401 (1977)

Portalski S. & Clegg A. J., Chem Eng Sci., Vol. 27, pp. 1257 (1972)

Portalski S., AIChE J., Vol.19, pp. 1244 (1973)

Reynolds W. C. & Potter M. C., J Fluid Mech., Vol.27, pp. 465 (1967)

Shagfeh E. S. G., Larson R. G. & Fredrickson G. H.,
J non-Newtonian Fluid Mech., Vol.31, pp. 87 (1989)

Shames, I., "Mechanics of Fluids", McGraw-Hill, New York (1962)

Shannon C. E., Proc. IRE, Vol. 37, pp. 10 (1949)

Sivashinsky G. & Michelson D. M., Prog. Theor. Phys., Vol. 63, pp. 2112 (1980)

Smith M. K., J. Fluid Mech., Vol. 217, pp. 469 (1990)

Squire H. B., Proc Roy Soc., A142, pp. 621 (1933)

Soh W. Y. & Goodrich J. W., J. Comput. Phys., Vol. 79, pp. 113 (1988)

Steger J. L., AIAA J., Vol. 16, pp. 679 (1978)

Strobel W. J. & Whitaker S., AIChE J., Vol. 15, pp. 527 (1969)

Stuart J. T., J Fluid Mech., Vol. 9, pp. 353 (1960)

Tailby S. R. & Portalski S., Trans. Inst. Chem. Engrs., Vol. 40, pp. 114 (1962)

Thomas P. D. & Middlehoff J. F., AIAA J., Vol. 18, pp. 652 (1980)

Ting L. L., Rheol Acta, Vol.14, pp. 503 (1975)

Tuann S. Y. & Mervyn D. O., Studies of Rectangular Cavity Flow with Reynolds Number by a Finite Element Method, University of British Columbia, Canada (1977)

Vinokur M., J. of Comput. Phys., Vol. 14, pp.1105 (1974)

Wang C. K., Seaborg J. J. & Lin S. P., Phys Fluids, Vol.2, pp. 1669 (1978)

Weaver H. J., Applications of Discrete and Continuous Fourier Analysis, John Wiley & Sons Inc. (1983)

Weinstein S. J., the Paper for AIChE's Spring National Meeting (1990)

Whitaker S., Ind. Engng Chem. Fundam., Vol. 3, pp. 132 (1964)

Yih C. S., Proceedings of the Second U.S. National Congress of Applied mechanics, pp. 623 (1955)

Yih C. S., Phys Fluids, Vol.6, pp. 321 (1963)

Yih C. S., Phys Fluids, Vol.8, pp. 1257 (1965)

APPENDIX
FORTRAN PROGRAM CODE

```
ZhG0001:      IMPLICIT REAL*8(A-H,O-Z)
ZhG0002:      CHARACTER BEGTM*24,STPTM*24
ZhG0003:      PARAMETER(M=2,LX=1001,LY=11,IG=2*LX-1,JG=2*LY-1)
ZhG0004:      PARAMETER(LX1=LX-1,LY1=LY-1,LX2=LX-2,LY2=LY-2)
ZhG0005:      PARAMETER(IG1=IG-1,JG1=JG-1)
ZhG0006:      COMMON/XY/X(IG,JG),Y(IG,JG)
ZhG0007:      COMMON/PSFE/PS(IG,JG),FE(IG,JG)
ZhG0008:      COMMON/ABG/BJ(IG,JG),A(IG,JG),B(IG,JG),G(IG,JG)
ZhG0009:      COMMON/DXY/XI(IG,JG),XJ(IG,JG),YI(IG,JG),YJ(IG,JG)
ZhG0010:      COMMON/DXYT/XT(IG,JG),YT(IG,JG)
ZhG0011:      COMMON/UVP/U(LX,LY),V(LX,LY),P(LX,LY)
ZhG0012:      COMMON/UVR/UR(LX,LY),VR(LX,LY)
ZhG0013:      COMMON/P_R/PR(LX,LY)
ZhG0014:      COMMON/UVPB/UB(LX,LY),VB(LX,LY),PB(LX,LY)
ZhG0015:      COMMON/DVELB/DUB(LX,LY),DVB(LX,LY)
ZhG0016:      COMMON/UV_B/ULFT(LY),URIT(LY),UBOT(LX)
ZhG0017:      1          ,VLFT(LY),VRIT(LY),VBOT(LX)
ZhG0018:      COMMON/UV_C/CUX1(LX,LY),CUY1(LX,LY),CVX1(LX,LY),CVY1(LX,LY)
ZhG0019:      1          ,CUX2(LX,LY),CUY2(LX,LY),CVX2(LX,LY),CVY2(LX,LY)
ZhG0020:      2          ,CU1(LX,LY),CV1(LX,LY),CU2(LX,LY),CV2(LX,LY)
ZhG0021:      3          ,CXX(LX,LY),CXY(LX,LY),CYY(LX,LY)
ZhG0022:      COMMON/BLK3/AMX(M,M,LX,2:LY1),BMX(M,M,LX,2:LY1)
ZhG0023:      1          ,CMX(M,M,LX,2:LY1),AMY(M,M,LY,2:LX1)
ZhG0024:      2          ,BMY(M,M,LY,2:LX1),CMY(M,M,LY,2:LX1)
ZhG0025:      COMMON/DP_C/XI2DJ(IG,JG),XJ2DJ(IG,JG),YI2DJ(IG,JG)
ZhG0026:      1          ,YJ2DJ(IG,JG),XIXJDJ(IG,JG),XIYIDJ(IG,JG)
ZhG0027:      2          ,XIYJDJ(IG,JG),XJYIDJ(IG,JG),XJYJDJ(IG,JG)
ZhG0028:      3          ,YIYJDJ(IG,JG),PLUS(IG,JG)
ZhG0029:      4          ,P1(IG,JG),P2(IG,JG),P3(IG,JG),P4(IG,JG)
ZhG0030:      5          ,P5(IG,JG),P6(IG,JG),P7(IG,JG),P8(IG,JG)
ZhG0031:      COMMON/ABGDJ/ADJ(IG,JG),BDJ(IG,JG),GDJ(IG,JG)
ZhG0032:      COMMON/DPHJ/XIHJ(LX,LY),XJHJ(LX,LY),YIHJ(LX,LY),YJHJ(LX,LY)
ZhG0033:      COMMON/BD/XI3(LX,M),XI4(LX,M),YI3(LX,M),YI4(LX,M)
ZhG0034:      1          ,XJ3(M,LY),XJ4(M,LY),YJ3(M,LY),YJ4(M,LY)
ZhG0035:      COMMON/COM22/Q1(LX,LY),Q2(LX,LY),Q3(LX,LY)
ZhG0036:      COMMON/FORCE/FX(LX,LY),FY(LX,LY)
ZhG0037:      COMMON/BLK3_FREE/AFREE(M,M,LX),BFREE(M,M,LX),CFREE(M,M,LX)
ZhG0038:      COMMON/FREE_UVP/FREEX(M,M,LX),FREEY(M,M,LX,3)
ZhG0039:      1          ,FP1(LX),FP2(LX,3),FP3(LX,3)
ZhG0040:      COMMON/R_FREE/R_VEL(M,LX),R_PRE(LX)
ZhG0041:      COMMON/WAVEP/PERCENT(LX),H(LX),AM(LX),PP(LX)
ZhG0042:      COMMON/F_M/FM(LX,LY),FM_LR(2,LY),FM_BT(LX)
ZhG0043:      DIMENSION XO(IG,JG),YO(IG,JG),PBO(LX,LY),PTIME(10)
ZhG0044:      1          ,UST(LY),VST(LY),PST(LY),U_RIT(LY),V_RIT(LY)
```

```
ZhG0045:        CALL UNIX
ZhG0046:        CALL FDATE(BEGTM)
ZhG0047:        OPEN(11,FILE='NEWINP.INP',STATUS='OLD')
ZhG0048:        READ(11,*) N_ORDER
ZhG0049:        READ(11,*) FLOW,DENS,VISC,TENS,ANGLE
ZhG0050:        READ(11,*) FAC,DT,DTOI,TOL,NPR,ENDTIME
ZhG0051:        READ(11,*) VEL_UPPER,PRE_UPPER
ZhG0052:        READ(11,*) (PTIME(I),I=1,5)
ZhG0053:        READ(11,*) (PTIME(I),I=6,10)
ZhG0054:        READ(11,*) AV,FV
ZhG0055:        CLOSE(11)
ZhG0056:        IF(N_ORDER.EQ.1) THEN
ZhG0057:        OPEN(10,FILE='SEE_1.SEE',STATUS='UNKNOWN',ACCESS='APPEND')
ZhG0058:        OPEN(12,FILE='XY_1.DAT',STATUS='UNKNOWN',ACCESS='APPEND')
ZhG0059:        ENDIF
ZhG0060:        IF(N_ORDER.EQ.2) THEN
ZhG0061:        OPEN(10,FILE='SEE_2.SEE',STATUS='UNKNOWN',ACCESS='APPEND')
ZhG0062:        OPEN(12,FILE='XY_2.DAT',STATUS='UNKNOWN',ACCESS='APPEND')
ZhG0063:        ENDIF
ZhG0064:        WRITE(10,9955) ANGLE,FLOW
ZhG0065:        WRITE(10,9956) DENS,VISC,TENS
ZhG0066:        WRITE(10,9960) DT,DTOI,FAC
ZhG0067:        WRITE(10,9980) AV,FV
ZhG0068:        WRITE(10,*)' ***'
ZhG0069: *      * SOME PARAMETERS *
ZhG0070:        PI=3.1415926535897932384
ZhG0071:        GRAV=980.665
ZhG0072:        KK=1
ZhG0073:        KSTOP=0
ZhG0074:        NTOI=250
ZhG0075:        PA=0.0
ZhG0076:        XLEN=200.0
ZhG0077:        YLEN=1.0
ZhG0078:        DPP=GRAV/DENS*(VISC/100.0/TENS)**3.0*VISC/100.0
ZhG0079:        WRITE(10,*)' Npp =',DPP
ZhG0080:        YLEN=YLEN/FAC
ZhG0081:        MIDX=LX1/2+1
ZhG0082:        ANGLE=ANGLE/180.0*PI
ZhG0083: *      * FLOW -- ml/min.  Width=4 cm
ZhG0084:        FLOW=FLOW/240.0
ZhG0085:        VISC=VISC/DENS/100.0
ZhG0086:        FV=2.0*PI*FV
ZhG0087: *      * FILM PARAMETER
ZhG0088: *      * Average u-velocity and Steady-state film thickness
ZhG0089: *      * as Characteristic Velocity and Length
ZhG0090: *      * Fr is dependent on Re for this flow system.
ZhG0091: *      * Re = Den*Flow/Visc    Flow -- per unit Width
ZhG0092: *      * Ua = (Visc*gSin(Ang)/3/Den)^(1/3)*Re^(2/3)
ZhG0093: *      * H  = (3Visc^2/Den^2/gSin(Ang))^(1/3)*Re^(1/3)
ZhG0094: *      * SS = Den*(3Visc^2*g^2*Sin(Ang)^2/Den^2)^(1/3)*Re^(1/3)
ZhG0095: *      * Fr = (Re Sin Ang/3)^0.5
ZhG0096:        RE=FLOW/VISC
ZhG0097:        FR2=RE*DSIN(ANGLE)/3.0
```

```
ZhG0098:       UAVE=(VISC*GRAV*DSIN(ANGLE)/3.0)**(1.0/3.0)*RE**(2.0/3.0)
ZhG0099:       HAVE=(3.0*VISC**2.0/GRAV/DSIN(ANGLE)*RE)**(1.0/3.0)
ZhG0100:       WE=TENS/DENS/UAVE**2.0/HAVE
ZhG0101:       WRITE(10,9957) HAVE,UAVE
ZhG0102:       WRITE(10,9950) RE,WE,FR2
ZhG0103: *     * CALCULATION Re, We, and Fr *
ZhG0104: *     * Surface u-velocity and (f)*Steady-state film thickness
ZhG0105: *     * as Characteristic Velocity and Length
ZhG0106: *     * Surface-u = 1.5*Average-u
ZhG0107:       USUR=1.5*UAVE
ZhG0108:       RE=FAC*HAVE*USUR/VISC
ZhG0109:       WE=TENS/DENS/USUR**2.0/HAVE/FAC
ZhG0110:       FR2=USUR**2.0/GRAV/HAVE/FAC
ZhG0111:       WRITE(10,9950) RE,WE,FR2
ZhG0112: *     * BCs u1: no-slip on the bottom
ZhG0113: *     *    u2: no-drag on the free surface
ZhG0114: *     *    p : p = Pa on the free surface
ZhG0115:       FXX=DSIN(ANGLE)/FR2
ZhG0116:       FYY=-DCOS(ANGLE)/FR2
ZhG0117:       YSTEP=HAVE/DFLOAT(LY1)
ZhG0118:       DO 100 J=1,LY
ZhG0119:       DO 101 I=1,LX
ZhG0120:       FX(I,J)=FXX
ZhG0121: 101   FY(I,J)=FYY
ZhG0122:       YY=DFLOAT(J-1)*YSTEP
ZhG0123:       UST(J)=(HAVE-0.5*YY)*YY*GRAV*DSIN(ANGLE)/VISC/USUR
ZhG0124:       VST(J)=0.0
ZhG0125: 100   PST(J)=PA+(HAVE-YY)*GRAV*DCOS(ANGLE)/USUR**2.0
ZhG0126:       TM=0.0
ZhG0127:       ITM=0
ZhG0128:       XSTEP=XLEN/DFLOAT(IG1)
ZhG0129:       DO 110 I=1,IG
ZhG0130:       XX=DFLOAT(I-1)*XSTEP
ZhG0131:       DO 110 J=1,JG
ZhG0132:       X(I,J)=XX
ZhG0133: 110   XO(I,J)=XX
ZhG0134:       YSTEP=YLEN/DFLOAT(JG1)
ZhG0135:       DO 113 J=1,JG
ZhG0136:       YY=DFLOAT(J-1)*YSTEP
ZhG0137:       DO 113 I=1,IG
ZhG0138:       Y(I,J)=YY
ZhG0139: 113   YO(I,J)=YY
ZhG0140:       DO 120 I=1,LX
ZhG0141:       DO 120 J=1,LY
ZhG0142:       U(I,J)=UST(J)
ZhG0143:       V(I,J)=VST(J)
ZhG0144: 120   P(I,J)=PST(J)
ZhG0145: 8080  TM=TM+DT
ZhG0146:       ITM=ITM+1
ZhG0147:       CALL GRID
ZhG0148:       CALL DPOSITION
ZhG0149:       DO 210 I=1,IG
ZhG0150:       DO 210 J=1,JG
```

```
ZhG0151:       XT(I,J)=(X(I,J)-XO(I,J))/DT
ZhG0152:       YT(I,J)=(Y(I,J)-YO(I,J))/DT
ZhG0153:       XO(I,J)=X(I,J)
ZhG0154: 210   YO(I,J)=Y(I,J)
ZhG0155:       CALL CONSTANT(RE,DT,PA,WE)
ZhG0156:       CALL COEF_MATRIX(DT,DTOI)
ZhG0157:       CALL BLK3_LU
ZhG0158:       DO 263 J=2,LY
ZhG0159:       JM1=J-1
ZhG0160:       JJ=2*JM1
ZhG0161:       U_RIT(J)=YI(IG1,JJ)*(U(LX,J)+U(LX1,J)-U(LX,JM1)-U(LX1,JM1))
ZhG0162:       1         -YJ(IG1,JJ)*(U(LX,J)+U(LX,JM1)-U(LX1,J)-U(LX1,JM1))
ZhG0163: 263   V_RIT(J)=XJ(IG1,JJ)*(V(LX,J)+V(LX,JM1)-V(LX1,J)-V(LX1,JM1))
ZhG0164:       1         -XI(IG1,JJ)*(V(LX,J)+V(LX1,J)-V(LX,JM1)-V(LX1,JM1))
ZhG0165:       DO 300 I=1,LX
ZhG0166:       DO 300 J=1,LY
ZhG0167:       DUB(I,J)=0.0
ZhG0168:       DVB(I,J)=0.0
ZhG0169:       UB(I,J)=0.0
ZhG0170:       VB(I,J)=0.0
ZhG0171:       PB(I,J)=0.0
ZhG0172: 300   PBO(I,J)=0.0
ZhG0173: *     * dis E = E at n+1 - E at n
ZhG0174:       DO 370 J=1,LY
ZhG0175: 370   UB(1,J)=UST(J)*AV*(DSIN(FV*TM)-DSIN(FV*(TM-DT)))
ZhG0176:       DO 400 ITOI=1,NTOI
ZhG0177:       ERRDUVB=0.0
ZhG0178:       CALL VELB_BLOCK(DT,DTOI)
ZhG0179:       DO 600 I=2,LX1
ZhG0180:       DO 600 J=2,LY1
ZhG0181:       A1=DMAX1(DABS(DUB(I,J)),DABS(DVB(I,J)))
ZhG0182:       IF(ERRDUVB.LT.A1) ERRDUVB=A1
ZhG0183:       UB(I,J)=UB(I,J)+DUB(I,J)
ZhG0184: 600   VB(I,J)=VB(I,J)+DVB(I,J)
ZhG0185:       CALL FREE_VEL
ZhG0186:       DO 633 J=2,LY
ZhG0187:       JM1=J-1
ZhG0188:       JJ=2*JM1
ZhG0189:       UB(LX,J)=(U_RIT(J)
ZhG0190:       1         +YI(IG1,JJ)*(UB(LX1,J)-UB(LX,JM1)-UB(LX1,JM1))
ZhG0191:       1         -YJ(IG1,JJ)*(UB(LX,JM1)-UB(LX1,J)-UB(LX1,JM1)))
ZhG0192:       2         /(YJ(IG1,JJ)-YI(IG1,JJ))
ZhG0193: 633   VB(LX,J)=(V_RIT(J)
ZhG0194:       1         +XJ(IG1,JJ)*(VB(LX,JM1)-VB(LX1,J)-VB(LX1,JM1))
ZhG0195:       1         -XI(IG1,JJ)*(VB(LX1,J)-VB(LX,JM1)-VB(LX1,JM1)))
ZhG0196:       2         /(XI(IG1,JJ)-XJ(IG1,JJ))
ZhG0197:       DO 650 I=2,LX1
ZhG0198:       IP1=I+1
ZhG0199:       IM1=I-1
ZhG0200:       UBX=FP1(IP1)*UB(IP1,LY)-FP1(IM1)*UB(IM1,LY)
ZhG0201:       UBY=3.0*FP2(I,1)*UB(I,LY)-4.0*FP2(I,2)*UB(I,LY1)
ZhG0202:       1         +FP2(I,3)*UB(I,LY2)
ZhG0203:       VBY=3.0*FP3(I,1)*VB(I,LY)-4.0*FP3(I,2)*VB(I,LY1)
```

```
ZhG0204:        1       +FP3(I,3)*VB(I,LY2)
ZhG0205: 650    PB(I,LY)=R_PRE(I)+0.5*(UBX-UBY-VBY)
ZhG0206: *      * OTHER PRESSURE BOUNDARY *
ZhG0207:        CALL PB_NBD(RE)
ZhG0208: *      * CORNER POINTS *
ZhG0209:        AA=PB(2,3)+PB(2,1)-PB(1,3)-2.0*(PB(2,2)-PB(1,2))
ZhG0210:        BB=PB(1,2)+PB(3,2)-PB(3,1)-2.0*(PB(2,2)-PB(2,1))
ZhG0211:        PB(1,1)=0.5*(AA+BB)
ZhG0212:        AA=PB(LX1,3)+PB(LX1,1)-PB(LX,3)+2.0*(PB(LX,2)-PB(LX1,2))
ZhG0213:        BB=PB(LX2,2)+PB(LX,2)-PB(LX2,1)-2.0*(PB(LX1,2)-PB(LX1,1))
ZhG0214:        PB(LX,1)=0.5*(AA+BB)
ZhG0215:        PB(1,LY)=PB(2,LY)+PB(2,LY2)-PB(1,LY2)
ZhG0216:        1       -2.0*(PB(2,LY1)-PB(1,LY1))
ZhG0217:        PB(LX,LY)=PB(LX1,LY)+PB(LX1,LY2)-PB(LX,LY2)
ZhG0218:        1       +2.0*(PB(LX,LY1)-PB(LX1,LY1))
ZhG0219:        CALL PB_INNER(BJ,DT)
ZhG0220:        ERRDPB=0.0
ZhG0221:        DO 700 I=1,LX
ZhG0222:        DO 700 J=1,LY
ZhG0223:        A2=DABS(PB(I,J)-PBO(I,J))
ZhG0224:        IF(ERRDPB.LT.A2) ERRDPB=A2
ZhG0225: 700    PBO(I,J)=PB(I,J)
ZhG0226:        IF(ERRDUVB.LT.TOL.AND.ERRDPB.LT.TOL) GOTO 8100
ZhG0227: 400    CONTINUE
ZhG0228: *      * Middle point on Bottom as
ZhG0229: *      * the Pressure Reference Point
ZhG0230: 8100   PBASE=PB(MIDX,1)
ZhG0231:        DO 750 I=1,LX
ZhG0232:        DO 750 J=1,LY
ZhG0233: 750    PB(I,J)=PB(I,J)-PBASE
ZhG0234:        ERRDUV=0.0
ZhG0235:        ERRDP=0.0
ZhG0236:        DO 800 I=1,LX
ZhG0237:        DO 800 J=1,LY
ZhG0238:        IF(DABS(UB(I,J)).LT.1.0D-10) UB(I,J)=0.0
ZhG0239:        IF(DABS(VB(I,J)).LT.1.0D-10) VB(I,J)=0.0
ZhG0240:        IF(DABS(PB(I,J)).LT.1.0D-10) PB(I,J)=0.0
ZhG0241:        A1=DMAX1(DABS(UB(I,J)),DABS(VB(I,J)))
ZhG0242:        A2=DABS(PB(I,J))
ZhG0243:        IF(ERRDUV.LT.A1) ERRDUV=A1
ZhG0244:        IF(ERRDP.LT.A2) ERRDP=A2
ZhG0245:        U(I,J)=U(I,J)+UB(I,J)
ZhG0246:        V(I,J)=V(I,J)+VB(I,J)
ZhG0247: 800    P(I,J)=P(I,J)+PB(I,J)
ZhG0248:        IF(ERRDUV.GT.VEL_UPPER) THEN
ZhG0249:        WRITE(10,*) ' VELOCITY UNSTABLE ! AT',TM
ZhG0250:        KSTOP=99
ZhG0251:        ENDIF
ZhG0252:        IF(ERRDP.GT.PRE_UPPER) THEN
ZhG0253:        WRITE(10,*) ' PRESSURE UNSTABLE ! AT',TM
ZhG0254:        KSTOP=99
ZhG0255:        ENDIF
ZhG0256:        DO 900 I=2,LX
```

```
ZhG0257:        II=2*I-1
ZhG0258:        XX=X(II,JG)-X(II-2,JG)
ZhG0259: 900    Y(II,JG)=(YO(II,JG)+V(I,LY)*DT+DT*U(I,LY)/XX*Y(II-2,JG))
ZhG0260:        2       /(1.0+DT*U(I,LY)/XX)
ZhG0261:        DO 910 II=2,IG-1,2
ZhG0262: 910    Y(II,JG)=0.5*(Y(II-1,JG)+Y(II+1,JG))
ZhG0263:        IF(ITM-ITM/NPR*NPR.EQ.0)
ZhG0264:        1       WRITE(10,9930) ITOI,ERRDUVB,ERRDPB,TM,ERRDUV,ERRDP
ZhG0265:        IF(KSTOP.EQ.99.OR.DABS(TM-PTIME(KK)).LT.DT/2.0) THEN
ZhG0266:        WRITE(12,9940) TM
ZhG0267:        DO 920 I=1,LX
ZhG0268:        II=2*I-1
ZhG0269:        PERCENT(I)=(Y(II,JG)-YLEN)/YLEN*100.0
ZhG0270: 920    WRITE(12,9900),X(II,JG),Y(II,JG),PERCENT(I)
ZhG0271:        CALL WAVE(LL1,LL2)
ZhG0272:        WRITE(10,9940) TM
ZhG0273:        WRITE(10,9926) (H(I),I=1,LL1)
ZhG0274:        DO 930 I=1,LL2
ZhG0275: 930    WRITE(10,9927) AM(I),PP(I)
ZhG0276:        IF(KSTOP.EQ.99) STOP
ZhG0277:        CALL FDATE(STPTM)
ZhG0278:        KK=KK+1
ZhG0279:        WRITE(10,9935) BEGTM,STPTM
ZhG0280:        ENDIF
ZhG0281:        IF(TM.LT.ENDTIME) GOTO 8080
ZhG0282: 9930   FORMAT(1X,I3,2(1X,E10.3),2X,F8.3,2(1X,E10.3))
ZhG0283: 9940   FORMAT(1X,'Time=',F8.3)
ZhG0284: 9950   FORMAT(1X,'Re=',F8.3,' We  =',F8.3,' Fr2 =',F8.3)
ZhG0285: 9955   FORMAT(1X,'Ang =',F5.1,' Deg.',' Q =',F6.1,' ml/min.')
ZhG0286: 9956   FORMAT(1X,'Den =',F7.3,' Visc =',F7.3,' Tens =',F7.3)
ZhG0287: 9957   FORMAT(1X,'H0 =',F7.4,' cm',' U0 =',F8.4,' cm/s')
ZhG0288: 9960   FORMAT(1X,'Dt=',F8.3,' Dtoi=',F8.3,' f = ',F4.1)
ZhG0289: 9980   FORMAT(1X,'AV=',F8.4,' FV  =',F6.2)
ZhG0290: 9900   FORMAT(1X,F7.3,1X,F10.6,2X,F10.6)
ZhG0291: 9905   FORMAT(1X,2(1X,F5.2,1X,F8.5))
ZhG0292: 9925   FORMAT(1X,3(1X,F10.5))
ZhG0293: 9926   FORMAT(1X,5(F8.5,1X))
ZhG0294: 9927   FORMAT(1X,2(F8.5,1X))
ZhG0295: 9935   FORMAT(1X,A24,2X,A24)
ZhG0296: 8888   STOP
ZhG0297:        END
ZhG0298:
ZhG0299:        SUBROUTINE UNIX
ZhG0300:        IMPLICIT REAL*8 (A-H,O-Z)
ZhG0301:        CALL ABRUPT_UNDERFLOW()
ZhG0302:        CALL GRADUAL_UNDERFLOW()
ZhG0303:        RETURN
ZhG0304:        END
ZhG0305:
ZhG0306:        SUBROUTINE GRID
ZhG0307:        IMPLICIT REAL*8(A-H,O-Z)
ZhG0308:        PARAMETER(LX=1001,LY=11,IG=2*LX-1,JG=2*LY-1)
ZhG0309:        PARAMETER(I1=IG-1,J1=JG-1)
```

```
ZhG0310:       COMMON/XY/X(IG,JG),Y(IG,JG)
ZhG0311:       COMMON/PSFE/PS(IG,JG),FE(IG,JG)
ZhG0312:       CALL UNIX
ZhG0313:       NUMBER=100
ZhG0314:       OMG=1.7
ZhG0315:       DO 30 I=1,IG
ZhG0316:       IM1=I-1
ZhG0317:       DO 30 J=1,JG
ZhG0318:       X(I,J)=(X(IG,J)-X(1,J))*DFLOAT(IM1)/DFLOAT(I1)+X(1,J)
ZhG0319: 30    Y(I,J)=(Y(I,JG)-Y(I,1))*DFLOAT(J-1)/DFLOAT(J1)+Y(I,1)
ZhG0320:       DO 50 I=2,I1
ZhG0321:       IP1=I+1
ZhG0322:       IM1=I-1
ZhG0323:       DO 50 J=1,JG
ZhG0324:       XX=X(IP1,J)-X(IM1,J)
ZhG0325:       YX=Y(IP1,J)-Y(IM1,J)
ZhG0326:       XXX=X(IP1,J)+X(IM1,J)-2.0*X(I,J)
ZhG0327:       YXX=Y(IP1,J)+Y(IM1,J)-2.0*Y(I,J)
ZhG0328: 50    FE(I,J)=-2.0*(XX*XXX+YX*YXX)/(XX*XX+YX*YX)
ZhG0329:       DO 60 J=2,J1
ZhG0330:       JP1=J+1
ZhG0331:       JM1=J-1
ZhG0332:       DO 60 I=1,IG
ZhG0333:       XY=X(I,JP1)-X(I,JM1)
ZhG0334:       YY=Y(I,JP1)-Y(I,JM1)
ZhG0335:       XYY=X(I,JP1)+X(I,JM1)-2.0*X(I,J)
ZhG0336:       YYY=Y(I,JP1)+Y(I,JM1)-2.0*Y(I,J)
ZhG0337: 60    PS(I,J)=-2.0*(XY*XYY+YY*YYY)/(XY*XY+YY*YY)
ZhG0338:       DO 130 K=1,NUMBER
ZhG0339:       RSD=0.0
ZhG0340:       DO 140 I=2,I1
ZhG0341:       IP1=I+1
ZhG0342:       IM1=I-1
ZhG0343:       DO 140 J=2,J1
ZhG0344:       JP1=J+1
ZhG0345:       JM1=J-1
ZhG0346:       XX=0.5*(X(IP1,J)-X(IM1,J))
ZhG0347:       XY=0.5*(X(I,JP1)-X(I,JM1))
ZhG0348:       YX=0.5*(Y(IP1,J)-Y(IM1,J))
ZhG0349:       YY=0.5*(Y(I,JP1)-Y(I,JM1))
ZhG0350:       XXY=X(IP1,JP1)-X(IP1,JM1)-X(IM1,JP1)+X(IM1,JM1)
ZhG0351:       YXY=Y(IP1,JP1)-Y(IP1,JM1)-Y(IM1,JP1)+Y(IM1,JM1)
ZhG0352:       AA=XY*XY+YY*YY
ZhG0353:       BB=0.5*(XX*XY+YX*YY)
ZhG0354:       GG=XX*XX+YX*YX
ZhG0355:       T=AA*FE(I,J)
ZhG0356:       D=GG*PS(I,J)
ZhG0357:       DAC=2.0*(AA+GG)
ZhG0358:       DX=(AA*(X(IP1,J)+X(IM1,J))+GG*(X(I,JP1)+X(I,JM1))
ZhG0359:       1         -BB*XXY+T*XX+D*XY)/DAC-X(I,J)
ZhG0360:       DY=(AA*(Y(IP1,J)+Y(IM1,J))+GG*(Y(I,JP1)+Y(I,JM1))
ZhG0361:       1         -BB*YXY+T*YX+D*YY)/DAC-Y(I,J)
ZhG0362:       X(I,J)=X(I,J)+OMG*DX
```

```
ZhG0363:       Y(I,J)=Y(I,J)+OMG*DY
ZhG0364:       E=DMAX1(DABS(DX),DABS(DY))
ZhG0365: 140   IF(RSD.LT.E) RSD=E
ZhG0366:       IF(RSD.LT.1.0D-6) GO TO 150
ZhG0367: 130   CONTINUE
ZhG0368: 150   RETURN
ZhG0369:       END
ZhG0370:
ZhG0371:       SUBROUTINE DPOSITION
ZhG0372:       IMPLICIT REAL*8(A-H,O-Z)
ZhG0373:       PARAMETER(LX=1001,LY=11,IG=2*LX-1,JG=2*LY-1)
ZhG0374:       PARAMETER(I1=IG-1,J1=JG-1,I2=IG-2,J2=JG-2)
ZhG0375:       COMMON/XY/X(IG,JG),Y(IG,JG)
ZhG0376:       COMMON/DXY/XI(IG,JG),XJ(IG,JG),YI(IG,JG),YJ(IG,JG)
ZhG0377:       COMMON/ABG/BJ(IG,JG),A(IG,JG),B(IG,JG),G(IG,JG)
ZhG0378:       CALL UNIX
ZhG0379:       DO 200 I=2,I1
ZhG0380:       IP1=I+1
ZhG0381:       IM1=I-1
ZhG0382:       XI(I,1)=X(IP1,1)-X(IM1,1)
ZhG0383:       YI(I,1)=Y(IP1,1)-Y(IM1,1)
ZhG0384:       XJ(I,1)=-3.0*X(I,1)+4.0*X(I,2)-X(I,3)
ZhG0385:       YJ(I,1)=-3.0*Y(I,1)+4.0*Y(I,2)-Y(I,3)
ZhG0386:       XI(I,JG)=X(IP1,JG)-X(IM1,JG)
ZhG0387:       YI(I,JG)=Y(IP1,JG)-Y(IM1,JG)
ZhG0388:       XJ(I,JG)=3.0*X(I,JG)-4.0*X(I,J1)+X(I,J2)
ZhG0389:       YJ(I,JG)=3.0*Y(I,JG)-4.0*Y(I,J1)+Y(I,J2)
ZhG0390:       DO 200 J=2,J1
ZhG0391:       JP1=J+1
ZhG0392:       JM1=J-1
ZhG0393:       XI(I,J)=X(IP1,J)-X(IM1,J)
ZhG0394:       YI(I,J)=Y(IP1,J)-Y(IM1,J)
ZhG0395:       XJ(I,J)=X(I,JP1)-X(I,JM1)
ZhG0396: 200   YJ(I,J)=Y(I,JP1)-Y(I,JM1)
ZhG0397:       DO 220 J=2,J1
ZhG0398:       JP1=J+1
ZhG0399:       JM1=J-1
ZhG0400:       XJ(1,J)=X(1,JP1)-X(1,JM1)
ZhG0401:       YJ(1,J)=Y(1,JP1)-Y(1,JM1)
ZhG0402:       XI(1,J)=-3.0*X(1,J)+4.0*X(2,J)-X(3,J)
ZhG0403:       YI(1,J)=-3.0*Y(1,J)+4.0*Y(2,J)-Y(3,J)
ZhG0404:       XJ(IG,J)=X(IG,JP1)-X(IG,JM1)
ZhG0405:       YJ(IG,J)=Y(IG,JP1)-Y(IG,JM1)
ZhG0406:       XI(IG,J)=3.0*X(IG,J)-4.0*X(I1,J)+X(I2,J)
ZhG0407: 220   YI(IG,J)=3.0*Y(IG,J)-4.0*Y(I1,J)+Y(I2,J)
ZhG0408:       XI(1,1)=-3.0*X(1,1)+4.0*X(2,1)-X(3,1)
ZhG0409:       YI(1,1)=-3.0*Y(1,1)+4.0*Y(2,1)-Y(3,1)
ZhG0410:       XJ(1,1)=-3.0*X(1,1)+4.0*X(1,2)-X(1,3)
ZhG0411:       YJ(1,1)=-3.0*Y(1,1)+4.0*Y(1,2)-Y(1,3)
ZhG0412:       XI(1,JG)=-3.0*X(1,JG)+4.0*X(2,JG)-X(3,JG)
ZhG0413:       YI(1,JG)=-3.0*Y(1,JG)+4.0*Y(2,JG)-Y(3,JG)
ZhG0414:       XJ(1,JG)=3.0*X(1,JG)-4.0*X(1,J1)+X(1,J2)
ZhG0415:       YJ(1,JG)=3.0*Y(1,JG)-4.0*Y(1,J1)+Y(1,J2)
```

```
ZhG0416:       XI(IG,1)=3.0*X(IG,1)-4.0*X(I1,1)+X(I2,1)
ZhG0417:       YI(IG,1)=3.0*Y(IG,1)-4.0*Y(I1,1)+Y(I2,1)
ZhG0418:       XJ(IG,1)=-3.0*X(IG,1)+4.0*X(IG,2)-X(IG,3)
ZhG0419:       YJ(IG,1)=-3.0*Y(IG,1)+4.0*Y(IG,2)-Y(IG,3)
ZhG0420:       XI(IG,JG)=3.0*X(IG,JG)-4.0*X(I1,JG)+X(I2,JG)
ZhG0421:       YI(IG,JG)=3.0*Y(IG,JG)-4.0*Y(I1,JG)+Y(I2,JG)
ZhG0422:       XJ(IG,JG)=3.0*X(IG,JG)-4.0*X(IG,J1)+X(IG,J2)
ZhG0423:       YJ(IG,JG)=3.0*Y(IG,JG)-4.0*Y(IG,J1)+Y(IG,J2)
ZhG0424:       DO 230 I=1,IG
ZhG0425:       DO 230 J=1,JG
ZhG0426:       A(I,J)=XJ(I,J)**2.0+YJ(I,J)**2.0
ZhG0427:       B(I,J)=XI(I,J)*XJ(I,J)+YI(I,J)*YJ(I,J)
ZhG0428:       G(I,J)=XI(I,J)**2.0+YI(I,J)**2.0
ZhG0429: 230   BJ(I,J)=XI(I,J)*YJ(I,J)-XJ(I,J)*YI(I,J)
ZhG0430:       RETURN
ZhG0431:       END
ZhG0432:
ZhG0433:       SUBROUTINE CONSTANT(RE,DT,PA,WE)
ZhG0434:       IMPLICIT REAL*8(A-H,O-Z)
ZhG0435:       PARAMETER(M=2,LX=1001,LY=11,IG=2*LX-1,JG=2*LY-1)
ZhG0436:       PARAMETER(LX1=LX-1,LY1=LY-1,LX2=LX-2,LY2=LY-2)
ZhG0437:       PARAMETER(IG2=IG-2,JG2=JG-2,JG4=JG-4)
ZhG0438:       COMMON/XY/X(IG,JG),Y(IG,JG)
ZhG0439:       COMMON/PSFE/PS(IG,JG),FE(IG,JG)
ZhG0440:       COMMON/UVP/U(LX,LY),V(LX,LY),P(LX,LY)
ZhG0441:       COMMON/FORCE/FX(LX,LY),FY(LX,LY)
ZhG0442:       COMMON/DXY/XI(IG,JG),XJ(IG,JG),YI(IG,JG),YJ(IG,JG)
ZhG0443:       COMMON/DXYT/XT(IG,JG),YT(IG,JG)
ZhG0444:       COMMON/ABG/BJ(IG,JG),A(IG,JG),B(IG,JG),G(IG,JG)
ZhG0445:       COMMON/UVR/UR(LX,LY),VR(LX,LY)
ZhG0446:       COMMON/P_R/PR(LX,LY)
ZhG0447:       COMMON/UV_B/ULFT(LY),URIT(LY),UBTM(LX)
ZhG0448:       1       ,VLFT(LY),VRIT(LY),VBTM(LX)
ZhG0449:       COMMON/BD/XI3(LX,M),XI4(LX,M),YI3(LX,M),YI4(LX,M)
ZhG0450:       1       ,XJ3(M,LY),XJ4(M,LY),YJ3(M,LY),YJ4(M,LY)
ZhG0451:       COMMON/DPHJ/XIHJ(LX,LY),XJHJ(LX,LY),YIHJ(LX,LY),YJHJ(LX,LY)
ZhG0452:       COMMON/DP_C/XI2DJ(IG,JG),XJ2DJ(IG,JG),YI2DJ(IG,JG)
ZhG0453:       1       ,YJ2DJ(IG,JG),XIXJDJ(IG,JG),XIYIDJ(IG,JG)
ZhG0454:       2       ,XIYJDJ(IG,JG),XJYIDJ(IG,JG),XJYJDJ(IG,JG)
ZhG0455:       3       ,YIYJDJ(IG,JG),PLUS(IG,JG)
ZhG0456:       4       ,P1(IG,JG),P2(IG,JG),P3(IG,JG),P4(IG,JG)
ZhG0457:       5       ,P5(IG,JG),P6(IG,JG),P7(IG,JG),P8(IG,JG)
ZhG0458:       COMMON/UV_C/CUX1(LX,LY),CUY1(LX,LY),CVX1(LX,LY),CVY1(LX,LY)
ZhG0459:       1       ,CUX2(LX,LY),CUY2(LX,LY),CVX2(LX,LY),CVY2(LX,LY)
ZhG0460:       2       ,CU1(LX,LY),CV1(LX,LY),CU2(LX,LY),CV2(LX,LY)
ZhG0461:       3       ,CXX(LX,LY),CXY(LX,LY),CYY(LX,LY)
ZhG0462:       COMMON/ABGDJ/ADJ(IG,JG),BDJ(IG,JG),GDJ(IG,JG)
ZhG0463:       COMMON/FREE_UVP/FREEX(M,M,LX),FREEY(M,M,LX,3)
ZhG0464:       1       ,FP1(LX),FP2(LX,3),FP3(LX,3)
ZhG0465:       COMMON/R_FREE/R_VEL(M,LX),R_PRE(LX)
ZhG0466:       COMMON/F_M/FM(LX,LY),FM_LR(2,LY),FM_BT(LX)
ZhG0467:       DIMENSION Q1(LX,LY),Q2(LX,LY),Q3(LX,LY),DD(LX,LY)
ZhG0468:       1       ,CUR(LX),W(LX,LY)
```

```
ZhG0469:        CALL UNIX
ZhG0470:        DO 10 II=1,IG
ZhG0471:        DO 10 JJ=1,JG
ZhG0472:        BB=1.0/BJ(II,JJ)
ZhG0473:        XI2DJ(II,JJ)=XI(II,JJ)**2.0*BB
ZhG0474:        XJ2DJ(II,JJ)=XJ(II,JJ)**2.0*BB
ZhG0475:        YI2DJ(II,JJ)=YI(II,JJ)**2.0*BB
ZhG0476:        YJ2DJ(II,JJ)=YJ(II,JJ)**2.0*BB
ZhG0477:        XIXJDJ(II,JJ)=XI(II,JJ)*XJ(II,JJ)*BB
ZhG0478:        XIYIDJ(II,JJ)=XI(II,JJ)*YI(II,JJ)*BB
ZhG0479:        XIYJDJ(II,JJ)=XI(II,JJ)*YJ(II,JJ)*BB
ZhG0480:        XJYIDJ(II,JJ)=XJ(II,JJ)*YI(II,JJ)*BB
ZhG0481:        XJYJDJ(II,JJ)=XJ(II,JJ)*YJ(II,JJ)*BB
ZhG0482:        YIYJDJ(II,JJ)=YI(II,JJ)*YJ(II,JJ)*BB
ZhG0483:        PLUS(II,JJ)=XIYJDJ(II,JJ)+XJYIDJ(II,JJ)
ZhG0484:        P1(II,JJ)=XJYJDJ(II,JJ)*YT(II,JJ)
ZhG0485:        1          -YJ2DJ(II,JJ)*XT(II,JJ)
ZhG0486:        P2(II,JJ)=YIYJDJ(II,JJ)*XT(II,JJ)
ZhG0487:        1          -XIYJDJ(II,JJ)*YT(II,JJ)
ZhG0488:        P3(II,JJ)=XJ2DJ(II,JJ)*YT(II,JJ)
ZhG0489:        1          -XJYJDJ(II,JJ)*XT(II,JJ)
ZhG0490:        P4(II,JJ)=XJYIDJ(II,JJ)*XT(II,JJ)
ZhG0491:        1          -XIXJDJ(II,JJ)*YT(II,JJ)
ZhG0492:        P5(II,JJ)=XIXJDJ(II,JJ)*YT(II,JJ)
ZhG0493:        1          -XIYJDJ(II,JJ)*XT(II,JJ)
ZhG0494:        P6(II,JJ)=XIYIDJ(II,JJ)*XT(II,JJ)
ZhG0495:        1          -XI2DJ(II,JJ)*YT(II,JJ)
ZhG0496:        P7(II,JJ)=XJYIDJ(II,JJ)*YT(II,JJ)
ZhG0497:        1          -YIYJDJ(II,JJ)*XT(II,JJ)
ZhG0498:        P8(II,JJ)=YI2DJ(II,JJ)*XT(II,JJ)
ZhG0499:        1          -XIYIDJ(II,JJ)*YT(II,JJ)
ZhG0500:        ADJ(II,JJ)=A(II,JJ)*BB
ZhG0501:        GDJ(II,JJ)=G(II,JJ)*BB
ZhG0502: 10     BDJ(II,JJ)=B(II,JJ)*BB
ZhG0503:        L=2*LX1
ZhG0504:        DO 13 J=2,LY1
ZhG0505:        JJ=2*J-1
ZhG0506:        FM_LR(1,J)=ADJ(2,JJ)*GDJ(2,JJ)-BDJ(2,JJ)**2.0
ZhG0507: 13     FM_LR(2,J)=ADJ(L,JJ)*GDJ(L,JJ)-BDJ(L,JJ)**2.0
ZhG0508:        DO 14 I=2,LX1
ZhG0509:        II=2*I-1
ZhG0510: 14     FM_BT(I)=ADJ(II,2)*GDJ(II,2)-BDJ(II,2)**2.0
ZhG0511:        DO 15 I=2,LX1
ZhG0512:        II=2*I-1
ZhG0513:        IE=II+1
ZhG0514:        IW=II-1
ZhG0515:        DO 15 J=2,LY1
ZhG0516:        JJ=2*J-1
ZhG0517: 15     FM(I,J)=ADJ(IE,JJ)+ADJ(IW,JJ)+GDJ(II,JJ+1)+GDJ(II,JJ-1)
ZhG0518:        DO 20 J=1,LY
ZhG0519:        JJ=2*J-1
ZhG0520:        XJ3(1,J)=1.5*XJ(1,JJ)/BJ(1,JJ)
ZhG0521:        YJ3(1,J)=1.5*YJ(1,JJ)/BJ(1,JJ)
```

```
ZhG0522:        XJ3(2,J)=1.5*XJ(IG,JJ)/BJ(IG,JJ)
ZhG0523:        YJ3(2,J)=1.5*YJ(IG,JJ)/BJ(IG,JJ)
ZhG0524:        XJ4(1,J)=2.0*XJ(3,JJ)/BJ(3,JJ)
ZhG0525:        YJ4(1,J)=2.0*YJ(3,JJ)/BJ(3,JJ)
ZhG0526:        XJ4(2,J)=2.0*XJ(IG2,JJ)/BJ(IG2,JJ)
ZhG0527: 20     YJ4(2,J)=2.0*YJ(IG2,JJ)/BJ(IG2,JJ)
ZhG0528:        DO 40 I=1,LX
ZhG0529:        II=2*I-1
ZhG0530:        XI3(I,1)=1.5*XI(II,1)/BJ(II,1)
ZhG0531:        YI3(I,1)=1.5*YI(II,1)/BJ(II,1)
ZhG0532:        XI3(I,2)=1.5*XI(II,JG)/BJ(II,JG)
ZhG0533:        YI3(I,2)=1.5*YI(II,JG)/BJ(II,JG)
ZhG0534:        XI4(I,1)=2.0*XI(II,3)/BJ(II,3)
ZhG0535:        YI4(I,1)=2.0*YI(II,3)/BJ(II,3)
ZhG0536:        XI4(I,2)=2.0*XI(II,JG2)/BJ(II,JG2)
ZhG0537:        YI4(I,2)=2.0*YI(II,JG2)/BJ(II,JG2)
ZhG0538:        DO 40 J=1,LY
ZhG0539:        JJ=2*J-1
ZhG0540:        H_J=0.5/BJ(II,JJ)
ZhG0541:        XIHJ(I,J)=XI(II,JJ)*H_J
ZhG0542:        XJHJ(I,J)=XJ(II,JJ)*H_J
ZhG0543:        YIHJ(I,J)=YI(II,JJ)*H_J
ZhG0544:        YJHJ(I,J)=YJ(II,JJ)*H_J
ZhG0545:        Q1(I,J)=U(I,J)**2.0+P(I,J)
ZhG0546:        Q2(I,J)=U(I,J)*V(I,J)
ZhG0547: 40     Q3(I,J)=V(I,J)**2.0+P(I,J)
ZhG0548:        DO 50 I=2,LX1
ZhG0549:        IP1=I+1
ZhG0550:        IM1=I-1
ZhG0551:        W(I,1)=(-XI3(I,1)*U(I,1)+XI4(I,1)*U(I,2)-XIHJ(I,3)*U(I,3)
ZhG0552:        2          -YI3(I,1)*V(I,1)+YI4(I,1)*V(I,2)-YIHJ(I,3)*V(I,3)
ZhG0553:        4          -XJHJ(IP1,1)*U(IP1,1)+XJHJ(IM1,1)*U(IM1,1)
ZhG0554:        5          -YJHJ(IP1,1)*V(IP1,1)+YJHJ(IM1,1)*V(IM1,1))
ZhG0555:        W(I,LY)=
ZhG0556:        1 (XI3(I,2)*U(I,LY)-XI4(I,2)*U(I,LY1)+XIHJ(I,LY2)*U(I,LY2)
ZhG0557:        1 +YI3(I,2)*V(I,LY)-YI4(I,2)*V(I,LY1)+YIHJ(I,LY2)*V(I,LY2)
ZhG0558:        4          -XJHJ(IP1,LY)*U(IP1,LY)+XJHJ(IM1,LY)*U(IM1,LY)
ZhG0559:        5          -YJHJ(IP1,LY)*V(IP1,LY)+YJHJ(IM1,LY)*V(IM1,LY))
ZhG0560:        DO 50 J=2,LY1
ZhG0561:        JP1=J+1
ZhG0562:        JM1=J-1
ZhG0563:        DD(I,J)=(YJHJ(IP1,J)*U(IP1,J)-YJHJ(IM1,J)*U(IM1,J)
ZhG0564:        1          -YIHJ(I,JP1)*U(I,JP1)+YIHJ(I,JM1)*U(I,JM1)
ZhG0565:        2          +XIHJ(I,JP1)*V(I,JP1)-XIHJ(I,JM1)*V(I,JM1)
ZhG0566:        3          -XJHJ(IP1,J)*V(IP1,J)+XJHJ(IM1,J)*V(IM1,J))
ZhG0567: 50     W(I,J)= (XIHJ(I,JP1)*U(I,JP1)-XIHJ(I,JM1)*U(I,JM1)
ZhG0568:        1          -XJHJ(IP1,J)*U(IP1,J)+XJHJ(IM1,J)*U(IM1,J)
ZhG0569:        2          -YJHJ(IP1,J)*V(IP1,J)+YJHJ(IM1,J)*V(IM1,J)
ZhG0570:        3          +YIHJ(I,JP1)*V(I,JP1)-YIHJ(I,JM1)*V(I,JM1))
ZhG0571:        DO 52 J=2,LY1
ZhG0572:        JP1=J+1
ZhG0573:        JM1=J-1
ZhG0574:        W(1,J)= (XIHJ(1,JP1)*U(1,JP1)-XIHJ(1,JM1)*U(1,JM1)
```

```
ZhG0575:       2         +YIHJ(1,JP1)*V(1,JP1)-YIHJ(1,JM1)*V(1,JM1)
ZhG0576:       3         +XJ3(1,J)*U(1,J)-XJ4(1,J)*U(2,J)+XJHJ(3,J)*U(3,J)
ZhG0577:       4         +YJ3(1,J)*V(1,J)-YJ4(1,J)*V(2,J)+YJHJ(3,J)*V(3,J))
ZhG0578: 52    W(LX,J)=(XIHJ(LX,JP1)*U(LX,JP1)-XIHJ(LX,JM1)*U(LX,JM1)
ZhG0579:       2         +YIHJ(LX,JP1)*V(LX,JP1)-YIHJ(LX,JM1)*V(LX,JM1)
ZhG0580:       3  -XJ3(2,J)*U(LX,J)+XJ4(2,J)*U(LX1,J)-XJHJ(LX2,J)*U(LX2,J)
ZhG0581:       4  -YJ3(2,J)*V(LX,J)+YJ4(2,J)*V(LX1,J)-YJHJ(LX2,J)*V(LX2,J))
ZhG0582:       W(1,1)=
ZhG0583:       1 (-XI3(1,1)*U(1,1)+XI4(1,1)*U(1,2)-XIHJ(1,3)*U(1,3)
ZhG0584:       2  -YI3(1,1)*V(1,1)+YI4(1,1)*V(1,2)-YIHJ(1,3)*V(1,3)
ZhG0585:       4  +XJ3(1,1)*U(1,1)-XJ4(1,1)*U(2,1)+XJHJ(3,1)*U(3,1)
ZhG0586:       5  +YJ3(1,1)*V(1,1)-YJ4(1,1)*V(2,1)+YJHJ(3,1)*V(3,1))
ZhG0587:       W(1,LY)=
ZhG0588:       1 (XI3(1,2)*U(1,LY)-XI4(1,2)*U(1,LY1)+XIHJ(1,LY2)*U(1,LY2)
ZhG0589:       2 +YI3(1,2)*V(1,LY)-YI4(1,2)*V(1,LY1)+YIHJ(1,LY2)*V(1,LY2)
ZhG0590:       4 +XJ3(1,LY)*U(1,LY)-XJ4(1,LY)*U(2,LY)+XJHJ(3,LY)*U(3,LY)
ZhG0591:       5 +YJ3(1,LY)*V(1,LY)-YJ4(1,LY)*V(2,LY)+YJHJ(3,LY)*V(3,LY))
ZhG0592:       W(LX,1)=
ZhG0593:       1 (-XI3(LX,1)*U(LX,1)+XI4(LX,1)*U(LX,2)-XIHJ(LX,3)*U(LX,3)
ZhG0594:       2  -YI3(LX,1)*V(LX,1)+YI4(LX,1)*V(LX,2)-YIHJ(LX,3)*V(LX,3)
ZhG0595:       4  -XJ3(2,1)*U(LX,1)+XJ4(2,1)*U(LX1,1)-XJHJ(LX2,1)*U(LX2,1)
ZhG0596:       5  -YJ3(2,1)*V(LX,1)+YJ4(2,1)*V(LX1,1)-YJHJ(LX2,1)*V(LX2,1))
ZhG0597:       W(LX,LY)=
ZhG0598:       1 (XI3(LX,2)*U(LX,LY)-XI4(LX,2)*U(LX,LY1)+XIHJ(LX,LY2)*U(LX,LY2)
ZhG0599:       3 +YI3(LX,2)*V(LX,LY)-YI4(LX,2)*V(LX,LY1)+YIHJ(LX,LY2)*V(LX,LY2)
ZhG0600:       4 -XJ3(2,LY)*U(LX,LY)+XJ4(2,LY)*U(LX1,LY)-XJHJ(LX2,LY)*U(LX2,LY)
ZhG0601:       5 -YJ3(2,LY)*V(LX,LY)+YJ4(2,LY)*V(LX1,LY)-YJHJ(LX2,LY)*V(LX2,LY))
ZhG0602: *     * LEFT (I=1) & RIGHT (I=LX1) *
ZhG0603: *     *  XI=X(IP1,J)-X(I,J)
ZhG0604: *     *  YJ=0.25*(Y(I,J+1)+Y(IP1,J+1)-Y(I,J-1)-Y(IP1,J-1))
ZhG0605:       DO 70 INDEX=1,2
ZhG0606:       IF(INDEX.EQ.1) I=1
ZhG0607:       IF(INDEX.EQ.2) I=LX1
ZhG0608:       IP1=I+1
ZhG0609:       II=2*I
ZhG0610:       IIP1=II+1
ZhG0611:       IIM1=II-1
ZhG0612:       DO 70 J=2,LY1
ZhG0613:       JJ=2*J-1
ZhG0614:       JP1=J+1
ZhG0615:       JM1=J-1
ZhG0616:       JJP2=JJ+2
ZhG0617:       JJM2=JJ-2
ZhG0618:       T1=FY(I,J)*XJ(II,JJ)-FX(I,J)*YJ(II,JJ)
ZhG0619:       T2=P1(IIP1,JJ)*U(IP1,J)-P1(IIM1,JJ)*U(I,J)
ZhG0620:       T3=P2(II,JJP2)*(U(IP1,JP1)+U(I,JP1))
ZhG0621:       1 -P2(II,JJM2)*(U(IP1,JM1)+U(I,JM1))
ZhG0622:       T4=P3(IIP1,JJ)*V(IP1,J)-P3(IIM1,JJ)*V(I,J)
ZhG0623:       T5=P4(II,JJP2)*(V(IP1,JP1)+V(I,JP1))
ZhG0624:       1 -P4(II,JJM2)*(V(IP1,JM1)+V(I,JM1))
ZhG0625:       T6=YJ2DJ(IIP1,JJ)*Q1(IP1,J)-YJ2DJ(IIM1,JJ)*Q1(I,J)
ZhG0626:       T7=YIYJDJ(II,JJP2)*(Q1(IP1,JP1)+Q1(I,JP1))
ZhG0627:       1 -YIYJDJ(II,JJM2)*(Q1(IP1,JM1)+Q1(I,JM1))
```

```
ZhG0628:       T8=2.0*(XJYJDJ(IIP1,JJ)*Q2(IP1,J)
ZhG0629:       1     -XJYJDJ(IIM1,JJ)*Q2(I,J))
ZhG0630:       T9=PLUS(II,JJP2)*(Q2(IP1,JP1)+Q2(I,JP1))
ZhG0631:       1 -PLUS(II,JJM2)*(Q2(IP1,JM1)+Q2(I,JM1))
ZhG0632:       T10=XJ2DJ(IIP1,JJ)*Q3(IP1,J)-XJ2DJ(IIM1,JJ)*Q3(I,J)
ZhG0633:       T11=XIXJDJ(II,JJP2)*(Q3(IP1,JP1)+Q3(I,JP1))
ZhG0634:       1 -XIXJDJ(II,JJM2)*(Q3(IP1,JM1)+Q3(I,JM1))
ZhG0635:       T12=(W(IP1,JP1)+W(I,JP1)-W(IP1,JM1)-W(I,JM1))/RE
ZhG0636:       EE=T1+T2-T4+T6-T8+T10+0.25*(T3-T5-T7+T9-T11-T12)
ZhG0637:       IF(INDEX.EQ.1) ULFT(J)=EE
ZhG0638:       IF(INDEX.EQ.2) URIT(J)=EE
ZhG0639:       T1=FY(I,J)*XI(II,JJ)-FX(I,J)*YI(II,JJ)
ZhG0640:       T2=P7(IIP1,JJ)*U(IP1,J)-P7(IIM1,JJ)*U(I,J)
ZhG0641:       T3=P8(II,JJP2)*(U(IP1,JP1)+U(I,JP1))
ZhG0642:       1 -P8(II,JJM2)*(U(IP1,JM1)+U(I,JM1))
ZhG0643:       T4=P5(IIP1,JJ)*V(IP1,J)-P5(IIM1,JJ)*V(I,J)
ZhG0644:       T5=P6(II,JJP2)*(V(IP1,JP1)+V(I,JP1))
ZhG0645:       1 -P6(II,JJM2)*(V(IP1,JM1)+V(I,JM1))
ZhG0646:       T6=YIYJDJ(IIP1,JJ)*Q1(IP1,J)-YIYJDJ(IIM1,JJ)*Q1(I,J)
ZhG0647:       T7=YI2DJ(II,JJP2)*(Q1(IP1,JP1)+Q1(I,JP1))
ZhG0648:       1 -YI2DJ(II,JJM2)*(Q1(IP1,JM1)+Q1(I,JM1))
ZhG0649:       T8=PLUS(IIP1,JJ)*Q2(IP1,J)-PLUS(IIM1,JJ)*Q2(I,J)
ZhG0650:       T9=2.0*(XIYIDJ(II,JJP2)*(Q2(IP1,JP1)+Q2(I,JP1))
ZhG0651:       1     -XIYIDJ(II,JJM2)*(Q2(IP1,JM1)+Q2(I,JM1)))
ZhG0652:       T10=XIXJDJ(IIP1,JJ)*Q3(IP1,J)-XIXJDJ(IIM1,JJ)*Q3(I,J)
ZhG0653:       T11=XI2DJ(II,JJP2)*(Q3(IP1,JP1)+Q3(I,JP1))
ZhG0654:       1 -XI2DJ(II,JJM2)*(Q3(IP1,JM1)+Q3(I,JM1))
ZhG0655:       T12=(W(IP1,J)-W(I,J))/RE
ZhG0656:       EE=T1+T2-T4+T6-T8+T10-T12+0.25*(T3-T5-T7+T9-T11)
ZhG0657:       IF(INDEX.EQ.1) VLFT(J)=EE
ZhG0658: 70    IF(INDEX.EQ.2) VRIT(J)=EE
ZhG0659: *     * BOTTOM (J=1) *
ZhG0660: *     *  XI=0.25*(X(I+1,J)+X(I+1,JP1)-X(I-1,J)-X(I-1,JP1))
ZhG0661: *     *  YJ=Y(I,JP1)-Y(I,J)
ZhG0662:       J=1
ZhG0663:       JP1=J+1
ZhG0664:       JJ=2*J
ZhG0665:       JJP1=JJ+1
ZhG0666:       JJM1=JJ-1
ZhG0667:       DO 80 I=2,LX1
ZhG0668:       II=2*I-1
ZhG0669:       IP1=I+1
ZhG0670:       IM1=I-1
ZhG0671:       IIP2=II+2
ZhG0672:       IIM2=II-2
ZhG0673:       T1=FY(I,J)*XJ(II,JJ)-FX(I,J)*YJ(II,JJ)
ZhG0674:       T2=P1(IIP2,JJ)*(U(IP1,JP1)+U(IP1,J))
ZhG0675:       1 -P1(IIM2,JJ)*(U(IM1,JP1)+U(IM1,J))
ZhG0676:       T3=P2(II,JJP1)*U(I,JP1)-P2(II,JJM1)*U(I,J)
ZhG0677:       T4=P3(IIP2,JJ)*(V(IP1,JP1)+V(IP1,J))
ZhG0678:       1 -P3(IIM2,JJ)*(V(IM1,JP1)+V(IM1,J))
ZhG0679:       T5=P4(II,JJP1)*V(I,JP1)-P4(II,JJM1)*V(I,J)
ZhG0680:       T6=YJ2DJ(IIP2,JJ)*(Q1(IP1,JP1)+Q1(IP1,J))
```

```
ZhG0681:        1 -YJ2DJ(IIM2,JJ)*(Q1(IM1,JP1)+Q1(IM1,J))
ZhG0682:        T7=YIYJDJ(II,JJP1)*Q1(I,JP1)-YIYJDJ(II,JJM1)*Q1(I,J)
ZhG0683:        T8=2.0*(XJYJDJ(IIP2,JJ)*(Q2(IP1,JP1)+Q2(IP1,J))
ZhG0684:        1     -XJYJDJ(IIM2,JJ)*(Q2(IM1,JP1)+Q2(IM1,J)))
ZhG0685:        T9=PLUS(II,JJP1)*Q2(I,JP1)-PLUS(II,JJM1)*Q2(I,J)
ZhG0686:        T10=XJ2DJ(IIP2,JJ)*(Q3(IP1,JP1)+Q3(IP1,J))
ZhG0687:        1  -XJ2DJ(IIM2,JJ)*(Q3(IM1,JP1)+Q3(IM1,J))
ZhG0688:        T11=XIXJDJ(II,JJP1)*Q3(I,JP1)-XIXJDJ(II,JJM1)*Q3(I,J)
ZhG0689:        T12=(W(I,JP1)-W(I,J))/RE
ZhG0690:        EE=T1+T3-T5-T7+T9-T11-T12+0.25*(T2-T4+T6-T8+T10)
ZhG0691:        UBTM(I)=EE
ZhG0692:        T1=FY(I,J)*XI(II,JJ)-FX(I,J)*YI(II,JJ)
ZhG0693:        T2=P7(IIP2,JJ)*(U(IP1,JP1)+U(IP1,J))
ZhG0694:        1 -P7(IIM2,JJ)*(U(IM1,JP1)+U(IM1,J))
ZhG0695:        T3=P8(II,JJP1)*U(I,JP1)-P8(II,JJM1)*U(I,J)
ZhG0696:        T4=P5(IIP2,JJ)*(V(IP1,JP1)+V(IP1,J))
ZhG0697:        1 -P5(IIM2,JJ)*(V(IM1,JP1)+V(IM1,J))
ZhG0698:        T5=P6(II,JJP1)*V(I,JP1)-P6(II,JJM1)*V(I,J)
ZhG0699:        T6=YIYJDJ(IIP2,JJ)*(Q1(IP1,JP1)+Q1(IP1,J))
ZhG0700:        1 -YIYJDJ(IIM2,JJ)*(Q1(IM1,JP1)+Q1(IM1,J))
ZhG0701:        T7=YI2DJ(II,JJP1)*Q1(I,JP1)-YI2DJ(II,JJM1)*Q1(I,J)
ZhG0702:        T8=PLUS(IIP2,JJ)*(Q2(IP1,JP1)+Q2(IP1,J))
ZhG0703:        1 -PLUS(IIM2,JJ)*(Q2(IM1,JP1)+Q2(IM1,J))
ZhG0704:        T9=2.0*(XIYIDJ(II,JJP1)*Q2(I,JP1)
ZhG0705:        1     -XIYIDJ(II,JJM1)*Q2(I,J))
ZhG0706:        T10=XIXJDJ(IIP2,JJ)*(Q3(IP1,JP1)+Q3(IP1,J))
ZhG0707:        1  -XIXJDJ(IIM2,JJ)*(Q3(IM1,JP1)+Q3(IM1,J))
ZhG0708:        T11=XI2DJ(II,JJP1)*Q3(I,JP1)-XI2DJ(II,JJM1)*Q3(I,J)
ZhG0709:        T12=(W(IP1,JP1)+W(IP1,J)-W(IM1,JP1)-W(IM1,J))/RE
ZhG0710:        EE=T1+T3-T5-T7+T9-T11+0.25*(T2-T4+T6-T8+T10-T12)
ZhG0711: 80     VBTM(I)=EE
ZhG0712:        DO 90 I=2,LX1
ZhG0713:        IP1=I+1
ZhG0714:        IM1=I-1
ZhG0715:        II=2*I-1
ZhG0716:        IE=II+1
ZhG0717:        IW=II-1
ZhG0718:        IIP2=II+2
ZhG0719:        IIM2=II-2
ZhG0720:        DO 90 J=2,LY1
ZhG0721:        JP1=J+1
ZhG0722:        JM1=J-1
ZhG0723:        JJ=2*J-1
ZhG0724:        JN=JJ+1
ZhG0725:        JS=JJ-1
ZhG0726:        JJP2=JJ+2
ZhG0727:        JJM2=JJ-2
ZhG0728:        REJJ=RE*BJ(II,JJ)**2.0
ZhG0729:        CXX(I,J)=A(II,JJ)/REJJ
ZhG0730:        CXY(I,J)=0.5*B(II,JJ)/REJJ
ZhG0731:        CYY(I,J)=G(II,JJ)/REJJ
ZhG0732:        UX=U(IP1,J)-U(IM1,J)
ZhG0733:        UY=U(I,JP1)-U(I,JM1)
```

```
ZhG0734:      VX=V(IP1,J)-V(IM1,J)
ZhG0735:      VY=V(I,JP1)-V(I,JM1)
ZhG0736:      C1=XIHJ(I,J)
ZhG0737:      C2=XJHJ(I,J)
ZhG0738:      C3=YIHJ(I,J)
ZhG0739:      C4=YJHJ(I,J)
ZhG0740:      XT_U=XT(II,JJ)-U(I,J)
ZhG0741:      XT_2U=XT_U-U(I,J)
ZhG0742:      YT_V=YT(II,JJ)-V(I,J)
ZhG0743:      YT_2V=YT_V-V(I,J)
ZhG0744:      CUX1(I,J)=XT_2U*C4-YT_V*C2+0.5*CXX(I,J)*FE(II,JJ)
ZhG0745:      CUY1(I,J)=YT_V*C1-XT_2U*C3+0.5*CYY(I,J)*PS(II,JJ)
ZhG0746:      CVX1(I,J)=U(I,J)*C2
ZhG0747:      CVY1(I,J)=-U(I,J)*C1
ZhG0748:      CU1(I,J)=-(2.0*(UX*C4-UY*C3)+VY*C1-VX*C2)
ZhG0749:      CV1(I,J)=-(UY*C1-UX*C2)
ZhG0750:      CUX2(I,J)=-V(I,J)*C4
ZhG0751:      CUY2(I,J)=V(I,J)*C3
ZhG0752:      CVX2(I,J)=XT_U*C4-YT_2V*C2+0.5*CXX(I,J)*FE(II,JJ)
ZhG0753:      CVY2(I,J)=YT_2V*C1-XT_U*C3+0.5*CYY(I,J)*PS(II,JJ)
ZhG0754:      CU2(I,J)=-(VX*C4-VY*C3)
ZhG0755:      CV2(I,J)=-(2.0*(VY*C1-VX*C2)+UX*C4-UY*C3)
ZhG0756:      A5=2.0*U(I,J)
ZhG0757:      B5=2.0*V(I,J)
ZhG0758:      UII=U(IP1,J)+U(IM1,J)-A5
ZhG0759:      UJJ=U(I,JP1)+U(I,JM1)-A5
ZhG0760:      VII=V(IP1,J)+V(IM1,J)-B5
ZhG0761:      VJJ=V(I,JP1)+V(I,JM1)-B5
ZhG0762:      UIJ=U(IP1,JP1)+U(IM1,JM1)-U(IP1,JM1)-U(IM1,JP1)
ZhG0763:      VIJ=V(IP1,JP1)+V(IM1,JM1)-V(IP1,JM1)-V(IM1,JP1)
ZhG0764:      U2I=Q1(IP1,J)-Q1(IM1,J)
ZhG0765:      U2J=Q1(I,JP1)-Q1(I,JM1)
ZhG0766:      UVI=Q2(IP1,J)-Q2(IM1,J)
ZhG0767:      UVJ=Q2(I,JP1)-Q2(I,JM1)
ZhG0768:      V2I=Q3(IP1,J)-Q3(IM1,J)
ZhG0769:      V2J=Q3(I,JP1)-Q3(I,JM1)
ZhG0770:      TTT=CXX(I,J)*FE(II,JJ)+2.0*(C4*XT(II,JJ)-C2*YT(II,JJ))
ZhG0771:      PPP=CYY(I,J)*PS(II,JJ)+2.0*(C1*YT(II,JJ)-C3*XT(II,JJ))
ZhG0772:      UR(I,J)=2.0*(FX(I,J)+TTT*UX+PPP*UY
ZhG0773:     1         +CXX(I,J)*UII-CXY(I,J)*UIJ+CYY(I,J)*UJJ
ZhG0774:     2         +C3*U2J-C4*U2I-C1*UVJ+C2*UVI)
ZhG0775:      VR(I,J)=2.0*(FY(I,J)+TTT*VX+PPP*VY
ZhG0776:     1         +CXX(I,J)*VII-CXY(I,J)*VIJ+CYY(I,J)*VJJ
ZhG0777:     2         +C3*UVJ-C4*UVI-C1*V2J+C2*V2I)
ZhG0778:      EE=0.5*(YJ(IIP2,JJ)*FX(IP1,J)-YJ(IIM2,JJ)*FX(IM1,J)
ZhG0779:     1    -YI(II,JJP2)*FX(I,JP1)-YI(II,JJM2)*FX(I,JM1)
ZhG0780:     2    +XI(II,JJP2)*FY(I,JP1)-XI(II,JJM2)*FY(I,JM1)
ZhG0781:     3    -XJ(IIP2,JJ)*FY(IP1,J)-XJ(IIM2,JJ)*FY(IM1,J))
ZhG0782:      TX1=P1(IE,JJ)*(U(IP1,J)-U(I,J))
ZhG0783:     1 -P1(IW,JJ)*(U(I,J)-U(IM1,J))
ZhG0784:      TX2=P2(IE,JJ)*(U(IP1,JP1)-U(IP1,JM1)+UY)
ZhG0785:     1 -P2(IW,JJ)*(U(IM1,JP1)-U(IM1,JM1)+UY)
ZhG0786:      TX3=P3(IE,JJ)*(V(IP1,J)-V(I,J))
```

```
ZhG0787:        1 -P3(IW,JJ)*(V(I,J)-V(IM1,J))
ZhG0788:        TX4=P4(IE,JJ)*(V(IP1,JP1)-V(IP1,JM1)+VY)
ZhG0789:        1 -P4(IW,JJ)*(V(IM1,JP1)-V(IM1,JM1)+VY)
ZhG0790:        TY1=P6(II,JN)*(V(I,JP1)-V(I,J))
ZhG0791:        1 -P6(II,JS)*(V(I,J)-V(I,JM1))
ZhG0792:        TY2=P5(II,JN)*(V(IP1,JP1)-V(IM1,JP1)+VX)
ZhG0793:        1 -P5(II,JS)*(V(IP1,JM1)-V(IM1,JM1)+VX)
ZhG0794:        TY3=P8(II,JN)*(U(I,JP1)-U(I,J))
ZhG0795:        1 -P8(II,JS)*(U(I,J)-U(I,JM1))
ZhG0796:        TY4=P7(II,JN)*(U(IP1,JP1)-U(IM1,JP1)+UX)
ZhG0797:        1 -P7(II,JS)*(U(IP1,JM1)-U(IM1,JM1)+UX)
ZhG0798:        X1=YJ2DJ(IE,JJ)*(Q1(IP1,J)-Q1(I,J))
ZhG0799:        1 -YJ2DJ(IW,JJ)*(Q1(I,J)-Q1(IM1,J))
ZhG0800:        X2=YIYJDJ(IE,JJ)*(Q1(IP1,JP1)-Q1(IP1,JM1)+U2J)
ZhG0801:        2 -YIYJDJ(IW,JJ)*(Q1(IM1,JP1)-Q1(IM1,JM1)+U2J)
ZhG0802:        X3=2.0*(XJYJDJ(IE,JJ)*(Q2(IP1,J)-Q2(I,J))
ZhG0803:        1    -XJYJDJ(IW,JJ)*(Q2(I,J)-Q2(IM1,J)))
ZhG0804:        X4=PLUS(IE,JJ)*(Q2(IP1,JP1)-Q2(IP1,JM1)+UVJ)
ZhG0805:        2 -PLUS(IW,JJ)*(Q2(IM1,JP1)-Q2(IM1,JM1)+UVJ)
ZhG0806:        X5=XJ2DJ(IE,JJ)*(Q3(IP1,J)-Q3(I,J))
ZhG0807:        1 -XJ2DJ(IW,JJ)*(Q3(I,J)-Q3(IM1,J))
ZhG0808:        X6=XIXJDJ(IE,JJ)*(Q3(IP1,JP1)-Q3(IP1,JM1)+V2J)
ZhG0809:        2 -XIXJDJ(IW,JJ)*(Q3(IM1,JP1)-Q3(IM1,JM1)+V2J)
ZhG0810:        Y1=YI2DJ(II,JN)*(Q1(I,JP1)-Q1(I,J))
ZhG0811:        1 -YI2DJ(II,JS)*(Q1(I,J)-Q1(I,JM1))
ZhG0812:        Y2=YIYJDJ(II,JN)*(Q1(IP1,JP1)-Q1(IM1,JP1)+U2I)
ZhG0813:        2 -YIYJDJ(II,JS)*(Q1(IP1,JM1)-Q1(IM1,JM1)+U2I)
ZhG0814:        Y3=2.0*(XIYIDJ(II,JN)*(Q2(I,JP1)-Q2(I,J))
ZhG0815:        2    -XIYIDJ(II,JS)*(Q2(I,J)-Q2(I,JM1)))
ZhG0816:        Y4=PLUS(II,JN)*(Q2(IP1,JP1)-Q2(IM1,JP1)+UVI)
ZhG0817:        3 -PLUS(II,JS)*(Q2(IP1,JM1)-Q2(IM1,JM1)+UVI)
ZhG0818:        Y5=XI2DJ(II,JN)*(Q3(I,JP1)-Q3(I,J))
ZhG0819:        1 -XI2DJ(II,JS)*(Q3(I,J)-Q3(I,JM1))
ZhG0820:        Y6=XIXJDJ(II,JN)*(Q3(IP1,JP1)-Q3(IM1,JP1)+V2I)
ZhG0821:        2 -XIXJDJ(II,JS)*(Q3(IP1,JM1)-Q3(IM1,JM1)+V2I)
ZhG0822:        RR=EE+DD(I,J)/DT*BJ(II,JJ)
ZhG0823:        2         -(TX1-TX3+0.25*(TX2-TX4))
ZhG0824:        3         -(TY1-TY3+0.25*(TY2-TY4))
ZhG0825:        4         -(X1-X3+X5-0.25*(X2-X4+X6))
ZhG0826:        5         -(Y1-Y3+Y5-0.25*(Y2-Y4+Y6))
ZhG0827: 90     PR(I,J)=RR
ZhG0828:        DO 140 I=1,LX
ZhG0829:        II=2*I-1
ZhG0830:        T3=ADJ(II,JG)*(XJ(II,JG)+BDJ(II,JG)*YJ(II,JG))
ZhG0831:        T4=ADJ(II,JG)*(YJ(II,JG)-BDJ(II,JG)*XJ(II,JG))
ZhG0832:        A2=ADJ(II,JG)**2.0
ZhG0833:        FREEX(1,1,I)=-(T3*YJ(II,JG)+A2*XI(II,JG)*XJ(II,JG))
ZhG0834:        FREEX(1,2,I)=T3*XJ(II,JG)-A2*XI(II,JG)*YJ(II,JG)
ZhG0835:        FREEX(2,1,I)=-(T4*YJ(II,JG)+A2*XJ(II,JG)*YI(II,JG))
ZhG0836:        FREEX(2,2,I)=T4*XJ(II,JG)-A2*YI(II,JG)*YJ(II,JG)
ZhG0837:        FREEY(1,1,I,1)=T3*YI(II,JG)-T4*XI(II,JG)
ZhG0838:        FREEY(2,2,I,1)=FREEY(1,1,I,1)
ZhG0839:        FREEY(1,2,I,1)=0.0
```

```
ZhG0840:       FREEY(2,1,I,1)=0.0
ZhG0841:       T3=ADJ(II,JG2)*(XJ(II,JG2)+BDJ(II,JG2)*YJ(II,JG2))
ZhG0842:       T4=ADJ(II,JG2)*(YJ(II,JG2)-BDJ(II,JG2)*XJ(II,JG2))
ZhG0843:       FREEY(1,1,I,2)=T3*YI(II,JG2)-T4*XI(II,JG2)
ZhG0844:       FREEY(2,2,I,2)=FREEY(1,1,I,2)
ZhG0845:       FREEY(1,2,I,2)=0.0
ZhG0846:       FREEY(2,1,I,2)=0.0
ZhG0847:       T3=ADJ(II,JG4)*(XJ(II,JG4)+BDJ(II,JG4)*YJ(II,JG4))
ZhG0848:       T4=ADJ(II,JG4)*(YJ(II,JG4)-BDJ(II,JG4)*XJ(II,JG4))
ZhG0849:       FREEY(1,1,I,3)=T3*YI(II,JG4)-T4*XI(II,JG4)
ZhG0850:       FREEY(2,2,I,3)=FREEY(1,1,I,3)
ZhG0851:       FREEY(1,2,I,3)=0.0
ZhG0852:       FREEY(2,1,I,3)=0.0
ZhG0853:       COM=RE*YJ(II,JG)
ZhG0854:       FP1(I)=2.0*ADJ(II,JG)/COM
ZhG0855:       FP2(I,1)=2.0*(BDJ(II,JG)/COM-XJ(II,JG)/(RE*A(II,JG)))
ZhG0856:       FP3(I,1)=2.0*XJ(II,JG)**2.0/A(II,JG)/COM
ZhG0857:       COM=RE*YJ(II,JG2)
ZhG0858:       FP2(I,2)=2.0*(BDJ(II,JG2)/COM-XJ(II,JG2)/(RE*A(II,JG2)))
ZhG0859:       FP3(I,2)=2.0*XJ(II,JG2)**2.0/A(II,JG2)/COM
ZhG0860:       COM=RE*YJ(II,JG4)
ZhG0861:       FP2(I,3)=2.0*(BDJ(II,JG4)/COM-XJ(II,JG4)/(RE*A(II,JG4)))
ZhG0862: 140   FP3(I,3)=2.0*XJ(II,JG4)**2.0/A(II,JG4)/COM
ZhG0863:       DO 160 I=2,LX1
ZhG0864:       IP1=I+1
ZhG0865:       IM1=I-1
ZhG0866:       II=2*I-1
ZhG0867:       IIP2=II+2
ZhG0868:       IIM2=II-2
ZhG0869:       XII=2.0*(X(IIP2,JG)+X(IIM2,JG)-2.0*X(II,JG))
ZhG0870:       YII=2.0*(Y(IIP2,JG)+Y(IIM2,JG)-2.0*Y(II,JG))
ZhG0871:       CUR(I)=(XI(II,JG)*YII-YI(II,JG)*XII)/G(II,JG)**1.5
ZhG0872:       UX1=FREEX(1,1,IP1)*U(IP1,LY)-FREEX(1,1,IM1)*U(IM1,LY)
ZhG0873:       VX1=FREEX(1,2,IP1)*V(IP1,LY)-FREEX(1,2,IM1)*V(IM1,LY)
ZhG0874:       UX2=FREEX(2,1,IP1)*U(IP1,LY)-FREEX(2,1,IM1)*U(IM1,LY)
ZhG0875:       VX2=FREEX(2,2,IP1)*V(IP1,LY)-FREEX(2,2,IM1)*V(IM1,LY)
ZhG0876:       UX3=FP1(IP1)*U(IP1,LY)-FP1(IM1)*U(IM1,LY)
ZhG0877:       UY1=3.0*FREEY(1,1,I,1)*U(I,LY)-4.0*FREEY(1,1,I,2)*U(I,LY1)
ZhG0878:      1        +FREEY(1,1,I,3)*U(I,LY2)
ZhG0879:       VY1=3.0*FREEY(1,2,I,1)*V(I,LY)-4.0*FREEY(1,2,I,2)*V(I,LY1)
ZhG0880:      1        +FREEY(1,2,I,3)*V(I,LY2)
ZhG0881:       UY2=3.0*FREEY(2,1,I,1)*U(I,LY)-4.0*FREEY(2,1,I,2)*U(I,LY1)
ZhG0882:      1        +FREEY(2,1,I,3)*U(I,LY2)
ZhG0883:       VY2=3.0*FREEY(2,2,I,1)*V(I,LY)-4.0*FREEY(2,2,I,2)*V(I,LY1)
ZhG0884:      1        +FREEY(2,2,I,3)*V(I,LY2)
ZhG0885:       UY3=3.0*FP2(I,1)*U(I,LY)-4.0*FP2(I,2)*U(I,LY1)
ZhG0886:      1        +FP2(I,3)*U(I,LY2)
ZhG0887:       VY3=3.0*FP3(I,1)*V(I,LY)-4.0*FP3(I,2)*V(I,LY1)
ZhG0888:      1        +FP3(I,3)*V(I,LY2)
ZhG0889:       R_VEL(1,I)=-(UX1+VX1+UY1+VY1)
ZhG0890:       R_VEL(2,I)=-(UX2+VX2+UY2+VY2)
ZhG0891: 160   R_PRE(I)=PA-WE*CUR(I)+0.5*(UX3-UY3-VY3)-P(I,LY)
ZhG0892:       RETURN
```

```
ZhG0893:        END
ZhG0894:
ZhG0895:        SUBROUTINE COEF_MATRIX(DT,DTOI)
ZhG0896:        IMPLICIT REAL*8(A-H,O-Z)
ZhG0897:        PARAMETER(M=2,LX=1001,LY=11,IG=2*LX-1,JG=2*LY-1)
ZhG0898:        PARAMETER(LX1=LX-1,LY1=LY-1,LX2=LX-2,LY2=LY-2)
ZhG0899:        COMMON/UV_C/CUX1(LX,LY),CUY1(LX,LY),CVX1(LX,LY),CVY1(LX,LY)
ZhG0900:        1       ,CUX2(LX,LY),CUY2(LX,LY),CVX2(LX,LY),CVY2(LX,LY)
ZhG0901:        2       ,CU1(LX,LY),CV1(LX,LY),CU2(LX,LY),CV2(LX,LY)
ZhG0902:        3       ,CXX(LX,LY),CXY(LX,LY),CYY(LX,LY)
ZhG0903:        COMMON/FREE_UVP/FREEX(M,M,LX),FREEY(M,M,LX,3)
ZhG0904:        1       ,FP1(LX),FP2(LX,3),FP3(LX,3)
ZhG0905:        COMMON/BLK3/AMX(M,M,LX,2:LY1),BMX(M,M,LX,2:LY1)
ZhG0906:        1       ,CMX(M,M,LX,2:LY1),AMY(M,M,LY,2:LX1)
ZhG0907:        2       ,BMY(M,M,LY,2:LX1),CMY(M,M,LY,2:LX1)
ZhG0908:        COMMON/BLK3_FREE/AFREE(M,M,LX),BFREE(M,M,LX),CFREE(M,M,LX)
ZhG0909:        DIMENSION WK1(M,M),WK2(M,M),WK3(M,M),WK4(M,M)
ZhG0910:        CALL UNIX
ZhG0911:        DTOI2=0.5*DTOI
ZhG0912:        DTDTOI2=0.5*DT*DTOI
ZhG0913:        DTDTOI4=0.25*DT*DTOI
ZhG0914:        DO 260 J=1,M
ZhG0915:        DO 260 I=1,M
ZhG0916:        DO 261 L=2,LY1
ZhG0917:        DO 261 K=1,LX,LX1
ZhG0918:        AMX(I,J,K,L)=0.0
ZhG0919:        BMX(I,J,K,L)=0.0
ZhG0920: 261    CMX(I,J,K,L)=0.0
ZhG0921:        DO 260 L=2,LX1
ZhG0922:        DO 260 K=1,LY,LY1
ZhG0923:        AMY(I,J,K,L)=0.0
ZhG0924:        BMY(I,J,K,L)=0.0
ZhG0925: 260    CMY(I,J,K,L)=0.0
ZhG0926:        DO 270 J=2,LY1
ZhG0927: *      * INNER POINTS WK1 -> T, WK2 -> A, WK3 -> P *
ZhG0928:        DO 271 I=2,LX1
ZhG0929:        WK1(1,1)=1.0+DTOI2-DTDTOI4*CU1(I,J)
ZhG0930:        WK1(1,2)=-DTDTOI4*CV1(I,J)
ZhG0931:        WK1(2,1)=-DTDTOI4*CU2(I,J)
ZhG0932:        WK1(2,2)=1.0+DTOI2-DTDTOI4*CV2(I,J)
ZhG0933:        WK2(1,1)=CUX1(I,J)
ZhG0934:        WK2(1,2)=CVX1(I,J)
ZhG0935:        WK2(2,1)=CUX2(I,J)
ZhG0936:        WK2(2,2)=CVX2(I,J)
ZhG0937:        WK3(1,1)=CXX(I,J)
ZhG0938:        WK3(1,2)=0.0
ZhG0939:        WK3(2,1)=0.0
ZhG0940:        WK3(2,2)=WK3(1,1)
ZhG0941:        DO 271 II=1,M
ZhG0942:        DO 271 JJ=1,M
ZhG0943:        AMX(II,JJ,I,J)=-DTDTOI4*(WK3(II,JJ)-WK2(II,JJ))
ZhG0944:        BMX(II,JJ,I,J)=WK1(II,JJ)+DTDTOI2*WK3(II,JJ)
ZhG0945: 271    CMX(II,JJ,I,J)=-DTDTOI4*(WK3(II,JJ)+WK2(II,JJ))
```

```
ZhG0946: *      * OLD BOUNDARY POINT *
ZhG0947:        DO 270 K=1,M
ZhG0948:        BMX(K,K,1,J)=1.0
ZhG0949: 270    BMX(K,K,LX,J)=1.0
ZhG0950:        DO 280 I=2,LX1
ZhG0951: *      * INNER POINTS WK1 -> 1/T, WK2 -> B, WK3 -> Q *
ZhG0952:        DO 281 J=2,LY1
ZhG0953:        WK1(1,1)=1.0+DTOI2-DTDTOI4*CU1(I,J)
ZhG0954:        WK1(1,2)=-DTDTOI4*CV1(I,J)
ZhG0955:        WK1(2,1)=-DTDTOI4*CU2(I,J)
ZhG0956:        WK1(2,2)=1.0+DTOI2-DTDTOI4*CV2(I,J)
ZhG0957:        CALL INVERS(WK1)
ZhG0958:        WK2(1,1)=CUY1(I,J)
ZhG0959:        WK2(1,2)=CVY1(I,J)
ZhG0960:        WK2(2,1)=CUY2(I,J)
ZhG0961:        WK2(2,2)=CVY2(I,J)
ZhG0962:        DO 282 II=1,M
ZhG0963:        DO 282 JJ=1,M
ZhG0964:        WK4(II,JJ)=0.0
ZhG0965:        DO 282 KK=1,M
ZhG0966: 282    WK4(II,JJ)=WK4(II,JJ)+WK1(II,KK)*WK2(KK,JJ)
ZhG0967:        DO 284 II=1,M
ZhG0968:        DO 284 JJ=1,M
ZhG0969: 284    WK2(II,JJ)=WK4(II,JJ)
ZhG0970:        WK3(1,1)=CYY(I,J)
ZhG0971:        WK3(1,2)=0.0
ZhG0972:        WK3(2,1)=0.0
ZhG0973:        WK3(2,2)=WK3(1,1)
ZhG0974:        DO 286 II=1,M
ZhG0975:        DO 286 JJ=1,M
ZhG0976:        WK4(II,JJ)=0.0
ZhG0977:        DO 286 KK=1,M
ZhG0978: 286    WK4(II,JJ)=WK4(II,JJ)+WK1(II,KK)*WK3(KK,JJ)
ZhG0979:        DO 288 II=1,M
ZhG0980:        DO 288 JJ=1,M
ZhG0981: 288    WK3(II,JJ)=WK4(II,JJ)
ZhG0982:        WK1(1,1)=1.0
ZhG0983:        WK1(1,2)=0.0
ZhG0984:        WK1(2,1)=0.0
ZhG0985:        WK1(2,2)=1.0
ZhG0986:        DO 281 II=1,M
ZhG0987:        DO 281 JJ=1,M
ZhG0988:        AMY(II,JJ,J,I)=-DTDTOI4*(WK3(II,JJ)-WK2(II,JJ))
ZhG0989:        BMY(II,JJ,J,I)=WK1(II,JJ)+DTDTOI2*WK3(II,JJ)
ZhG0990: 281    CMY(II,JJ,J,I)=-DTDTOI4*(WK3(II,JJ)+WK2(II,JJ))
ZhG0991: *      * OLD BOUNDARY POINT *
ZhG0992:        DO 280 K=1,M
ZhG0993:        BMY(K,K,1,I)=1.0
ZhG0994: 280    BMY(K,K,LY,I)=1.0
ZhG0995:        DO 300 J=1,M
ZhG0996:        DO 300 I=1,M
ZhG0997:        DO 310 K=1,LX,LX1
ZhG0998:        AFREE(I,J,K)=0.0
```

```
ZhG0999:        BFREE(I,J,K)=0.0
ZhG1000: 310    CFREE(I,J,K)=0.0
ZhG1001:        DO 300 K=2,LX1
ZhG1002:        AFREE(I,J,K)=-FREEX(I,J,K-1)
ZhG1003:        BFREE(I,J,K)=3.0*FREEY(I,J,K,1)
ZhG1004: 300    CFREE(I,J,K)=FREEX(I,J,K+1)
ZhG1005: *      * OLD CORNER POINT *
ZhG1006:        DO 320 K=1,M
ZhG1007:        BFREE(K,K,1)=1.0
ZhG1008: 320    BFREE(K,K,LX)=1.0
ZhG1009:        RETURN
ZhG1010:        END
ZhG1011:
ZhG1012:        SUBROUTINE BLK3_LU
ZhG1013:        IMPLICIT REAL*8(A-H,O-Z)
ZhG1014:        PARAMETER(M=2,LX=1001,LY=11,LX1=LX-1,LY1=LY-1)
ZhG1015:        COMMON/BLK3/AMX(M,M,LX,2:LY1),BMX(M,M,LX,2:LY1)
ZhG1016:        1       ,CMX(M,M,LX,2:LY1),AMY(M,M,LY,2:LX1)
ZhG1017:        2       ,BMY(M,M,LY,2:LX1),CMY(M,M,LY,2:LX1)
ZhG1018:        COMMON/BLK3_FREE/AFREE(M,M,LX),BFREE(M,M,LX),CFREE(M,M,LX)
ZhG1019:        DIMENSION WK(M,M)
ZhG1020:        CALL UNIX
ZhG1021:        DO 1000 NUM=2,LY1
ZhG1022:        DO 110 I=1,M
ZhG1023:        DO 110 J=1,M
ZhG1024: 110    WK(I,J)=BMX(I,J,1,NUM)
ZhG1025:        CALL INVERS(WK)
ZhG1026:        DO 112 I=1,M
ZhG1027:        DO 112 J=1,M
ZhG1028: 112    BMX(I,J,1,NUM)=WK(I,J)
ZhG1029:        DO 114 I=1,M
ZhG1030:        DO 114 J=1,M
ZhG1031:        WK(I,J)=0.0
ZhG1032:        DO 114 K=1,M
ZhG1033: 114    WK(I,J)=WK(I,J)+BMX(I,K,1,NUM)*CMX(K,J,1,NUM)
ZhG1034:        DO 116 I=1,M
ZhG1035:        DO 116 J=1,M
ZhG1036: 116    CMX(I,J,1,NUM)=WK(I,J)
ZhG1037:        DO 138 L=2,LX
ZhG1038:        DO 130 I=1,M
ZhG1039:        DO 130 J=1,M
ZhG1040:        XX=0.0
ZhG1041:        DO 132 K=1,M
ZhG1042: 132    XX=XX+AMX(I,K,L,NUM)*CMX(K,J,L-1,NUM)
ZhG1043: 130    WK(I,J)=BMX(I,J,L,NUM)-XX
ZhG1044:        CALL INVERS(WK)
ZhG1045:        DO 134 I=1,M
ZhG1046:        DO 134 J=1,M
ZhG1047: 134    BMX(I,J,L,NUM)=WK(I,J)
ZhG1048:        IF(L.EQ.LX) GOTO 1000
ZhG1049:        DO 136 I=1,M
ZhG1050:        DO 136 J=1,M
ZhG1051:        WK(I,J)=0.0
```

```
ZhG1052:        DO 136 K=1,M
ZhG1053: 136    WK(I,J)=WK(I,J)+BMX(I,K,L,NUM)*CMX(K,J,L,NUM)
ZhG1054:        DO 138 I=1,M
ZhG1055:        DO 138 J=1,M
ZhG1056: 138    CMX(I,J,L,NUM)=WK(I,J)
ZhG1057: 1000   CONTINUE
ZhG1058:        DO 2000 NUM=2,LX1
ZhG1059:        DO 210 I=1,M
ZhG1060:        DO 210 J=1,M
ZhG1061: 210    WK(I,J)=BMY(I,J,1,NUM)
ZhG1062:        CALL INVERS(WK)
ZhG1063:        DO 212 I=1,M
ZhG1064:        DO 212 J=1,M
ZhG1065: 212    BMY(I,J,1,NUM)=WK(I,J)
ZhG1066:        DO 214 I=1,M
ZhG1067:        DO 214 J=1,M
ZhG1068:        WK(I,J)=0.0
ZhG1069:        DO 214 K=1,M
ZhG1070: 214    WK(I,J)=WK(I,J)+BMY(I,K,1,NUM)*CMY(K,J,1,NUM)
ZhG1071:        DO 216 I=1,M
ZhG1072:        DO 216 J=1,M
ZhG1073: 216    CMY(I,J,1,NUM)=WK(I,J)
ZhG1074:        DO 238 L=2,LY
ZhG1075:        DO 230 I=1,M
ZhG1076:        DO 230 J=1,M
ZhG1077:        YY=0.0
ZhG1078:        DO 232 K=1,M
ZhG1079: 232    YY=YY+AMY(I,K,L,NUM)*CMY(K,J,L-1,NUM)
ZhG1080: 230    WK(I,J)=BMY(I,J,L,NUM)-YY
ZhG1081:        CALL INVERS(WK)
ZhG1082:        DO 234 I=1,M
ZhG1083:        DO 234 J=1,M
ZhG1084: 234    BMY(I,J,L,NUM)=WK(I,J)
ZhG1085:        IF(L.EQ.LY) GOTO 2000
ZhG1086:        DO 236 I=1,M
ZhG1087:        DO 236 J=1,M
ZhG1088:        WK(I,J)=0.0
ZhG1089:        DO 236 K=1,M
ZhG1090: 236    WK(I,J)=WK(I,J)+BMY(I,K,L,NUM)*CMY(K,J,L,NUM)
ZhG1091:        DO 238 I=1,M
ZhG1092:        DO 238 J=1,M
ZhG1093: 238    CMY(I,J,L,NUM)=WK(I,J)
ZhG1094: 2000   CONTINUE
ZhG1095:        DO 310 I=1,M
ZhG1096:        DO 310 J=1,M
ZhG1097: 310    WK(I,J)=BFREE(I,J,1)
ZhG1098:        CALL INVERS(WK)
ZhG1099:        DO 312 I=1,M
ZhG1100:        DO 312 J=1,M
ZhG1101: 312    BFREE(I,J,1)=WK(I,J)
ZhG1102:        DO 314 I=1,M
ZhG1103:        DO 314 J=1,M
ZhG1104:        WK(I,J)=0.0
```

```
ZhG1105:          DO 314 K=1,M
ZhG1106: 314      WK(I,J)=WK(I,J)+BFREE(I,K,1)*CFREE(K,J,1)
ZhG1107:          DO 316 I=1,M
ZhG1108:          DO 316 J=1,M
ZhG1109: 316      CFREE(I,J,1)=WK(I,J)
ZhG1110:          DO 338 L=2,LX
ZhG1111:          DO 330 I=1,M
ZhG1112:          DO 330 J=1,M
ZhG1113:          XX=0.0
ZhG1114:          DO 332 K=1,M
ZhG1115: 332      XX=XX+AFREE(I,K,L)*CFREE(K,J,L-1)
ZhG1116: 330      WK(I,J)=BFREE(I,J,L)-XX
ZhG1117:          CALL INVERS(WK)
ZhG1118:          DO 334 I=1,M
ZhG1119:          DO 334 J=1,M
ZhG1120: 334      BFREE(I,J,L)=WK(I,J)
ZhG1121:          IF(L.EQ.LX) GOTO 3000
ZhG1122:          DO 336 I=1,M
ZhG1123:          DO 336 J=1,M
ZhG1124:          WK(I,J)=0.0
ZhG1125:          DO 336 K=1,M
ZhG1126: 336      WK(I,J)=WK(I,J)+BFREE(I,K,L)*CFREE(K,J,L)
ZhG1127:          DO 338 I=1,M
ZhG1128:          DO 338 J=1,M
ZhG1129: 338      CFREE(I,J,L)=WK(I,J)
ZhG1130: 3000     RETURN
ZhG1131:          END
ZhG1132:
ZhG1133:          SUBROUTINE INVERS(X)
ZhG1134:          IMPLICIT REAL*8(A-H,O-Z)
ZhG1135:          PARAMETER(M=2)
ZhG1136:          DIMENSION X(M,M),U(M,M),B(M,M),XL(M,M),Z(M)
ZhG1137:          CALL UNIX
ZhG1138:          DO 200 J=1,M
ZhG1139:          B(J,J)=1.0
ZhG1140:          XL(J,1)=X(J,1)
ZhG1141: 200      U(1,J)=X(1,J)/XL(1,1)
ZhG1142:          DO 500 I=2,M
ZhG1143:          U(I,I)=1.0
ZhG1144:          TT=0.0
ZhG1145:          DO 400 K=1,I-1
ZhG1146: 400      TT=TT+XL(I,K)*U(K,I)
ZhG1147:          XL(I,I)=X(I,I)-TT
ZhG1148:          DO 500 J=I+1,M
ZhG1149:          TT=0.0
ZhG1150:          DO 600 K=1,I-1
ZhG1151: 600      TT=TT+XL(J,K)*U(K,I)
ZhG1152:          XL(J,I)=(X(J,I)-TT)
ZhG1153:          TT=0.0
ZhG1154:          DO 700 K=1,I-1
ZhG1155: 700      TT=TT+XL(I,K)*U(K,J)
ZhG1156: 500      U(I,J)=(X(I,J)-TT)/XL(I,I)
ZhG1157:          DO 800 M1=1,M
```

```
ZhG1158:       Z(1)=B(1,M1)/XL(1,1)
ZhG1159:       DO 900 I=2,M
ZhG1160:       TT=0.0
ZhG1161:       DO 1000 K=1,I-1
ZhG1162: 1000  TT=TT+XL(I,K)*Z(K)
ZhG1163: 900   Z(I)=(B(I,M1)-TT)/XL(I,I)
ZhG1164:       X(M,M1)=Z(M)
ZhG1165:       DO 800 I=M-1,1,-1
ZhG1166:       TT=0.0
ZhG1167:       DO 1100 K=M,I+1,-1
ZhG1168: 1100  TT=TT+U(I,K)*X(K,M1)
ZhG1169: 800   X(I,M1)=Z(I)-TT
ZhG1170:       RETURN
ZhG1171:       END
ZhG1172:
ZhG1173:       SUBROUTINE FREE_VEL
ZhG1174:       IMPLICIT REAL*8(A-H,O-Z)
ZhG1175:       PARAMETER(M=2,LX=1001,LY=11)
ZhG1176:       PARAMETER(LX1=LX-1,LY1=LY-1,LX2=LX-2,LY2=LY-2)
ZhG1177:       COMMON/UVPB/UB(LX,LY),VB(LX,LY),PB(LX,LY)
ZhG1178:       COMMON/BLK3_FREE/AFREE(M,M,LX),BFREE(M,M,LX),CFREE(M,M,LX)
ZhG1179:       COMMON/FREE_UVP/FREEX(M,M,LX),FREEY(M,M,LX,3)
ZhG1180:       1         ,FP1(LX),FP2(LX,3),FP3(LX,3)
ZhG1181:       COMMON/R_FREE/R_VEL(M,LX),R_PRE(LX)
ZhG1182:       DIMENSION WK(M),DFR(M,LX)
ZhG1183:       CALL UNIX
ZhG1184:       DO 450 I=2,LX1
ZhG1185:       UBY=4.0*FREEY(1,1,I,2)*UB(I,LY1)-FREEY(1,1,I,3)*UB(I,LY2)
ZhG1186:       VBY=4.0*FREEY(1,2,I,2)*VB(I,LY1)-FREEY(1,2,I,3)*VB(I,LY2)
ZhG1187:       DFR(1,I)=R_VEL(1,I)+UBY+VBY
ZhG1188:       UBY=4.0*FREEY(2,1,I,2)*UB(I,LY1)-FREEY(2,1,I,3)*UB(I,LY2)
ZhG1189:       VBY=4.0*FREEY(2,2,I,2)*VB(I,LY1)-FREEY(2,2,I,3)*VB(I,LY2)
ZhG1190: 450   DFR(2,I)=R_VEL(2,I)+UBY+VBY
ZhG1191: *     * OLD CORNER POINTS *
ZhG1192:       DFR(1,1)=UB(1,LY)
ZhG1193:       DFR(2,1)=VB(1,LY)
ZhG1194:       DFR(1,LX)=UB(LX,LY)
ZhG1195:       DFR(2,LX)=VB(LX,LY)
ZhG1196:       DO 452 I=1,M
ZhG1197:       TT=0.0
ZhG1198:       DO 454 K=1,M
ZhG1199: 454   TT=TT+BFREE(I,K,1)*DFR(K,1)
ZhG1200: 452   DFR(I,1)=TT
ZhG1201:       DO 460 L=2,LX
ZhG1202:       DO 462 I=1,M
ZhG1203:       TT=0.0
ZhG1204:       DO 464 K=1,M
ZhG1205: 464   TT=TT+AFREE(I,K,L)*DFR(K,L-1)
ZhG1206: 462   WK(I)=DFR(I,L)-TT
ZhG1207:       DO 460 I=1,M
ZhG1208:       DFR(I,L)=0.0
ZhG1209:       DO 460 K=1,M
ZhG1210: 460   DFR(I,L)=DFR(I,L)+BFREE(I,K,L)*WK(K)
```

```
ZhG1211:        DO 470 L=LX1,1,-1
ZhG1212:        DO 470 I=1,M
ZhG1213:        TT=0.0
ZhG1214:        DO 472 K=1,M
ZhG1215: 472    TT=TT+CFREE(I,K,L)*DFR(K,L+1)
ZhG1216: 470    DFR(I,L)=DFR(I,L)-TT
ZhG1217:        DO 400 I=1,LX
ZhG1218:        UB(I,LY)=DFR(1,I)
ZhG1219: 400    VB(I,LY)=DFR(2,I)
ZhG1220:        RETURN
ZhG1221:        END
ZhG1222:
ZhG1223:        SUBROUTINE VELB_BLOCK(DT,DTOI)
ZhG1224:        IMPLICIT REAL*8(A-H,O-Z)
ZhG1225:        PARAMETER(M=2,LX=1001,LY=11)
ZhG1226:        PARAMETER(LX1=LX-1,LY1=LY-1,LX2=LX-2,LY2=LY-2)
ZhG1227:        COMMON/UVPB/UB(LX,LY),VB(LX,LY),PB(LX,LY)
ZhG1228:        COMMON/DVELB/DUB(LX,LY),DVB(LX,LY)
ZhG1229:        COMMON/UVR/UR(LX,LY),VR(LX,LY)
ZhG1230:        COMMON/BLK3/AMX(M,M,LX,2:LY1),BMX(M,M,LX,2:LY1)
ZhG1231:        1       ,CMX(M,M,LX,2:LY1),AMY(M,M,LY,2:LX1)
ZhG1232:        2       ,BMY(M,M,LY,2:LX1),CMY(M,M,LY,2:LX1)
ZhG1233:        COMMON/UV_C/CUX1(LX,LY),CUY1(LX,LY),CVX1(LX,LY),CVY1(LX,LY)
ZhG1234:        1       ,CUX2(LX,LY),CUY2(LX,LY),CVX2(LX,LY),CVY2(LX,LY)
ZhG1235:        2       ,CU1(LX,LY),CV1(LX,LY),CU2(LX,LY),CV2(LX,LY)
ZhG1236:        3       ,CXX(LX,LY),CXY(LX,LY),CYY(LX,LY)
ZhG1237:        COMMON/DPHJ/XIHJ(LX,LY),XJHJ(LX,LY),YIHJ(LX,LY),YJHJ(LX,LY)
ZhG1238:        DIMENSION
DMX(M,LX),DMY(M,LY),WK(M),Q1(LX,LY),Q2(LX,LY),Q3(LX,LY)
ZhG1239:        1       ,DQ1(LX,LY),DQ2(LX,LY),DQ3(LX,LY)
ZhG1240:        CALL UNIX
ZhG1241:        DT2=0.5*DT
ZhG1242:        DTDTOI2=0.5*DT*DTOI
ZhG1243:        DTDTOI4=0.25*DT*DTOI
ZhG1244:        DO 300 I=1,LX
ZhG1245:        DO 300 J=1,LY
ZhG1246:        Q1(I,J)=UB(I,J)**2.0+PB(I,J)
ZhG1247:        Q2(I,J)=UB(I,J)*VB(I,J)
ZhG1248:        Q3(I,J)=VB(I,J)**2.0+PB(I,J)
ZhG1249:        DQ1(I,J)=DUB(I,J)**2.0+2.0*UB(I,J)*DUB(I,J)
ZhG1250:        DQ2(I,J)=DUB(I,J)*DVB(I,J)+DUB(I,J)*VB(I,J)+UB(I,J)*DVB(I,J)
ZhG1251: 300    DQ3(I,J)=DVB(I,J)**2.0+2.0*VB(I,J)*DVB(I,J)
ZhG1252: *      ** J=CONST. X-SWEEP **
ZhG1253:        DO 400 J=2,LY1
ZhG1254:        JP1=J+1
ZhG1255:        JM1=J-1
ZhG1256:        DO 450 I=2,LX1
ZhG1257:        IP1=I+1
ZhG1258:        IM1=I-1
ZhG1259:        XX=XIHJ(I,J)
ZhG1260:        XY=XJHJ(I,J)
ZhG1261:        YX=YIHJ(I,J)
ZhG1262:        YY=YJHJ(I,J)
```

```
ZhG1263:        Q2X=Q2(IP1,J)-Q2(IM1,J)
ZhG1264:        Q2Y=Q2(I,JP1)-Q2(I,JM1)
ZhG1265:        UBXY=UB(IP1,JP1)+UB(IM1,JM1)-UB(IP1,JM1)-UB(IM1,JP1)
ZhG1266:        VBXY=VB(IP1,JP1)+VB(IM1,JM1)-VB(IP1,JM1)-VB(IM1,JP1)
ZhG1267:        UNL=YY*(Q1(IP1,J)-Q1(IM1,J))-YX*(Q1(I,JP1)-Q1(I,JM1))
ZhG1268:        1  +XX*Q2Y-XY*Q2X+CXY(I,J)*UBXY
ZhG1269:        VNL=YY*Q2X-YX*Q2Y+CXY(I,J)*VBXY
ZhG1270:        1  +XX*(Q3(I,JP1)-Q3(I,JM1))-XY*(Q3(IP1,J)-Q3(IM1,J))
ZhG1271:        Q2X=DQ2(IP1,J)-DQ2(IM1,J)
ZhG1272:        Q2Y=DQ2(I,JP1)-DQ2(I,JM1)
ZhG1273:        UBXY=DUB(IP1,JP1)+DUB(IM1,JM1)-DUB(IP1,JM1)-DUB(IM1,JP1)
ZhG1274:        VBXY=DVB(IP1,JP1)+DVB(IM1,JM1)-DVB(IP1,JM1)-DVB(IM1,JP1)
ZhG1275:        DUNL=YY*(DQ1(IP1,J)-DQ1(IM1,J))-YX*(DQ1(I,JP1)-DQ1(I,JM1))
ZhG1276:        1  +XX*Q2Y-XY*Q2X+CXY(I,J)*UBXY
ZhG1277:        DVNL=YY*Q2X-YX*Q2Y+CXY(I,J)*VBXY
ZhG1278:        1  +XX*(DQ3(I,JP1)-DQ3(I,JM1))-XY*(DQ3(IP1,J)-DQ3(IM1,J))
ZhG1279:        A5=2.0*UB(I,J)
ZhG1280:        B5=2.0*VB(I,J)
ZhG1281:        UBX=UB(IP1,J)-UB(IM1,J)
ZhG1282:        UBY=UB(I,JP1)-UB(I,JM1)
ZhG1283:        UBXX=UB(IP1,J)+UB(IM1,J)-A5
ZhG1284:        UBYY=UB(I,JP1)+UB(I,JM1)-A5
ZhG1285:        VBX=VB(IP1,J)-VB(IM1,J)
ZhG1286:        VBY=VB(I,JP1)-VB(I,JM1)
ZhG1287:        VBXX=VB(IP1,J)+VB(IM1,J)-B5
ZhG1288:        VBYY=VB(I,JP1)+VB(I,JM1)-B5
ZhG1289:        UXSWP=DTDTOI4*DUNL+DTOI*(UB(I,J)-DT2*(CU1(I,J)*UB(I,J)
ZhG1290:        1         +CV1(I,J)*VB(I,J)+CUX1(I,J)*UBX+CVX1(I,J)*VBX
ZhG1291:        2         +CUY1(I,J)*UBY+CVY1(I,J)*VBY+CXX(I,J)*UBXX
ZhG1292:        3         +CYY(I,J)*UBYY-UNL))
ZhG1293:        VXSWP=DTDTOI4*DVNL+DTOI*(VB(I,J)-DT2*(CU2(I,J)*UB(I,J)
ZhG1294:        1         +CV2(I,J)*VB(I,J)+CUX2(I,J)*UBX+CVX2(I,J)*VBX
ZhG1295:        2         +CUY2(I,J)*UBY+CVY2(I,J)*VBY+CXX(I,J)*VBXX
ZhG1296:        3         +CYY(I,J)*VBYY-VNL))
ZhG1297:        DMX(1,I)=DTDTOI2*UR(I,J)-UXSWP
ZhG1298: 450    DMX(2,I)=DTDTOI2*VR(I,J)-VXSWP
ZhG1299: *      * OLD BOUNDARY *
ZhG1300:        DO 451 K=1,M
ZhG1301:        DMX(K,1)=0.0
ZhG1302: 451    DMX(K,LX)=0.0
ZhG1303:        DO 452 I=1,M
ZhG1304:        TT=0.0
ZhG1305:        DO 454 K=1,M
ZhG1306: 454    TT=TT+BMX(I,K,1,J)*DMX(K,1)
ZhG1307: 452    DMX(I,1)=TT
ZhG1308:        DO 460 L=2,LX
ZhG1309:        DO 462 I=1,M
ZhG1310:        TT=0.0
ZhG1311:        DO 464 K=1,M
ZhG1312: 464    TT=TT+AMX(I,K,L,J)*DMX(K,L-1)
ZhG1313: 462    WK(I)=DMX(I,L)-TT
ZhG1314:        DO 460 I=1,M
ZhG1315:        DMX(I,L)=0.0
```

```
ZhG1316:        DO 460 K=1,M
ZhG1317: 460    DMX(I,L)=DMX(I,L)+BMX(I,K,L,J)*WK(K)
ZhG1318:        DO 470 L=LX1,1,-1
ZhG1319:        DO 470 I=1,M
ZhG1320:        TT=0.0
ZhG1321:        DO 472 K=1,M
ZhG1322: 472    TT=TT+CMX(I,K,L,J)*DMX(K,L+1)
ZhG1323: 470    DMX(I,L)=DMX(I,L)-TT
ZhG1324:        DO 400 I=1,LX
ZhG1325:        DUB(I,J)=DMX(1,I)
ZhG1326: 400    DVB(I,J)=DMX(2,I)
ZhG1327: *      ** I=CONST. Y-SWEEP **
ZhG1328:        DO 500 I=2,LX1
ZhG1329:        DO 510 J=2,LY1
ZhG1330:        DMY(1,J)=DUB(I,J)
ZhG1331: 510    DMY(2,J)=DVB(I,J)
ZhG1332: *      * OLD BOUNDARY *
ZhG1333:        DO 515 K=1,M
ZhG1334:        DMY(K,1)=0.0
ZhG1335: 515    DMY(K,LY)=0.0
ZhG1336:        DO 552 J=1,M
ZhG1337:        TT=0.0
ZhG1338:        DO 554 K=1,M
ZhG1339: 554    TT=TT+BMY(J,K,1,I)*DMY(K,1)
ZhG1340: 552    DMY(J,1)=TT
ZhG1341:        DO 560 L=2,LY
ZhG1342:        DO 562 J=1,M
ZhG1343:        TT=0.0
ZhG1344:        DO 564 K=1,M
ZhG1345: 564    TT=TT+AMY(J,K,L,I)*DMY(K,L-1)
ZhG1346: 562    WK(J)=DMY(J,L)-TT
ZhG1347:        DO 560 J=1,M
ZhG1348:        DMY(J,L)=0.0
ZhG1349:        DO 560 K=1,M
ZhG1350: 560    DMY(J,L)=DMY(J,L)+BMY(J,K,L,I)*WK(K)
ZhG1351:        DO 570 L=LY1,1,-1
ZhG1352:        DO 570 J=1,M
ZhG1353:        TT=0.0
ZhG1354:        DO 572 K=1,M
ZhG1355: 572    TT=TT+CMY(J,K,L,I)*DMY(K,L+1)
ZhG1356: 570    DMY(J,L)=DMY(J,L)-TT
ZhG1357:        DO 500 J=1,LY
ZhG1358:        DUB(I,J)=DMY(1,J)
ZhG1359: 500    DVB(I,J)=DMY(2,J)
ZhG1360:        RETURN
ZhG1361:        END
ZhG1362:
ZhG1363:        SUBROUTINE PB_NBD(RE)
ZhG1364:        IMPLICIT REAL*8(A-H,O-Z)
ZhG1365:        PARAMETER(M=2,LX=1001,LY=11,IG=2*LX-1,JG=2*LY-1)
ZhG1366:        PARAMETER(LX1=LX-1,LY1=LY-1,LX2=LX-2,LY2=LY-2)
ZhG1367:        COMMON/DXY/XI(IG,JG),XJ(IG,JG),YI(IG,JG),YJ(IG,JG)
ZhG1368:        COMMON/UVP/U(LX,LY),V(LX,LY),P(LX,LY)
```

```
ZhG1369:       COMMON/UVPB/UB(LX,LY),VB(LX,LY),PB(LX,LY)
ZhG1370:       COMMON/ABGDJ/ADJ(IG,JG),BDJ(IG,JG),GDJ(IG,JG)
ZhG1371:       COMMON/UV_B/ULFT(LY),URIT(LY),UBOT(LX)
ZhG1372:       1        ,VLFT(LY),VRIT(LY),VBOT(LX)
ZhG1373:       COMMON/DP_C/XI2DJ(IG,JG),XJ2DJ(IG,JG),YI2DJ(IG,JG)
ZhG1374:       1        ,YJ2DJ(IG,JG),XIXJDJ(IG,JG),XIYIDJ(IG,JG)
ZhG1375:       2        ,XIYJDJ(IG,JG),XJYIDJ(IG,JG),XJYJDJ(IG,JG)
ZhG1376:       3        ,YIYJDJ(IG,JG),PLUS(IG,JG)
ZhG1377:       4        ,P1(IG,JG),P2(IG,JG),P3(IG,JG),P4(IG,JG)
ZhG1378:       5        ,P5(IG,JG),P6(IG,JG),P7(IG,JG),P8(IG,JG)
ZhG1379:       COMMON/BD/XI3(LX,M),XI4(LX,M),YI3(LX,M),YI4(LX,M)
ZhG1380:       1        ,XJ3(M,LY),XJ4(M,LY),YJ3(M,LY),YJ4(M,LY)
ZhG1381:       COMMON/DPHJ/XIHJ(LX,LY),XJHJ(LX,LY),YIHJ(LX,LY),YJHJ(LX,LY)
ZhG1382:       COMMON/COM22/Q1(LX,LY),Q2(LX,LY),Q3(LX,LY)
ZhG1383:       COMMON/F_M/FM(LX,LY),FM_LR(2,LY),FM_BT(LX)
ZhG1384:       DIMENSION WB(LX,LY)
ZhG1385:       CALL UNIX
ZhG1386: *     * VORTICITY *
ZhG1387:       DO 10 I=2,LX1,LX1-2
ZhG1388:       IP1=I+1
ZhG1389:       IM1=I-1
ZhG1390:       DO 10 J=2,LY1
ZhG1391:       JP1=J+1
ZhG1392:       JM1=J-1
ZhG1393: 10    WB(I,J)=(XIHJ(I,JP1)*UB(I,JP1)-XIHJ(I,JM1)*UB(I,JM1)
ZhG1394:       1        -XJHJ(IP1,J)*UB(IP1,J)+XJHJ(IM1,J)*UB(IM1,J)
ZhG1395:       2        -YJHJ(IP1,J)*VB(IP1,J)+YJHJ(IM1,J)*VB(IM1,J)
ZhG1396:       3        +YIHJ(I,JP1)*VB(I,JP1)-YIHJ(I,JM1)*VB(I,JM1))
ZhG1397:       DO 20 I=2,LX1
ZhG1398:       IP1=I+1
ZhG1399:       IM1=I-1
ZhG1400:       DO 20 J=2,LY1,LY1-2
ZhG1401:       JP1=J+1
ZhG1402:       JM1=J-1
ZhG1403: 20    WB(I,J)=(XIHJ(I,JP1)*UB(I,JP1)-XIHJ(I,JM1)*UB(I,JM1)
ZhG1404:       1        -XJHJ(IP1,J)*UB(IP1,J)+XJHJ(IM1,J)*UB(IM1,J)
ZhG1405:       2        -YJHJ(IP1,J)*VB(IP1,J)+YJHJ(IM1,J)*VB(IM1,J)
ZhG1406:       3        +YIHJ(I,JP1)*VB(I,JP1)-YIHJ(I,JM1)*VB(I,JM1))
ZhG1407:       DO 30 J=2,LY1
ZhG1408:       JP1=J+1
ZhG1409:       JM1=J-1
ZhG1410:       WB(1,J)=(XIHJ(1,JP1)*UB(1,JP1)-XIHJ(1,JM1)*UB(1,JM1)
ZhG1411:       2        +YIHJ(1,JP1)*VB(1,JP1)-YIHJ(1,JM1)*VB(1,JM1)
ZhG1412:       3        +XJ3(1,J)*UB(1,J)-XJ4(1,J)*UB(2,J)+XJHJ(3,J)*UB(3,J)
ZhG1413:       4        +YJ3(1,J)*VB(1,J)-YJ4(1,J)*VB(2,J)+YJHJ(3,J)*VB(3,J))
ZhG1414: 30    WB(LX,J)=(XIHJ(LX,JP1)*UB(LX,JP1)-XIHJ(LX,JM1)*UB(LX,JM1)
ZhG1415:       2         +YIHJ(LX,JP1)*VB(LX,JP1)-YIHJ(LX,JM1)*VB(LX,JM1)
ZhG1416:       3  -XJ3(2,J)*UB(LX,J)+XJ4(2,J)*UB(LX1,J)-XJHJ(LX2,J)*UB(LX2,J)
ZhG1417:       4  -YJ3(2,J)*VB(LX,J)+YJ4(2,J)*VB(LX1,J)-YJHJ(LX2,J)*VB(LX2,J))
ZhG1418:       DO 40 I=2,LX1
ZhG1419:       IP1=I+1
ZhG1420:       IM1=I-1
ZhG1421:       WB(I,1)=(-XI3(I,1)*UB(I,1)+XI4(I,1)*UB(I,2)-XIHJ(I,3)*UB(I,3)
```

```
ZhG1422:      2        -YI3(I,1)*VB(I,1)+YI4(I,1)*VB(I,2)-YIHJ(I,3)*VB(I,3)
ZhG1423:      4       -XJHJ(IP1,1)*UB(IP1,1)+XJHJ(IM1,1)*UB(IM1,1)
ZhG1424:      5       -YJHJ(IP1,1)*VB(IP1,1)+YJHJ(IM1,1)*VB(IM1,1))
ZhG1425: 40   WB(I,LY)=(XI3(I,2)*UB(I,LY)-XI4(I,2)*UB(I,LY1)
ZhG1426:      1       +XIHJ(I,LY2)*UB(I,LY2)+YI3(I,2)*VB(I,LY)
ZhG1427:      2       -YI4(I,2)*VB(I,LY1)+YIHJ(I,LY2)*VB(I,LY2)
ZhG1428:      4       -XJHJ(IP1,LY)*UB(IP1,LY)+XJHJ(IM1,LY)*UB(IM1,LY)
ZhG1429:      5       -YJHJ(IP1,LY)*VB(IP1,LY)+YJHJ(IM1,LY)*VB(IM1,LY))
ZhG1430:      WB(1,1)=
ZhG1431:      1 (-XI3(1,1)*UB(1,1)+XI4(1,1)*UB(1,2)-XIHJ(1,3)*UB(1,3)
ZhG1432:      2 -YI3(1,1)*VB(1,1)+YI4(1,1)*VB(1,2)-YIHJ(1,3)*VB(1,3)
ZhG1433:      4 +XJ3(1,1)*UB(1,1)-XJ4(1,1)*UB(2,1)+XJHJ(3,1)*UB(3,1)
ZhG1434:      5 +YJ3(1,1)*VB(1,1)-YJ4(1,1)*VB(2,1)+YJHJ(3,1)*VB(3,1))
ZhG1435:      WB(1,LY)=
ZhG1436:      1 (XI3(1,2)*UB(1,LY)-XI4(1,2)*UB(1,LY1)+XIHJ(1,LY2)*UB(1,LY2)
ZhG1437:      2 +YI3(1,2)*VB(1,LY)-YI4(1,2)*VB(1,LY1)+YIHJ(1,LY2)*VB(1,LY2)
ZhG1438:      4 +XJ3(1,LY)*UB(1,LY)-XJ4(1,LY)*UB(2,LY)+XJHJ(3,LY)*UB(3,LY)
ZhG1439:      5 +YJ3(1,LY)*VB(1,LY)-YJ4(1,LY)*VB(2,LY)+YJHJ(3,LY)*VB(3,LY))
ZhG1440:      WB(LX,1)=
ZhG1441:      1 (-XI3(LX,1)*UB(LX,1)+XI4(LX,1)*UB(LX,2)-XIHJ(LX,3)*UB(LX,3)
ZhG1442:      2 -YI3(LX,1)*VB(LX,1)+YI4(LX,1)*VB(LX,2)-YIHJ(LX,3)*VB(LX,3)
ZhG1443:      4 -XJ3(2,1)*UB(LX,1)+XJ4(2,1)*UB(LX1,1)-XJHJ(LX2,1)*UB(LX2,1)
ZhG1444:      5 -YJ3(2,1)*VB(LX,1)+YJ4(2,1)*VB(LX1,1)-YJHJ(LX2,1)*VB(LX2,1))
ZhG1445:      WB(LX,LY)=
ZhG1446:      1 (XI3(LX,2)*UB(LX,LY)-XI4(LX,2)*UB(LX,LY1)+XIHJ(LX,LY2)*UB(LX,LY2)
ZhG1447:      3 +YI3(LX,2)*VB(LX,LY)-YI4(LX,2)*VB(LX,LY1)+YIHJ(LX,LY2)*VB(LX,LY2)
ZhG1448:      4 -XJ3(2,LY)*UB(LX,LY)+XJ4(2,LY)*UB(LX1,LY)-XJHJ(LX2,LY)*UB(LX2,LY)
ZhG1449:      5 -YJ3(2,LY)*VB(LX,LY)+YJ4(2,LY)*VB(LX1,LY)-YJHJ(LX2,LY)*VB(LX2,LY))
ZhG1450:      DO 50 I=1,LX
ZhG1451:      DO 50 J=1,LY
ZhG1452:      Q1(I,J)=UB(I,J)**2.0+2.0*U(I,J)*UB(I,J)
ZhG1453:      Q2(I,J)=UB(I,J)*VB(I,J)+U(I,J)*VB(I,J)+V(I,J)*UB(I,J)
ZhG1454: 50   Q3(I,J)=VB(I,J)**2.0+2.0*V(I,J)*VB(I,J)
ZhG1455: *    * LEFT (I=1) & RIGHT (I=LX1) *
ZhG1456: *    *  XI=X(IP1,J)-X(I,J)
ZhG1457: *    *  YJ=0.25*(Y(I,J+1)+Y(IP1,J+1)-Y(I,J-1)-Y(IP1,J-1))
ZhG1458:      DO 100 K=1,2
ZhG1459:      IF(K.EQ.1) I=1
ZhG1460:      IF(K.EQ.2) I=LX1
ZhG1461:      IP1=I+1
ZhG1462:      II=2*I
ZhG1463:      IIP1=II+1
ZhG1464:      IIM1=II-1
ZhG1465:      DO 100 J=2,LY1
ZhG1466:      JJ=2*J-1
ZhG1467:      JP1=J+1
ZhG1468:      JM1=J-1
ZhG1469:      JJP2=JJ+2
ZhG1470:      JJM2=JJ-2
ZhG1471:      T2=P1(IIP1,JJ)*UB(IP1,J)-P1(IIM1,JJ)*UB(I,J)
ZhG1472:      T3=P2(II,JJP2)*(UB(IP1,JP1)+UB(I,JP1))
ZhG1473:      1 -P2(II,JJM2)*(UB(IP1,JM1)+UB(I,JM1))
ZhG1474:      T4=P3(IIP1,JJ)*VB(IP1,J)-P3(IIM1,JJ)*VB(I,J)
```

```
ZhG1475:       T5=P4(II,JJP2)*(VB(IP1,JP1)+VB(I,JP1))
ZhG1476:       1 -P4(II,JJM2)*(VB(IP1,JM1)+VB(I,JM1))
ZhG1477:       T6=YJ2DJ(IIP1,JJ)*Q1(IP1,J)-YJ2DJ(IIM1,JJ)*Q1(I,J)
ZhG1478:       T7=YIYJDJ(II,JJP2)*(Q1(IP1,JP1)+Q1(I,JP1))
ZhG1479:       1 -YIYJDJ(II,JJM2)*(Q1(IP1,JM1)+Q1(I,JM1))
ZhG1480:       T8=2.0*(XJYJDJ(IIP1,JJ)*Q2(IP1,J)-XJYJDJ(IIM1,JJ)*Q2(I,J))
ZhG1481:       T9=PLUS(II,JJP2)*(Q2(IP1,JP1)+Q2(I,JP1))
ZhG1482:       1 -PLUS(II,JJM2)*(Q2(IP1,JM1)+Q2(I,JM1))
ZhG1483:       T10=XJ2DJ(IIP1,JJ)*Q3(IP1,J)-XJ2DJ(IIM1,JJ)*Q3(I,J)
ZhG1484:       T11=XIXJDJ(II,JJP2)*(Q3(IP1,JP1)+Q3(I,JP1))
ZhG1485:       1  -XIXJDJ(II,JJM2)*(Q3(IP1,JM1)+Q3(I,JM1))
ZhG1486:       T12=(WB(IP1,JP1)+WB(I,JP1)-WB(IP1,JM1)-WB(I,JM1))/RE
ZhG1487:       UL=-T2+T4-T6+T8-T10-0.25*(T3-T5-T7+T9-T11-T12)
ZhG1488:       T2=P7(IIP1,JJ)*UB(IP1,J)-P7(IIM1,JJ)*UB(I,J)
ZhG1489:       T3=P8(II,JJP2)*(UB(IP1,JP1)+UB(I,JP1))
ZhG1490:       1 -P8(II,JJM2)*(UB(IP1,JM1)+UB(I,JM1))
ZhG1491:       T4=P5(IIP1,JJ)*VB(IP1,J)-P5(IIM1,JJ)*VB(I,J)
ZhG1492:       T5=P6(II,JJP2)*(VB(IP1,JP1)+VB(I,JP1))
ZhG1493:       1 -P6(II,JJM2)*(VB(IP1,JM1)+VB(I,JM1))
ZhG1494:       T6=YIYJDJ(IIP1,JJ)*Q1(IP1,J)-YIYJDJ(IIM1,JJ)*Q1(I,J)
ZhG1495:       T7=YI2DJ(II,JJP2)*(Q1(IP1,JP1)+Q1(I,JP1))
ZhG1496:       1 -YI2DJ(II,JJM2)*(Q1(IP1,JM1)+Q1(I,JM1))
ZhG1497:       T8=PLUS(IIP1,JJ)*Q2(IP1,J)-PLUS(IIM1,JJ)*Q2(I,J)
ZhG1498:       T9=2.0*(XIYIDJ(II,JJP2)*(Q2(IP1,JP1)+Q2(I,JP1))
ZhG1499:       1     -XIYIDJ(II,JJM2)*(Q2(IP1,JM1)+Q2(I,JM1)))
ZhG1500:       T10=XIXJDJ(IIP1,JJ)*Q3(IP1,J)-XIXJDJ(IIM1,JJ)*Q3(I,J)
ZhG1501:       T11=XI2DJ(II,JJP2)*(Q3(IP1,JP1)+Q3(I,JP1))
ZhG1502:       1  -XI2DJ(II,JJM2)*(Q3(IP1,JM1)+Q3(I,JM1))
ZhG1503:       T12=(WB(IP1,J)-WB(I,J))/RE
ZhG1504:       VL=-T2+T4-T6+T8-T10+T12-0.25*(T3-T5-T7+T9-T11)
ZhG1505:       IF(K.EQ.1) THEN
ZhG1506:       PX=(BDJ(II,JJ)*(VLFT(J)-VL)-GDJ(II,JJ)*(ULFT(J)-UL))/FM_LR(1,J)
ZhG1507:       PB(I,J)=PB(IP1,J)-PX
ZhG1508:       ENDIF
ZhG1509:       IF(K.EQ.2) THEN
ZhG1510:       PX=(BDJ(II,JJ)*(VRIT(J)-VL)-GDJ(II,JJ)*(URIT(J)-UL))/FM_LR(2,J)
ZhG1511:       PB(IP1,J)=PB(I,J)+PX
ZhG1512:       ENDIF
ZhG1513: 100   CONTINUE
ZhG1514: *     * BOTTOM (J=1) *
ZhG1515: *     *  XI=0.25*(X(I+1,J)+X(I+1,JP1)-X(I-1,J)-X(I-1,JP1))
ZhG1516: *     *  YJ=Y(I,JP1)-Y(I,J)
ZhG1517:       J=1
ZhG1518:       JP1=J+1
ZhG1519:       JJ=2*J
ZhG1520:       JJP1=JJ+1
ZhG1521:       JJM1=JJ-1
ZhG1522:       DO 200 I=2,LX1
ZhG1523:       II=2*I-1
ZhG1524:       IP1=I+1
ZhG1525:       IM1=I-1
ZhG1526:       IIP2=II+2
ZhG1527:       IIM2=II-2
```

```
ZhG1528:       T2=P1(IIP2,JJ)*(UB(IP1,JP1)+UB(IP1,J))
ZhG1529:       1 -P1(IIM2,JJ)*(UB(IM1,JP1)+UB(IM1,J))
ZhG1530:       T3=P2(II,JJP1)*UB(I,JP1)-P2(II,JJM1)*UB(I,J)
ZhG1531:       T4=P3(IIP2,JJ)*(VB(IP1,JP1)+VB(IP1,J))
ZhG1532:       1 -P3(IIM2,JJ)*(VB(IM1,JP1)+VB(IM1,J))
ZhG1533:       T5=P4(II,JJP1)*VB(I,JP1)-P4(II,JJM1)*VB(I,J)
ZhG1534:       T6=YJ2DJ(IIP2,JJ)*(Q1(IP1,JP1)+Q1(IP1,J))
ZhG1535:       1 -YJ2DJ(IIM2,JJ)*(Q1(IM1,JP1)+Q1(IM1,J))
ZhG1536:       T7=YIYJDJ(II,JJP1)*Q1(I,JP1)-YIYJDJ(II,JJM1)*Q1(I,J)
ZhG1537:       T8=2.0*(XJYJDJ(IIP2,JJ)*(Q2(IP1,JP1)+Q2(IP1,J))
ZhG1538:       1     -XJYJDJ(IIM2,JJ)*(Q2(IM1,JP1)+Q2(IM1,J)))
ZhG1539:       T9=PLUS(II,JJP1)*Q2(I,JP1)-PLUS(II,JJM1)*Q2(I,J)
ZhG1540:       T10=XJ2DJ(IIP2,JJ)*(Q3(IP1,JP1)+Q3(IP1,J))
ZhG1541:       1  -XJ2DJ(IIM2,JJ)*(Q3(IM1,JP1)+Q3(IM1,J))
ZhG1542:       T11=XIXJDJ(II,JJP1)*Q3(I,JP1)-XIXJDJ(II,JJM1)*Q3(I,J)
ZhG1543:       T12=(WB(I,JP1)-WB(I,J))/RE
ZhG1544:       UL=-T3+T5+T7-T9+T11+T12-0.25*(T2-T4+T6-T8+T10)
ZhG1545:       T2=P7(IIP2,JJ)*(UB(IP1,JP1)+UB(IP1,J))
ZhG1546:       1 -P7(IIM2,JJ)*(UB(IM1,JP1)+UB(IM1,J))
ZhG1547:       T3=P8(II,JJP1)*UB(I,JP1)-P8(II,JJM1)*UB(I,J)
ZhG1548:       T4=P5(IIP2,JJ)*(VB(IP1,JP1)+VB(IP1,J))
ZhG1549:       1 -P5(IIM2,JJ)*(VB(IM1,JP1)+VB(IM1,J))
ZhG1550:       T5=P6(II,JJP1)*VB(I,JP1)-P6(II,JJM1)*VB(I,J)
ZhG1551:       T6=YIYJDJ(IIP2,JJ)*(Q1(IP1,JP1)+Q1(IP1,J))
ZhG1552:       1 -YIYJDJ(IIM2,JJ)*(Q1(IM1,JP1)+Q1(IM1,J))
ZhG1553:       T7=YI2DJ(II,JJP1)*Q1(I,JP1)-YI2DJ(II,JJM1)*Q1(I,J)
ZhG1554:       T8=PLUS(IIP2,JJ)*(Q2(IP1,JP1)+Q2(IP1,J))
ZhG1555:       1 -PLUS(IIM2,JJ)*(Q2(IM1,JP1)+Q2(IM1,J))
ZhG1556:       T9=2.0*(XIYIDJ(II,JJP1)*Q2(I,JP1)-XIYIDJ(II,JJM1)*Q2(I,J))
ZhG1557:       T10=XIXJDJ(IIP2,JJ)*(Q3(IP1,JP1)+Q3(IP1,J))
ZhG1558:       1  -XIXJDJ(IIM2,JJ)*(Q3(IM1,JP1)+Q3(IM1,J))
ZhG1559:       T11=XI2DJ(II,JJP1)*Q3(I,JP1)-XI2DJ(II,JJM1)*Q3(I,J)
ZhG1560:       T12=(WB(IP1,JP1)+WB(IP1,J)-WB(IM1,JP1)-WB(IM1,J))/RE
ZhG1561:       VL=-T3+T5+T7-T9+T11-0.25*(T2-T4+T6-T8+T10-T12)
ZhG1562:       PY=(ADJ(II,JJ)*(VBOT(I)-VL)-BDJ(II,JJ)*(UBOT(I)-UL))/FM_BT(I)
ZhG1563: 200   PB(I,J)=PB(I,JP1)-PY
ZhG1564:       RETURN
ZhG1565:       END
ZhG1566:
ZhG1567:       SUBROUTINE PB_INNER(BJ,DT)
ZhG1568:       IMPLICIT REAL*8(A-H,O-Z)
ZhG1569:       PARAMETER(M=2,LX=1001,LY=11,IG=2*LX-1,JG=2*LY-1)
ZhG1570:       PARAMETER(LX1=LX-1,LY1=LY-1,LX2=LX-2,LY2=LY-2)
ZhG1571:       COMMON/UVPB/UB(LX,LY),VB(LX,LY),PB(LX,LY)
ZhG1572:       COMMON/P_R/PR(LX,LY)
ZhG1573:       COMMON/DP_C/XI2DJ(IG,JG),XJ2DJ(IG,JG),YI2DJ(IG,JG)
ZhG1574:      1        ,YJ2DJ(IG,JG),XIXJDJ(IG,JG),XIYIDJ(IG,JG)
ZhG1575:      2        ,XIYJDJ(IG,JG),XJYIDJ(IG,JG),XJYJDJ(IG,JG)
ZhG1576:      3        ,YIYJDJ(IG,JG),PLUS(IG,JG)
ZhG1577:      4        ,P1(IG,JG),P2(IG,JG),P3(IG,JG),P4(IG,JG)
ZhG1578:      5        ,P5(IG,JG),P6(IG,JG),P7(IG,JG),P8(IG,JG)
ZhG1579:       COMMON/ABGDJ/ADJ(IG,JG),BDJ(IG,JG),GDJ(IG,JG)
ZhG1580:       COMMON/DPHJ/XIHJ(LX,LY),XJHJ(LX,LY),YIHJ(LX,LY),YJHJ(LX,LY)
```

```
ZhG1581:       COMMON/COM22/Q1(LX,LY),Q2(LX,LY),Q3(LX,LY)
ZhG1582:       COMMON/F_M/FM(LX,LY),FM_LR(2,LY),FM_BT(LX)
ZhG1583:       DIMENSION R(LX,LY),DB(LX,LY),BJ(IG,JG)
ZhG1584:       CALL UNIX
ZhG1585:       NUMBER=100
ZhG1586:       OMG=1.7
ZhG1587: *     * DB *
ZhG1588:       DO 1 I=2,LX1
ZhG1589:       IP1=I+1
ZhG1590:       IM1=I-1
ZhG1591:       DO 1 J=2,LY1
ZhG1592:       JP1=J+1
ZhG1593:       JM1=J-1
ZhG1594: 1     DB(I,J)=(YJHJ(IP1,J)*UB(IP1,J)-YJHJ(IM1,J)*UB(IM1,J)
ZhG1595:       1         -YIHJ(I,JP1)*UB(I,JP1)+YIHJ(I,JM1)*UB(I,JM1)
ZhG1596:       2         +XIHJ(I,JP1)*VB(I,JP1)-XIHJ(I,JM1)*VB(I,JM1)
ZhG1597:       3         -XJHJ(IP1,J)*VB(IP1,J)+XJHJ(IM1,J)*VB(IM1,J))
ZhG1598:       DO 10 I=2,LX1
ZhG1599:       IP1=I+1
ZhG1600:       IM1=I-1
ZhG1601:       II=2*I-1
ZhG1602:       IE=II+1
ZhG1603:       IW=II-1
ZhG1604:       DO 10 J=2,LY1
ZhG1605:       JP1=J+1
ZhG1606:       JM1=J-1
ZhG1607:       JJ=2*J-1
ZhG1608:       JN=JJ+1
ZhG1609:       JS=JJ-1
ZhG1610:       TX1=P1(IE,JJ)*(UB(IP1,J)-UB(I,J))
ZhG1611:       1  -P1(IW,JJ)*(UB(I,J)-UB(IM1,J))
ZhG1612:       COM=UB(I,JP1)-UB(I,JM1)
ZhG1613:       TX2=P2(IE,JJ)*(UB(IP1,JP1)-UB(IP1,JM1)+COM)
ZhG1614:       1  -P2(IW,JJ)*(UB(IM1,JP1)-UB(IM1,JM1)+COM)
ZhG1615:       TX3=P3(IE,JJ)*(VB(IP1,J)-VB(I,J))
ZhG1616:       1  -P3(IW,JJ)*(VB(I,J)-VB(IM1,J))
ZhG1617:       COM=VB(I,JP1)-VB(I,JM1)
ZhG1618:       TX4=P4(IE,JJ)*(VB(IP1,JP1)-VB(IP1,JM1)+COM)
ZhG1619:       1  -P4(IW,JJ)*(VB(IM1,JP1)-VB(IM1,JM1)+COM)
ZhG1620:       TY1=P6(II,JN)*(VB(I,JP1)-VB(I,J))
ZhG1621:       1  -P6(II,JS)*(VB(I,J)-VB(I,JM1))
ZhG1622:       COM=VB(IP1,J)-VB(IM1,J)
ZhG1623:       TY2=P5(II,JN)*(VB(IP1,JP1)-VB(IM1,JP1)+COM)
ZhG1624:       1  -P5(II,JS)*(VB(IP1,JM1)-VB(IM1,JM1)+COM)
ZhG1625:       TY3=P8(II,JN)*(UB(I,JP1)-UB(I,J))
ZhG1626:       1  -P8(II,JS)*(UB(I,J)-UB(I,JM1))
ZhG1627:       COM=UB(IP1,J)-UB(IM1,J)
ZhG1628:       TY4=P7(II,JN)*(UB(IP1,JP1)-UB(IM1,JP1)+COM)
ZhG1629:       1  -P7(II,JS)*(UB(IP1,JM1)-UB(IM1,JM1)+COM)
ZhG1630:       X1=YJ2DJ(IE,JJ)*(Q1(IP1,J)-Q1(I,J))
ZhG1631:       1 -YJ2DJ(IW,JJ)*(Q1(I,J)-Q1(IM1,J))
ZhG1632:       COM=Q1(I,JP1)-Q1(I,JM1)
ZhG1633:       X2=YIYJDJ(IE,JJ)*(Q1(IP1,JP1)-Q1(IP1,JM1)+COM)
```

```
ZhG1634:      2 -YTYJDJ(IW,JJ)*(Q1(IM1,JP1)-Q1(IM1,JM1)+COM)
ZhG1635:      X3=2.0*(XJYJDJ(IE,JJ)*(Q2(IP1,J)-Q2(I,J))
ZhG1636:      1     -XJYJDJ(IW,JJ)*(Q2(I,J)-Q2(IM1,J)))
ZhG1637:      COM=Q2(I,JP1)-Q2(I,JM1)
ZhG1638:      X4=PLUS(IE,JJ)*(Q2(IP1,JP1)-Q2(IP1,JM1)+COM)
ZhG1639:      2 -PLUS(IW,JJ)*(Q2(IM1,JP1)-Q2(IM1,JM1)+COM)
ZhG1640:      X5=XJ2DJ(IE,JJ)*(Q3(IP1,J)-Q3(I,J))
ZhG1641:      1 -XJ2DJ(IW,JJ)*(Q3(I,J)-Q3(IM1,J))
ZhG1642:      COM=Q3(I,JP1)-Q3(I,JM1)
ZhG1643:      X6=XIXJDJ(IE,JJ)*(Q3(IP1,JP1)-Q3(IP1,JM1)+COM)
ZhG1644:      2 -XIXJDJ(IW,JJ)*(Q3(IM1,JP1)-Q3(IM1,JM1)+COM)
ZhG1645:      Y1=YI2DJ(II,JN)*(Q1(I,JP1)-Q1(I,J))
ZhG1646:      1 -YI2DJ(II,JS)*(Q1(I,J)-Q1(I,JM1))
ZhG1647:      COM=Q1(IP1,J)-Q1(IM1,J)
ZhG1648:      Y2=YTYJDJ(II,JN)*(Q1(IP1,JP1)-Q1(IM1,JP1)+COM)
ZhG1649:      2 -YTYJDJ(II,JS)*(Q1(IP1,JM1)-Q1(IM1,JM1)+COM)
ZhG1650:      Y3=2.0*(XIYIDJ(II,JN)*(Q2(I,JP1)-Q2(I,J))
ZhG1651:      2     -XIYIDJ(II,JS)*(Q2(I,J)-Q2(I,JM1)))
ZhG1652:      COM=Q2(IP1,J)-Q2(IM1,J)
ZhG1653:      Y4=PLUS(II,JN)*(Q2(IP1,JP1)-Q2(IM1,JP1)+COM)
ZhG1654:      3 -PLUS(II,JS)*(Q2(IP1,JM1)-Q2(IM1,JM1)+COM)
ZhG1655:      Y5=XI2DJ(II,JN)*(Q3(I,JP1)-Q3(I,J))
ZhG1656:      1 -XI2DJ(II,JS)*(Q3(I,J)-Q3(I,JM1))
ZhG1657:      COM=Q3(IP1,J)-Q3(IM1,J)
ZhG1658:      Y6=XIXJDJ(II,JN)*(Q3(IP1,JP1)-Q3(IM1,JP1)+COM)
ZhG1659:      2 -XIXJDJ(II,JS)*(Q3(IP1,JM1)-Q3(IM1,JM1)+COM)
ZhG1660: 10   R(I,J)=PR(I,J)+DB(I,J)/DT*BJ(II,JJ)
ZhG1661:      2         -(TX1-TX3+0.25*(TX2-TX4))
ZhG1662:      3         -(TY1-TY3+0.25*(TY2-TY4))
ZhG1663:      4         -(X1-X3+X5-0.25*(X2-X4+X6))
ZhG1664:      5         -(Y1-Y3+Y5-0.25*(Y2-Y4+Y6))
ZhG1665:      DO 100 K=1,NUMBER
ZhG1666:      RSD=0.0
ZhG1667:      DO 75 I=2,LX1
ZhG1668:      IP1=I+1
ZhG1669:      IM1=I-1
ZhG1670:      II=2*I-1
ZhG1671:      IE=II+1
ZhG1672:      IW=II-1
ZhG1673:      DO 75 J=2,LY1
ZhG1674:      JP1=J+1
ZhG1675:      JM1=J-1
ZhG1676:      JJ=2*J-1
ZhG1677:      JN=JJ+1
ZhG1678:      JS=JJ-1
ZhG1679:      T1=ADJ(IE,JJ)*PB(IP1,J)+ADJ(IW,JJ)*PB(IM1,J)
ZhG1680:      T2=GDJ(II,JN)*PB(I,JP1)+GDJ(II,JS)*PB(I,JM1)
ZhG1681:      COM=PB(I,JP1)-PB(I,JM1)
ZhG1682:      T3=(BDJ(IE,JJ)*(PB(IP1,JP1)-PB(IP1,JM1)+COM)
ZhG1683:      2 -BDJ(IW,JJ)*(PB(IM1,JP1)-PB(IM1,JM1)+COM))
ZhG1684:      COM=PB(IP1,J)-PB(IM1,J)
ZhG1685:      T4=(BDJ(II,JN)*(PB(IP1,JP1)-PB(IM1,JP1)+COM)
ZhG1686:      2 -BDJ(II,JS)*(PB(IP1,JM1)-PB(IM1,JM1)+COM))
```

```
ZhG1687:        RHS=T1+T2-0.25*(T3+T4)-R(I,J)
ZhG1688:        DPB=RHS/FM(I,J)-PB(I,J)
ZhG1689:        E=DABS(DPB)
ZhG1690:        IF(RSD.LT.E) RSD=E
ZhG1691: 75     PB(I,J)=PB(I,J)+OMG*DPB
ZhG1692:        IF(RSD.LT.1.0D-6) GOTO 150
ZhG1693: 100    CONTINUE
ZhG1694: 150    RETURN
ZhG1695:        END
ZhG1696:
ZhG1697:        SUBROUTINE WAVE(N1,N2)
ZhG1698:        IMPLICIT REAL*8(A-H,O-Z)
ZhG1699:        PARAMETER(LX=1001,LY=11,IG=2*LX-1,JG=2*LY-1)
ZhG1700:        COMMON/XY/X(IG,JG),Y(IG,JG)
ZhG1701:        COMMON/WAVEP/PER(LX),H(LX),AM(LX),XX(LX)
ZhG1702:        CALL UNIX
ZhG1703:        N1=0
ZhG1704:        N2=0
ZhG1705:        R1=PER(1)
ZhG1706:        R2=PER(2)
ZhG1707:        X1=X(1,JG)
ZhG1708:        X2=X(3,JG)
ZhG1709:        IF(R2.GE.R1) INDEX=1
ZhG1710:        IF(R2.LT.R1) INDEX=-1
ZhG1711:        DO 10 I=5,IG,2
ZhG1712:        K=(I+1)/2
ZhG1713:        R3=PER(K)
ZhG1714:        X3=X(I,JG)
ZhG1715:        IF((R3/R2).LT.0.0) THEN
ZhG1716:        N1=N1+1
ZhG1717:        H(N1)=0.5*(X2+X3)
ZhG1718:        ENDIF
ZhG1719:        IF((INDEX.EQ.1 .AND.R3.LT.R2).OR.
ZhG1720:        1  (INDEX.EQ.-1.AND.R3.GT.R2)) THEN
ZhG1721:        N2=N2+1
ZhG1722:        AM(N2)=R2
ZhG1723:        XX(N2)=X2
ZhG1724:        INDEX=-INDEX
ZhG1725:        ENDIF
ZhG1726:        R1=R2
ZhG1727:        R2=R3
ZhG1728:        X1=X2
ZhG1729: 10     X2=X3
ZhG1730:        RETURN
ZhG1731:        END
```